

**Biologically Inspired Computational Models Relating
Vection, Optokinetic Nystagmus (OKN) And
Visually Induced Motion Sickness (VIMS)**

by

JI, Ting Ting

A Thesis Submitted to
The Hong Kong University of Science and Technology
in Partial Fulfillment of the Requirements for
the Degree of Doctor of Philosophy
in Industrial Engineering and Engineering Management

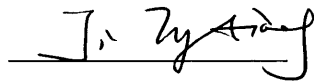
April 2008, Hong Kong

Authorization

I hereby declare that I am the sole author of the thesis.

I authorize the Hong Kong University of Science and Technology to
lend this thesis to other institutions or individuals for the purpose of
scholarly research.

I further authorize the Hong Kong University of Science and Technology
to reproduce the thesis by photocopying or by other means, in
total or in part, at the request of other institution or individuals for the
purpose of scholarly research.

A handwritten signature in black ink, appearing to read 'Ji, Ting Ting', written over a horizontal line.

Ji, TING TING

**Biologically Inspired Computational Models Relating
Vection, Optokinetic Nystagmus (OKN) And
Visually Induced Motion Sickness (VIMS)**


by

Jl, Ting Ting

This is to certify that I have examined the above PhD thesis
and have found that it is complete and satisfactory in all respects,
and that any and all revisions required by
the thesis examination committee have been made.



Dr. Richard H.Y. So Supervisor



Professor Chung-Yee Lee Head

Department of Industrial Engineering and Logistics Management

25 June 2008

Acknowledgements

My foremost thanks go to my advisor, Professor Richard H.Y. So. I thank him for his insights and suggestions that has helped shape my research and teaching skills, and for his thoughtful advice that inspired my research interest. His visionary thoughts and energetic working style have influenced me greatly.

I also thank the thesis committee members, Professor Daniel Chow at the Hong Kong Polytechnic University, Professor Ravindra Goonetilleke and Professor Fugee Tsung in the Department of Industrial Engineering and Logistics Management, Professor Bertram Shi in the Department of Electronic & Computer Engineering, and Professor Penger Tong in the Department of Physics at the Hong Kong University of Science and Technology, for their helpful discussions and valuable comments to the thesis, which has helped improve the quality of this work greatly.

I greatly appreciate the helps of my researcher partner, Mr. Eric Chow, on the hardware setup and programming of visual stimuli. I am also grateful to all the technicians in IELM, especially, Mr. Denil Chan, Mr. Kwok Chu Tin, Mr. Kwok Kuen Yung, Mr. Stanley SZE, for their supports on equipment setup and maintenance. Also I would like to thank the Hong Kong Research Grants Council for supporting this research study. Also I would like to thank my classmates and friends in Hong Kong. Their friendship has made my life at HKUST more colorful and memorable.

Finally, I would like to dedicate this thesis to my husband, Wang Lei, for his unreserved understanding and consistent support. His encouragement made it possible to accomplish my studies in Hong Kong. Words cannot adequately describe my appreciation of him.

TABLE OF CONTENTS

TitlePage	i
Authorization Page.....	ii
Signature Page.....	iii
Acknowledgements	iv
Table of Contents	v
List of Figures	xiii
List of Tables	xxi
Acronyms	xxiv
Abstract	xxv
CHAPTER 1 INTRODUCTION.....	1
1.1 Motivations.....	1
1.2 Literature review.....	5
1.2.1 Major theories of VIMS.....	5
1.2.1.1 Neural mismatch theory.....	5
1.2.1.2 Extraocular afference hypothesis.....	8
1.2.1.3 Postural instability theory.....	10
1.2.1.4 Subjective vertical-conflict theory.....	12
1.2.1.5 Summary.....	14
1.2.2 Three VIMS related responses.....	15
1.2.2.1 Vection and VIMS.....	15
1.2.2.2 Optokinetic nystagmus (OKN) and VIMS.....	22
1.2.2.3 Involuntary posture sway (IPS) and VIMS.....	23
1.2.2.4 Summary.....	24
1.2.3 Mathematical models of VIMS.....	24
1.2.3.1 Oman's neural mismatch model.....	24

1.2.3.2 Bos and Bles' subjective vertical-conflict model.....	27
1.2.3.3 Summary.....	28
1.3 Research rationale.....	29
1.3.1 Research gaps.....	29
1.3.2 Objectives and scope.....	30
1.3.3 Methodology overview.....	32
1.4 Thesis organization.....	34
CHAPTER 2 A BIOLOGICALLY INSPIRED COMPUTATIONAL MODEL RELATING VECTION AND VIMS (MODEL ONE).....	40
2.1 Introduction	40
2.2 Motivation.....	42
2.3 Model scope and assumptions.....	43
2.4 Model development.....	44
2.4.1 Neural based roadmap relating vection and VIMS.....	45
2.4.2 Conceptual model.....	53
2.4.3 Computational model.....	55
2.4.3.1 Module 1(M1): a visual-vestibular sensory integration network for vection perception.....	58
2.4.3.2 Module 2 (M2): a supervised learning adaptation network.....	61
2.4.3.3 Module 3 (M3): a symptom dynamic network.....	64
2.4.4 Model simulation.....	66
2.5 Comparison of model simulated data and empirical data of Stern et al. (1990)...	68
2.6 Conclusion.....	71
CHAPTER 3 A BIOLOGICALLY INSPIRED COMPUTATIONAL MODEL RELATING OKN AND VIMS (MODEL TWO).....	72
3.1 Introduction.....	72

3.2 Motivation	75
3.3 Model scope and assumptions.....	76
3.4 Model development.....	77
3.4.1 Neural based roadmap relating OKN and VIMS.....	77
3.4.2 Conceptual model.....	86
3.4.3 Computational model.....	87
3.4.3.1 Module 1(M1): a visual-vestibular sensory integration network for OKN generation.....	89
3.4.3.2 Module 2 (M2): a supervised learning adaptation network.....	93
3.4.3.3 Module 3 (M3): a symptom dynamic network.....	94
3.4.4 Model simulation.....	95
3.5 Comparison of model simulated data and empirical data of Webb and Griffin (2002).....	97
3.6 Discussion.....	100
3.7 Conclusion.....	102
CHAPTER 4 OVERVIEW OF MODEL VALIDATION EXPERIMENTS.....	103
4.1 Introduction.....	103
4.2 Motivations.....	106
4.3 OKN suppression in experiment one.....	106
4.4 Vection suppression in experiment two.....	108
4.5 Methods.....	110
4.5.1 Apparatus and visual stimuli.....	110
4.5.2 Participants.....	114
4.5.3 Measures.....	116
4.5.3.1 Nausea severity.....	117
4.5.3.2 Simulator Sickness Questionnaire (SSQ)	121

4.5.3.3 Vection velocity and vection intensity.....	123
4.5.3.4 EOG records of optokinetic nystagmus (OKN)	125
4.5.3.5 Visual acuity at near point and motion sickness susceptibility....	129
CHAPTER 5 EXPERIMENT ONE: VECTION AND VIMS AS A FUNCTION OF ROTATION VELOCITY OF AN OPTOKINETIC STIMULI IN THE ABSENCE OF OKN.....	132
5.1 Objective and hypotheses.....	133
5.2 Methods.....	134
5.2.1 Participants.....	134
5.2.2 Visual stimuli.....	134
5.2.3 Design of experiment (DOE)	135
5.2.4 Procedure.....	137
5.2.5 Measures.....	139
5.2.6 Statistical analysis.....	141
5.3 Results.....	142
5.3.1 EOG recording data.....	142
5.3.2 Vection velocity (perceived self-rotation velocity)	143
5.3.3 7-point nausea rating.....	148
5.3.4 Nausea ratio scale data.....	153
5.3.5 Simulator Sickness Questionnaire Scores.....	157
5.3.6 Correlation analysis of vection related measures, 7-point nausea rating, nausea ratio scale data, and post SSQ-Nausea score.....	164
5.3.7 Visual acuity at near point and motion sickness susceptibility.....	167
5.4 Discussions.....	168
5.5 Conclusions.....	172

CHAPTER 6 EXPERIMENT TWO: OKN AND VIMS AS A FUNCTION OF ROTATION VELOCITY OF AN OPTOKINETIC STIMULI IN THE ABSENCE OF VECTION.....	174
6.1 Objective and hypotheses.....	175
6.2 Methods.....	176
6.2.1 Participants.....	176
6.2.2 Visual stimuli.....	177
6.2.3 Design of experiment (DOE)	177
6.2.4 Procedure.....	179
6.2.5 Measures.....	182
6.2.6 Statistical analysis.....	184
6.3 Results.....	186
6.3.1 Vection intensity.....	186
6.3.2 OKN slow-phase velocity (SPV), OKN gain, and foveal retinal slip velocity.....	187
6.3.3 7-point nausea rating.....	192
6.3.4 Nausea ratio scale data.....	198
6.3.5 Simulator Sickness Questionnaire Scores.....	201
6.3.6 Correlation analysis of OKN related measures, 7-point nausea rating, nausea ratio scale data, and post SSQ-Nausea score.....	208
6.3.7 Visual acuity at near point and motion sickness susceptibility.....	211
6.4 Discussions.....	212
6.5 Conclusions.....	215
CHAPTER 7 MODEL VALIDATIONS.....	217
7.1 Motivations.....	217
7.2 Methodology overview.....	218

7.3 Pre-validation stage of model one.....	223
7.4 Validation stage of model one.....	224
7.4.1 Model predicted nausea severity as a function of time.....	224
7.4.2 Model predicted nausea severity as a function of velocity.....	227
7.5 Pre-validation stage of model two.....	228
7.6 Validation stage of model two.....	230
7.6.1 Model predicted nausea severity as a function of time.....	230
7.6.2 Model predicted nausea severity as a function of velocity.....	232
7.7 Conclusions.....	234
CHAPTER 8 MODEL SIMULATED INDIVIDUAL DIFFERENCES AND MODEL SENSITIVITY ANALYSIS.....	236
8.1 Motivations.....	236
8.2 Methodology overview.....	238
8.3 Model one simulated individual differences in latency of vection onset, vection build-up time, and vection velocity's steady state.....	240
8.4 Model one's sensitivity analysis and model one simulated individual differences in nausea severity.....	243
8.5 Model two simulated individual differences in OKN SPV, OKN gain and foveal retinal slip velocity.....	250
8.6 Model two's sensitivity analysis and model two simulated individual differences in nausea severity.....	251
8.7 Discussions.....	261
8.8 Conclusions.....	263
CHAPTER 9 CONCLUSIONS.....	265
9.1 Conclusions.....	265
9.2 Limitations and future research areas.....	270

Appendix 2-1 Transfer functions of M1 in model one.....	277
Appendix 2-2 Transfer functions of M3 in model one and two.....	279
Appendix 3-1 Transfer functions of M1 in model two.....	280
Appendix 4-1 Pre-exposure and post-exposure Simulator Sickness Questionnaires (SSQ) (Kennedy et al., 1993)	283
Appendix 4-2 Calculations of SSQ total scores and three sub-scores (Kennedy et al., 1993)	285
Appendix 4-3 A motion sickness susceptibility survey questionnaire (So et al., 1999).....	286
Appendix 4-4 A motion sickness susceptibility questionnaire (MSSQ)-Short (Golding, 2006)	289
Appendix 5-1 Individual vection velocity time series.....	290
Appendix 5-2 Individual 7-point nausea rating time series.....	297
Appendix 5-3 Individual nausea ratio scale time series.....	304
Appendix 5-4 individual plots of pre-& post-exposure SSQ scores.....	311
Appendix 5-5 four-level balanced Latin Square technique.....	321
Appendix 5-6 Instruction of experiment one.....	322
Appendix 5-7 Consent form.....	327
Appendix 5-8 Instruction of measuring visual acuity at near point by an “OPTEC®2000” visual tester.....	328
Appendix 5-9 Graybiel scale (Graybiel et al., 1968) used in Hu et al.(1989)	331
Appendix 6-1 The diameter (in the unit of degree) of central visual field used in experiment two fine tuned for each subject across three non-zero velocity conditions to fully suppress vection perception.....	332
Appendix 6-2 Instruction of experiment two.....	333
Appendix 6-3 Individual plots of OKN SPV calculated from eye position data of	

EOG recording (negative value since OKN slow-phase had negative slope). Mean and SD of time series was listed.....	336
Appendix 6-4 Individual plots of 7-point nausea rating time series.....	344
Appendix 6-5 Individual plots of modulus equalized nausea ratio scale data.....	351
Appendix 6-6 individual plots of pre-& post-exposure SSQ scores.....	358
Appendix 7-1 grouping in experiment one.....	366
Appendix 7-2 grouping in experiment two.....	367
Bibliography.....	368

LIST OF FIGURES

Figure 1.1 Reason’s neural mismatch model (Reason, 1978)	6
Figure 1.2 Diagram of cerebellar circuit reported by Doya, 1999.....	20
Figure 1.3 Oman’s mathematical model of motion sickness (Oman, 1982; 1990) ...	26
Figure 1.4 Subjective vertical conflict model for passive vertical motion (Bos and Bles, 1998)	28
Figure 1.5 Schematic representation of the research methodology employed in this study.....	34
Figure 1.6 Flow chart of thesis organization.....	39
Figure 2.1 Neural centers related tovection perception and VIMS generation summarized from neuroscience literature.....	47
Figure 2.2 Roadmap relatingvection and VIMS summarized from related neuroscience literature.....	52
Figure 2.3 Three-module conceptual model relatingvection and VIMS. Details are stated in text.....	54
Figure 2.4 Block diagram of M1 of model one.....	61
Figure 2.5 Block diagram of M2 of model one.....	64
Figure 2.6 Block diagram of M3 of model one.....	66
Figure 2.7 Block diagram of model one relatingvection and VIMS.....	67
Figure 2.8 Comparing model one’s output with empirical data of Stern et al. (1990)	70
Figure 3.1 Block diagram of the working mechanism of OKN suppression induced VIMS alleviation.....	80
Figure 3.2. Neural centers related to slow-phase OKN and VIMS generation summarized from neuroscience literature.....	83
Figure 3.3 Roadmap relating OKN and VIMS summarized from related neuroscience	

literature.....	85
Figure 3.4 Three-module conceptual model relating OKN and VIMS.....	86
Figure 3.5 Block diagram of M1 of model two.....	93
Figure 3.6 Block diagram of M2 of model two.....	94
Figure 3.7 Block diagram of M3 of model two.....	95
Figure 3.8 Block diagram of model two relating OKN and VIMS	96
Figure 3.9 Comparing model two's output with empirical data of Webb & Griffin (2002)	99
Figure 3.10 Relationship of model one and model two and the difference of their visual inputs.....	101
Figure 4.1 OKN suppression achieved by fixating on 1deg eye fixation point.....	108
Figure 4.2 (a) Physical layout of multi-projection system consisting of three projects and one curved projection screen (b) Geometrical transformation between viewing distance and field of view (FOV)	112
Figure 4.3 (a) Subject in standing position viewing virtual optokinetic drum rotating in yaw direction at constant velocity. (b) Subject wearing five EOG electrodes for eye position data recording.....	113
Figure 4.4 Horizontal and vertical eye position time courses recorded in an eye calibration session.....	126
Figure 5.1 The 4 conditions of experiment one.....	136
Figure 5.2 Vection velocity (median of 14 subjects') as function of exposure duration. for three non-zero rotation velocity conditions.....	144
Figure 5.3 Normality test of vection velocity (average over 30min)	146
Figure 5.4 Variance homogeneity test of vection velocity (average over 30min)	146

Figure 5.5 Linear relationships between the vection velocity and the rotation velocity of the optokinetic stimuli.....	148
Figure 5.6 Median, 25 th and 75 th percentile of nausea rating as a function of exposure duration for four rotation velocity conditions.....	151
Figure 5.7 Observed linear increasing trend of 7-point nausea rating at 30min as a function of drum rotation velocity.....	153
Figure 5.8 Median, 25 th and 75 th percentile of nausea ratio scale data as a function of exposure duration for four rotation velocity conditions.....	154
Figure 5.9 Normality test of (a) modulus equalized nausea ratio scale data.....	155
Figure 5.10 Normality test of modulus equalized nausea ratio scale data.....	156
Figure 5.11 Observed linear increasing trend of the nausea ratio scale data at 30 min as a function of the rotation velocity of the optokinetic stimuli.....	157
Figure 5.12 Mean and SE (standard error) of Pre- and Post- exposure SSQ total scores and sub-scores for condition of 0dps, 2dps, 14dps, and 34dps.....	160
Figure 5.13 Observed linear increasing trend of post SSQ-N as a function of drum rotation velocity.....	162
Figure 5.14 Difference (Post-Pre) SSQ total score and three sub-scores for rotation velocity of 0dps, 2dps, 14dps, and 34dps.....	163
Figure 5.15 Main effect plots of rotation velocity.....	165
Figure 5.16 Observed linear increasing trend of nausea severity measured by nausea ratio scale (Median of 14 subjects) as a function of vection velocity (Median of 14 subjects)	165
Figure 5.17 Scatter plots and correlation coefficients (Spearman's rho) summarized for correlation analysis.....	167
Figure 5.18 Scatter plots and correlation coefficients (Spearman's rho) of visual acuity at near point and 7-point nausea rating data in (a) 14 dps and (b) 34 dps	

condition.....	168
Figure 6.1 The 4 conditions of experiment two.....	178
Figure 6.2 Comparing (a) OKN gain, (b) OKN SPV, and (c) foveal retinal slip velocity's median level of experiment two with results of Koenig et al., 1978.....	190
Figure 6.3 Linear relationships between the foveal retinal slip velocity and the rotation velocity of the optokinetic stimuli.....	192
Figure 6.4 Median, 25 th and 75 th percentile nausea rating as a function of exposure duration for four velocity conditions.....	195
Figure 6.5 Observed inverted shape relationship between nausea severity measured by 7-point nausea rating and drum rotation velocity	196
Figure 6.6 Median, 25 th and 75 th percentile of nausea ratio scale data as a function of exposure duration for four velocity conditions.....	199
Figure 6.7 Observed inverted shape relationship between nausea severity measured by nausea ratio scale and drum rotation velocity.....	201
Figure 6.8 Mean and SE (standard error) of Pre- and Post- exposure SSQ total scores and sub-scores.....	205
Figure 6.9 Observed inverted shape relationship between nausea severity measured by post SSQ-Nausea and drum rotation velocity.....	206
Figure 6.10 Post-Pre SSQ total scores and three sub-scores in four conditions of rotation velocity of image pattern.....	207
Figure 6.11 Main effect plots of the rotation velocity of the image pattern.....	209
Figure 6.12 Scatter plots and correlation coefficients (Spearman's rho) summarized for correlation analysis.....	210
Figure 6.13 Observed linear increasing trend of nausea severity measured by nausea ratio scale (Median of 14 subjects) as a function of the foveal retinal slip velocity	

(Median of 14 subjects)	211
Figure 6.14 Mapping of retinal slip velocity levels between experiment one and two.....	214
Figure 6.15 Model one simulated nausea severity at drum rotation velocity levels of 14dps, 34dps, 70dps, and 94dps.....	215
Figure 7.1 Comparison of model simulated / predicted nausea severity levels with empirical data as functions of exposure duration for three optokinetic stimuli rotation velocity conditions: rotating at (a) 2, (b) 14, and (c) 34 degrees per second (dps)	225
Figure 7.2 Comparison of model simulated/predicted nausea severity levels with empirical data as functions of exposure duration for (a) 34dps group I and (c) II as well as (b) 14dps group I and (d) II.....	226
Figure 7.3 Comparison of model simulated/predicted nausea severity levels with empirical data as functions of rotation velocity of the optokinetic stimuli from 2dps, to 14dps, then to 34dps.....	227
Figure 7.4 Comparison of model simulated/predicted nausea severity levels with empirical data as functions of rotation velocity of the optokinetic stimuli from 2dps, to 14dps, then to 34dps of (a) group I subjects and (b) group II subjects.....	228
Figure 7.5 Comparison of model simulated/predicted nausea severity levels with empirical data as functions of exposure duration for three optokinetic stimuli rotation velocity conditions: rotating at (a) 60dps, (b) 90dps, and (c) 30dps.....	231
Figure 7.6 comparison of model simulated/predicted nausea severity levels with empirical data as functions of exposure duration for (a) 90dps group I and (c) group II as well as (b) 60dps group I and (d) group II.....	232
Figure 7.7 Comparison of model simulated/predicted nausea severity levels with	

empirical data as functions of rotation velocity of the optokinetic stimuli from 30dps, to 60dps, then to 90dps.....	233
Figure 7.8 Comparison of model simulated/predicted nausea severity levels with empirical data as functions of rotation velocity of the optokinetic stimuli from 30dps, to 60dps, then to 90dps of (a) group I subjects and (b) group II subjects.....	234
Figure 8.1 Model simulated latency of vection onset as a function of τ_{ω} and ξ	241
Figure 8.2 a) Model simulated vection onset time as function of τ_{ω} given ξ equal to 1.6dps as suggested by Telban & Cardullo, 2001; b) Model simulated vection build-up time as a function of τ_{va}	241
Figure 8.3 Model simulated vection velocity's steady state varied in its empirical interquantile range in the velocity condition of (a) 2dps, (b) 14dps, and (c) 34dps and (d) model simulated individual differences in vection gain as a function of parameter Φ	242
Figure 8.4 Comparison of model simulated/predicted nausea severity levels with empirical data as functions of exposure duration for thee optokinetic stimuli velocity conditions: rotating at (a) 2dps, (b) 14dps, and (c) 34dps.....	245
Figure 8.5 Comparison of model simulated/predicted nausea severity levels with empirical data as functions of rotation velocity from 2dps, to 14dps, and to 34dps.....	245
Figure 8.6 Comparing model one simulated data distribution with empirical data distribution collected from experiment one.....	247
Figure 8.7 Comparison of model simulated/predicted nausea severity levels with empirical data as a function of rotation velocity from 2dps, to 14pds, and to 34dps.....	248

Figure 8.8 Comparison of model simulated nausea severity levels with empirical data as functions of exposure duration for (a) 34dps group I and (c) II as well as (b) 14dps group I and (d) group II.....	249
Figure 8.9 Comparison of model simulated/predicted nausea severity levels with empirical data as functions of rotation velocity from 2dps, to 14dps, and to 34dps for (a) group I subjects and (b) group II subjects.....	249
Figure 8.10 Model simulated OKN SPV varied in its empirical interquantile range in the velocity condition of (a) 30dps, (b) 60dps, and (c) 90dps and (d) model simulated individual differences in OKN gain as a function of parameter $W_{r,3}$	251
Figure 8.11 comparison of model simulated/predicted nausea severity levels with empirical data as functions of exposure duration for thee optokinetic stimuli velocity conditions: rotating at (a) 30dps, (b) 60dps, and (c) 90dps.....	252
Figure 8.12 Comparison of model simulated/predicted nausea severity levels with empirical data as functions of rotation velocity from 30dps, to 60dps, and to 90dps.....	253
Figure 8.13 comparison of model simulated/predicted nausea severity levels with empirical data as functions of exposure duration for thee optokinetic stimuli velocity conditions: rotating at (a) 30dps, (b) 60dps, and (c) 90dps.....	255
Figure 8.14 Comparison of model simulated/predicted nausea severity levels with empirical data as functions of rotation velocity from 30dps, to 60dps, and to 90dps.....	255
Figure 8.15 Comparing model two simulated data distribution with empirical data distribution collected from experiment two.....	256
Figure 8.16 Comparison of model simulated/predicted nausea severity levels with empirical data as a function of rotation velocity from 30dps, to 60pds, and to 90dps.....	257

Figure 8.17 Model simulated nausea severity levels as function of drum velocity given the average of top three and the average of bottom three vection velocity levels listed in Table 6.7.....	258
Figure 8.18 Comparison of model simulated nausea severity levels with empirical data as functions of exposure duration for (a) 90dps group I and (c) II as well as (b) 60dps group I and (d) group II.....	259
Figure 8.19 Comparison of model simulated/predicted nausea severity levels with empirical data as functions of rotation velocity of (a) group I subjects and (b) group II subjects.....	260
Figure 8.20 Variation of OKN SPV results of experiment two given a range of EOG unit mapping constants (* EUMC) measured in EOG calibration session.....	262

LIST OF TABLES

Table 4.1 7-point nausea rating scale proposed by Golding & Kerguelen (1992) ...	121
Table 4.2 4-point vection rating scale (Webb & Griffin, 2002)	125
Table 5.1 Velocity conditions in Hu et al., 1989 and their corresponding retinal slip velocities calculated by using OKN gains reported by Koenig et al., 1978.....	137
Table 5.2 Vection velocity averaged over 30min in three non-zero velocity conditions.....	147
Table 5.3: Student-Newman-Kuels (SNK) tests on the effects of rotation velocity on vection velocity (average over 30min)	147
Table 5.4 Student-Newman-Kuels (SNK) test on the effect of rotation velocity on 7-point nausea rating data (average over 30min)	151
Table 5.5 Student-Newman-Kuels (SNK) test on the effects of rotation velocity on nausea severity at 30min measured by 7-point nausea rating.....	152
Table 5.6 Student-Newman-Kuels (SNK) test on the effect of rotation velocity on modulus equalized nausea ratio scale (average over 30min)	155
Table 5.7 Student-Newman-Kuels (SNK) test on the effects of rotation velocity on modulus equalized nausea ratio scale data at 30min.....	156
Table 5.8 Student-Newman-Kuels (SNK) tests on significance of health state fluctuation measured by pre-exposure SSQ scores across four rotation velocity conditions.....	161
Table 5.9 Student-Newman-Kuels (SNK) tests on the effects of rotation velocity on sickness severity measured by post SSQ total score and three sub-scores.....	162
Table 5.10 Student-Newman-Kuels (SNK) tests on the effect of rotation velocity on difference (Post-Pre) SSQ total score and three sub-scores.....	164
Table 6.1 (a) EOG unit mapping constant calculated from horizontal eye position	

data recorded during eye calibration. (b) The lower bound of OKN SPV in the unit of degree per second (dps)	188
Table 6.2 Average values of (a) OKN SPV (b) OKN gain, and (c) foveal retinal slip velocity.....	190
Table 6.3 Student-Newman-Kuels (SNK) tests on the effect of rotation velocity of image pattern on (a) OKN SPV, (b) OKN gain, and (c) the foveal retinal slip velocity.....	191
Table 6.4 Student-Newman-Kuels (SNK) tests on the effect of rotation velocity of the image pattern on 7-point nausea rating (a) averaged over 30mins and (b) at 30min.....	195
Table 6.5 Student-Newman-Kuels (SNK) tests on the effect of the rotation velocity on the nausea severity measured by 7-point nausea rating (a) averaged over the first 18min (b) at 18min. 0dps, 30dps, 60dps, and 90dps was labeled as 1, 2, 3, and 4, respectively.....	198
Table 6.6 Student-Newman-Kuels (SNK) tests on the effect of rotation velocity of the image pattern on nausea ratio scale data (a) averaged over 30mins and (b) at 30min.....	200
Table 6.7 Student-Newman-Kuels (SNK) tests on the effects of the rotation velocity of the image pattern on sickness severity measured by post SSQ total score and three sub-scores.....	204
Table 6.8 Student-Newman-Kuels (SNK) tests on the effect of rotation velocity on difference (Post-Pre) SSQ total score and three sub-scores.....	207
Table 8.1 Model simulated vection velocity's steady state levels and their corresponding parameter Φ plotted in Figure 8.3.....	243
Table 8.2 25 th percentile, 50 th percentile, and 75 th percentile of vection velocity reported in experiment one.....	246

Table 8.3 Top three and bottom three vection velocity levels in 2dps, 14dps and 34dps rotation velocity conditions.....	248
Table 8.4 vection velocity medians, 75 th percentile, and 25 th percentiles of 2dps, 14dps, and 34dps drum velocity condition for group I and II subjects.....	250
Table 8.5 Model simulated OKN SPVs and their corresponding parameter $W_{r,3}$ plotted in Figure 8.9.....	251
Table 8.6 Means and 95% confidence intervals of OKN SPV and foveal retina slip velocity levels reported by experiment two.....	254
Table 8.7 The top three and bottom three retinal slip velocity levels reported by experiment two.....	258
Table 8.8 Means and 95% confidence intervals of foveal retinal slip velocity of 30dps, 60dps, and 90dps velocity condition for group I and group II subjects.....	260

ACRONYMS

ADALINE	Adaptive linear neural network
CN	Deep cerebellar nuclei
CNS	Central nervous system
CV	Circular vection
DOE	Design of experiment
EOG	Electrooculogram
EUMC	EOG unit mapping constant
FOV	Field of view
GC	Granule cells
ION	Inferior olivary nucleus
IPS	Involuntary postural sway
LMS	Least mean square error
LV	Linear vection
MS	Motion sickness
OKN	Optokinetic nystagmus
OKNe	Early component of optokinetic nystagmus
OKNd	Delayed component of optokinetic nystagmus
OTO	Otolith
PC	Purkinje cells
PI	Postural instability
PIVC	Parietal-insular vestibular cortex
SCC	Semicircular canals
SPV	Slow-phase velocity
SSQ	Simulator Sickness Questionnaire
SVC	Subjective-vertical conflict
VIMS	Visually induced motion sickness
VN	Vestibular nucleus
VR	Virtual reality

**Biologically Inspired Computational Models Relating Vection, Optokinetic
Nystagmus (OKN) And
Visually Induced Motion Sickness (VIMS)**

by JI, Ting Ting

Department of Industrial Engineering and Logistics Management
The Hong Kong University of Science and Technology

Abstract

Motivated by recent debates on the role of vection and optokinetic nystagmus (OKN) in VIMS generation, two biologically inspired computational models are developed to simulate the connections between vection and VIMS (model one), and the connections between OKN and VIMS (model two), respectively. Both models are new and consistent with their respective VIMS theories and neuroscience knowledge concerning VIMS. Results of simulation of models one and two successfully reproduce sickness severity levels that are comparable to the empirical data published in Stern et al. (1990) and Webb and Griffin (2002), respectively.

A literature review reveals a lack of empirical study reporting the isolated effects of vection and OKN on ratio scale data of VIMS severity. Consequently, two empirical experiments are conducted to validate the two models, respectively. Experiment one examines the effects of circular vection (CV) on VIMS severity in the absence of OKN while watching visual stripe patterns rotating in the yaw axis at different velocities. Experiment two examines the effect of optokinetic nystagmus (OKN) on VIMS severity in the absence of vection while watching visual stripe patterns rotating in the yaw axis at different velocities. Both experiments one and two report a significant main effect of rotation velocity of the optokinetic stimuli on VIMS

severity. Experiment one reports a linear relationship between the vection velocity and VIMS severity. Experiment two reports a nonlinear relationship between the foveal retinal slip velocity and VIMS severity. Such results indicate that either vection alone or OKN alone can induce VIMS and their effects change significantly as the visual stimuli velocity changes.

Results of model validation indicate that both models can simulate the average VIMS severity levels as functions of rotation velocities of the stripe patterns. In addition, sensitivity analyses are conducted to identify the model parameters contributing to inter-subject variations in VIMS severity. This enables both models to simulate not only the mean VIMS severity levels, but also the inter-subject variations. Model one and model two can simulate inter-subject variations in VIMS severity by manipulating inter-subject variations in three vection related measures (latency of vection onset, vection build-up time, the steady state of vection velocity) and three OKN related measures (OKN slow-phase velocity, OKN gain, and foveal retinal slip velocity), respectively. Such results are consistent with the understanding that both vection and OKN play a significant role in VIMS generation.

In addition, both experiments report significant correlation among the three VIMS severity measures: (i) 7-point nausea rating, (ii) SSQ nausea score, and (iii) nausea ratio scale data collected by free-modulus magnitude estimation. It is proposed the free-modulus magnitude estimation, as a supplement to the two ordinal scales for measuring VIMS severity, can benefit future VIMS studies.

CHAPTER 1

INTRODUCTION

SUMMARY

This chapter first presents the motivations for launching this study. After that, major VIMS theories are reviewed, previous findings of empirical studies and neurobiological studies related to the three VIMS related responses are summarized, and previous work on mathematical modeling of motion sickness are presented. Finally, research rationale, including research gaps, objectives, scope and methodology overview, is elaborated in detail.

1.1 Motivations

Visually induced motion sickness (VIMS) is commonly considered as a variant of motion sickness (Reason, 1978; Hettinger and Ricco, 1992). It is defined as a syndrome that ‘occasionally occurs when physically stationary individuals view compelling visual representation of self motion’ and characterized by ‘syndromes normally associated with classic motion sickness’, such as nausea, stomach awareness, fullness of the head, etc (Hettinger and Ricco, 1992).

VIMS is considered to be a major ergonomics concern with the use of virtual reality (VR) technology (Stanney et al., 1998) since human subjects can generate VIMS after VR environment exposure. It is reported that 88% of the participants experienced sickness symptoms and specifically, 71% experienced nausea. This led to a nearly 50% dropout rate after 1 hour of VR environment exposure. To widely apply VR technology in the civil and military industry, for instance, in training, entertainment, education, medical etc, research questions for VIMS have to be answered (Stanney and Kingdon, 2002).

Researchers around the world have already spent a great amount of effort on this research topic since 1978. Varied VIMS theories and models were proposed and several human responses were reported to be associated with VIMS generation. Recently, the competing role of two VIMS related responses; vection and optokinetic nystagmus (OKN, a type of involuntary eye movement for gaze stabilization provoked by rotational visual disturbances) in VIMS generation, has become a bone of contention between two camps of researchers who favor one over the other. Unfortunately, claims on each side have supportive and opposing evidence. Therefore, no confirmative conclusions have ever been drawn. Consequently, the author was motivated to study the relations between the two VIMS related responses

(vection and OKN) and VIMS generation.

A literature review revealed that different types of VIMS studies emphasize on different aspects. (i) Empirical studies make scientific statements on the basis of statistical results. The focus is to identify the factors that have significant effects on VIMS related measures (Hu et al., 1989; Webb and Griffin, 2002, etc). (ii) Studies of conceptual model development provided a general conceptual framework to explain the occurrence of VIMS over a wide range of apparently diverse circumstances (Reason, 1978; Benson, 1984). (iii) Studies of mathematical modeling substantiated conceptual notions by mathematical equations. The quantitative models can not only predict results of empirical studies, but also provide logical explanations on previous empirical findings (Oman, 1982 and 1990). (iv) Neurobiological studies focused on uncovering neural mechanisms of VIMS generation. For example, neural centers directly mediating elicitation of VIMS symptoms, such as nausea and vomiting had been identified in mammals by neuroscientists (Balaban and Porter, 1998; Yates et al., 1998).

Standing on the shoulders of giants, a research study can further the understanding of VIMS generation by exploring a deeper layer of VIMS's working mechanism if such

a study satisfies the following requirements: first, the study should develop a mathematical model to simulate the entire process of VIMS generation from raw visual and vestibular stimuli to elicitation of VIMS symptoms. Secondly, the model should be built on the basis of a VIMS theory. Thirdly, the model should work in a way that is relevant to the operation of the human central nervous system. Fourth, the model should be able to explain the association betweenvection (or OKN) and VIMS reported empirically. Fifth, the model should be validated against empirical data.

It is expected that this type of research work can produce informative results as a useful addition to recent debates that are mentioned above. Furthermore, this move supports the ultimate goal of ‘studying human by building a human through quantitative modeling’ of computational ergonomics (So and Lor, 2004) and is consistent with the call for a more quantitative model of human performance and behavior (Byrne & Gray, 2003). However, such a study was not found after a thorough literature review.

The following sections summarize previous research findings on VIMS. Such a review helps identify a few research gaps. After the objectives and scope are

carefully defined, a methodology overview of this research study is presented.

1.2 Literature review

This section is composed of three parts: (i) review of major VIMS theories, (ii) review of empirical studies and neurobiological studies related to VIMS, and (iii) review of studies on mathematical modeling of VIMS generation.

1.2.1 Major theories of VIMS

1.2.1.1 Neural mismatch theory

The earliest idea of ‘neural mismatch’ can be traced back to the following statement made by Irwin (1881) (refer to Reason, 1978, pp819): ‘In the visual vertigo of seasickness there appears to be a discord between the immediate or true visual impressions and a certain visual habit or visual sense of the fitness and order of things, which passes into consciousness as a distressing feeling of uncertainty, dizziness and nausea’. This concept was expounded and developed into a complete theory by Reason around 100 years later. Borrowing an earlier idea of ‘correlation storage’ by Held (1961), the neural mismatch theory built a necessary linkage between neural mismatch notion and protective adaptation of motion sickness. As shown in Figure 1.1, Reason proposed two structural components to explain the

mechanism of motion sickness generation and adaptation: one is a neural store responsible for storing previous experiences or expectations of sensory input patterns; the other is a comparator responsible for detecting the discrepancies between the current sensory input pattern and one stored pattern selected out of the neural store by an efference copy if available. A neural mismatch signal is produced in the comparator to trigger various neural mechanisms mediating motion sickness symptoms, such as nausea and vomiting. The sustained neural mismatch signal also updates the retrieval strategy in the ‘neural store’ until new rules are built to select expected sensory input pattern that satisfy the match criteria much better, which eventually leads to diminution and disappearance of motion sickness symptoms; i.e., protective adaptation of motion sickness (Reason, 1978).

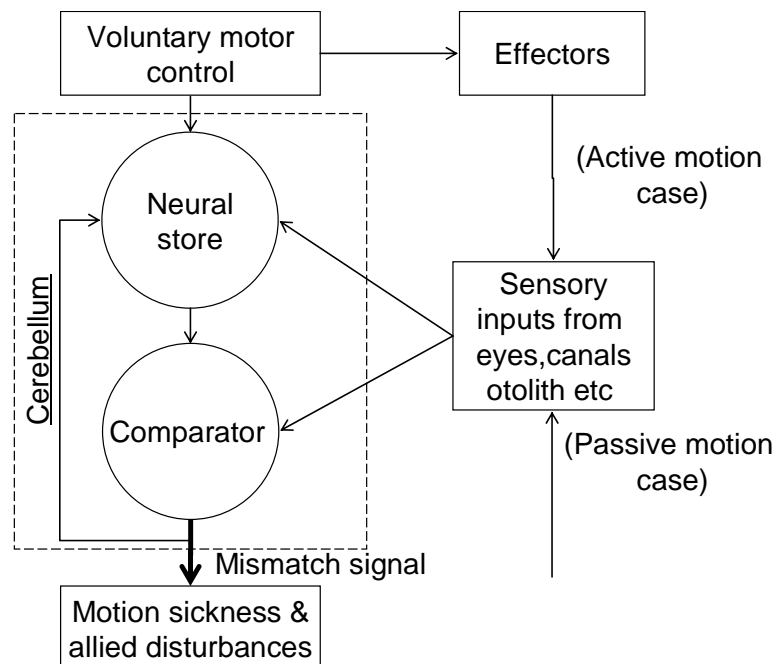


Figure 1.1 Reason's neural mismatch model (Reason, 1978).

The neural mismatch theory classifies all types of motion sickness provocative stimuli into six categories of sensory rearrangements. Type 2 visual-vestibular rearrangements (visual signal in the absence of an expected corresponding vestibular signal) are especially widely investigated by a large amount of VIMS empirical studies (Hettinger, et al., 1990; Kennedy, et al., 1990; Yang and Pei, 1991; Howarth, 2002; Flanagan, et al., 2004; Bonato, et al., 2005; see the review by Hettinger & Riccio, 1992). Generally, type 2 visual-vestibular rearrangements occur when human subjects viewed rotating visual content or translational moving along different axes, but lack corresponding vestibular motion information. Such visual-vestibular sensory integration can simultaneously produce a visually induced illusion of rotational or translational self-motion; that is, circular vection (CV) or linear vection (LV) (Brandt, et al., 1973; Dichgans and Brandt, 1978; Howard, 1986b; Flanagan, et al., 2002; 2004; see the review by Hettinger & Riccio, 1992).

In summary, the neural mismatch theory indicates that the visual-vestibular sensory integration, as the central mechanism of vection generation, is essential for explaining VIMS generation. A good knowledge of the role of such visual-vestibular sensory integration in VIMS generation will help explain the strong association between vection and VIMS reported by groups of empirical studies (Hettinger, et al.,

1990; Stern, et al., 1990; Hu et al., 1989; Flanagan, et al., 2002).

1.2.1.2 Extraocular afference hypothesis

On the basis of the crucial role of the vestibular system in motion sickness (Cheung, et al., 1991; Kennedy, et al., 1968) and highly correlated relation between the vestibular system activity and extraocular motor control activity (Waespe & Henn, 1977; Keller & Daniels, 1975), it was hypothesized by Ebenholtz et al. (1994) that motion sickness resulted from the conflicts among eye movements controlled by competing oculomotor systems and associated afferences of abnormal extraocular muscle tractions. It was proposed that these extraocular afference signals of sensory organs of eye muscles ultimately stimulated the vagus nerve through a pathway running from the ciliary ganglion to motor neurons of the vagus nerve (Katz and Bigger, 1970), which is believed to be a critical neural center in the vestibular-autonomic neural circuit responsible for eliciting VIMS symptoms, such as nausea and vomiting (Ebenhotz, et al., 1994; Balaban & Porter, 1998).

For the purpose of directly approving the extraocular afference hypothesis, first, the afferent signals from extraocular muscles should be completely blocked by retrobulbar injection and then, the subject should be exposed in a provocative

environment to see whether the subject is immune to motion sickness (Ebenholtz, et al., 1994). Although related research work has not been conducted, abundant empirical results strongly support the significant effect of optokinetic nystagmus (OKN), a type of involuntary eye movement for gaze stabilization under rotational visual disturbance, on VIMS severity (Hu, et al., 1997; Hu and Stern, 1998; Stern, et al. 1990; Webb and Griffin, 2002; May, et al. 2001; Flanagan, et al. 2002; 2004). Such strong association between OKN and VIMS indicate that the possibility is high that OKN-related information plays a major role in the process of VIMS generation.

The extraocular afference hypothesis is still under testing and has not been formed as a complete theory and modeled conceptually or mathematically. Although general statements are made about the extensive connections between the oculomotor control system, vestibular system and about the involvement of eye afferent signals in autonomic activities, no speculation has been made on the detailed working mechanisms relating OKN and VIMS generation. However, the success of the extraocular afferent hypothesis resides in the fact that it points out the role of OKN governed under various oculomotor systems in VIMS. It is consistent with the observations on human subjects that numerous oculomotor systems are engaged under exposure to both rotational (Miyoshi, 1985) and linear (Niemann et al., 1999)

optokinetic stimuli; in this case, where VIMS generally occurs (Ebenholtz, 1992).

Logically, a good knowledge of the working mechanism of OKN can serve to substantiate the general statements made by Ebenholtz et al. (1994) about the role of OKN in VIMS and helps to clarify interactive relations among vection, OKN and VIMS, which continues to be a disputable research question (Webb & Griffin, 2002; 2003; Stern, et al., 1990; Flanagan, et al., 2002; 2004).

1.2.1.3 Postural instability theory

Although the neural mismatch theory is widely accepted, it is acknowledged worldwide that the existence of neural mismatch is common, which leads to adaptive changes in the control of behavior, but the actual elicitation of motion sickness symptoms, such as vomiting, is rare. Motivated by such an observation, Riccio and Stoffregan (1991) argued that motion sickness was not triggered by the mismatch between current and expected sensory input patterns per se. They proposed a postural instability theory as an alternative to the traditional neural mismatch theory. The theme of postural instability theory is that one of the primary behavioral goals in humans is to maintain postural stability in the environment, which is defined as ‘the state in which uncontrolled movements of the perception and action systems are

minimized' (Riccio and Stoffregen, 1991, pp.202). Whenever the environment changes in an abrupt or significant way, in many cases, postural stability will be lost if the control strategies are not available due to lack of experience. Gradually, the control strategy is learned and postural stability is attained once again. When someone has degradedly lost postural stability rather than outright lost stability, they are in a state of postural instability. Therefore, the theory states that the cause of motion sickness is prolonged postural instability.

Although some studies succeed in identifying the association between postural instability and VIMS (Stoffregen & Smart, 1998; Owen, et al., 1998; Stoffregen, et al., 2000), others reported results contradicting the inference of the postural instability theory (Warwick-Evans & Beaumont, 1991; Warwick-Evans, et al., 1998). It was argued that postural instability was a necessary precursor of motion sickness; more specifically, both a necessary and sufficient condition of motion sickness (Riccio & Stoffregen, 1991). However, the question of the ways that this sustained postural instability is linked to the activation of the neural center directly eliciting VIMS symptoms has not been answered. Moreover, the role of the enormous amount of reflexive eye movements and intensive vection sensations was not considered in the postural instability theory.

Instead of considering postural instability theory as an alternative of the neural mismatch theory, it is believed that the true value of the postural instability theory is its insights on the role of the posture control system in VIMS generation. It is reasonable to infer that an understanding of the working mechanism of posture control; specifically, control of involuntary postural sway, can provide considerable implications on the underlying mechanism of VIMS generation.

1.2.1.4 Subjective vertical-conflict theory

Subjective vertical-conflict theory (SV-conflict theory), in fact, can be considered as a variant of the original neural mismatch theory by redefining or simplifying the six sensory arrangement categories. It is proposed that there is only one type of conflict out of all six types of conflicts classified by Reason (1978). It is named as ‘subjective vertical conflict’, which is ‘necessary and sufficient to explain all different kinds of motion sickness’ (Bles et al., 1998, pp481). In other words, there should be a comparator for comparing a ‘sensed vertical’ obtained from integrated sensory information; i.e., visual, vestibular and somatosensory information, and the ‘subjective vertical’ or ‘expected vertical’ obtained from previous experiences (or a memory unit). In addition, the discrepancy between the sensed and expected vertical

are quantified as a 'difference vector' to trigger elicitation of VIMS symptoms and update the information of the expected vertical in the neural store.

Although the SV-conflict theory evolved from the original ideas of the neural mismatch theory, there are different predictions made with regards to the nauseogenicity of motion sickness. The SV-conflict theory predicts that as long as the subjective vertical stayed aligned with the sensed vertical, no motion sickness would occur, even with large differences between sensed and expected sensory information. Following this logic, the rotation of an optokinetic drum around the earth-vertical axis is hypothesized to be non-nauseogenic. This inference is consistent with the findings of several European research groups where VIMS incidence is lower than 1% by using large optokinetic drums and is consistent with their observations that VIMS was only occasionally observed during sudden onsets of surround motion (Bles et al., 1998). On the contrary, the neural mismatch theory infers that motion sickness would occur in such circumstances since a nauseogenic conflict signal is produced when a seated subject is exposed to circular optokinetic stimulation and lack corresponding vestibular motion information. This inference is supported by many VIMS studies (Stern et al., 1990; Hu et al., 1997; Andre et al., 1996; Hu and Hui, 1997). Moreover, a recent empirical study with careful drum and head position

alignment provides negative evidence for the SV-conflict theory and positive evidence for the neural mismatch theory (Bonato, Bubka & Story, 2005). It reported that the visual-vestibular conflict produced VIMS under head fixation. It also argued that the hastened onset of motion sickness in a tilted drum resulted from a sensory conflicting regarding sensed and expected passive self-motion, but not a vertical discrepancy as suggested in the SV-conflict theory.

It is still premature to make any conclusions on the validity of the SV-conflict theory without further supporting evidence. However, it would be a wise decision to carefully align and fixate the head position in future VIMS empirical studies in order to avoid introducing vertical discrepancy as a potential confounding factor. Given such a requirement on head fixation, unfortunately, there is no way to investigate the role of involuntary head sways in VIMS generation.

1.2.1.5 Summary

In summary, the neural mismatch theory indicates that vection is essential for understanding the underlying mechanism of VIMS generation. Likewise, OKN and involuntary postural sway are also suggested to be crucial for explaining VIMS in the extraocular afference hypothesis and postural instability theory, respectively. In the

next section, inter-relations between the three VIMS related responses and VIMS will be elaborated.

1.2.2 Three VIMS related responses

1.2.2.1 Vection and VIMS

Hettinger et al. (1990) made the first attempt to build a connection between vection and VIMS. It was proposed that vection was a necessary condition for VIMS elicitation, inferred from an observation in a fix-based flight simulator where a larger percentage of individuals became sick in a group of subjects reporting vection relative to the group of subjects reporting no vection.

Inspired by a comprehensive empirical study conducted by Brandt et al. (1973) on circular vection (CV) perception, a large number of empirical studies on the relation between vection and VIMS were conducted in a rotating optokinetic drum (a metal cylinder drum having a image pattern of vertical pairs of black and white stripes attached to its inner wall) in the thirty following years (Stern et al., 1990; Hu et al., 1997; Hu and Stern, 1998; Webb & Griffin, 2002; Flanagan et al., 2002; Bonato et al., 2004). Unfortunately, such provocative visual stimuli generally produce vection and OKN simultaneously. A few researchers assumed VIMS provoked by a rotating

optokinetic drum was ‘vection-induced’ although they also acknowledged that OKN was related with VIMS generation. Hu et al. (1997) reported that VIMS severity is affected by spatial frequency of the optokinetic drum pattern. It was proposed that the effect of image spatial frequency on VIMS was mediated by the number of horizontal eye movements (OKN cycles). Hu and Stern (1998) reported that the frequency of OKN is positively correlated with the CV rating as well as VIMS rating. However, they both referred vection as the major cause of VIMS although the effect of vection and OKN coupled together.

An empirical study attempted to decouple the effect of vection and OKN on VIMS, but failed. Stern et al. (1990) reported that both eye fixation and field of view (FOV) restriction reduce VIMS severity. They admitted that such results could not be used to decide whether CV or OKN was indeed the causative factor of VIMS since the manipulation of one resulted in drastic reduction of the other. Flanagan et al. (2002) gave it another try, but also failed, since their experimental design could not manipulate OKN and CV separately as well.

Webb and Griffin (2003) succeeded in manipulating the vection intensity level independent of the eye movement level under restricted FOV. Results of the

correlation analysis indicate that vection intensity and VIMS level can vary independently. However, this study uses laterally moving dots in a restricted FOV (48*36) as the visual stimuli instead of wide FOV optokinetic drum and provides no comments on the pattern of perceived self-motion (CV or LV). It was difficult to compare their results with previous results of circular vection optokinetic drum studies under wide FOV.

Hu et al. (1989) reported that the drum rotation velocity, given a fixed spatial frequency, influenced the intensity of VIMS symptoms in the presence of vection and OKN. Among the 15dps, 30dps, 60dps and 90dps drum rotation velocity conditions, 60dps drum rotation velocity produces the highest VIMS severity level. It was concluded that this curvilinear relationship (an inverted 'U' shape) between velocity of drum rotation and VIMS severity is mediated by a similar curvilinear relationship between the velocity of drum rotation and strength of vection experienced by the subjects. However, the effects of drum rotation velocity on VIMS in the absence of OKN have not been investigated.

Compared with studies on the relation between CV and VIMS, the number of studies on the relation between LV and VIMS is much smaller. So et al. (2002) reported a

similar pattern of recorded nausea rating and vection rating as a function of fore-and aft navigation speed and exposure duration, but gave no comments on whether nausea and vection rating were correlated. Chen (2006) reported a strong linear correlation relationship between linear vection and VIMS severity level in 30 min VR simulation. However, the head movements of the subjects were not controlled and concomitant reflexive eye movements were not monitored. Therefore, discrepancy between perceived and subjective vertical, involuntary head sways as well as OKN can confound the effect of vection on VIMS.

Motivated by the recent debates on the role of vection in VIMS generation, literature reviews on neural mechanism related to vection perception and VIMS symptoms elicitation were conducted. It is expected that such reviews can provide some evidence or implications for the connection between vection and VIMS inferred from the neural mismatch theory. In particular, the role of vection in VIMS is supported if the two neural circuits share some core functional units and vice versa.

A review of related neurobiological studies revealed that the brainstem can be indispensable in the generation of VIMS symptoms based on several evidence listed as follows: first, it is widely accepted that an intact vestibular labyrinth is the only

necessary condition for VIMS generation and the vestibular nuclei in the brainstem is one of the main targets of signal from the vestibular labyrinth (Money & Wood, 1968; Kennedy, et al., 1968). Secondly, the vestibular nuclei in the brainstem is a central structure in the vestibulo-autonomic network which had been identified in mammals as the underlying neural substrate directly mediating VIMS symptom elicitation, such as nausea. (Balaban & Porter, 1998; Yates, et al., 1998)

Evidence indicate that the cerebellum is also essential for VIMS generation. The cerebellum is found to be a specialized organism for supervised learning (Doya, 1999) which is capable of implementing computations required for VIMS protective adaptation. As illustrated in Figure 1.2, first, the cerebellum receives current perceived sensory inputs from the vestibular nuclei via both climbing fiber routes (reaches into Purkinje cells of vestibulo-cerebellum through the inferior olivary nucleus) and mossy fiber routes (reaches into Purkinje cells of vestibulo-cerebellum through the granule cells of vestibulo-cerebellum). Secondly, Purkinje cells in cerebellar cortex linearly combine massive numbers of granule cell outputs running along parallel fibers to generate sensory prediction. Thirdly, the sensory prediction output of the Purkinje cells can be modified since the weights of the parallel fiber-Purkinje cell synapses are tunable under the control of error signal (difference

between perceived sensory input and sensory prediction) transmitted by climbing fibers from the inferior olivary nucleus (ION), which is the origin of an important afferent system of cerebellar cortex. Therefore, the cerebellum can be the seat of the neural store and comparator in light of the original neural mismatch theory. Last but not least, the output of the vestibular part of cerebellum (consisting of partial posterior vermis and the whole flocculus-paraflocculus lobe) is reported to be involved in cerebellar modulation of the vestibulo-autonomic circuit via the vestibular nuclei (Balaban & Porter, 1998). Therefore, the output of the cerebellum is capable of carrying formed neural mismatch signal into the vestibular nuclei, which in turn, trigger the whole vestibulo-autonomic circuits to elicit VIMS symptoms.

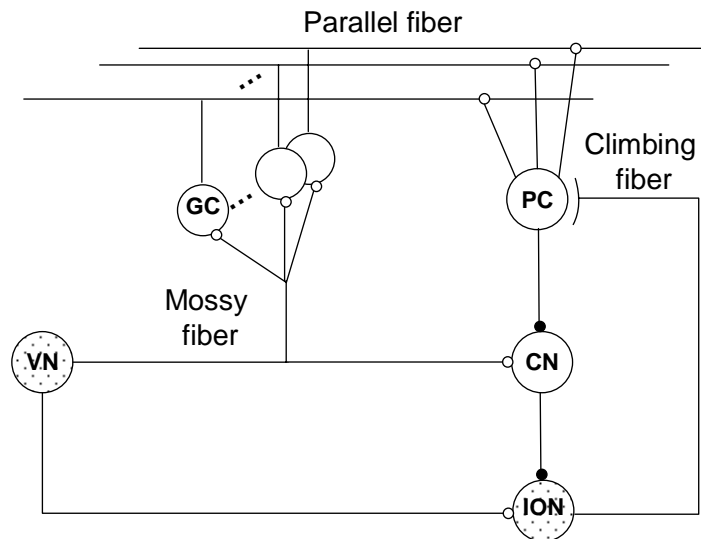


Figure 1.2 Diagram of cerebellar circuit reported by Doya, 1999. **GC**, granule cells; **PC**, Purkinje cells; **CN**, deep cerebellar nuclei; **ION**, inferior olivary nucleus; **VN**, vestibular nucleus; ○, excitatory connection; ●, inhibitory connection. Dot filled pattern labels the neurons in the brainstem and the others are in the cerebellum.

The strong association between neural activities of the vestibular nuclei and visual-vestibular sensory integration, as suggested in several electrophysiological studies, indicates a potential role of the brainstem in vection perception (Dichgans & Brandt, 1972; Henn, et al., 1974; Daunton & Thomsen, 1979). Moreover, a multi-sensory convergence terminal formed by the brainstem, thalamus and human homologue of PIVC is suggested to be directly involved in the process of vection perception as proposed by a recent brain imaging study in humans (Brandt et al., 1998). This terminal receives both visual input via the human homologue of PIVC and vestibular input via the vestibular nuclei. It is proposed that the human homologue of PIVC further cooperates with certain areas in the primary visual cortex and motion-sensitive cortex or other higher level cortex regions to directly mediate vection perception (Brandt, et al., 1998, Bense, et al., 2005).

Moreover, the cerebellum should not be excluded from the neural circuit of vection perception in consideration of its ample signal exchanges with the brainstem. As well, a study on motion perception deficit resulting from damage to the posterior vermis neurons provides supporting evidence for a potential role of the cerebellum in visual motion processing as well as perception of self-motion illusion (Nawrot & Rizzo, 1995).

In summary, two essential functional units in vection perception network; the cerebellum and the brainstem, are shared by protective adaptation and symptom dynamic networks of VIMS (see more details in Section 2.4.1). The signal exchanges between the network of vection perception and VIMS symptom elicitation manifest a connection between vection and VIMS generation. Such observation is consistent with the inference of Reason's neural mismatch theory.

1.2.2.2 Optokinetic nystagmus (OKN) and VIMS

Eye fixation is found to be able to significantly reduce VIMS severity (Stern, et al., 1990). However, such an effect of OKN on VIMS can be easily obscured by the effect of vection since OKN and vection generally occur together. Several studies tried to decouple the effects of OKN and vection on VIMS, but failed due to synergistic interaction between OKN and vection (Stern et al., 1990; Flanagan et al., 2002).

An empirical study successfully manipulated the OKN amplitude level independent of vection intensity level in a restricted FOV virtual optokinetic drum and reported a significant effect of eye fixation on VIMS suppression (Webb & Griffin, 2002).

However, no specific comments were given on whether OKN alone could induce VIMS in the absence of vection perception. Moreover, this study had only one velocity and one control condition. Therefore, the relation between VIMS severity and the drum rotation velocity was not investigated.

Literature review on the neural mechanism of OKN generation and VIMS symptoms elicitation revealed that the brainstem and cerebellum, as two essential function units in VIMS generation, are also indispensable for OKN generation (see Section 3.4.1). The signal exchanges between the network of OKN generation and VIMS symptom elicitation manifest a connection between OKN and VIMS generation. Such an observation is consistent with the inference of Ebenholtz's extraocular afference hypothesis.

1.2.2.3 Involuntary postural sway (IPS) and VIMS

Postural instability revealed as involuntary posture sway (IPS) is another possible cause factor of VIMS as suggested by the postural instability theory and related empirical studies. However, the absolute effect of IPS on VIMS can be confounded by vertical discrepancy given no control of head movements. Furthermore, the role of IPS in VIMS can be easily obscured by the effect of vection as well as OKN since

there are ample interactions among the three VIMS related responses as reported by empirical studies (Postural sway and vection: Kawakita, et al., 2000; Postural sway and eye movement: Jahn, et al., 2002; Pereira, et al., 2001; Brandt et al., 1986; Hunter & Hoffman, 2001). Therefore, the possible role of IPS in VIMS is beyond the scope of this study.

1.2.2.4 Summary

In summary, a literature review on empirical studies and neurobiological studies revealed that both vection and OKN are critical in VIMS generation. Such inference is consistent with inferences from the neural mismatch theory and extraocular afference hypothesis.

1.2.3 Mathematical models of VIMS

1.2.3.1 Oman's neural mismatch model

Oman (1982; 1990) proposed a mathematical representation of Reason's neural mismatch theory (see Figure 1.3). For the first time, the neural mismatch signal was quantitatively defined as the discrepancy between actual sensory input coded by sensory organs and expected sensory input estimated from internal CNS dynamic models of sensory organs and body. The protective adaptation of MS was explained

by gradually reducing the neural mismatch signal under sustained provocative exposure. It was proposed that the sensory prediction was driven towards the actual sensory input by an adaptive Kalman filter in which a tunable filter gain matrix was adjusted by an optimal strategy. The neural mismatch signal was then passed into a network of nausea symptom dynamic to produce a nausea magnitude estimate output. A rectified neural mismatch signal was first transmitted along two parallel, interacting pathways containing fast and slow dynamic elements, respectively. The fast and slow path response was transformed into nausea magnitude estimates by a threshold-power law element. The threshold was added to explain individual differences in motion sickness susceptibility. The power law element was added in light of Stevens' power law on the relation between the magnitude of a physical stimulus and its perceived intensity or strength. Specifically for motion sickness, the physical stimulus is a summation of fast and slow path response and the perceived intensity or strength is the nausea magnitude estimate.

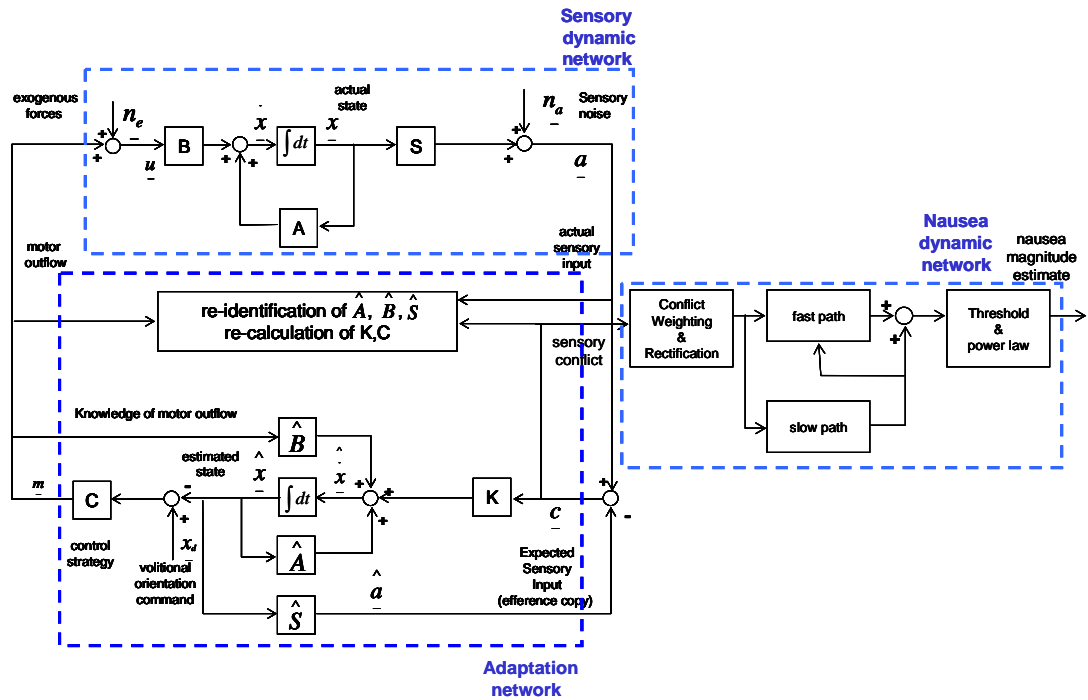


Figure 1.3 Oman's mathematical model of motion sickness (Oman, 1982; 1990)

In summary, the Oman's mathematical neural mismatch model has a three-module structure as shown in Figure 1.3. Module one is the sensory dynamic network to detect visual and vestibular stimuli signals and encodes actual sensory input. Module two is an adaptation network computing the expected sensory input and neural mismatch signal. Module three is a nausea dynamic network transferring the neural mismatch signal into an estimated nausea magnitude level. Oman's model provides a general framework for motion sickness modeling. However, a hypothetical neural mismatch signal, as the outcome of a provocative stimulus, has to be presumed in order to simulate corresponding nausea severity time course. For example, to predict the nausea level reported by a subject exposed to 3 successive 10 min intervals

5RPM Coriolis stimulation with 5 mins resting period in between, the corresponding neural mismatch signal is presumed to be a periodic square wave having a 10 min high level and 5 min low level. The request for pre-knowledge of neural mismatch signal raises the entry barrier for applying Oman's model to VIMS severity prediction. Moreover, the emphases of Oman's model are not on the relations among vection, OKN, and VIMS.

1.2.3.2 Bos and Bles's subjective vertical-conflict model

Little improvement was made on Oman's quality work until Bos and Bles (1998). An additional module was added to Oman's mathematical model for calculating the sensed vertical (V_{sens}) and subjective or expected vertical (V_{exp}). The difference between V_{sens} and V_{exp} instead of Oman's neural mismatch signal is believed to generate motion sickness (Bles et al., 1998). As shown in Figure 1.4, the mathematical formulation of subjective vertical model is once simplified to make a prediction for passive vertical motion induced motion sickness. The model simulated data is compared with empirical seasickness incidence data from literature. The model output is found to show a good resemblance with empirical data.

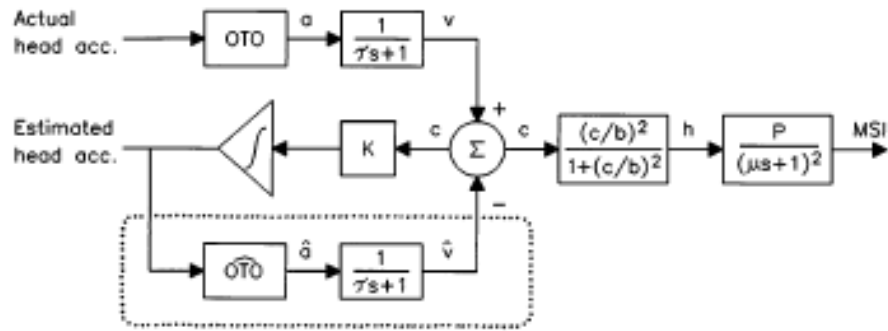


Figure 1.4 Subjective vertical conflict model for passive vertical motion (Bos and Bles, 1998)

The subjective vertical conflict model took in the otolith-related vestibular signal only. The contribution of visual signal and canal-related vestibular signal (with head rotation) in generation of seasickness was ignored. The emphases of their model were not on the relations amongvection, OKN, and VIMS

1.2.3.3 Summary

Reviews of the current available mathematical models of motion sickness indicate that neither Oman's model nor Bos and Bles's model has the intention to explain the association betweenvection and VIMS severity or between OKN and VIMS severity. Such reviews help identify a research gap with regards to the mathematical modeling of VIMS related tovection and OKN.

1.3 Research rationale

This section specifies the research gaps identified from the literature review, defines research objectives and scope, and finally, provides an overview of the methodology employed in this study.

1.3.1 Research gaps

Research gap 1: Literature review on VIMS theories, empirical studies and neurobiological studies revealed that there exists a connection between vection and VIMS as well as between OKN and VIMS. However, mathematical models which can substantiate such connections have not been proposed.

Research gap 2: Literature review on mathematical modeling of motion sickness revealed that a mathematical model aimed to simulate VIMS from both raw visual and vestibular signal, in a way that is relevant to operations of human central nervous system, is not found.

Research gap3: Literature review on mathematical modeling of motion sickness revealed that none of the current available models aimed to account for individual differences in vection perception, OKN related measures and VIMS severity is

reported empirically.

Research gap 4: Literature review on empirical studies revealed that the effect of drum rotation velocity on VIMS severity in the absence of OKN and vection has not been investigated separately. It is still unknown whether such relation between VIMS severity and drum rotation velocity is linear or nonlinear, although Hu et al. (1989) reported an inverted-U shape given that both vection and OKN were present.

1.3.2 Objectives and scope

Four objectives were set up to fill each research gap.

Objective 1: Propose two mathematical models to explain the relations among vection, OKN and VIMS. Model one aims to substantiate the connection between vection and VIMS inferred from the neural mismatch theory. Model two aims to substantiate the connection between OKN and VIMS inferred from the extraocular afference hypothesis.

Objective 2: Propose two mathematical models to simulate the entire process from raw visual and vestibular sensory stimuli to the occurrence of VIMS, in a way that will be relevant to the operation of the human central nervous system. Model one

takes in visual and vestibular inputs to simulate VIMS related to vection perception.

Model two takes in visual and vestibular inputs to simulate VIMS related to OKN generation.

Objective 3: Propose two mathematical models which can account for individual differences in vection perception, OKN generation, and VIMS severity reported in empirical studies. Model one accounts for individual differences in three vection related measures; i.e., latency of vection onset, vection build-up time, and vection velocity's steady state. Model two accounts for inter-subject variations in three OKN related measures; i.e., in OKN slow-phase velocity, OKN gain and foveal retinal slip velocity. Both models can account for individual differences in VIMS severity.

Objective 4: Conduct two empirical experiments. Experiment one examines the effect of drum rotation velocity on VIMS severity in the absence of OKN. Experiment two examines the effect of drum rotation velocity on VIMS severity in the absence of vection.

As the first attempt to simulating VIMS from raw visual and vestibular stimuli, the parameters of models one and two were initially constrained to simulate VIMS

provoked inside an optokinetic image pattern having black and white striped pairs rotating at a constant velocity along the earth-vertical axis. Such stimulus is commonly employed worldwide to provoke vection, OKN and VIMS (Stern et al., 1990; Hu et al., 1997; Hu & Stern, 1998; Webb & Griffin, 2002; Flanagan et al., 2002; Bonato et al., 2004). It is worth pointing out that this research work emphasizes on studying the individual relations between vection and VIMS, and OKN and VIMS. Detailed mechanisms underlying the well-known interaction of the effect of vection and OKN on VIMS are beyond this scope. To reduce problem complexity, postural sway is not investigated in this study, although it can also contribute to VIMS inferred from related theory and empirical studies. Head movement is assumed to be controlled across different velocity conditions in both models and empirical experiments.

1.3.3 Methodology overview

To build a theoretical framework for modeling VIMS elicitation related to vection perception and VIMS elicitation related to OKN generation, multi-aspect knowledge is congregated in this study. As illustrated in Figure 5.1, first, a neural basis roadmap of the entire process from raw visual and vestibular inputs to vection perception (or OKN generation) and eventually to VIMS symptoms' elicitation is inferred from

VIMS related neuroscience literature. Secondly, a multi-module conceptual model is constructed upon the roadmap. Thirdly, searching in various published computational models and neural networks, appropriate models or neural networks are employed to achieve computational implementation of each conceptual model with a known function requirement. Fourth, model one (or model two) simulated by one single computer program is constructed by combining all three computerized modules together and by appropriate parameter tuning. Fifth, model simulated data are compared with empirical ratio scale data for model validation. The data was collected from two model validation experiments. Aside from the purpose of model validation, the two experiments can fill research gap 4. In addition, detailed model simulations are used to demonstrate whether the two models have the flexibility to account for individual differences in vection perception, OKN generation as well as VIMS severity. The final outcome of this study will be two biologically inspired computational models; one relating vection and VIMS, and the other relating OKN and VIMS. Therefore, research gaps 1, 2 and 3 will be filled.

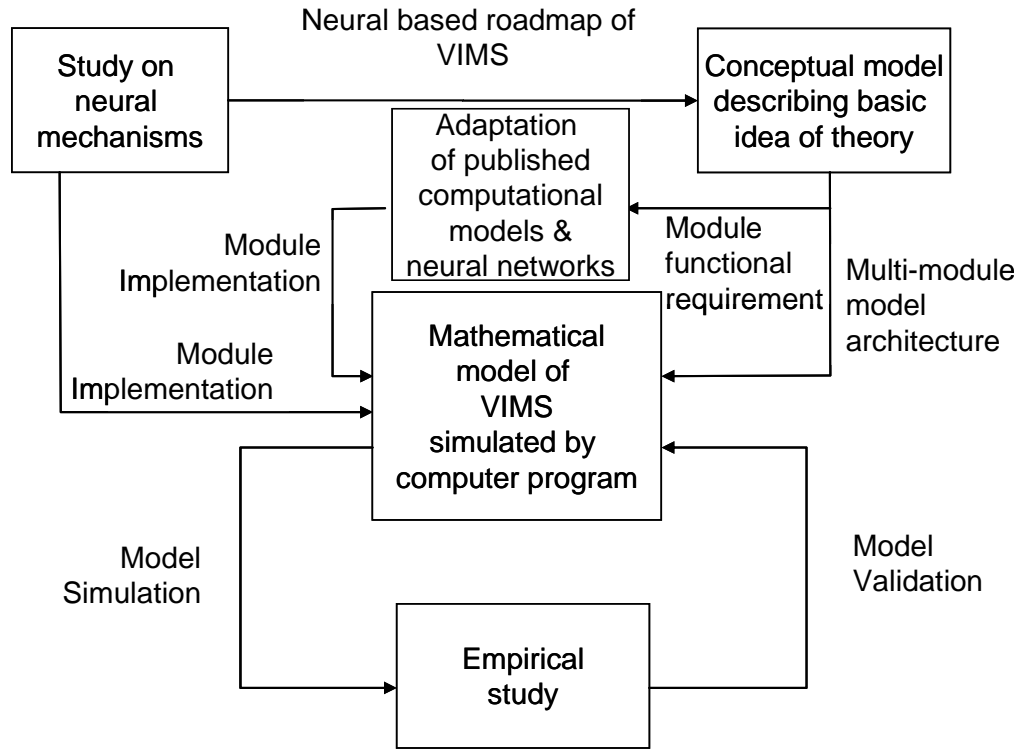


Figure 1.5 Schematic representation of the research methodology employed in this study. See text for more details.

1.4 Thesis organization

This research is mainly composed of two contributions: first, two mathematical models are proposed to simulate the entire process of VIMS elicitation mediated by vection perception (model one) and OKN generation (model two). Secondly, two empirical experiments are conducted to study the relation between vection and VIMS in the absence of OKN (experiment one) and the relation between OKN and VIMS in the absence of vection (experiment two). The empirical data are not only used to uncover the effect of drum rotation velocity on VIMS in the absence of vection or OKN, but also used to validate the two mathematical models that were developed.

The following is an outline of the thesis (see Figure 1.6).

Chapter 1: this chapter first presents the motivations for launching this study. After that, major VIMS theories are reviewed, previous findings of empirical studies and neurobiological studies related to the three VIMS related responses are summarized, and previous work on mathematical modeling of motion sickness are presented. Finally, the research rationale, including research gaps, objectives, scope and methodology overview, is elaborated in detail.

Chapter 2: This chapter presents a biologically inspired computational model that simulates the entire process from sensory stimuli to the occurrence of VIMS mediated by vection perception (model one). Motivations behind the construction of model one will be presented. After the model scope and assumptions are carefully defined, details of model development are documented. Model one consists of three modules: (i) a visual-vestibular integration network of vection perception, (ii) a supervised-learning adaptation network, and (iii) a symptoms dynamic network. Finally, the model predicted sickness severity is compared with published empirical data (Stern et al., 1990) for a demonstration of model one's predictive ability.

Chapter 3: This chapter presents a biologically inspired computational model that simulates the entire process from sensory stimuli to the occurrence of VIMS mediated by OKN generation (model two). Motivations behind the construction of model two will be presented. After the model scope and assumptions are carefully defined, details of model development are documented. Model two consists of three modules: (i) a visual-vestibular integration network of OKN generation, (ii) a supervised-learning adaptation network, and (iii) a symptoms dynamic network. Finally, the model predicted sickness severity is compared with published empirical data (Webb and Griffin, 2002) for a demonstration of model two's predictive ability.

Chapter 4: This chapter presents the motivations behind the two empirical validation studies. Relevant literature are reviewed to justify the methodology adopted to suppress OKN and vection in experiments one and two, respectively. Detailed methodologies are presented with results of pilot tests.

Chapter 5: This chapter presents the hypotheses, methods and results of experiment one. The relation between VIMS severity and drum rotation velocity in the absence of OKN is examined. Results are compared with reports by Hu et al. (1989). The ratio scale data of vection velocity and VIMS severity are collected.

Chapter 6: This chapter presents the hypotheses, methods and results of experiment two. The relation between VIMS severity and drum rotation velocity in the absence of vection is examined. Results are compared with reports by Hu et al. (1989). The ratio scale data of VIMS severity and objective data of OKN related measures are collected.

Chapter 7: This chapter presents model simulations used to validate model one (relating vection and VIMS) and model two (relating OKN and VIMS). Motivations behind the model validations are presented first. After a brief overview of the validating methods, the simulated (in the stage of “pre-validation”)/predicted (in the stage of “validation”) data of models one and two will be compared with empirical data collected in experiments one and two, respectively. Results indicate that both models one and two have satisfactory performances with regards to VISM severity predictions in different rotation velocity conditions.

Chapter 8: In this chapter, motivations behind simulations of individual differences and model sensitivity analysis are presented first. After a brief methodology overview, detailed motion simulations are used to demonstrate that model one can

simulate individual differences in three vection related measures reported in experiment one. Likewise, model two is demonstrated to be able to simulate individual differences in three OKN related measures reported in experiment two. In addition, results of model sensitivity analysis indicate that model one simulated individual differences in vection velocity can explain part of the variation of nausea severity reported in experiment one. Model two simulated individual differences in foveal retinal slip velocity can explain part of the variation of nausea severity reported in experiment two.

Chapter 9: This chapter concludes the thesis with a review of the major contributions of the research and an outlook of future research directions.

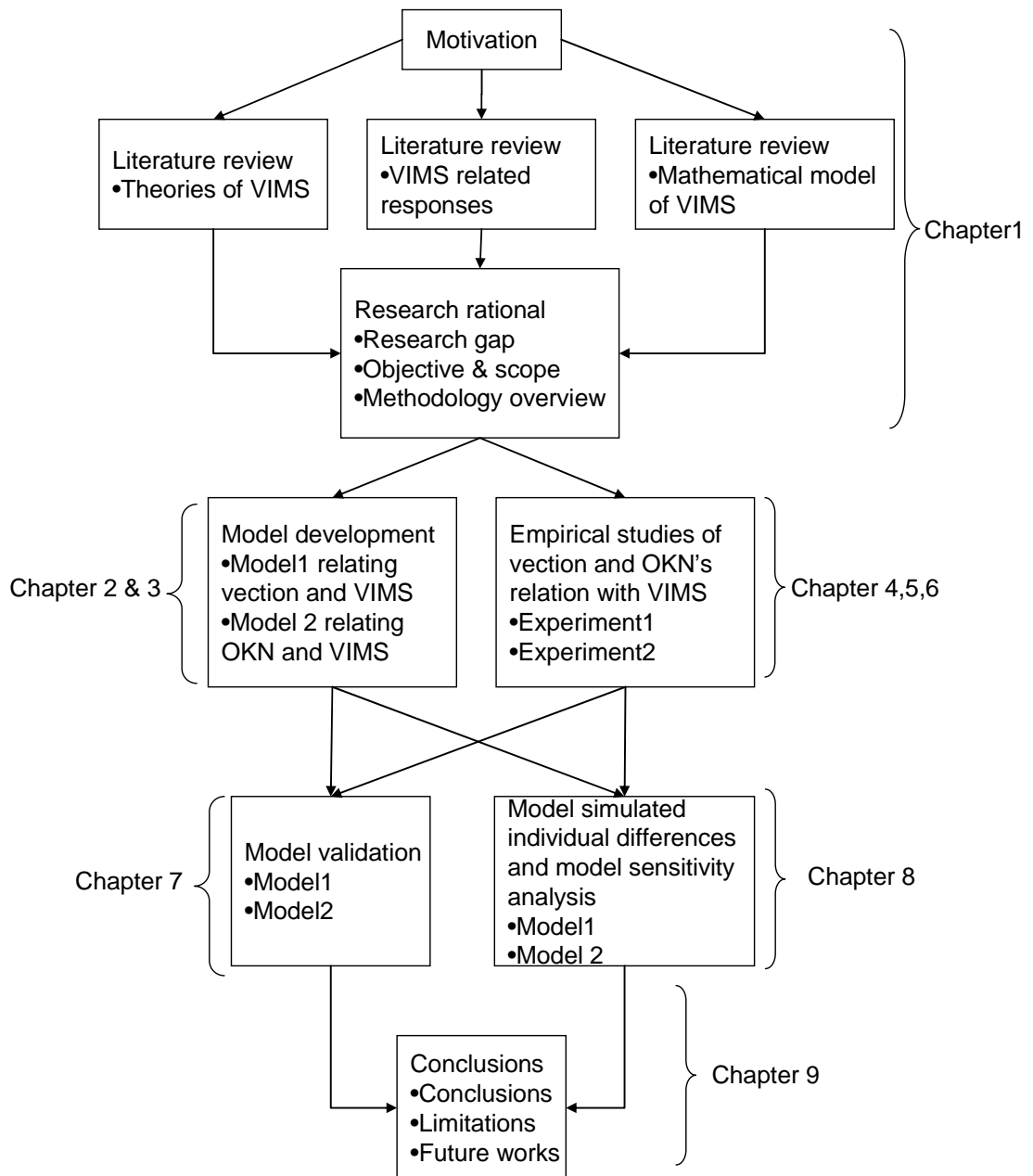


Figure1.6 Flow chart of thesis organization

CHAPTER 2

A BIOLOGICALLY INSPIRED COMPUTATIONAL MODEL RELATING VECTION AND VIMS (MODEL ONE)

SUMMARY

This chapter presents a biologically inspired computational model that simulates an entire process from sensory stimuli to the occurrence of VIMS mediated by vection perception (model one). The motivations behind the construction of model one are presented. After the model scope and assumptions are carefully defined, details of the model development are documented. Model one consists of three modules: (i) a visual-vestibular integration network of vection perception, (ii) a supervised learning adaptation network, and (iii) a symptoms dynamic network. Finally, the model predicted sickness severity is compared with published empirical data for a demonstration of model one's predictive ability.

2.1 Introduction

The well-known neural mismatch theory indicates that visual-vestibular integration,

as the central mechanism of vection perception, is also essential for explaining motion sickness generation (Reason, 1978). This connection between vection and motion sickness inferred from the neural mismatch theory was later built based on the empirical findings of Hettinger et al. It was proposed that vection was a necessary condition for VIMS elicitation based on an observation that a larger percentage of individuals became sick in the group of subjects reporting vection relative to the group reporting no vection (Hettinger et al., 1990).

However, there are recent debates on the role of vection in VIMS generation. On the one hand, the term “vection-induced motion sickness” is frequently used (Hu et al. 1997, Hu & Stern, 1998, Stern et al., 1990). On the other hand, some researchers propose that vection is a factor that can explain part of VIMS, but it is not the only factor that can do so (Flanagan et al., 2002). Moreover, there is an empirical study that successfully disassociates change of VIMS severity from change of vection intensity level under a constraint of restricted FOV (Webb & Griffin, 2003). As well, it was once concluded that vection is not the primary cause of sickness with optokinetic stimuli (Webb & Griffin, 2002).

In this study, it is proposed that developing a mathematical model to simulate the

whole process from raw visual and vestibular stimuli to vection perception and finally, to VIMS symptoms' elicitation can be a useful addition to the recent healthy debates; in particular, if the model's structure is consistent with biological facts on visual and vestibular interactions. As mentioned in Section 1.2.3, previous quality work on mathematical modeling of motion sickness was reviewed. Both Oman (1982, 1990) and Bos and Bles (1998) reported models concerning motion sickness. Oman's model successfully simulated a sickness severity time course from a hypothetical sensory conflict time series signal. Bos & Bles's model successfully simulated a range of motion sickness incidence index from otolith-related vestibular signals. Unfortunately, the emphases of their models were not on vection. Such reviews help identify a research gap with regards to the mathematical modeling of VIMS that is related to vection perception.

2.2 Motivation

Motivated by the research gap mentioned in the last section, a computational model substantiating the connection between vection and VIMS (model one) is constructed. It should be noted that it was not the intention of the author to argue that vection is the only cause of VIMS. In fact, a biologically inspired model relating OKN and VIMS is also developed (see details in Chapter 3). The objective of this study is to

further the understanding of the cause of VIMS through model development. Currently, the author believes that VIMS is poly-symptomatic and caused by multi-factors associated with visual and vestibular interactions. It is the author's firm conviction that if vection is not a cause of VIMS, then model one and its validation experiment will demonstrate the disassociation between vection and VIMS.

2.3 Model scope and assumptions

As the first attempt to simulate VIMS from raw visual and vestibular stimuli, the parameters of model one was initially constrained to simulate VIMS provoked by a yaw-direction rotating optokinetic image pattern with black & white striped pairs along the earth-vertical axis. Such stimulus is commonly employed worldwide to provoke vection and VIMS (Stern et al., 1990; Hu et al., 1997; Hu & stern, 1998; Webb & Griffin, 2002; Flanagan et al., 2002; Bonato et al., 2004). Theoretically, model one can be generalized to simulate VIMS provoked by other types of visual stimuli. Possible expansions of model one will be discussed in Chapter 9.

Since evidence has demonstrated that vection is not the sole causal factor of VIMS, assumptions have been made to isolate the effect of vection on MS from the influence of other factors. First, it is assumed that optokinetic nystagmus (OKN) is

fully suppressed by eye fixation to isolate the effect ofvection from OKN (see details in Section 4.3). Secondly, it is assumed that head movement is fully constrained by head fixation and the rostrocaudal axis of the head is carefully aligned along the earth-vertical axis to isolate the effect ofvection from subjective-vertical conflict (SVC). Thirdly, it is assumed that individuals with his or her head fixed can use an external instrument to stabilize his/her body. For example, using hand holders or sitting in a chair for the purpose of isolating the effect ofvection from postural instability (PI).

2.4 Model development

This section describes each step for constructing model one. First, a neural basis roadmap of the entire process, from raw visual and vestibular inputs tovection perception and eventually, to the elicitation of VIMS symptoms, was inferred from VIMS related neuroscience literature. Secondly, a multi-module conceptual model was constructed on the roadmap. Thirdly, searching in various published computational models and neural networks, appropriate models or neural networks were employed to achieve computational implementation of each conceptual model with a known function requirement. Fourth, model one simulated by one single computer program was constructed by combining all three computerized modules

together and appropriate parameter tuning. Finally, simulated data of model one was compared with data of an empirical study. The final outcome of this chapter is one single computational model simulating the entire process from sensory stimuli to occurrence of VIMS related to vection perception, in a way that is relevant to the operation of the human central nervous system. It is named “a biologically inspired computational model relating vection and VIMS”.

2.4.1 Neural based roadmap relating vection and VIMS

Reviews of VIMS related neuroscience literature were an essential starting point for the development of model one. By integrating current understandings on neural circuits or neural mechanisms of vection perception and VIMS symptom generation, it is possible to identify a linkage between vection and VIMS generation, which is much harder to achieve empirically. A neural based roadmap relating vection and VIMS inferred from such reviews was employed as the substrate of model one construction.

Neural center related vection perception and VIMS generation are summarized in Figure 2.1. The vestibular nuclei; the main target of the input of the vestibular nerve (the eighth cranial nerve) and the entrance of the vestibulo-autonomic circuit, is

essential for VIMS generation (Howard, 1986b; Balaban and Porter, 1998). The vestibular nuclei, together with the thalamus and the human homologue of parietal-insular vestibular cortex (PIVC), form a visual-vestibular sensory convergence terminal which can be involved in the neural circuit of vection perception (Guldin & Grusser, 1998; Brandt, 1999). Visual stimuli received by the retina receptors is transmitted along the motion-sensitive pathway running from the magnocellular–dorsal stream to posterior parietal cortex and then transformed into signals regarding visual surround movements with respect to the retina (Rolls and Deco, 2002). Such information is eventually passed into the sensory convergence terminal via the PIVC (Guldin & Grusser, 1998). Vestibular input carrying information of head movements is extracted by the inner ear vestibular organ receptors (SCC: semicircular canals; OTO: otolith) and passed into the same sensory convergence terminal via the vestibular nuclei (Howard, 1986b).

In consideration of the intensive signal interchanges happening between the vestibular nuclei and vestibulo-cerebellum, the perceived self-motion velocity formed in the visual-vestibular convergence center can be transmitted into the vestibulo-cerebellum via the vestibular nuclei. The vestibulo-cerebellum, as a specialized organism for supervised learning computation underlying VIMS

protective adaptation (Doya, 1999), is capable of generating sensory prediction from sensory input carrying perceived self-motion velocity and then forming neural mismatch signals. Consequently, such neural mismatch signals are used as self-modification error signals and in turn, passed in the vestibular nuclei to trigger the vestibulo-autonomic neural circuit which directly mediates the VIMS symptoms, such as nausea (Balaban & Porter, 1998).

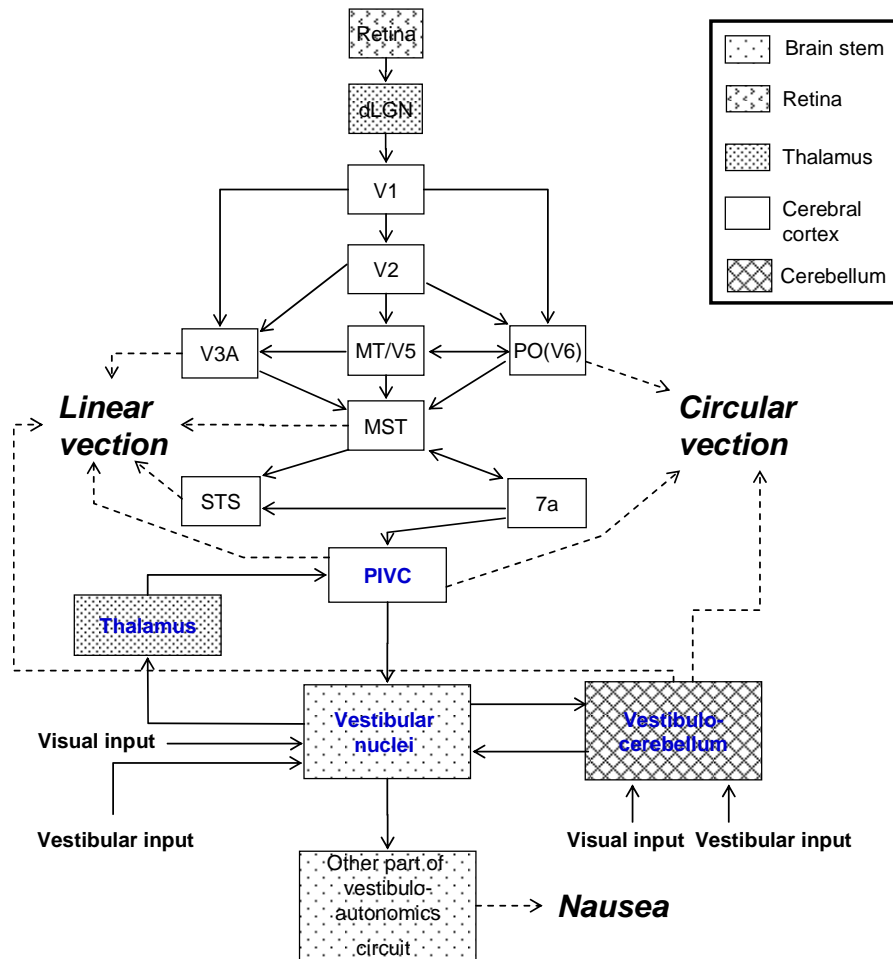


Figure 2.1 Neural centers related to vection perception and VIMS generation summarized from neuroscience literature. Rectangular blocks indicate specific areas within the cerebral cortex, thalamus, brain stem, cerebellum, etc., distinguished by different patterns. Arrows indicate the anatomical connections between these areas. Names of critical neural structures are color coded in blue. Dashed lines represent that detailed neural mechanisms from the responses of certain neural centers to the final formation of nausea and vection perception are unknown.

In summary, thorough reviews of neuroscience literature indicate that two neural structures serve as the signal interchanging terminal in between neural circuitries of vection and elicitation of VIMS symptoms. They are the brainstem and the cerebellum. Detailed evidence is listed below to further justify such observations.

Let us start from the argument that the brainstem is indispensable in the generation of VIMS symptoms. First, it is widely accepted that an intact vestibular labyrinth is the necessary condition for MS generation. Bearing in mind that the vestibular nuclei in the brainstem is a main target of signal from the vestibular labyrinth (Money & Wood, 1968; Kennedy et al., 1968), it would be unexpected if the vestibular nuclei did not play a role in the elicitation of VIMS symptoms. Secondly, the vestibular nuclei in the brainstem is a central structure of the vestibulo-autonomic network which has been identified in mammals as an underlying neural substrate directly mediating elicitation of sickness symptoms, such as nausea (Balaban & Porter, 1998; Yates et al., 1998).

There is evidence that indicate the brainstem also plays an essential role in vection perception. Several electrophysiological studies have already provided evidence

without a doubt that visual-vestibular sensory convergence, which is critical for vection perception, does happen in the vestibular nuclei in mammal brainstems (Dichgans & Brandt, 1972; Henn et al., 1974; Daunton & Thomsen, 1979). Moreover, recent brain imaging studies discovered that a visual-vestibular sensory convergence terminal formed by the brainstem, thalamus and human homologue of PIVC could be directly involved in the process of vection perception in humans (Brandt et al., 1998).

Likewise, various evidence indicates that the cerebellum is critical for VIMS generation. The cerebellum is found to be the specialized organism for supervised learning (Doya, 1999). As shown in Figure 1.2, granule cells of the cerebellum receive the current perceived sensory input from the vestibular nuclei in the brainstem via both climbing fiber routes and mossy fiber routes. Purkinje cells in cerebellar cortex combine massive numbers of granule cell outputs running along parallel fibers to generate corresponding sensory predictions. Sensory prediction outputs of Purkinje cells are modifiable since connection strengths of parallel fiber-Purkinje cell synapse are tuned by an error signal. The error signal is the difference or mismatch between the perceived sensory input and the corresponding cerebellar sensory prediction, based on an optimization learning rule. The error

signal is projected back to the cerebellum via climbing fibers from the inferior olivary nucleus (ION) in the brainstem, which is the origin of an important afferent system of cerebellar cortex. Gradually, the cerebellar sensory prediction is driven towards the perceived sensory input. Consequently, the error signal diminishes and eventually disappears. In short, this supervised-learning computation circuit composed of cerebellar nuclei, cerebellar cortex cells and brainstem nuclei is capable of implementing neural mismatch computation and VIMS protective adaptation. These computations are the basic working mechanisms underlying Reason's neural mismatch theory. The vestibule-cerebellum consists of the partial posterior vermis and whole flocculus-paraflocculus lobe. This vestibular part of the cerebellum is reported to be involved in cerebellar modulation of the vestibulo-autonomic circuit (Balaban & Porter, 1998). Such results indicate that the output of the vestibule-cerebellum most likely carries the formed neural mismatch signals into the vestibular nuclei in the brainstem to trigger the whole vestibulo-autonomic circuits which mediate elicitation of VIMS symptoms.

Last, but not least, although current neuroscience studies regarding human vection perception mainly place their focus on the brainstem and vestibular cortex regions, but seldom on the cerebellum, it is not wise to exclude the cerebellum out of the

neural circuit of vection perception in consideration of ample signal interchanges between the cerebellum and brainstem. Recent findings of a cerebellar lesion study in humans reinforce this concern since motion perception deficit is reported to have resulted from damage to the posterior vermis neurons in the cerebellum (Nawrot & Rizzo, 1995). Such results indicate that the cerebellum has a potential role in visual motion processing as well as perception of self-motion illusions, although related neural mechanisms have not been discovered.

The neural basis roadmap relating vection and VMS is summarized in Figure 2.2. On the one hand, visual input carries information of visual surround movements with respect to the retina into the visual-vestibular sensory convergence terminal via the vestibular cortex. On the other hand, vestibular input carries information of the head movement with respect to the earth into the same sensory convergence terminal via the brainstem. In consideration of the intensive signal interchanges that exist between the brainstem and cerebellum, the perceived self-motion velocity formed in the visual-vestibular convergence terminal is transmitted into the cerebellum via the brainstem. The cerebellum, as a specialized organism for supervised learning computation underlying VIMS protective adaptation, generates the corresponding sensory prediction output given that the sensory input is carrying the perceived

self-motion velocity. Cooperating with the ION in the brainstem, the cerebellum computes a neural mismatch signal as a self-modification error signal and a trigger signal of the vestibulo-autonomic circuitry. The vestibulo-autonomic circuitry receives the trigger signal from the cerebellum via the vestibular nuclei in the brainstem and then directly mediates the elicitation of VIMS symptoms, such as nausea.

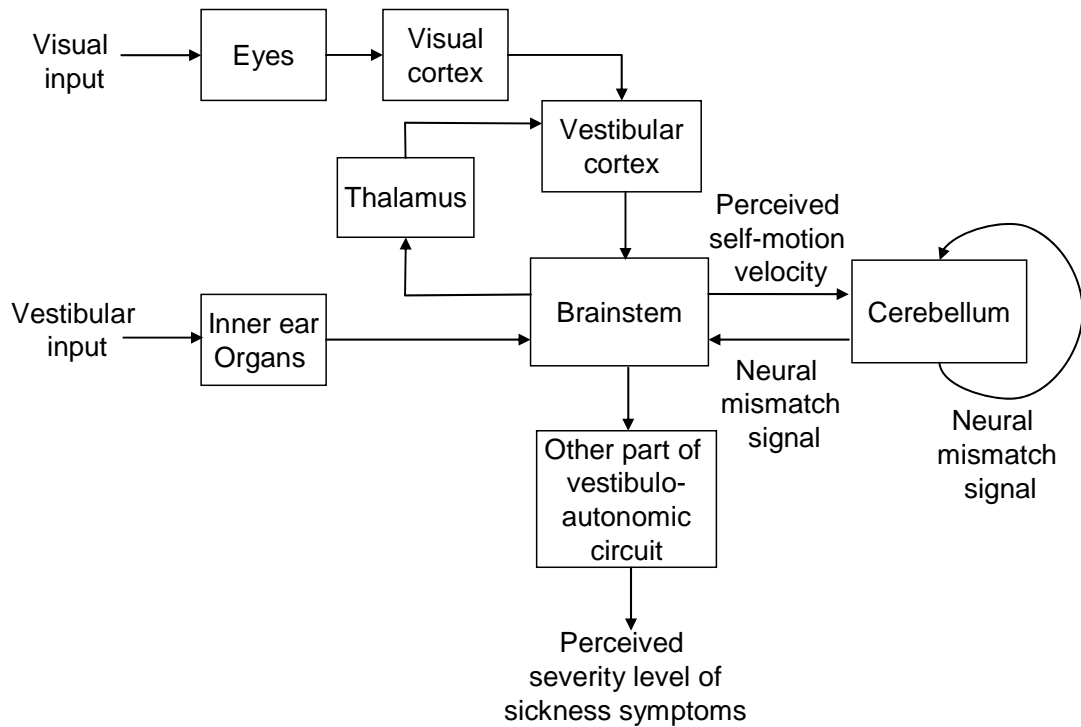


Figure 2.2 Roadmap relating vection and VIMS summarized from related neuroscience literature. Each block represents a specific neural structure in humans related to vection and elicitation of VIMS symptoms. Arrows represent interchanging corresponding signals flowing in neural structures through anatomical connections. For clarity, not all relevant areas are depicted (e.g., the posterior parietal cerebral cortex as a relay of visual and vestibular cortex, the inferior olivary nucleus relaying neural mismatch signal back to the cerebellum) and arrows do not always correspond to the direction of anatomical connections. See text for details.

In short, reviews of neural mechanisms reveal a direct link between vection perception and elicitation of VIMS symptoms, consistent with implications from the neural mismatch theory. Although VIMS is generally provoked in the presence of both vection and OKN; theoretically VIMS can be induced in the presence of vection alone. In other words, VIMS provoked by a rotating optokinetic image pattern is probably directly mediated by vection perception alone when OKN is fully suppressed. In light of Reason's neural mismatch theory, it is proposed that the perceived self-motion velocity is the sensory input directly contributing to VIMS generation.

2.4.2 Conceptual model

Based upon the neural basis roadmap presented in the last section, a three-module architecture of model one is proposed (see Figure 2.3). Module1 (M1) is a visual-vestibular sensory integration network converging a visual input (visual surround velocity with respect to the retina) and a vestibular input (head movement velocity with respect to the earth) to output a perceived self-motion velocity with respect to the earth. Module2 (M2) is a supervised learning adaptation network simulating the function of the cerebellum. It receives the perceived self-motion velocity and generates a corresponding sensory prediction and a neural mismatch

signal based on an optimization learning rule. Module3 (M3) is a Stevens' power law-based symptoms dynamic network triggered by the neural mismatch signal to estimate subjective sickness severity.

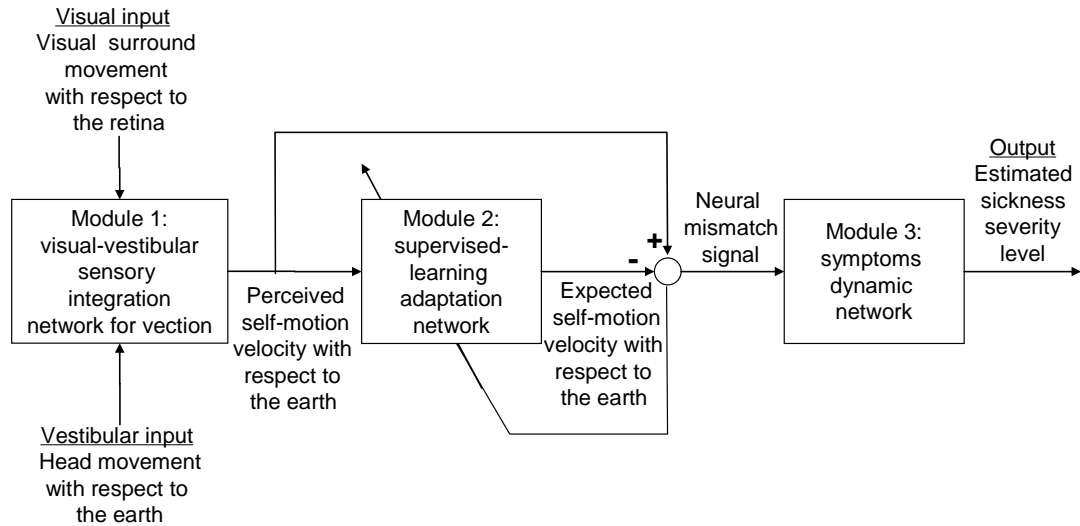


Figure 2.3 Three-module conceptual model relating vection and VIMS. Details are stated in text.

As discussed in Chapter 1, Oman's motion sickness model has a similar three-module structure. Oman's sensory dynamic network provides a generalized framework for coding nonintegrated visual and vestibular input into a single sensory input without specifying its embedded information content. Consistent with Oman's three-module framework, model one employs 'the perceived self-motion velocity with respect to the earth' as the information carried by sensory input to the adaptation network.

Moreover, Oman adopted the Kalman filter (also known as the Kalman-Bucy filter or Kalman-Bucy-Wonham filter), incorporating it with the movement control strategy matrix (labeled as “c”) and internal models of sensory and body dynamics (labeled as \hat{A} , \hat{B} , and \hat{S}) to implement the supervised learning protective adaptation of motion sickness. On the one hand, Oman’s work did not specify the type of optimal strategy for calculating the sensory prediction. On the other hand, the Kalman filter could not be the only solution to implementing VIMS protective adaptation. In this study, an adaptive filter implemented by an adaptive linear neural network is employed to simulate the function of cerebellum because signal transmissions and computations in this adaptive filter have their counterpart neural substrates in the cerebellar neural circuit. In short, model one is an outcome of customizing Oman’s generic framework of motion sickness generation to serve the specific purpose of relating vection and VIMS.

2.4.3 Computational model

In model one, variables of visual and vestibular input are defined in a right-handed orthogonal head-fixed frame of reference in which its rostrocaudal axis with positive values for the top of the head are aligned with the earth-vertical axis. Although this coordination can be simply defined as space-fixed, it is defined in such way so that it

is possible that the model assumption regarding head fixation can be relaxed in future model extensions if necessary. In such coordination, the movement of visual stimuli is constrained to a yaw-direction rotation along the earth-vertical axis. This is to modelvection and VIMS provoked by viewing a yaw-direction rotating image pattern of black & white striped pairs.

In model one, the sensory input variables were: (i) rotation velocity of peripheral visual surround with respect to the earth ω_{vis} (+ve means rotating to the left of the viewer), (ii) vestibular signal representing the velocity of head rotation with respect to the earth ω_{vest} . Other variables included: the perceived self-rotating velocity (vection velocity) with respect to the earth ω_{per} , the expected or predicted self-rotating velocity with respect to the earth ω_{exp} , and the neural mismatch signal ω_{mis} defined as the difference between ω_{per} and ω_{exp} . The output of model one, the model simulated subjective nausea severity level O_{nausea} , was a non-negative scalar. The foveal visual input was excluded in model one due to the following two reasons. First, peripheral vision is found to be dominant over fovea vision in circularvection generation (Brandt et al., 1973). Secondly, the foveal visual input in the case of model one was actually minute since the fovea area of the retina was occluded by an eye fixation spot subtending one degree FOV.

Thanks to previous excellent research work on modeling vection and sickness symptoms generation, it is much easier to build a computational model simulating the complete process from raw visual and vestibular stimuli to VIMS elicitation. Instead of modeling from a draft, appropriate published computational models or neural networks are employed to implement each of the three conceptual modules. Since the conceptual model itself is a biologically inspired representation which is the most critical feature of this study, it is less important whether the selected computational models are fully biologically plausible. In model one, the “biological level” of model implementation and the resulting computation complexity were carefully balanced. Eventually, three computational models were chosen and each customized to meet specific function requirements of a conceptual module. First, a visual-vestibular interaction model for human vection perception (Telban & Cardullo, 2001) was employed to implement M1. Secondly, a supervised-learning adaptive filter with the least mean square error (LMS) learning rule (Widrow & Hoff, 1960) was employed to implement M2. Thirdly, a nausea path dynamics model (Oman, 1982; 1990) was employed to implement M3. Related mathematical implementation and customization of each module are documented in detail in the following three sections, respectively.

2.4.3.1 Module 1 (M1): a visual-vestibular sensory integration network for vection perception

Telban and Cardullo (2001)'s visual-vestibular interaction model for the motion perception of humans is modified and adopted in M1. The decision was made based on the fact that this vection model could achieve computations of visual-vestibular integration requested by M1.

It is reported that visual-vestibular integration, as the central mechanism of vection perception, is not a simple linear summation of visual and vestibular input. Instead, the perceived self-motion velocity is a summation of two weighted sensory inputs. Those weightings can be controlled by certain weighting logic based on perceived conflicts (Young, 1977). Telban and Cardullo's model succeeded in implementing this nonlinear signal processing of visual-vestibular integration as shown in Equation 2-1:

$$\omega_{per} = T_{scc} \omega_{vest} + T_{opto} [K(T_{vis} \omega_{vis})] \quad (2-1)$$

where T_{scc} , T_{vis} , and T_{opto} are transfer functions modeling semicircular canal dynamics, visual receptor dynamics and low pass frequency response of optokinetic influence on vection perception, respectively. (See Appendix 2-1) The weighting of

vestibular input is fixed at 1 while the weighting of visual input is defined by a function K .

In the original work of Telban & Cardullo (2001), K was a function of a variable of the perceived conflict measure ω_{err} and a variable of the conflict threshold ξ . K 's value varied in a range from 0 to 1. This form of weighting logic function forced the vection velocity (perceived self-motion velocity) to eventually reach a level equal to the rotation velocity of image pattern. In such a case, vection saturation was achieved, i.e., a visual illusion where a subject felt self rotation only and the rotating image pattern was instead, perceived to be still. However, in real life, some participants did not experience vection saturation during exposure to rotating optokinetic stimuli (Stern et al, 1990; Danieli et al., 1996). Therefore, in model one, the definition of function K is modified by adding a parameter Φ to account for the individual differences in human vection perception as shown in Equation 2-2:

$$K = \Phi \cos \frac{\pi}{\xi} \omega_{err} + \Phi \quad (2-2)$$

where Φ is the newly added parameter having a value between 0 and 0.5. Φ can be tuned to zero to simulate zero vection velocity and tuned to 0.5 to simulate vection saturation after latency of vection onset and build-up. The weighting K in model one varies in a range from 0 to 2Φ . ξ is defined to equal the mean yaw direction

vestibular indifference motion threshold reported by Benson et al.(1989), following Telban and Cardullo (2001). Likewise, the perceived conflict measure ω_{err} is defined by Equation 2-3:

$$\omega_{err} = T_{ao} \left| T_{scc} \omega_{vest} - \hat{T}_{scc} T_{vis} \omega_{vis} \right| \quad (2-3)$$

where \hat{T}_{scc} is the transfer function of the internal model of the semicircular canal dynamics chosen to be equal to T_{scc} . It is defined as such to transform two sensory inputs with different frequency components into a common representation to obtain a measure of high-frequency mismatch. T_{ao} is the transfer function of a high pass filter (see details in Appendix 2-1) having a time constant τ_w cooperating with the conflict threshold ξ to decide latency of vection onset.

As illustrated in the block diagram of M1 (see Figure 2.4), inputting the time series of a zero head rotating velocity with respect to the earth ω_{vest} and a constant peripheral visual surround velocity ω_{vis} for an exposure period, the output of M1 is a time series of the vection velocity (the perceived self-rotating velocity) ω_{per} . The latency of vection onset is decided by the conflict threshold ξ and the time constant τ_w of T_{ao} . The vection build-up time defined as the time interval after vection onset to a steady state at $2\phi\omega_{vis}$ is determined by the time constant τ_{va} of T_{opto} . The steady state or the maximum level of vection velocity is determined by parameter Φ .

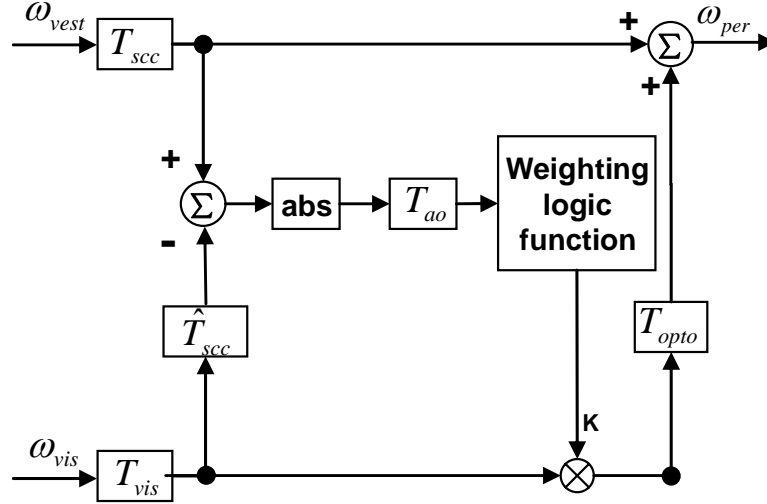


Figure 2.4 Block diagram of M1. The weighting logic function K is defined by Equation 2-2 which is modified from the original work of Telban and Cardullo (2001) to account for individual differences in vection perception. The absolute function taking the absolute value of its input is labeled as “abs”

2.4.3.2 Module 2 (M2): a supervised learning adaptation network

This module was implemented as a supervised-learning adaptive filter. The adaptive filter facilitating M2’s predictive ability was composed of an adaptive linear neural network (ADALINE) and tapped unit delay lines. The employment of such a linear adaptive filter brought about two benefits: (i) it can achieve computations underlying motion sickness protective adaptation in a way consistent to the working mechanism of Reason’s neural mismatch model, and (ii) signal transmissions and computations in this adaptive filter have their counterpart neural substrates in the cerebellar neural circuit.

As illustrated in the block diagram of M2 (see Figure 2.5), the input signal ω_{per} is

first transformed into a M-component input vector $U = [u_1, u_2, \dots, u_M]^T$ by M-1 unit delay functions D in a tapped unit delay line $\tilde{D} = [1, D, \dots, D^{M-1}]^T$ as defined in Equation 2-4:

$$U = \tilde{D}\omega_{per} \quad (2-4)$$

Referring to the cerebellar neural circuit proposed by Doya (1999), the mossy fiber-granule cells input network cooperating with some attached Golgi cells can realize the various delays in the tapped unit delay line \tilde{D} . The prediction output of the supervised-learning adaptive filter ω_{exp} is a linear combination of the M components of U weighted by a tunable weighting vector plus a tunable bias b as defined in Equation 2-5:

$$\omega_{exp} = U^T W + b \quad (2-5)$$

The prediction output signal ω_{exp} is a representation of Purkinje cell output formed by gathering parallel fiber signals u_1, u_2, \dots, u_M together through synaptic connections having various strengths w_1, w_2, \dots, w_M . Consequently, the neural mismatch signal ω_{mis} is calculated by Equation 2-6:

$$\omega_{mis} = \omega_{per} - \omega_{exp} \quad (2-6)$$

The inferior olivary nucleus (ION) in the brainstem can work as the comparator of the input ω_{per} from the vestibular nuclei and the prediction output ω_{exp} from the Purkinje cell to compute the neural mismatch signal ω_{mis} . ω_{mis} is then fed back to

the computation loop of the prediction output ω_{exp} in a iterative manner to make ω_{exp} a step closer to ω_{per} and eventually, exactly equal to ω_{per} . In other words, this supervised-learning adaptive filter eventually makes an accurate prediction of input by minimizing the mean square of the neural mismatch signal ω_{mis} . This convergence of prediction output and input is achieved by adjusting the components of weighting vector $W = [w_1, w_2, \dots, w_M]^T$ and the bias b from zero in the step with dW and db , respectively, defined by a LMS learning rule in Equation 2-7:

$$\begin{cases} dW = lr \omega_{\text{mis}} U \\ db = lr \omega_{\text{mis}} \end{cases} \quad (2-7)$$

where lr is the learning rate of the adaptive filter. A larger lr means learning or adapting faster and vice versa. Indeed, the cerebellar neural circuit is capable of self modification since the synaptic connection strength of parallel fiber-Purkinje cells is under the control of neural mismatch signals that ω_{mis} sent from the ION's climbing fibers. The efferent of cerebellar cortex can carry the neural mismatch signal ω_{mis} into the vestibular nuclei in the brainstem to trigger the whole vestibulo-autonomics neural circuit for eliciting VIMS symptoms, such as nausea.

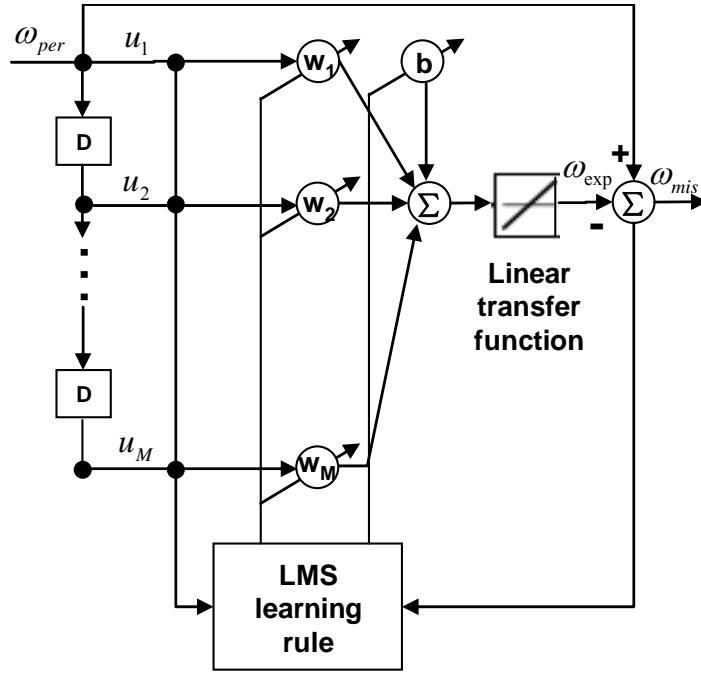


Figure 2.5 Block diagram of M2 consisting of a tapped unit delay line and an adaptive linear neural network (ADALINE). The LMS learning rule is defined by Equation 2-7. The linear transfer function's input and output are equal.

2.4.3.3 Module 3 (M3): a symptom dynamic network

Oman (1990)'s nausea path dynamic model was modified to implement M3. It took in the neural mismatch or sensory conflict signal (ω_{mis}) and outputted the model simulated subjective nausea severity (O_{nausea}). It is worth pointing out that sensory conflict weighting in the nausea path dynamic model originally proposed by Oman is unnecessary for M3's implementation since M3's input (ω_{mis}) itself is already a sensory signal integrated from weighted visual and vestibular input. As illustrated in the block diagram of M3 (see Figure 2.6), ω_{mis} is directly processed by Equation 2-8:

$$\tilde{\omega}_{mis} = |\omega_{mis}| / c \quad (2-8)$$

where c is a positive free parameter and $\tilde{\omega}_{mis}$ is named “the pre-processed neural mismatch signal”. This rectification was originally proposed by Oman to account for an empirical finding that stimuli resulting in opposite sign neural mismatch produced the same type and intensity of nausea. After that, $\tilde{\omega}_{mis}$ is passed into two parallel, interacting pathways. One contains a fast dynamic element T_{fast} and the other contains a slow dynamic element T_{slow} (Appendix 2-2). The distinction between the slow and fast component is made to match the phenomenological description of Bock and Oman, 1982. Furthermore, the slow path output acts as a multiplicative factor of the fast path input to account for an empirical observation where the fast path responded much stronger when prolonged provocative stimulation raised the slow path output. The overall response of the two pathways I is defined in Equation

$$2-9: I = T_{slow} \tilde{\omega}_{mis} + T_{fast} [(T_{slow} \tilde{\omega}_{mis}) \tilde{\omega}_{mis}] \quad (2-9)$$

The M3’s output O_{nausea} is then calculated by feeding I into a threshold-power law element defined in Equation 2-10:

$$\begin{cases} O_{nausea} = a(I - I_0)^b, & I \geq I_0 \\ O_{nausea} = 0, & 0 \leq I < I_0 \end{cases} \quad (2-10)$$

where I_0 is a sickness threshold indispensable for modeling MS. The threshold is added to explain an observation that adaptation to an atypical motion environment can occur without experience of MS symptoms (Benson, 1984). “ a ” and “ b ” are the constant and exponent of Stevens’ power law function, respectively. As proposed by

Oman, human's subjective magnitude estimation is considered as a representation of Stevens' power law even though the putative mismatch stimulus is an internal one in the case of motion sickness elicitation.

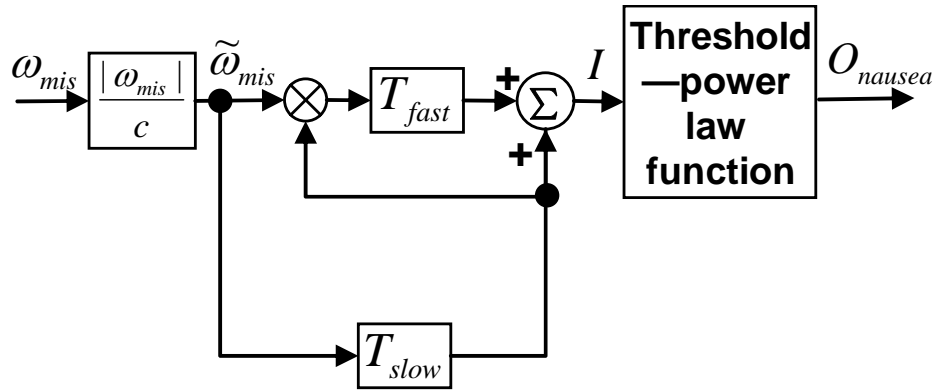
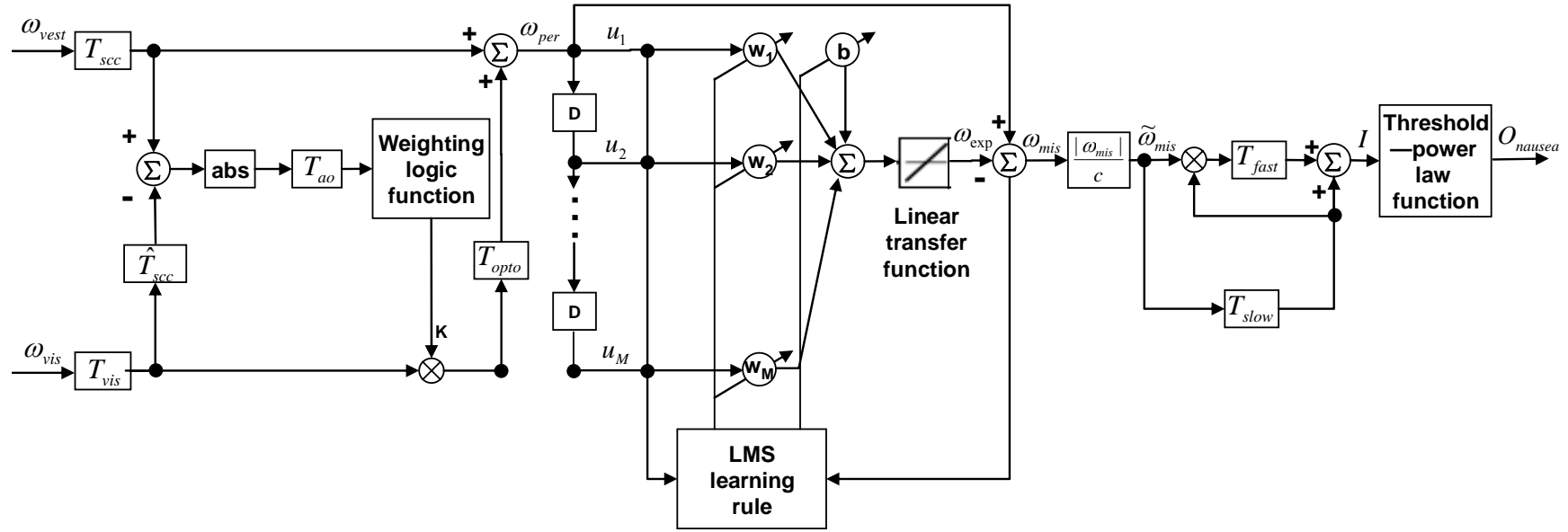


Figure 2.6 Block diagram of M3. The threshold-power law function is defined by Equation 2-10

2.4.4 Model simulation

Figure 2.7 shows a block diagram of model one relating vection and VIMS. The model is implemented by the Matlab-Simulink® software package. A fourth-order variable-step Dromand-Prince algorithm is used for model simulation (the ode45 function in Simulink). In total, model one has eight free parameters, including a parameter in weighting logic function used to simulate the level of the vection's steady state (Φ), number of components of input vector U (M), learning rate of the adaptive filter (lr), a constant c , the gain of the transfer function T_{fast} and T_{slow} (k), threshold (I_0), constant (a) and exponent (b) of Stevens' power law function.



69

Figure 2.7 Block diagram of model one relating vection and VIMS. Visual input ω_{vis} is the peripheral visual surround rotating velocity with respect to the earth. Vestibular input ω_{vest} is the head rotating velocity with respect to the earth. Both of the inputs are defined in a right-handed orthogonal head-fixed frame of reference. The neural mismatch signal ω_{mis} is defined as the difference between the perceived (ω_{per}) and expected (ω_{exp}) self-motion velocity with respect to the earth. Model one's scalar output O_{nausea} is the severity of the model simulated subjective nausea. Model one assumes that (i) OKN has been fully suppressed by eye fixation, and (ii) head movement has been fully constrained by head fixation and the rostrocaudal axis of head has been carefully aligned along the earth-vertical axis, and (iii) individuals with his or her head fixed have an external instrument for body stabilization. The weighting logic function is defined by Equation 2-2. The LMS learning rule is defined by Equation 2-7. The threshold-power law function is defined by Equation 2-10. The input and output of the linear transfer function are equal.

2.5 Comparison of model simulated data and empirical data of Stern et al. (1990)

To demonstrate model one's predictive ability, empirical data reported by Stern et al., (1990) was chosen as the benchmark of model one's output. In the empirical study,vection and VIMS was provoked in a yaw-direction rotating optokinetic drum at a constant velocity of 60 degrees per second (dps). There were, in total, three conditions in this experiment: (i) control conditions without eye fixation and FOV restrictions; (ii) fixation conditions with eye fixation only and without FOV restrictions; (iii) restricted field conditions with FOV restrictions only and without fixation conditions. In particular, the data with "eye fixation" was selected in consideration of model one's assumption regarding OKN suppression. Moreover, head movement was constrained by a chin rest so that model one's assumption regarding head fixation was satisfied. The exposure duration was up to 12 min (stopped at any time when requested by subject). Subjective vection intensity and sickness severity were rated every 2 min. Vection intensity was rated by referring to a common anchor point at which a subject perceived vection saturation and gave a rating of "10". Sickness severity was rated on Graybiel's motion sickness scale with a possible range from a minimum of 0 to a maximum of 50 (Graybiel et al., 1968, Appendix 5-9). Specifically, closer model predictions of subjective discomfort to the

mean sickness severity reported by Stern et al. (1990) resulted in the better predictive ability of model one.

In this case, model one's two inputs were $\omega_{vis}(t) = -60\text{dps}$ and $\omega_{vest}(t) = 0\text{dps}$. Model one's eight free parameters are set to a set of values determined through a process of trial and error and with reference to literature where appropriate ($\Phi = 0.35$, $M = 5$, $lr = 2^{-8}$, $c = 60$, $k = 0.8$, $I_0 = 0.05$, $a = 0.96$, and $b = 0.65$). The first step was to tune the parameter Φ in weighting logic function K (in module 1) to 0.35 so that the model simulated vection gain (G_v) was equal to 0.7 (see Equation 2-2 and Figure 8.3). The parameter M (the number of components of input vector U in module 2), lr (the learning rate of the adaptive filter in module 2), and k (transfer function gain of fast and slow dynamic elements in module 3) was determined through a process of trial and error ($M = 5$, $lr = 2^{-8}$, and $k = 0.8$). The parameter c (in module 3) was set to 60 dps for normalization purposes. Finally, the parameter I (the threshold), a and b (the constant and exponent of Stevens' power law function) was tuned to minimize the mean square error (MSE) measuring the difference between the model simulated nausea severity time course and an empirical nausea severity time course reported by Stern et al (1990). Figure 2.8 shows that model one's output, a time course of model simulated subjective nausea severity, is enclosed in the 95% confidence interval (CI)

envelop, calculated from Stern et al.(1990)’s empirical data. Such results indicate that model one has the capability to simulate time series of sickness severity reported empirically if all model assumptions are satisfied.

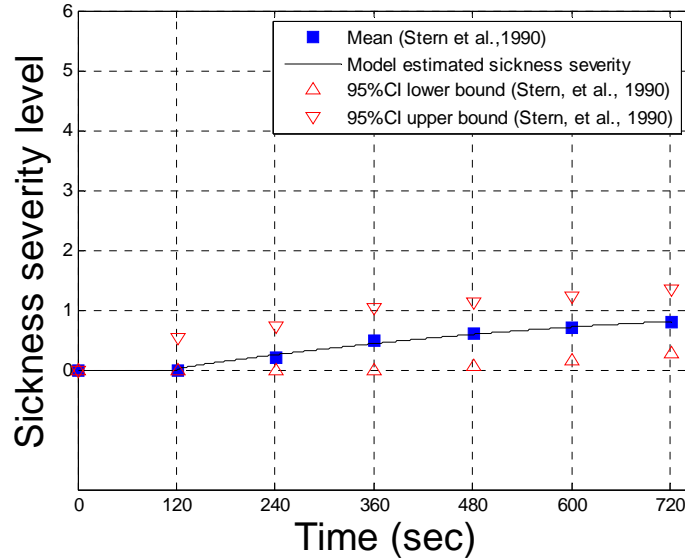


Figure 2.8 Comparing model one’s output with empirical data of Stern et al. (1990), given inputs of $\omega_{vis}(t) = -60\text{dps}$ and $\omega_{vest}(t) = 0\text{dps}$, and $t = 1 \dots T$ where $T = 720\text{sec}$

It is acknowledged that further work needs to be conducted to validate model one due to the following two reasons. First, nausea data were collected as ordinal data but not ratio scale data in Stern et al (1990)’s study while the model outputs are supposed to be compared with ratio scale data. Secondly, model one should be validated under more than one condition of rotation velocity of image pattern. A review of literature indicated that suitable ratio scale nausea data with VIMS studies could not be found. To validate model one (see details in Chapter 7), an empirical experiment having three different non-zero velocity condition and a control condition was conducted.

Related results are presented in Chapters 4 and 5. In such an experiment, the ratio scale data of nausea severity was collected for model validation purpose. Given individual differences in vection perception and sickness elicitation reported in experiment one, more model simulations will be implemented to test whether model one is capable of accounting for such individual differences in Chapter 8.

2.6 Conclusion

Model one relating vection and VIMS is successfully developed by modifying two published computational models: (i) the human vection perception model of Telban and Cardullo (2001) and (ii) Oman's (1990) nausea path dynamic model. The former model does not concern VIMS while the latter model is the first published computational model concerning motion sickness. To simulate sensory adaptation, a supervised-learning adaptive filter with a least mean square (LMS) learning rule (Widrow and Hoff, 1990) is also adopted in our model. The three-module architecture of model one is consistent with the structure of the neural circuitry underlying vection perception and VIMS elicitation. Model simulation produced sickness severity prediction that is comparable to empirical data published in Stern et al. (1990). Such results are consistent with expectations based on Reason (1978)'s neural mismatch theory (see Chapter 1) and related neural mechanism.

CHAPTER 3

A BIOLOGICALLY INSPIRED COMPUTATIONAL MODEL RELATING OKN AND VIMS (MODEL TWO)

SUMMARY

This chapter presents a biologically inspired computational model that simulates the entire process from sensory stimuli to the occurrence of VIMS mediated by OKN generation (model two). Motivations behind the construction of model two are presented. After the model scope and assumptions are carefully defined, details of the model development are documented. Model two consists of three modules: (i) a visual-vestibular integration network of OKN generation, (ii) a supervised-learning adaptation network, and (iii) a symptoms dynamic network. Finally, the model predicted sickness severity is compared with published empirical data for a demonstration of the predictive ability of model two.

3.1 Introduction

The extraocular afference hypothesis proposed by Ebenholtz et al. (1994) indicates

that activities of the oculomotor control system governing optokinetic nystagmus (OKN) should be associated with the elicitation of VIMS symptoms. OKN is a type of reflexive eye movement for gaze stabilization provoked by rotational visual disturbances, such as a yaw-direction rotating image pattern of black and white striped pairs. Such a hypothesis was made based on the following evidence: (i) two neurophysiological studies with monkeys reported that the activity of oculomotor control system is strongly associated with the activity of the vestibular system (Waespe & Henn, 1977b; Keller & Daniels, 1975), and (ii) several empirical studies with humans reported a critical role of the vestibular system in VIMS generation (Cheung et al., 1991; Kennedy et al., 1968). It is not the first time that the oculomotor control system has been pointed out to play an essential in motion sickness elicitation. A similar argument was proposed earlier in the poison theory (Treisman, 1977). It was proposed that the cooperation of the oculomotor movement control system with the head movement control system was critical for motion sickness generation, serving as a “toxin early warning system”. Bearing in mind that the OKN and VIMS symptoms can be provoked simultaneously and generally, OKN occurs before any VIMS symptoms, there might be a relation between OKN and VIMS as suggested by the extraocular afference hypothesis. Furthermore, such a hypothesis can be used to explain the significant depression of VIMS severity by

OKN suppression (Webb & Griffin, 2002).

Generally, VIMS elicitation happens in the presence of both vection and OKN. Consequently, the effect of OKN in VIMS generation can be easily obscured by the effect of vection. For instance, the effects of OKN and vection confound together when eye fixation significantly reduces both OKN magnitude and vection intensity (Stern et al., 1990; Flanagan et al., 2002). In such a case, no firm conclusions can be made for OKN's contribution in VIMS generation. An empirical study successfully manipulated OKN amplitude independently from vection intensity, from one condition to the other in an optokinetic drum with restricted FOV. A significant sickness severity difference between the two conditions was reported (Webb & Griffin, 2002). However, no specific comments were given on whether OKN alone can induce VIMS in the absence of vection. It was once reported that a type of visual stimulus is capable of provoking OKN alone without vection perception. The visual stimulus consisted of a central visual field and peripheral visual field rotating in opposite directions (Brandt et al., 1973). However, no comments were given on whether such visual stimuli can eventually provoke VIMS.

In this study, it is proposed that developing a mathematical model speculating

detailed working mechanisms relating OKN to VIMS can be an informative way to further the understanding of the cause of VIMS. As mentioned in Section 1.2.3, Oman's (1990) quality work on motion sickness modeling is reviewed. Oman's generic model, in an amazingly compact formation, constructs a uniform framework for VIMS generation. Due to its generic nature, the emphases of Oman's model are not on vection. The motion sickness model from Bos and Bles (1998) did not emphasize OKN either. Such reviews of previous work on mathematical modeling of motion sickness help identify a research gap with regards to the mathematical modeling of VIMS related to OKN.

3.2 Motivation

Motivated by the research gap mentioned in the last section, a computational model substantiating the connection between OKN and VIMS (model two) was constructed. It is worth pointing out that it was not the intention of the author to argue that OKN (or vection) was the only cause of VIMS, or favor one over the other. Currently, the author believes that VIMS is poly-symptomatic and caused by multi-factors associated with visual and vestibular interactions. Aside from model one relating vection and VIMS that was presented in Chapter 2, model two relating OKN and VIMS is also constructed and presented in this chapter. Similar to the discussion in

Section 2.2, if OKN is indeed not a cause of VIMS, then model two and its validation experiment will demonstrate the disassociation between OKN and VIMS.

3.3 Model scope and assumptions

In this study, the parameters of model two are initially constrained to simulate OKN and VIMS provoked by a yaw-direction rotating image pattern of black and white striped pairs along the earth-vertical axis. Similar visual stimuli are commonly employed around the world to provoke OKN and VIMS (Stern et al., 1990; Hu et al., 1997; Hu & Stern, 1998; Webb & Griffin, 2002; Flanagan et al., 2002; Bonato et al., 2004). Theoretically, model two can be generalized to simulate VIMS provoked by other types of visual stimuli. Possible expansions of model two will be discussed in Chapter 9.

Since evidence exist that demonstrate OKN is not the sole causal factor of VIMS, assumptions have been made to isolate the effects of OKN on motion sickness from the influence of other factors. First, it is assumed that vection perception is completely suppressed by a type of visual stimuli having central and peripheral visual fields rotating in opposite directions to isolate the effects of OKN from vection (see details in Section 4.4). Secondly, it is assumed that head movement is fully

constrained by head fixation and the rostrocaudal axis of head is carefully aligned along the earth-vertical axis to isolate the effects of OKN from the subjective-vertical conflict (SVC). Thirdly, it is assumed that individuals with his or her head fixed can use an external instrument to stabilize his/her body. For example, using hand holders or sitting in a chair for the purpose of isolating the effects of OKN from postural instability (PI).

3.4 Model development

Model two was developed step by step in the same way that model one was constructed (Section 2.4). The only difference is that the objective this time is to relate OKN and VIMS, instead of vection and VIMS. The final outcome of this chapter is one single computational model simulating the entire process from sensory stimuli to occurrence of VIMS related to OKN, in a way that is relevant to the operation of the human central nervous system. It is named “a biologically inspired computational model relating OKN and VIMS”.

3.4.1 Neural based roadmap relating OKN and VIMS

OKN is a combination of slow eye movement (slow-phase) for gaze stabilization and fast eye movement (fast-phase) for eye position resetting. It is widely accepted that

in humans, the fast-phase OKN is governed by the saccadic system while the slow-phase OKN has two components involving relatively separated, but interactive neural pathways; namely, an early component (OKNe) and a delayed component (OKNd). As illustrated in Figure 3.1, the OKN motor control system receives two types of visual signals given a wide-angle visual stimulus. One is a foveal retinal slip velocity (e_f) defined as the velocity of a visual surround in the central visual field (w_c) minus the slow-phase OKN velocity (e). The other is a peripheral retinal slip velocity (e_p) defined as the velocity of a visual surround in the peripheral visual field (w_p) minus the same slow-phase OKN velocity (e) (Buttner & Buttner-Ennever, 1988; Miles, 1998; Fletcher et al., 1990). It is reported that OKN suppression by eye fixation alleviates VIMS severity. This finding has already been confirmed by several empirical studies (Stern et al., 1990; Webb & Griffin, 2002; Flanagan et al., 2002). Logically, the working mechanism underlying such an effect can help identify a connection between OKN and VIMS.

In the case of eye fixation, the entrance of the peripheral retinal slip velocity (e_p) to the OKNd pathway was switched off (open S_2) to prevent this nonzero signal from transmitting in, for the purpose of stabilizing the target image on the fovea. At the same time, the entrance of the foveal retinal slip velocity (e_f) to both OKNe and

OKN_d pathways (Murator & Zee, 1979) was switched off (open S_3) simultaneously since the central visual surround velocity (w_c) in this case was equal to zero, given the fovea was occluded by an eye fixation point (Schmid et al., 1979). Consequently, the foveal retinal slip velocity (e_f) and the slow-phase OKN velocity (e) were reduced to zero while the peripheral retinal slip velocity (e_p) increased up to a level that was equal to the peripheral visual field velocity (w_p). Logically, the suppressed sickness severity by eye fixation could be the outcome of any of these changes in e_f , e_p , or e . However, various evidence indicate that the reduced foveal retinal slip velocity (e_f) was a superior explanation over the others. First, manipulation of a peripheral retinal slip velocity (e_p) independent of a foveal retinal slip velocity (e_f) was found to have no significant effect on sickness severity (Webb & Griffin, 2003). Secondly, a decreased slow-phase OKN velocity (e) resulting from a decreased visual acuity at near point was reported to exacerbate motion sickness instead of alleviating it, in the condition of no eye fixation (Webb, 2000). Therefore, the reduced foveal retinal slip velocity (e_f) can be directly responsible for the reduction of sickness severity induced by eye fixation, as proposed by Webb (2000). Such working mechanism of OKN suppression induced VIMS alleviation is summarized in Figure 3.1.

As mentioned in Section 3.3, model two should simulate VIMS elicitation in the presence of OKN alone and in the absence of vection. This model assumption is satisfied by inputting a special type of visual stimulus consisting of a central visual field and a peripheral visual field having opposite rotation directions (see details in Section 4.4). In such circumstances, the entrance of the peripheral visual field velocity to the OKN_d pathway was switched off (open S_1), controlled by a sign comparator (Schmid et al., 1979). In summary, although the OKN motor control system received two visual signals, only the foveal retinal slip velocity is critical for both OKN and VIMS generation under the model assumption of complete vection suppression.

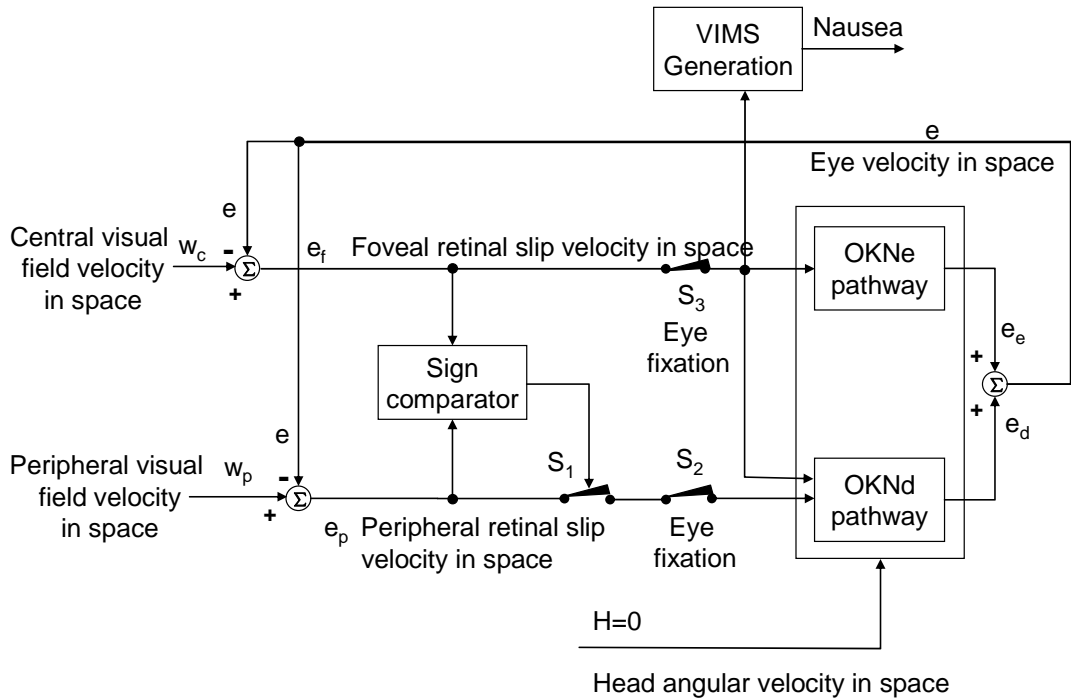


Figure 3.1 Block diagram of the working mechanism of OKN suppression induced VIMS alleviation. In this case, OKN and VIMS are provoked by a yaw-direction rotating image pattern of black & white striped pairs. S_1 , S_2 , and S_3 are normal-close switches.

In short, the connection between OKN and VIMS in the absence ofvection can be directly mediated by the foveal retinal slip velocity (e_f). Such deduction is sequentially supported by related neural mechanisms. As illustrated in Figure 3.2, the two neural centers, the brainstem and cerebellum, which are shown to be critical for VIMS generation (see Section 2.4.1), are also indispensable for generating OKN. The retinal slip velocity, defined as the velocity of visual surround minus the slow-phase velocity of OKN (SPV), is extracted by the retinal receptors and the motion-sensitive regions in the cerebral cortex. Such information is then encoded by neurons in the nucleus of the optic tract (NOT) and in the target nuclei of the accessory optic tract (AOT) in the brainstem (Fletcher et al., 1990; Fuchs & Mustari, 1993). The encoded foveal retinal slip velocity; namely, the perceived foveal retinal slip velocity, is capable of reaching into the protective adaptation network in the vestibulo-cerebellum via both mossy fiber (from the vestibular nuclei in the brainstem to the granule cells of the vestibule-cerebellum) and climbing fiber routes (from the ION in the brainstem to the Purkinje cells of the vestibule-cerebellum).

As shown in Figure 3.2, the neural circuit of slow-phase OKN is composed of two neural pathways: (i) the OKN_e pathway from the NOT/AOT to the dorsolateral

pontine nuclei (DLPN) in the brainstem, and then to the vestibule-cerebellum, and finally, to the vestibular nuclei (Fuchs & Mustari, 1993; Krauzlis, 2005), and (ii) the OKN_d pathway from the NOT/AOT to the ION, and then to the vestibule-cerebellum, and finally, to the vestibular nuclei (Mustari & Fuchs, 1990; Howard, 1986b; Simpson et al., 1988). The vestibular nuclei is the final eye motor nuclei integrating the visual signal from the OKN_e and OKN_d pathways and the vestibular signal encoded by the vestibular organs (SCC: semicircular canals; OTO: otolith), the vestibular ganglion, and the eighth cranial nerve (the vestibular nerve) (Howard, 1986b; Wilson & Jones, 1979). Such final eye motor nuclei in the brainstem sends both eye velocity and eye position signals via the ascending medial longitudinal fasciculus (MLF) into the pool of ocular motor nuclei of CNIII, IV, VI (the third, fourth and fifth cranial nerves). The pool of ocular motor nuclei then controls extraocular muscles via their lower motor neurons to generation OKN eye movements (Buttner & Buttner-Ennever, 1988).

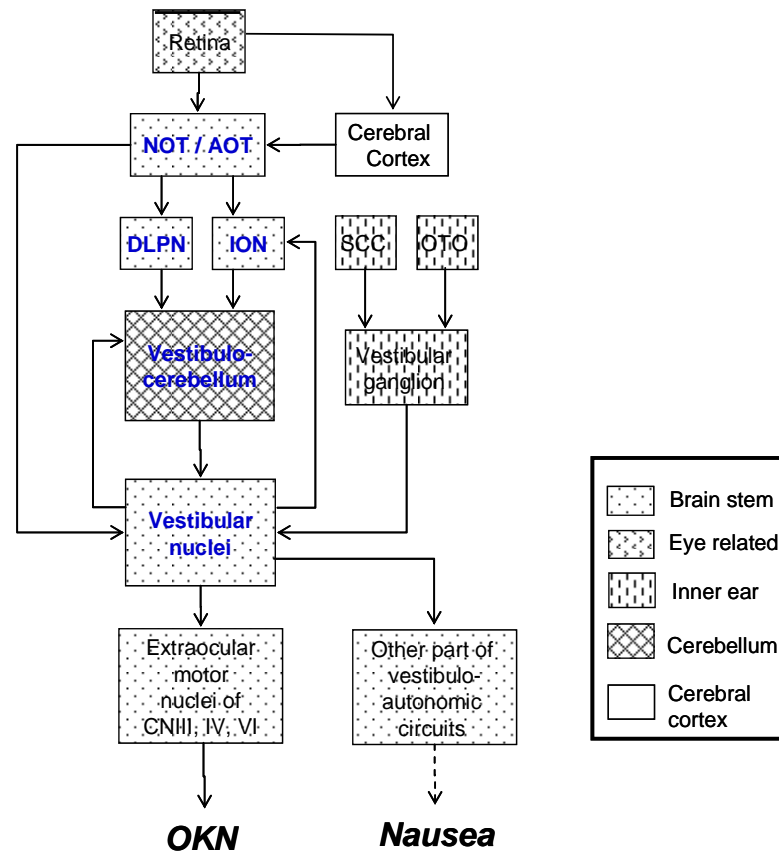


Figure3.2. Neural centers related to slow-phase OKN and VIMS generation summarized from neuroscience literature. Rectangular blocks indicate specific areas within the cerebral cortex, brain stem, cerebellum, etc., distinguished by different fill patterns. For clarity, not all relevant areas are depicted (e.g., the nucleus prepositus hypoglossi and the interstitial nucleus of Cajal in the neural integrator), and arrows do not always correspond to direct anatomical connections. Critical neural structures are color coded in blue. Dashed line represents that detailed neural mechanisms from the responses of vestibule-autonomic circuit to the final formation of nausea perception are unknown.

The neural basis roadmap relating OKN and VIMS in the absence of vection perception is summarized in Figure 3.3. On the one hand, a visual input carries information of the central visual field velocity in space into the vestibular nuclei in the brainstem via the human's visual system. On the other hand, a vestibular input carries information of the head movement in space into the same neural center in the

brainstem via the human's vestibular system. Such visual and vestibular inputs are integrated in the OKN oculomotor control system formed by the brainstem and the cerebellum. The vestibular nuclei in the brainstem serving as the final eye motor nuclei generate the OKN eye commands. Such information is then fed back into the computational loop of the perceived foveal retinal slip velocity encoded by the human's accessory optic system (NOT/AOT). The resulting perceived foveal retinal slip velocity in space is then passed into the cerebellum via the brainstem by both mossy and climbing fiber routes. The cerebellum, as a specialized organism for supervised learning computation underlying VIMS protective adaptation, generates the corresponding sensory prediction output given that the sensory input is carrying the perceived foveal retinal slip velocity in space. Cooperating with the ION in the brainstem, the cerebellum computes a neural mismatch signal as a self-modification error signal and a trigger signal of the vestibulo-autonomic circuitry. The vestibulo-autonomic circuitry receives the trigger signal from the cerebellum via the vestibular nuclei in the brainstem and then directly mediates elicitation of VIMS symptoms, such as nausea.

In short, reviews of neural mechanisms reveal a direct link between OKN and VIMS elicitation of symptoms, consistent with implications from the extraocular afference

hypothesis. Although VIMS is generally provoked in the presence of both vection and OKN, theoretically, VIMS can be induced in the presence of OKN alone. In other words, VIMS provoked by a rotating optokinetic image pattern is probably directly mediated by OKN alone when vection perception is fully suppressed. In light of Ebenholtz's extraocular afference hypothesis, it is proposed that the perceived foveal retinal slip velocity is the sensory input directly contributing to VIMS generation.

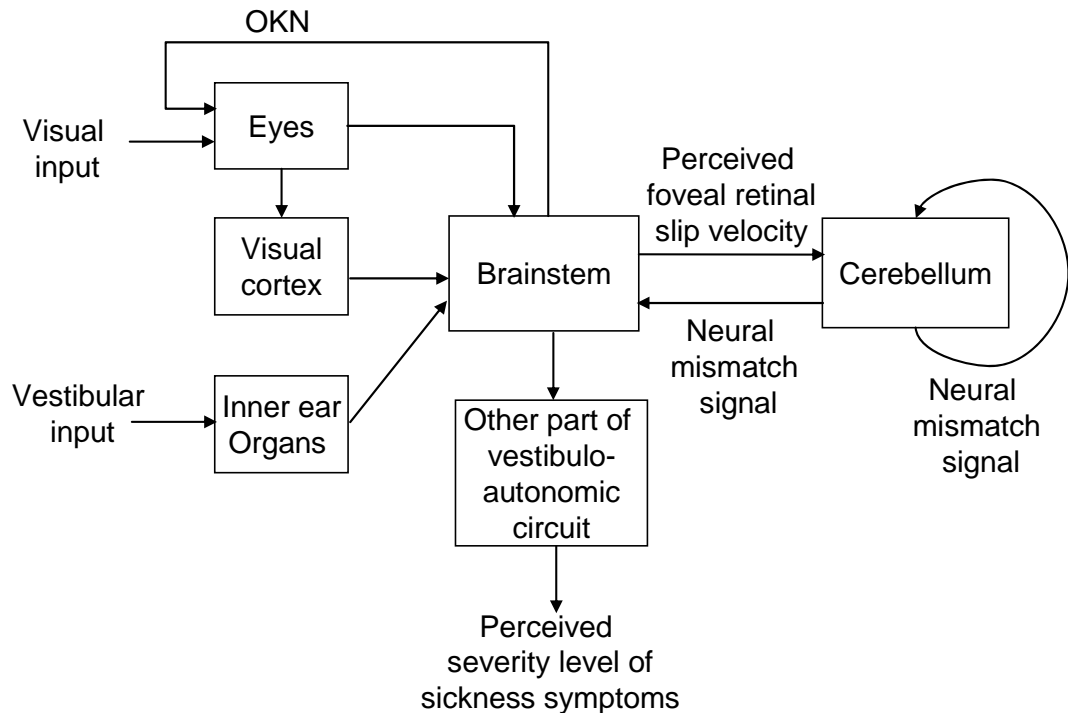


Figure 3.3 Roadmap relating OKN and VIMS summarized from related neuroscience literature. Each block represents a specific neural structure in humans that are related to optokinetic nystagmus (OKN) and VIMS generation. Arrows represent the interchanging signals flowing along anatomical connections among the neural structures. For clarity, not all relevant areas and signals are depicted (e.g., the inferior olivary nucleus relaying neural mismatch signals back to the cerebellum; the signal sent from the cerebellum to brainstem for computing OKN motor commands; the direct visual signal sent from the retina to the brainstem) and arrows do not always correspond to the direction of anatomical connections.

3.4.2 Conceptual model

Based upon the neural basis roadmap presented in the last section, a three-module architecture of model two is proposed (See Figure 3.4). Module1 (M1) is a visual-vestibular sensory integration network converging a visual input (the central visual field velocity in space) and a vestibular input (the head velocity in space) to output a perceived fovea retinal slip velocity in space. Module2 (M2) is a supervised-learning adaptation network simulating the function of the cerebellum. It receives the perceived foveal retinal slip velocity in space and generates a corresponding sensory prediction and a neural mismatch signal based on an optimization learning rule. Module3 (M3) is a Stevens' power law-based symptoms dynamic network triggered by the neural mismatch signal to estimate subjective sickness severity.

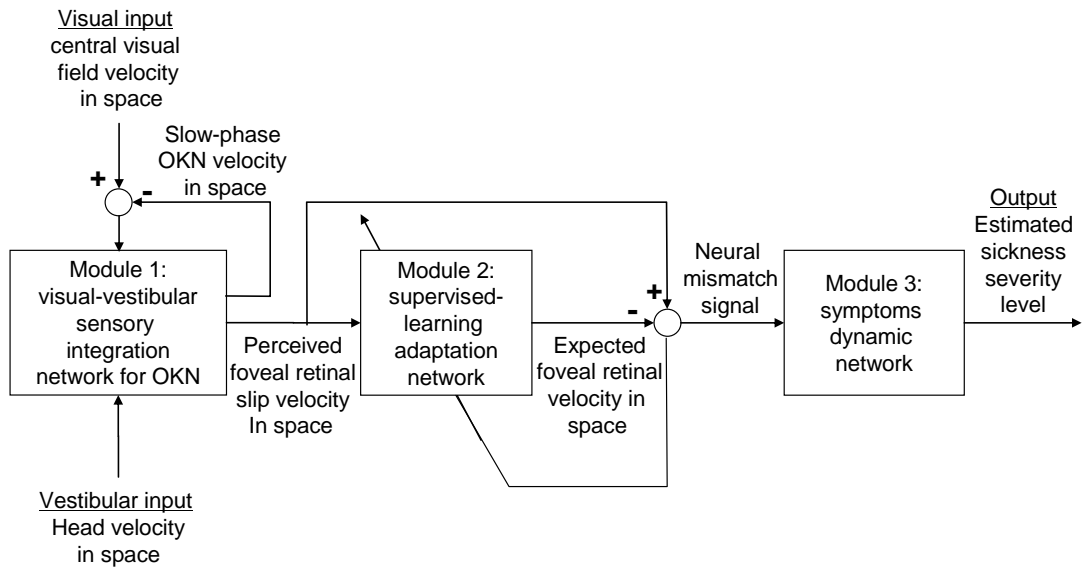


Figure 3.4 Three-module conceptual model relating OKN and VIMS

Comparing this conceptual model relating OKN and VIMS with the one relatingvection and VIMS, it is obvious that the two conceptual models have the same M2 and M3. The input of M2 is different in these two models. A perceived self-motion velocity in space is employed in model one while a perceived foveal retinal slip velocity in space is employed in model two.

3.4.3 Computational model

In model two, sensory input variables are defined in a right-handed orthogonal head-fixed frame of reference (x,y,z) where the x, y and z-axes are the naso-occipital interaural and rostrocaudal axes with positive values forward, to the left and to the top of the head, respectively. For rotation, the x, y and z-axes represent roll, pitch and yaw rotations with positive values clockwise, downward, and to the left, respectively. Consequently, sensory input variables are three-dimension vectors. The movement of visual stimuli was constrained to a yaw-direction rotation along the earth-vertical axis to model OKN and VIMS provoked by viewing a yaw-direction rotating image pattern of black & white striped pairs. In this case, all sensory input variables had zero x and y components ([0,0,z]).

In model two, the sensory input variables were: (i) central visual surround angular velocity in space r_v , (ii) head angular velocity in space ω . Other variables included: the OKN slow-phase velocity (SPV) in space r , the perceived foveal retinal slip velocity in space r_e^{per} , the expected or predicted foveal retinal slip velocity in space r_e^{exp} , and the neural mismatch signal r_e^{mis} . The output of model two, the model simulated subjective nausea severity O_{nausea} , was a scalar. The peripheral visual surround angular velocity in space was not excluded in model two since such signals were not used in computation of the OKN SPV and the foveal retinal slip velocity under the model assumption of completevection suppression.

Similar to the method discussion in Section 2.4.3, three computational models are employed and customized to meet specific functional requirements of the three conceptual modules, respectively. First, a visual-vestibular interaction model for human's OKN generation (Zupan et al., 2002) is employed to implement M1. Secondly, a supervised-learning adaptive filter with the least mean square error (LMS) learning rule (Widrow & Hoff, 1960) is employed to implement M2. Thirdly, a nausea path dynamics model (Oman, 1982; 1990) is employed to implement M3. Related mathematical implementation and customization of each module are documented in detail in the following three sections, respectively.

3.4.3.1 Module 1(M1): a visual-vestibular sensory integration network for OKN generation

The visual-vestibular sensory weighting model for human's slow-phase OKN by Zupan et al. (2002) was employed in M1. The decision was made based on the fact that this OKN model could achieve computations of visual-vestibular interaction requested by M1. It is worth mentioning that Zupan's original OKN model had no intentions to isolate central and peripheral visual fields for detecting central and peripheral visual field velocities separately. However, for the purpose of satisfying the model assumption of completevection perception in model two, the central visual surround velocity was the only visual input of M1. The output of M1, the perceived foveal retinal slip (r_e^{per}) is defined by Equation 3-1:

$$r_e^{per} = T_{rs}(r_v - r) \quad (3-1)$$

where T_{rs} is a 3D transfer function matrix (Appendix 3-1) modeling the part of the visual system extracting angular information from the foveal retinal slip velocity ($r_v - r$). The OKN slow-phase velocity (SPV) in space (r) is a summation of head angular velocity in space (ω) and slow-phase eye angular velocity in the head (e) defined by Equation 3-2:

$$r = \omega + e = T_{eye}e_M \quad (3-2)$$

where T_{eye} is a 3D transfer function matrix (Appendix 3-1) modeling the eye plant dynamics transforming eye command e_M into eye velocity e . The total eye command e_M is the sum of OKN_e eye command e_P and OKN_d eye command e_R defined by Equation 3-3:

$$e_M = e_P + e_R \quad (3-3)$$

Since it is widely accepted that OKN_e is governed by the smooth pursuit system, Robinson's smooth pursuit model (Robinson et al., 1986) is employed to compute e_P as defined in Equation 3-4:

$$e_P = T_{OKNe} \Pi_{yz} (\hat{\omega} + \tilde{e} + r_e^{per}) \quad (3-4)$$

where T_{OKNe} is a 3D transfer function matrix (Appendix 3-1) modeling the OKN_e motor control dynamics transforming the central estimate of external visual disturbance into the OKN_e motor command. Π_{yz} represents a projection of 3D vector onto the (y,z) plane to yield smooth pursuit motor command with a zero torsional component. The M1 output, the perceived foveal retinal slip velocity (r_e^{per}) is fed back into the loop of OKN_e motor control to make an estimate of r_v together with \tilde{e} and $\hat{\omega}$. \tilde{e} is a sensory estimate of the slow-phase eye angular velocity in head e . \tilde{e} is equal to e if the internal model of eye plant dynamics, implemented by a 3D transfer function \hat{T}_{eye} , is a perfect match of eye plant dynamics itself T_{eye} (Appendix 3-1) as defined by Equation 3-5:

$$\tilde{e} = \hat{T}_{eye} \hat{e}_M = T_{eye} e_M = e \quad (3-5)$$

where \hat{e}_M is the efference copy of total eye command e_M . OKN_d eye command e_R compensates for the central estimates of head angular velocity in space ($\hat{\omega}$) and eye angular velocity in space (\hat{r}) as defined by Equation 3-6:

$$e_R = -\hat{\omega} - \hat{r} \quad (3-6)$$

\hat{r} and $\hat{\omega}$ are computed by weighted averaging various intermediate estimates of r and ω , captured by different sensory systems as defined by Equations 3- 7 and 3-8:

$$\hat{r} = W_{r,1} \tilde{r} + W_{r,2} (\tilde{\omega} + \tilde{e}) + W_{r,3} (\hat{\omega}_2 + \tilde{e}) \quad (3-7)$$

$$\hat{\omega} = W_{\omega,1} \tilde{\omega} + W_{\omega,2} \hat{\omega}_2 + W_{\omega,3} (\tilde{r} - \tilde{e}) \quad (3-8)$$

where the sensory weights $W_{r,1}$, $W_{r,2}$, $W_{r,3}$, $W_{\omega,1}$, $W_{\omega,2}$, and $W_{\omega,3}$ are free parameters in a range of zero to one. $W_{r,3}$ is the only one found to affect the OKN slow-phase velocity (SPV) noticeably. Referring back to the original OKN model by Zupan, two more sensory inputs (head linear velocity in space v and gravity g), are defined to compute a intermediate estimate of ω ($\hat{\omega}_2$) via the processing layers of “frequency completion” and “estimation conversion”. However, $\hat{\omega}_2$ is equal to zero, given the model assumption of head fixation in model two. The sensory estimate of eye angular velocity in space (\tilde{r}) and head angular velocity in space ($\tilde{\omega}$) are defined by Equations 3-9 and 3-10, respectively:

$$\tilde{r} = T_{rs} (r - r_v) + (I - \hat{T}_{rs}) \hat{r} \quad (3-9)$$

$$\tilde{\omega} = T_{scc} \omega + (I - \hat{T}_{scc}) \hat{\omega} \quad (3-10)$$

where $I - \hat{T}_{rs}$ is a dynamics complementary internal model of T_{rs} , and $I - \hat{T}_{scc}$ is a dynamics complementary internal model of T_{scc} characterizing sensory dynamics of semicircular canals (Appendix 3-1). As illustrated in the block diagram M1 (see Figure 3.5), given the time series of a zero head angular velocity in space ω and a constant central visual surround angular velocity in space r_v for an exposure period as input of M1, the output of M1 is a time series of the perceived foveal retinal slip velocity in space r_e^{per} . The computation of OKN SPV in space (r) involves three processing layers; frequency completion, estimation conversion, and weighted averaging, and two neural pathways; OKN_e and OKN_d motor control pathways. The OKN gain defined as the OKN SPV in space (r) over the central visual field velocity in space (r_v) is found to have a negative linear relation with free parameter $W_{r,3}$ (see details in Chapter 8).

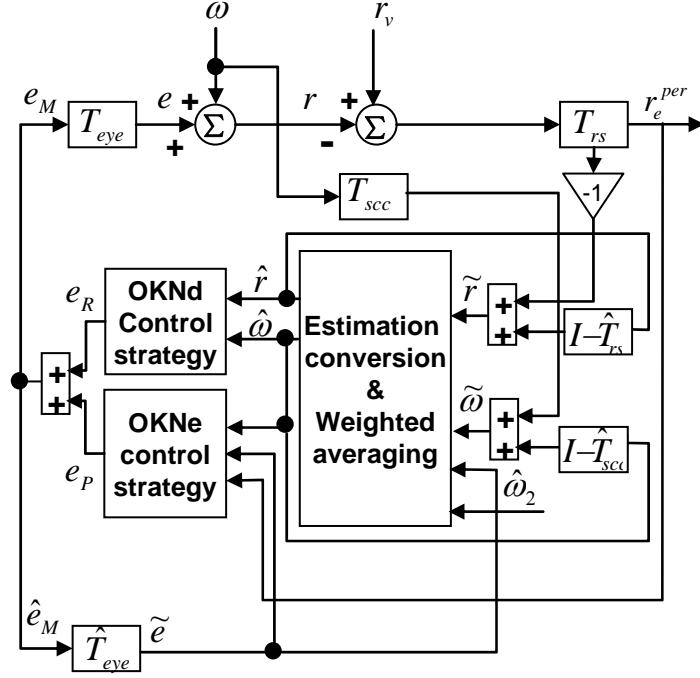


Figure 3.5 Block diagram of M1. The OKNd control strategy is defined by Equation 3-6. The OKNe control strategy is defined by Equation 3-4. The estimation conversion and weighted averaging are defined by Equations 3-7 and 3-8 together. Two inputs of M1 are the central visual field velocity in space (r_v) and head angular velocity in space (ω). Output of M1 is the perceived foveal retinal slip velocity (r_e^{per})

3.4.3.2 Module 2 (M2): a supervised learning adaptation network

This module was implemented by a supervised-learning adaptive filter (see details in Section 2.4.3.2). This adaptive filter took in a perceived foveal retinal slip velocity in space (r_e^{per}) and outputted a predicted or expected foveal retinal slip velocity in space (r_e^{exp}). Meanwhile, a neural mismatch signal (r_e^{mis}) is calculated by subtracting the prediction output from the input as defined in Equation 3-11: $r_e^{mis} = r_e^{per} - r_e^{exp}$.

Although the same type of adaptive filter was employed by model one's M2, the

mathematical implementation of such an adaptive filter in model two was different from the one in model one. The M2 variables in model two are all 3D vectors instead of 1D since the M2 input was not a single dimensional vector like the one in model one. All the unit delay functions D in the tapped unit delay line and the tunable weightings of parallel fiber signals w_1, w_2, \dots, w_M were 3×3 diagonal matrix. Three separated LMS learning rules each defined by Equation 2-7 and three separated linear transfer functions are employed to control the three dimensions, respectively.

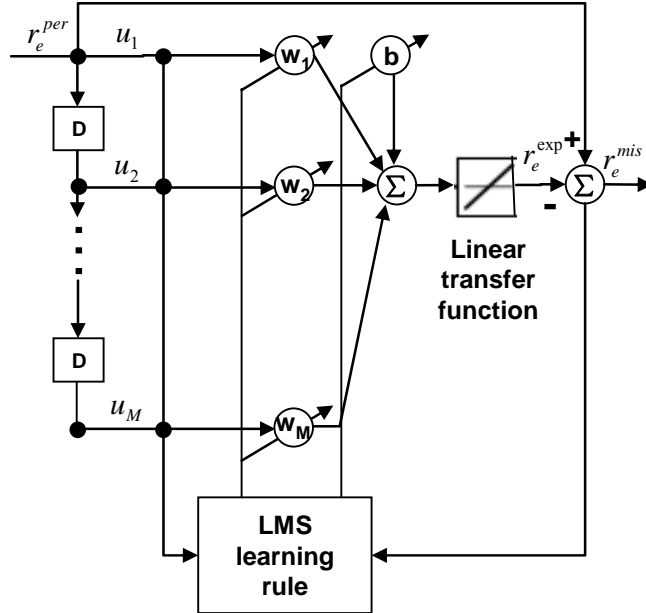


Figure 3.6 Block diagram of M2. The LMS learning rule and the linear transfer function are defined in the same way as model one (see details in Section 2.4.3.2)

3.4.3.3 Module 3(M3): a symptom dynamic network

Oman's (1990) nausea path dynamic model was employed to implement M3. It took in a neural mismatch signal r_e^{mis} and outputted the model simulated subjective nausea severity (O_{nausea}). Since O_{nausea} is defined as a scalar, the 3D input vector r_e^{mis}

is transformed into a scalar variable before passing into the fast and slow dynamic elements as defined in Equation 3-12: $\tilde{\omega}_{mis} = \|r_e^{mis}\|/c$, where the pre-processed neural mismatch signal ($\tilde{\omega}_{mis}$) is the Euclidean norm of 3D vector r_e^{mis} divided by a positive free parameter c . The total response of fast path and slow path I and the threshold-power law function are defined in the same way as model one.

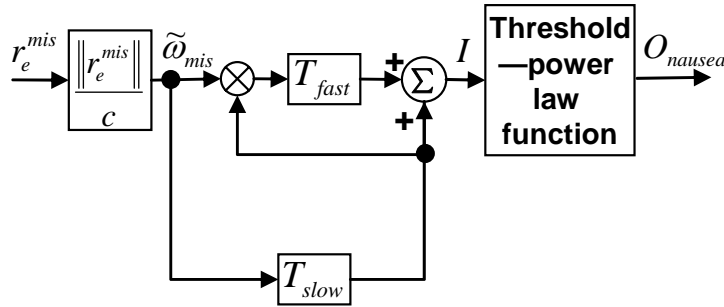


Figure 3.7 Block diagram of M3. The threshold-power law function is defined by Equation 2-10

3.4.4 Model simulation

Figure 3.8 shows a block diagram of model two relating OKN and VIMS. The model is implemented by the Matlab-Simulink® software package. A fourth-order variable-step Dromand-Prince algorithm is used for model simulation. In total, model two has eight free parameters, including a M1 parameter used to tune OKN gain ($W_{r,3}$), a number of components of input vector U (M), the learning rate of the adaptive filter (lr), a constant c , the gain of the transfer function T_{fast} and T_{slow} (k), the threshold (I_0), the constant (a) and exponent (b) of power law function.

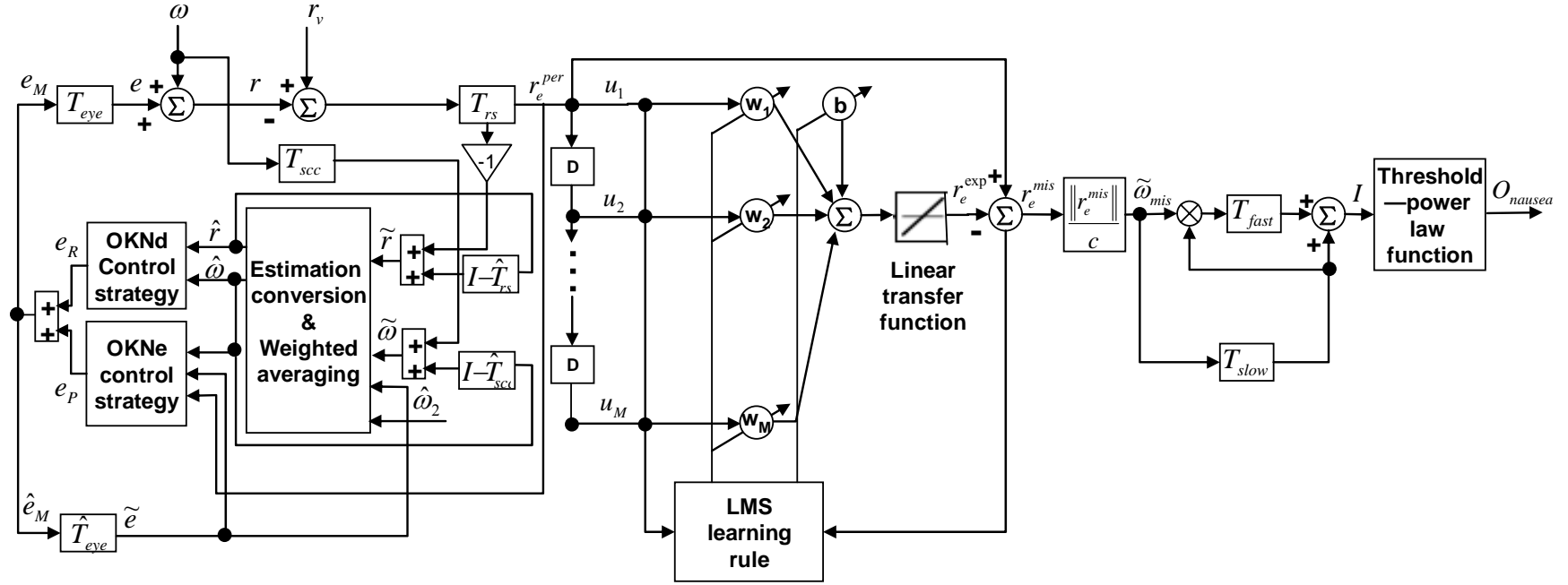


Figure 3.8 Block diagram of model two relating OKN and VIMS. Visual input (r_v) is the central visual surround angular velocity in space. Vestibular input (ω) is the head angular velocity in space. The neural mismatch signal (r_e^{mis}) is defined as the difference between the perceived (r_e^{per}) and expected (r_e^{exp}) foveal retinal slip velocity in space. Model two's scalar output (O_{ausea}) is the severity of the model simulated subjective nausea.

3.5 Comparison of model simulated data and empirical data of Webb & Griffin (2002)

To demonstrate the predictive ability of model two, empirical data reported by Webb & Griffin (2002) was chosen as the benchmark of model two's output. In this empirical study, OKN and VIMS are provoked by a yaw-direction rotating virtual optokinetic drum at a constant velocity of 30 degree per second (dps) presented by a VR4 head-mounted display (HMD). There were two experimental conditions: (i) eye fixation condition, and (ii) no eye fixation condition. Moreover, the head movements of subjects were restrained by the use of a strap attached to the HMD. Subjective vection intensity and sickness severity were rated every 5 min by a 4-point vection rating and a 7-point nausea rating, respectively. The exposure duration was up to 30 min (stopped when subject reported a rating of 6 on the 7-point nausea scale, indicating moderate nausea and wanting to stop). Since model two could only simulate the effect of OKN alone on VIMS severity level in the absence of vection, the difference of sickness severity levels in the non-fixation and fixation conditions representing the part of sickness suppressed by eye fixation was compared with model simulated data. Specifically, closer model predictions of subjective sickness severity to the difference of mean sickness scores in the two conditions reported by Webb & Griffin (2002) resulted in the better predictive ability of model two.

In this case, the two inputs of model two are $r_v(t)=[0.0.60]\text{dps}$ and $\omega(t)=[0,0,0]\text{dps}$.

The eight free parameters of model two are set to a set of values determined through a process of trial and error and with references to literature where appropriate ($W_{r,3}=0.025$, $M=5$, $lr=2^{-8}$, $c=30$, $k=0.8$, $I_0=0.001$, $a=1$, and $b=0.65$). $W_{r,3}$ was set to the level of 0,025 as proposed by Zupan et al. (2002) to simulate the case when OKN gain is equal to 0.97 since Webb & Griffin (2002) didn't report any OKN related measures. The parameter M , lr , and k was determined through a process of trail and error ($M=5$, $lr=2^{-8}$, and $k=0.8$). The parameter c (in module 3) was set to 30 dps for normalization purposes. Finally, the parameter I (the threshold), a and b (the constant and exponent of Stevens' power law function) was tuned to minimize the mean square error (MSE) measuring the difference between the model simulated nausea severity time course and an empirical nausea severity time course reported by Webb & Griffin (2002). Figure 3.9 shows that model two's output $O_{\text{nausea}}(t)$, a time course of model simulated subjective nausea severity, is very close to the six mean difference scores calculated from empirical data of Webb & Griffin (2002). The mean square error of model simulated data and empirical data is 0.017. The 95% confidence intervals (CI) are not shown in Figure 3.9 since such data was not reported in Webb & Griffin (2002). Such results indicate that model two has the capability to simulate time series of sickness severity reported empirically.

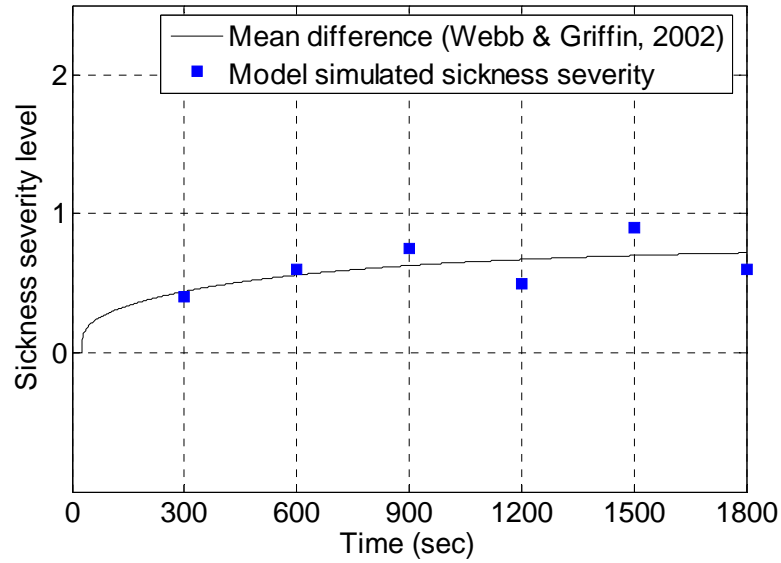


Figure 3.9 Comparing model two's output with empirical data of Webb & Griffin (2002), given inputs of $r_v(t)=[0.0,0.60]$ dps and $\omega(t)=[0,0,0]$ dps, and $t=1\dots T$ where $T=1800$ sec

It is acknowledged that further work needs to be conducted to validate model two due to the following three reasons: first,vection is provoked together with OKN and VIMS in the two conditions from Webb & Griffn (2002), which does not satisfy the assumption of model two. Secondly, nausea data are not collected as ratio scale data in Webb & Griffin's (2002) study. Thirdly, model two should validate under more than one condition, the rotation velocity of the image pattern. A review of literature indicates that suitable ratio scale data with VIMS studies can not be found. To validate model two (see details in Chapter 7), an empirical experiment having three different non-zero velocity conditions and a control condition will be conducted. Related results will be presented in Chapters 4 and 6. In such an experiment, the ratio

scale data of nausea severity will be collected for model validation purposes. Given individual differences in OKN SPV and sickness elicitation reported in experiment two, more model simulations will be implemented to test whether model two is capable of accounting for such individual differences (see details in Chapter 8).

3.6 Discussion

In this section, the author would like to emphasize the difference of visual inputs of model one and model two. As illustrated in Figure 3.10, model one takes into only the peripheral retinal slip velocity (e_p) and model two takes into only the foveal retinal slip velocity (e_f). Under the assumption of fully suppressed OKN facilitated by an eye fixation point, e_p is non-zero and e_f is zero. Consequently model one is activated and model two is not. Under the assumption of fully suppressedvection achieved by viewing central and peripheral visual field rotating in opposite directions, both e_f and e_p are non-zero. However, the model two is deactivated by the mechanism of sign comparator detecting the discrepancy of rotating directions of central and peripheral visual field as proposed by Schmid et al.(1979). Consequently, only model one is activated under such circumstances. This particular conceptual framework indicated that the neural network of veciton-induced VIMS and OKN-induced VIMS could work separately or together with certain levels of overlap,

depending on which visual input path is switched on.

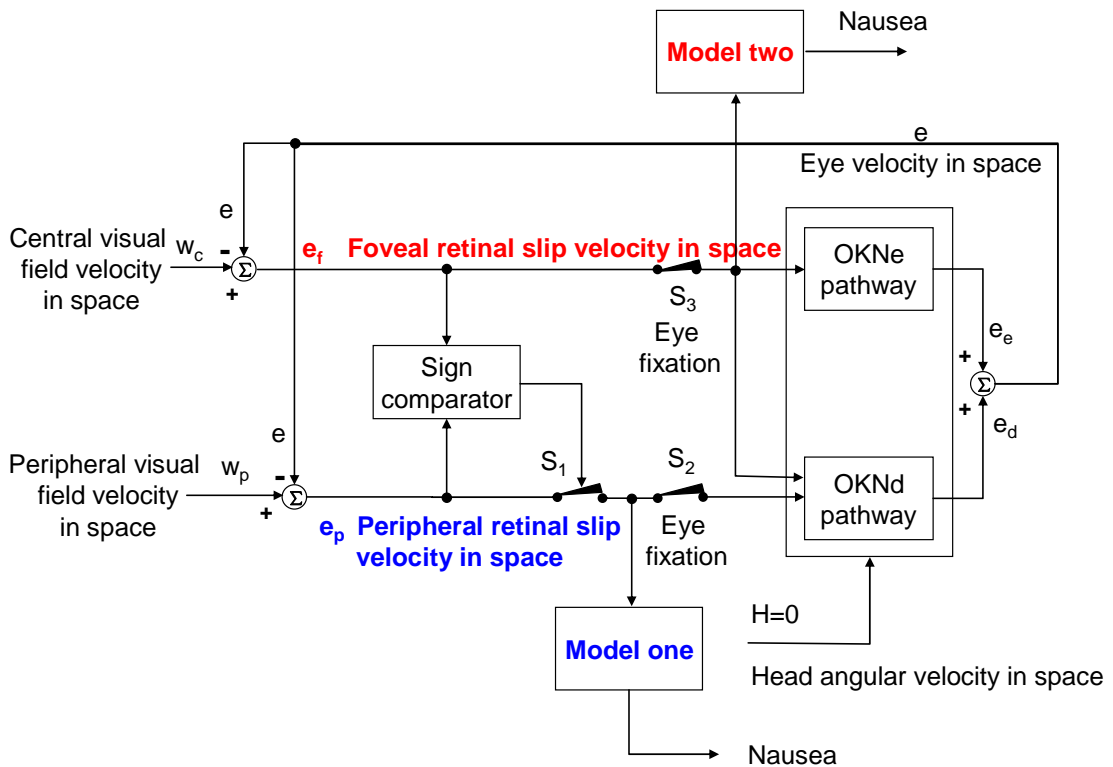


Figure 3.10 Relationship of model one and model two and the difference of their visual inputs. The vestibular input of model one and model two is not shown for simplicity

The author intended to emphasize the independent visual inputs of model one and model two, but not the independency of working mechanisms of model one and model two. Actually, there are intensive overlaps between computational networks of the two models in terms of visual and vestibular signal processing, sickness protective adaptation, and mediating of nausea responses. Therefore, the conceptual model illustrated in Figure 3.10 is only valid when only one of the two mechanisms is activated, i.e., either vection alone (assumption of model one) or OKN alone (assumption of model two). As discussed in section 9.2, modeling the synergistic

interaction of effects of vection and OKN on VIMS is out of the scope of this study.

3.7 Conclusion

Model two relating OKN and VIMS is successfully developed by modifying two published computational models: (i) the human OKN SPV model in Zupan et al. (2002) and (ii) Oman's (1990) nausea path dynamic model. The former does not concern VIMS and the latter is the first published computational model on motion sickness. Similar to Model one, a supervised-learning adaptive filter with a least mean square (LMS) learning rule is adopted to simulate the habituation effects of human to continuous exposure (Widrow and Hoff, 1990). The three-module architecture of model two is consistent to the structure of the neural circuitry underlying OKN and VIMS elicitation. Model simulation produced prediction of sickness severity that is comparable to empirical data published in Webb and Griffin (2002). Such results are consistent with expectations based on Ebenholtz et al.'s (1994) extraocular afference hypothesis (see Chapter 1) and related neural mechanism.

CHAPTER 4

OVERVIEW OF MODEL

VALIDATION EXPERIMENTS

SUMMARY

This chapter presents the motivations behind the two empirical validation studies. Relevant literature are reviewed to justify the methodology adopted to suppress OKN and vection in experiments one and two, respectively. Detailed methodologies are presented with the results of pilot tests.

4.1 Introduction

Reviews of literature indicate two possible major causes of VIMS: (i) vection (visually induced illusion of self-motion) and (ii) OKN (optokinetic nystagmus, a type of reflexive eye movement for gaze stabilization under rotational visual disturbance). Indeed, there are two camps of researchers who favor one cause over the other. On the one hand, vection has been referred as the major cause of VIMS in many studies involving optokinetic drums (Hu et al., 1997, Hu and Stern, 1998, Stern et al., 1990). On the other hand, vection has been successfully dissociated with changes of VIMS severity levels when the field of view (FOV) is restricted (Webb

and Griffin, 2003). Moreover, it was reported that eye fixation reduces VIMS, but has no effect on vection in restricted FOV. It was concluded that vection is not the primary cause of sickness with optokinetic stimuli and VIMS can be reduced by OKN suppression (Webb and Griffin, 2002).

To resolve these conflicting views among current VIMS researchers, some empirical studies attempt to isolate the effects of vection and OKN on VIMS. Initially, eye fixation and FOV restriction were used to manipulate OKN and vection independently, but later it was found that OKN and vection would change simultaneously instead of independently for either way (Stern, et al., 1990; Flanagan et al., 1990). Webb and Griffin (2003) succeeded in varying the vection intensity level independent of the eye movement magnitude under restricted FOV. Correlation between the vection intensity level and VIMS level indicated that VIMS and vection are not correlated. However, this study uses laterally moving dots in restricted FOV ($48^{\circ} \times 36^{\circ}$) as visual stimuli instead of wide FOV optokinetic drum and does not provide comments on the pattern of perceived self-motion (CV or LV). Consequently, there are difficulties in comparing their results with previous results of CV optokinetic drum studies under a wide FOV. Moreover, no comments are given on whether vection can induce VIMS in the absence of OKN. Webb and Griffin (2002)

successfully manipulated OKN magnitude levels independent of vection intensity levels in a restricted FOV virtual optokinetic drum and reported a significant effect of eye fixation on VIMS suppression. However, no comments were given on whether OKN can induce VIMS in the absence of vection.

Hu et al. (1989) reported that drum rotation velocity, given a fixed spatial frequency, influenced the intensity of VIMS symptoms in the presence of vection and OKN. Among the 15 dps, 30 dps, 60 dps and 90 dps drum rotation velocity conditions, the 60 dps drum rotation velocity produced the highest VIMS severity level. It was concluded that this curvilinear relationship (an inverted 'U' shape) between velocity of drum rotation and VIMS severity is mediated by a similar curvilinear relationship between the velocity of drum rotation and strength of vection experienced by the subjects. However, the effects of drum rotation velocity on VIMS in the absence of vection and OKN have not been investigated separately.

In short, there exists a gap in conducting experiments to study ratio scaled measures of VIMS in the presence of vection without OKN and in the presence of OKN without vection.

4.2 Motivations

Aside from filling the gap as reported in the last section, another important motivation of the experiments is to validate the computational models that were developed. In Chapters 2 and 3 of this thesis, computational models were reported to relate vection and VIMS as well as OKN and VIMS. Although the models were shown to successfully simulate sickness ratings as a function of exposure duration that are consistent with those reported in Stern et. al (1990), and Webb and Griffin (2002), since neither studies used ratio scale data and both did not publish the individual raw data, two validating empirical experiments are conducted. Experiment one examines the effect of drum rotation velocity in the absence of OKN on VIMS and vection. Experiment two examines the effect of drum rotation velocity in the absence of vection on VIMS and OKN.

4.3 OKN suppression in experiment one

To examine the effect of drum rotation velocity on VIMS in the presence of vection and in the absence of OKN, experiment one requires a method which can completely suppress OKN; in the mean time, it does not eliminate vection perception. Webb and Griffin (2002) reported that eye fixation completely suppressed OKN in an optokinetic drum. Other researchers also reported similar findings (Stern et al., 1990;

Flanagan et al., 2002). All studies reported that eye fixation does not eliminate vection perception.

Different studies used eye fixation points with different sizes. Stern et al. (1990) used a cross subtending about 2.3 deg. Webb and Griffin (2002) used a cross subtending about 8 deg. The eye fixation point used in Flanagan et al. (2002) was projected from a laser pointer and its size was not specified. Brandt et al. (1973) conducted a comprehensive study on vection perception in an optokinetic drum, using an eye fixation point subtending 1 deg. To verify whether 1 deg eye fixation point can completely suppress OKN, a pilot test was conducted involving 4 female subjects using the same experimental setup with experiment one. All 4 subjects participated in experiment one as well.

Visual stimuli took the form of an optokinetic drum rotating at a speed of 34 dps. The subject first experienced a no-eye fixation condition for 1 min and then followed by an eye fixation condition for another 1 min. EOG records confirmed that OKN can be completely suppressed by a 1 deg eye fixation point for all 4 subjects. As shown in Figure 4.1, the difference of the horizontal EOG signal between an eye fixation condition and no-fixation condition is obvious. In the no-fixation condition, an OKN

slow-phase component (having a smaller slope) is followed by an OKN fast-phase component (having a larger slope). In the eye fixation condition, there is no similar repetitive pattern. In fact, EOG records of experiment one showed that a 1 deg eye fixation point completely suppressed OKN for over 30 min for all subjects. Related results will be presented in Chapter 5.

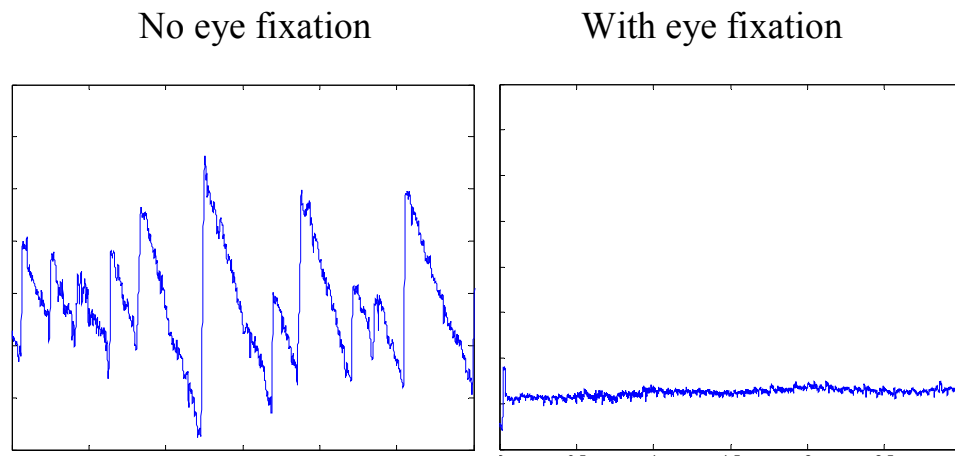


Figure 4.1 OKN suppression achieved by fixating on a 1 deg eye fixation point. The horizontal eye position data is the subject's EOG data recorded in a previous pilot test.

4.4 Vection suppression in experiment two

Likewise, experiment two requires a method that completely suppresses vection without elimination of OKN. Brandt et al. (1973) created a special visual stimulus having a central and peripheral visual field rotating in opposite directions in an optokinetic drum. The circular central visual field rotating in an opposite direction to the peripheral visual field was created by reflecting a visual pattern behind the subject with a mirror. When the diameter of the central visual field was adjusted to

about 100 deg, vection perception was fully suppressed in the optokinetic drum rotating at a speed of 60 dps. Under such circumstances, OKN followed a rotation direction of the central visual field. However, these observations were derived from the individual subject's data and thus no confirmative conclusion can be drawn. Literature reviews indicate that no such empirical studies are repeated and published.

A pilot test was conducted to investigate the effect of the size of the central visual field on vection perception using the same group of subjects and same experimental setup of experiment two. The size of central visual field was varied from 80 pixels (9 degrees) to 1580 pixels (180 degrees) at a stepping size of 100 pixels. For each size of the central visual field, the subject was exposed to 4 different drum rotation velocities in sequence; i.e., 15 dps, 30 dps, 60 dps, and 90 dps. (after Hu et al., 1989) Therefore, each subject was required to experience 64 different trials. In each trial, the subject was instructed to report whether she experienced illusion of self-rotation (vection) to the left or to the right. If no such illusion of self-rotation was reported, the trial continued for 90 sec and then ceased. There was a break up to 3 min between the two trials to avoid provoking sickness. The results of the pilot test helped to identify a specific range of diameters of the central visual field in which the vection perception was fully suppressed for 90 sec for each subject in each drum rotation

velocity condition. As a matter of fact, results of experiment two show that vection perception can be fully suppressed for over a 30 min exposure period by having subjects view opposite rotating central and peripheral visual fields. Related results will be presented in detail in Chapter 6.

4.5 Methods

This section describes the methods used in experiments one and two. The experimental setup, including the apparatus and visual stimuli, will be described first. This is followed by some details of the participants and a description of the different measures taken that are related to vection, OKN, sickness severity, visual acuity and motion sickness susceptibility.

4.5.1 Apparatus and visual stimuli

In experiment one, a virtual optokinetic drum (height of 120 cm, diameter of 230 cm) with 24 pairs of uneven widths of black and white stripes (each pair subtending 15° at the subjects' eyes; white stripe is 9.3 deg and black stripe is 5.7 deg) was used to provoke circular vection (CV) and VIMS. The visual stimuli were set up so that they were as close as possible to that of Hu et al. (1989), in order to compare the results of experiment one to those reported in Hu et al. (1989). The drum was rotated in a yaw

direction at a constant velocity along the earth-vertical axis. The spatial frequency of the visual stimuli was 0.067cycle/deg, which was outside the range of 2 to 4 cycle/degree sensitivity peak of photosensitivity epilepsy (Harding and Harding, 2007).

As illustrated in Figure 4.2, the virtual drum covering $200^{\circ} \times 55^{\circ}$ FOV is displayed on a curved wide-angle screen (dimension: $183\text{cm} \times 460\text{cm}$, model: Da-Lite Matter White) by a multi-projection system in a light tight room. The black and white stripes are drawn by calling functions defined in the Direct Draw library in the Visual Basic (2005 express edition) language. All stimuli are presented at a refresh rate of 60Hz and $1920\text{p} \times 480\text{p}$ resolution by a NVIDIA GeForce 7600GT graphics card running on an Intel® core 2™computer (2.4GHz CPU, 2GB memory). An external hardware, Matrox Triple Head2Go, was used to split a frame of black and white stripes into three images, each projected by one projector. Each image has about 6 degree overlap with its adjacent image for the purpose of presenting a seamless wide-angle rotating visual pattern. Gradient image blending programmed by Visual Basic was used to fade the edges formed by image overlapping. Figure 4.3(a) shows a subject standing inside the virtual drum with her chin resting on a chin rest to fixate the position of her head. The chin rest was mounted on a self-designed metal bracket

((120(h) × 100(l) × 50(w)cm) which was used as external instrument to help subjects stabilize their bodies.

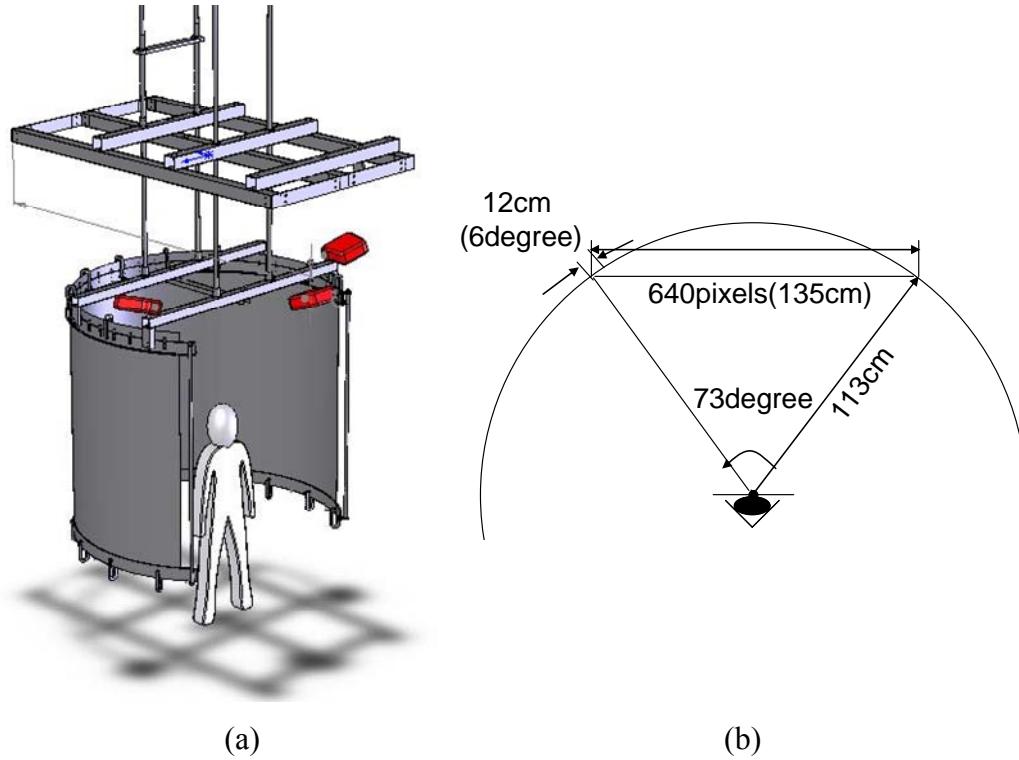


Figure 4.2 (a) Physical layout of multi-projection system consisting of three projects and one curved projection screen (b) Geometrical transformation between viewing distance and FOV.

The same set of apparatus was used in experiment two. However, the content of the visual stimuli used in experiment two was dramatically different. The visual stimuli in the central and peripheral visual fields moved in opposite direction at a constant velocity for the purpose of completely suppressingvection perception. The diameter of the central visual field, having an opposite rotation direction with peripheral visual field, was technically adjustable in a range from 0 pixels to 1920 pixels.

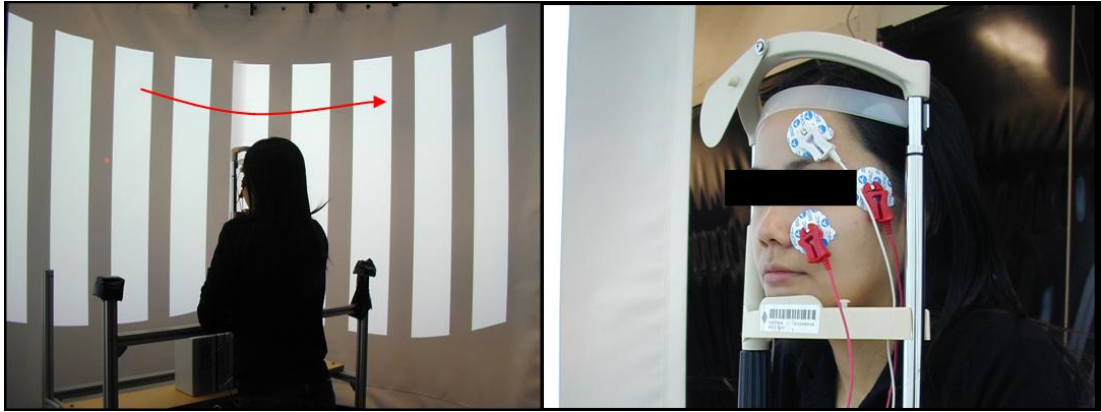


Figure 4.3 a) Subject in a standing position viewing the virtual optokinetic drum rotating in a yaw direction at constant velocity. The red arrow is added to the figure to indicate the drum rotating direction. The head of the subject is fixated by a standard optometry chinrest which has a forehead rest and an adjustable chin rest height. Subjects were requested to hold the self-made metal bracket for stabilizing their bodies. b) Subject wearing five EOG electrodes for eye position data recording. The attachment positions of the electrodes are recommended by the EOG100C menu.

Eye movements were tracked and recorded using an electrooculogram amplifier module (EOG100C, BIOPAC[®]) and an EOG data acquisition and analysis software (AcqKnowledge, BIOPAC[®]). The EOG signal gain was set to the highest level, which is 5000. The sampling rate was set to 200 sample/sec in consideration of both anti-aliasing and limited memory capability. The EOG100C output selection was set to “normal” to capture eye position signals. The frequency response of the EOG module was set to a range of 0.05Hz to 35 Hz with the 50Hz notch filter open. Figure 4.3(b) shows a subject wearing EOG electrodes. Four electrodes are attached around the eye sockets of the participant for capturing eye movements in horizontal and vertical planes and one electrode is attached to the participant’s arm as the ground.

Each pair of horizontal and vertical electrodes is carefully aligned to avoid crosstalk of horizontal and vertical signal channels. A video camera was set up to capture the entire drum exposure period of each participant. Each video clip was visually inspected by the experimenter. No subject was found to close her eyes except during normal eye blinking.

An OPTEC[®] 2000 vision tester was used to measure the near point visual acuity (both eyes and with each eye separately). This vision tester can measure the near point visual acuity at 14 in (35.56 cm) and far point visual acuity at 20 ft (6.1 m). The test visual stimuli were 14 sets (in different sizes) of four Landolt rings, each having different orientations and placed in a position of “up”, “down”, “left” or “right”. Three rings were unbroken and one was broken. Subject was requested to report which ring was unbroken among the four for each set of Landolt rings, from the largest to the smallest set. The range that the visual acuity was able to measure was 20/200 (scored as 1) to 20/13 (scored as 14). All visual acuity parameters were measured in a light tight room, given that all lights were off.

4.5.2 Participants

It was reported that Chinese female subjects are hypo-susceptible to motion sickness

(Stern et al., 1996). To amplify the “output” signal of nausea severity as much as possible in the experimental setup described previously, only Chinese females were recruited in experiments one and two. There is evidence suggesting that the difference between male and female susceptibility can be partially explained by the magnitude of fluctuation in motion sickness susceptibility across women’s menstrual cycle (Golding et al., 2005). However, in the Chinese culture, the information of a woman’s menstrual cycle is very private. Generally, it is very rude to ask a woman, especially an unmarried one, information about her menstrual cycle. Most of the female subjects recruited in the two experiments were single females. Therefore, there was no way to perfectly control the individual subject’s motion sickness susceptibility across different drum velocity conditions that was experienced in different days without knowing information about the menstrual cycles.

It was known that the female subjects had the highest susceptibility during the period of “menstruation” (Golding et al., 2005). Usually during menstruation, women experience some unpleasant symptoms, such as tiredness and menstrual pain. Therefore, the pre-exposure simulator sickness questionnaire (see details in Section 4.4.3.2) is used to quantify the pre-exposure health state of the subjects. If a subject reported “moderately” for any symptom of the pre-exposure SSQ, her experiment

session would be delayed and she was required to come back on another day. In fact, the experimenter contacted each subject several hours before each experiment run to check their general state of health so that such schedule delays rarely happened. It was hoped that such control could avoid making female subjects experience any experimental condition during their menstruation, which could bias the results of experiments one and two. Moreover, the balanced Latin square (see details in Chapter 5) used to dampen the learning effect or order effect in experiments one and two, also helped alleviate the bias resulting from such motion sickness susceptibility fluctuations across the menstrual cycle.

Last but not least, all subjects were kept in the dark with regards to the hypothesis under investigation to avoid psychological hinting as much as possible. For experiment one, subjects were told that the objective was to measure how well they could maintain eye fixation given a disturbing visual background. For experiment two, subjects were told that the objective was to measure their involuntary eye movements triggered by a rotating visual pattern and to find the diameter of the central visual field that could fully suppress their vection perception.

4.5.3 Measures

This section gives details on methods or scales which were used in experiments one and two to measure sickness severity, vection perception, eye positions, visual acuity and motion sickness susceptibility.

4.5.3.1 Nausea severity

In experiments one and two, the subjective nausea severity level was measured by two methods over a 30 min exposure period at 2 min intervals. One method was the free modulus magnitude estimation (Stevens, 1971; McGee, 1998) and the other was a 7-point nausea rating (Golding and Kerguelen, 1992).

“Free modulus” means that there is no anchor point set for magnitude estimation in each experimental session. Subjects were requested to report how much their sensation of nausea was induced and how the strength of nausea changed over the 30 min by assigning a number. At the moment when a participant opened her eyes in a main experimental session, she should report “zero” if she did not have any sensation of nausea or report any number that she thought was appropriate if she had some sensation of nausea. At the 2 min intervals, the participant was requested to report another number representing her current nausea severity level. Participants were requested to make the ratios of the two successive non-zero number equal to the ratio

of two levels of nausea severity levels that they perceived at the corresponding time. In other words, a subject was required to double her reported non-zero number when she felt her nausea severity level double and half her reported non-zero number when she felt her nausea severity level was half reduced. Subjects had the freedom to assign the number in any format. The only restriction imposed on the numbers assigned was that they should be positive. The experiment reminded the subject of her last assigned number 2 min before she reported a new number.

“Free modulus” was preferred for the nausea severity magnitude estimation than the “fixed modulus” in experiments one and two. In general, it is difficult to set an anchor point for nausea severity magnitude estimation without introducing the confounding factor of motion sickness adaptation. It originates from the fact that provocation of nausea needs a much longer time, relative to the time needed forvection perception. Moreover, some low susceptibility subjects can report zero nausea severity after a long exposure time to the rotating drum. There was no way to set a common anchor point for these types of subjects. Such potential subject screening in the “fixed modulus” magnitude estimation would never happen in the “free modulus” magnitude estimation of nausea severity.

Since no common anchor point was provided in the free modulus magnitude estimation, the raw ratio scale data needed to be adjusted to a common modulus for eliminating related inter-subject and intra-subject variability. The data conversion method adopted was the modulus equalization by Stevens (Stevens, 1971). Since a new scale was created for each subject in each condition, each time series of nausea ratio scale data was defined as a set for data conversion in modulus equalization. The steps of modulus equalization are listed below:

1. Convert raw data estimates to their logarithmic values.
2. Calculate the mean of each set of log estimates to obtain each set modulus.
3. Calculate the mean of all the log estimates to obtain the common modulus.
4. Subtract the common modulus from each set modulus to obtain the constant offset of each set from the common modulus.
5. Subtract the set constant from the log estimates in each set to obtain normally distributed data adjusted to a common modulus.
6. Take the antilog of all the normally distributed adjusted data values to obtain data ready for parametric analysis.

The transformed ratio scale data can be compared across subjects and conditions.

The transformed data, rather than the raw data, was used in model simulation and data analysis.

It should be noted that all subjects had practiced the free modulus magnitude estimation method by estimating the lengths of 20 lines (from 1 cm to 20 cm at a stepping change of 1 cm) presented in random order on 20 sheets of paper right before each experimental session. Regression analysis was implemented immediately to obtain the R square. If the R square value was smaller than 0.9, then the subject was requested to do the test again until her R square value was no less than 0.9. No subject was found to have difficulties in using the free modulus magnitude estimation method to estimate line length.

The 7-point nausea rating has been used by several studies to capture successive ratings of motion sickness experienced over time (Webb and Griffin, 2002; 2003). To avoid confusion potentially caused by reporting nausea severity level that used two different methods, subjects were requested to report A to G instead 0 to 6 as shown in Table 4.1.

Using these two methods to measure nausea severity simultaneously has three advantages. First, the ratio scale data can capture minute changes of nausea severity within each level of the 7-point nausea rating. Secondly, the categorical data helps

attach certain meanings to corresponding ratio scale numbers. Thirdly, the experimenter can cross check the nausea severity reported by subjects in two different methods so that some human errors can be identified instantaneously and appropriate corrections can be made. For example, if a subject reports the same number (free modulus magnitude estimation) with the one reported 2 minutes ago while she reports a different rating in the 7-point nausea rating scale, it means that this subject made a mistake in self-reporting subjective nausea severity. Under this circumstance, the experimenter will notice that the subject has made a mistake and she will need to report the nausea severity level again in an appropriate way.

Table 4.1 7-point nausea rating scale proposed by Golding and Kerguelen (1992). Subject reported A-G instead of 0-6 to avoid confusing numbers from the free-modulus magnitude estimation and numbers from the 7-point nausea rating

Reporting	Rating	Description
A	0	No symptoms
B	1	Any symptpom, however slight
C	2	Mild symptoms (e.g. stomach awareness, but no nausea)
D	3	Mild nausea
E	4	Mild to moderate nausea
F	5	Moderate nausea but can continue
G	6	Moderate nausea and want to stop

4.5.3.2 Simulator Sickness Questionnaire (SSQ)

The SSQ employing a 4-point rating scale (0=none, 1=slight, 2=moderate, 3=severe)

to indicate 21 motion sickness symptoms that was also used to measure VIMS severity. (Kennedy *et al.*, 1993, Appendix 4-1) Participants were asked to complete a pre-exposure SSQ before each exposure and a post-exposure SSQ right after each exposure, from which one total score (SSQ-Total Score) and three sub scores (SSQ-Nausea, SSQ-Oculomotor, SSQ-Disorientation) indicating VIMS severity level could be calculated to quantify the severity level of VIMS. (Kennedy *et al.*, 1993, Appendix 4-2)

As discussed in Section 4.4.2, pre-SSQ was used to control the pre-exposure health state of subjects across 4 conditions. A subject reporting “moderate” for any symptoms of pre-exposure SSQ was asked to come back on another day in order to avoid bias caused by potential intra-subject variability of the pre-exposure health state across conditions. ANOVA analysis and post-hoc SNK test on pre-SSQ total scores and 3 sub scores helped reveal whether the health state of the subjects right before commencing an experiment had a significant fluctuation over 4 drum rotation velocity conditions conducted on different days. ANOVA analysis and post-hoc SNK test on post-SSQ scores was used to examine whether drum rotation velocity had a significant main effect on VIMS assuming that the pre-exposure health states of the subjects for the 4 conditions were not significantly different from each other. Aside

from that, the SSQ difference scores (post-pre scores) representing the change in symptoms over the whole exposure period was analyzed in the same way as well. Kennedy et al. (1993) argued against the use of post-pre scores since SSQ employs a category scale rather than ratio scale. However, post-pre scores have been used by other researchers (Chen, 2006; Diels, 2008). Therefore, data analysis on post-pre scores was documented in this study simply for comparison.

4.5.3.3 Vection velocity and vection intensity

In experiment one, vection velocity (perceived self-rotation velocity) was measured by the fixed modulus magnitude estimation method. (Stevens, 1971, Kennedy et al., 1996) For the purpose of setting an anchor point for the vection velocity magnitude estimation, before the main testing in experiment one, the subject was exposed to a pre-test that was up to 90 sec in which the subject viewed the same rotating drum in the main test. If the subject experienced vection saturation; i.e., a visual illusion that she was the one rotating and the drum was still (Hu et al., 1989), she was requested to take this level of vection velocity as reference “100”. If the subject did not experience vection saturation during the 90 sec pre-test, she was requested to take the initial perceived drum rotation velocity as reference “100”. It is worth mentioning that all of the subjects who were randomly recruited for experiment one experienced

vection in the pre-test. There was a 5 min rest period in between the pre-test and main test. During the main test, subjects were requested to continuously report a number representing their vection velocity (perceived self-rotating velocity) using an appropriate reference. For example, if a subject experienced vection saturation in a pre-test, she needed to report 100 when she experienced vection saturation again or report 50 when she perceived a half reduced vection velocity during the following main test. “Free modulus” was not employed in this case since the absolute self-rotation velocity in the unit of degree per second (dps) was the measure of interest in experiment one.

In experiment two, the vection intensity defined as the degree of “compellingness” of the sensation of body rotation (Brandt et al., 1973) was measured at 2 min intervals by a 4-point vection scale as shown in Table 4.2 (Webb and Griffin, 2002): 0=drum only; 1=drum and self (intermittent); 2=drum and self (continuously); 3=self only. This measure was taken to monitor whether vection perception had been fully suppressed over the 30 min exposure period.

Table 4.2 4-point vection rating scale (Webb and Griffin, 2002)

Perception of what is moving	Meaning
Drum only	You perceive that the only thing moving is the drum (with opposite rotating central and peripheral visual fields)
Drum and self (intermittent)	You perceive the drum to be moving but also experience periods of self motion
Drum and self (continuously)	You perceive the drum to be moving and simultaneously experience continuous self motion
Self only	You perceive the drum to be stationary and experience continuous self motion only

4.5.3.4 EOG records of optokinetic nystagmus (OKN)

In both experiments, the eye position data in the horizontal and vertical plane were continuously recorded using EOG (Electro-oculography) during each exposure session. In experiment one, EOG recording was used to monitor whether OKN was fully suppressed by eye fixation. In experiment two, OKN related eye position data was used to calculate OKN slow-phase velocity (SPV), OKN gain was defined as OKN SPV over drum rotation velocity, and the foveal retinal slip velocity defined as the rotation velocity of central visual field minus OKN SPV. OKN was identified as a sequence of repetitive eye movement cycles consisting of a quick saccade (fast-phase OKN) followed by a relatively smaller change in amplitude over a longer duration (slow-phase OKN).

The unit of the raw eye position data is volt (V). To transform V into degree, eye calibration was run before each experiment session for each subject in experiment two. Subjects were asked to horizontally move their eyes across a pair of black and white stripes (subtending 15 deg) back and forth for 3 times. Considering that the OKN followed the direction of the central visual field which moved to the left of the viewer, eye calibration first started with a rotation to the left of the viewer then followed by a rotation to the right of the viewer (defined as one cycle). A subject was requested to complete 3 cycles. The horizontal and vertical eye position data are recorded as illustrated in Figure 4.4.

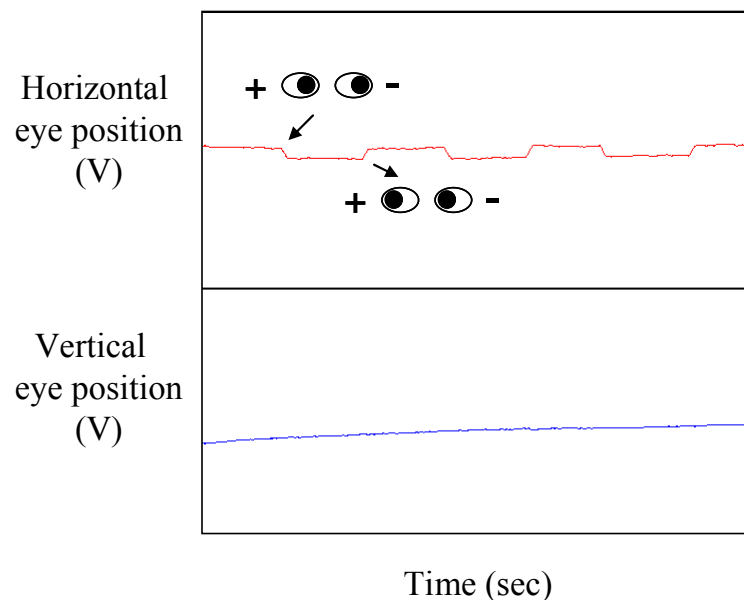


Figure 4.4 Horizontal and vertical eye position time courses recorded in an eye calibration session. Since the positive electrode was attached to the right temple of the subject and the negative electrode was attached to her left temple, eye position signal decreased when her eyes rotated to the left and vice versa.

The eye position signal decreased when eye balls moved to the left of the viewer and increased when eye balls moved to the right of the viewer. The EOG data in the horizontal channel showed that the subject correctly followed instructions from the experimenter and EOG data in the vertical channel showed that there was no cross-talk between two channels. The average of six voltage changes each generated by one eye rotation was named as an EOG unit mapping constant, used to transform EOG records of experiment two from a unit of V into a unit of degree. In other words, if the EOG unit mapping constant of a subject was equal to 1V, 1V EOG signal change captured in the 30 min main test meant a 15 deg eye rotation for the subject. It should be noted that eye calibration was implemented before each experiment session for each subject since the EOG unit mapping constant of the same subject could be a bit different due to minute differences in attachment positions of EOG electrodes in the 4 conditions.

After the EOG unit mapping constant was calculated for each experiment session, OKN SPV was derived from raw EOG signal by a matlab-based algorithm. First, raw EOG signal was passed into a first-order low pass filter having a cut-off frequency at 10Hz to move high frequency noise. OKN frequency in all velocity conditions was smaller than 5Hz, therefore; no OKN information was thrown away. Secondly, all of

the OKN cycles within the first 3 sec were compared to identify the one slow-phase component having the slowest slope. Three sec was larger than the mean charge time of the OKNe component reported by Robinson (1981). This minimum slope (in a unit of volt per sample) was considered to be the lower bound of OKN SPV of the whole time series (Equation 4-1). The upper bound (in a unit of volt per sample) is a value calculated from corresponding drum rotation velocity, sampling rate of EOG records, and the ratio of the EOG unit mapping constant to 15 degree (Equation 4-2):

$$\text{Lower Bound of SPV} = \min \{(\text{voltage changes of each OKN slow-phase component within the first 3 sec} / \text{the number of data samples covered by that component})\} \quad (4-1)$$

$$\text{Upper Bound of SPV} = (\text{drum velocity} / \text{sampling rate}) \times (\text{the EOG unit mapping constant} / 15 \text{ deg}) \quad (4-2)$$

Thirdly, the OKN cycles were distilled from the raw time series knowing the lower bound and upper bound. Finally, the SPV (degree per second) of each successive sample pair in the new time series is calculated by Equation 4-3:

$$\text{SPV} = \text{voltage change between the pair of successive samples} \times \text{sampling rate} \times 15 \text{ degree} / \text{the EOG unit mapping constant} \quad (4-3)$$

After the OKN SPV time series were derived from the raw EOG signal, OKN gain time series and foveal retinal slip velocity time series were derived by definition.

4.5.3.5 Visual acuity at near point and motion sickness susceptibility

For both experiments one and two, visual acuity at the near point for the left eye, right eye and both eyes were measured for each participant right before the first experiment run in a light tight environment. Subjects inspected 14 sets of Landolt rings in sequence, from the largest to the smallest set, and reported which ring was unbroken among the four in the same set. Visual acuity was scored on a scale from 1 (20/200-low visual acuity) to 14 (20/13-high visual acuity) where 14 meant subjects gave correct answers for all 14 sets and 1 meant subjects only gave correct answers for the first set. The experimenter stopped the test after 2 consecutive wrong answers. All subjects in experiments one and two had visual acuity higher or equal to 9 (20/22) for both eyes.

Before commencing experiment one or two, previous susceptibility to motion sickness was taken by asking subjects to fill in a motion sickness susceptibility survey questionnaire (So et al., 1999, Appendix 4-3) and a MSSQ-short questionnaire (Golding, 2006, Appendix 4-4). For the motion sickness susceptibility survey, subjects were requested to classify their previous susceptibility to motion sickness into one of the following categories: “Not at all”, “Slightly”, “Moderately”,

and “Very Extremely”. The MSSQ-short was a revised version (only 18 items on one page) of the MSSQ-Long (54 items on two and a half pages) with a compromise between length and validity. The questionnaire asked for frequency of previous motion sickness occurrences in cars, buses, trains, aircraft, small boats, ships, swings, roundabouts and big dippers for ages up to 12 and for the past 10 years, respectively. The frequency of previous motion sickness occurrences were classified into 5 categories: “Not Applicable-Never Traveled”, “Never Felt Sick”, “Rarely Felt Sick”, “Sometimes Felt Sick”, and “Frequently Felt Sick”. A MSSQ-short raw score (possible range from a minimum of 0 to a maximum of 54) was derived from the MSSQ-short questionnaire to quantify previous susceptibility to motion sickness. (Appendix 4-4) The MSSQ-short raw score of experiment one 19.5 (SD=12.6) and score of experiment two 14.6 (SD=7.6) were larger than the female mean MSSQ-short 13.93 (SD =10.37) reported in Golding (2006). This result was expected since Chinese females were reported to be hypo-susceptible in comparison to females of other races (Stern, et al., 1996).

The motion sickness susceptibility survey questionnaire and MSSQ-short questionnaire were used simultaneously for cross-checking. It should be noted that the susceptibility measured by both methods are previous susceptibility to motion

sickness rather than the current susceptibility as discussed in Golding (2005) which can be different for the same female subject during her menstrual cycle. As discussed in Section 4.4.2, pre-SSQ was used to quantify the current susceptibility (or pre-exposure health state) of each subject before each exposure period.

CHAPTER 5

EXPERIMENT ONE: VECTION AND VIMS AS A FUNCTION OF ROTATION VELOCITY OF AN OPTOKINETIC STIMULI IN THE ABSENCE OF OKN

SUMMARY

Recently, the competing roles of vection and OKN in VIMS generation are a bone of contention between two camps of researchers who favor one over the other. A review of literature indicates that the effect of rotation velocity of optokinetic stimuli on VIMS severity with vection, but without OKN has not been studied. To fill this gap and collect ratio scale data for validating model one, an experiment is conducted. Fourteen participants were exposed to an optokinetic stimuli consisting of vertical oriented black and white striped pairs of unequal width (Hu et al., 1989; Stern et al., 1990) rotating along the earth-vertical axis at a constant velocity of 0 degree per second (dps), 2 dps, 14 dps and 34 dps. OKN was suppressed across all 4 conditions by eye fixation. Consistent with implications from the VISM theory (see Chapter 1) and related neural mechanisms (see Chapter 2), vection velocity is found to be significantly correlated with VIMS severity and also mediated a significant main effect on VIMS severity in the absence of OKN. Unexpectedly, a monotonic

increasing relation between rotation velocity of the optokinetic stimuli and VIMS severity instead of a curvilinear relation is found in experiment one. Possible reasons were documented. Since both ratio scale and ordinal nausea data were collected, a comparison of the data can form a reference for future VIMS studies.

5.1 Objective and hypotheses

The objective of this experiment is to study the relation betweenvection and VIMS severity in the absence of OKN while watching a wide FOV simulated optokinetic drum pattern rotating in the yaw direction around the earth-vertical axis. It is hypothesized that the rotating velocity of the patterns has a significant main effect on thevection velocity (perceived self-rotating velocity) (H1.1) and VIMS severity level (H1.2) withvection and without OKN. Based on implications from Hu et al. (1990), it is hypothesized that the relation between the rotation velocity of the optokinetic stimuli and nausea ratio scale data (H2.1) can be described by a high-order polynomial function peaking at a rotation velocity of 14 dps. Based on the results of Kennedy et al. (1996), the relation between the rotation velocity of the optokinetic stimuli andvection velocity is hypothesized to be described by a first-order polynomial (linear) function (H2.2). Last but not least, it is hypothesized that the relation between thevection velocity and nausea ratio scale data can be described by a high-order polynomial function (H2.3).

5.2 Methods

5.2.1 Participants

Fifteen Chinese females participated in experiment one. These subjects were university students ranging from 22 to 28 years of age. Each one was paid for her participation. All of the participants were consenting volunteers who were healthy and free of medication or illness. The Human Subject and Research Ethics Committee at the Hong Kong University of Science and Technology approved the experiments. Fourteen out of the fifteen subjects were involved throughout the whole experiment. One subject quit the experiment after experiencing a condition related to high photosensitivity. The phenomenon of photosensitivity will be discussed in detail in Section 5.3.3. Therefore, the data from 14 subjects were used in the data analysis. The mean MSSQ-Short raw score for the participants in experiment one was 19.5 (SD=12.6), indicating that a sample with only Chinese females are more susceptible to motion sickness than the average population (see Section 4.5.3.5).

5.2.2 Visual stimuli

The visual stimuli used to provoke vection and VIMS was a vertical black and white visual pattern rotating in a yaw direction along the earth-vertical axis at a constant

rotation velocity projected on a cylindrical screen. Each pair of black and white stripes subtended a 15 degree field of view (FOV) with a 9.3 degree black stripe and a 5.7 degree white stripe. The same visual pattern, printed on wallpaper and attached to the inner wall of a cylindrical metal drum (named as an optokinetic drum or circularvection drum), was used by Hu et al. (1989) to investigate the effect of the rotation velocity of the optokinetic stimuli on VIMS in the presence of bothvection and OKN. A red eye fixation point subtending 1 degree FOV on a projection screen was positioned in the subjects' line of sight to fully suppress OKN.

5.2.3 Design of experiment (DOE)

As illustrated in Figure 5.1, experiment one has 4 conditions, each administered in 30 min sessions: A) viewing the static optokinetic drum pattern with eye fixation; B) viewing the rotating optokinetic drum pattern with eye fixation at 14 dps rotation velocity; C) viewing the rotating optokinetic drum pattern with eye fixation at 34 dps rotation velocity; D) viewing the rotating optokinetic drum pattern with eye fixation at 2 dps rotation velocity. Experiment one used a within-subject design in consideration of high inter-subject variations invection perception and VIMS severity. A balanced Latin square (4 levels) technique (Appendix 5-5) was used to counterbalance the order of the presentation of the 4 rotation velocities to each

subject. Fourteen participants were randomly assigned a condition that had 4 possible sequence of orders. To dampen the effect of habituation, the time interval between the two experiment runs for each subject was at least 7 days.

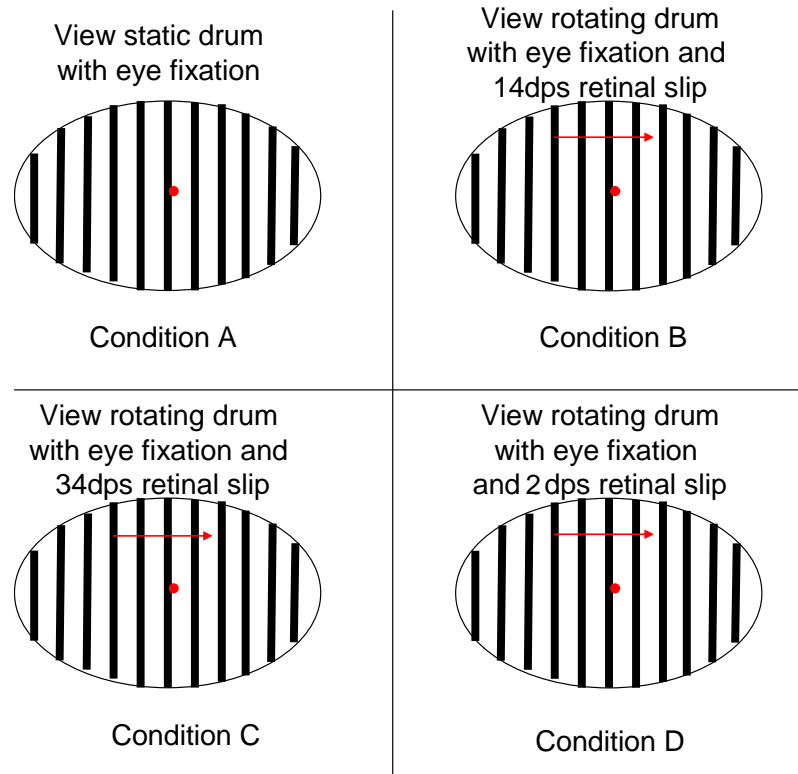


Figure 5.1 The 4 conditions of experiment one. The arrows in red are added in the figure to show the direction of rotation. The red dot subtending 1 deg at the eye is used for eye fixation.

The 3 non-zero velocity conditions were chosen on purpose to make the retinal slip velocity of each condition; that is, 2 dps, 14 dps and 34 dps, closer to the retinal slip velocity levels of 30 dps, 60 dps and 90 dps rotation velocity conditions in Hu et al. (1989) as much as possible respectively. Since Hu et al. (1989) did not report OKN gain or OKN slow-phase velocity (SPV) in each velocity condition, the mapping

between the retinal slip velocity and rotation velocity was calculated based on OKN gain data reported by Koenig et al. (1978), which has a similar experiment setting as that of Hu et al. (1989); i.e., rotating circularvection drum having 24 pairs of black and white stripes. The condition with 1.35 dps retinal slip velocity corresponding to 15 dps rotation velocity in Hu et al.(1989, was not selected since this value was calculated from a hypothetical OKN gain equal to the one of 30 dps rotation velocity. This was because Koenig et al. (1978) did not investigate OKN gain in the 15 dps rotation velocity condition.

Table 5.1 Velocity conditions in Hu et al. (1989) and their corresponding retinal slip velocities calculated by using OKN gains reported by Koenig et al. (1978).

Drum speed (dps) (Hu et al., 1989)	OKN gain (Koenig et al., 1978)	OKN spv (dps)	Retinal slip velocity (dps)
15	0.91*	13.65	1.35
30	0.91	27.3	2.7
60	0.72	43.2	16.8
90	0.63	56.7	33.3

* 15 dps drum rotating velocity was not investigated in Koenig et al.(1978). Its OKN gain is assumed in this table to be equal to the one of 30 dps drum rotating velocity.

5.2.4 Procedure

First, participants were requested to read experiment one instructions (Appendix 5-6). Secondly, participants read and signed a consent form (Appendix 5-7). Thirdly, a line length estimation test that included 20 line segments with different lengths was

implemented to provide familiarity with the free modulus magnitude estimation method (Stevens, 1971; McGee, 1998). Fourth, visual acuity at the near point for both eyes and each individual eye were measured and recorded following the instructions of the vision tester menu (Appendix 5-8). Fifth, the participant was requested to complete a motion sickness susceptibility survey questionnaire (So et al., 1999, Appendix 4-3) and a MSSQ-short questionnaire (Golding, 2006, Appendix 4-4) to indicate their previous susceptibility to motion sickness. Sixth, participants completed a pre-exposure Simulation Sickness Questionnaire (SSQ, Appendix 4-1) after becoming familiar with the literal meanings of various VIMS symptoms. Seventh, a subject viewed a constant rotating optokinetic drum pattern for 30 mins. She was requested to report her subjective nausea severity level using the free modulus magnitude estimation (Stevens, 1971; McGee, 1998) and 7-point nausea rating (Golding & Kerguelen, 1992) every 2 min. For conditions B, C and D, the subject was also requested to continuously report her vection velocity (perceived self-rotating velocity) continuously using the fixed modulus magnitude estimation method (Stevens, 1971, Kennedy et al., 1996). Therefore, right before the main testing of conditions B, C and D, the subject would be exposed to a pre-test up to 90 sec for the purpose of identifying an appropriate anchor point for vection velocity magnitude estimation. There was a 5 min break in between the pre-test and main test.

The EOG electrodes were worn after the rest period and right before the main test. Then the subject was requested to close her eyes until the experimenter asked her to open her eyes and maintain eye fixation. The EOG recording started at the moment when the subject opened her eyes for the main test. The experimenter terminated the visual stimuli and EOG recording up to 30 mins or a time point at which the subject wanted to stop the exposure immediately (reporting a rating of 6 on the 7-point nausea scale). Finally, the subject completed a post-exposure SSQ (Appendix 4-1).

5.2.5 Measures

Visual acuity at near point and previous susceptibility to motion sickness were measured before the first experiment session. It should be noted that these two measurements are used to quantify characteristics of the group of participants, but not used for subject screening.

During the 30 min exposure period, participants rated their nausea severity every 2 min using the free modulus magnitude estimation and 7-point nausea rating. The raw ratio scale data from free modulus magnitude estimation were then transformed by modulus equalization so that the transformed ratio scale data were comparable across different subjects and experimental conditions.

Vection velocity, defined as the perceived velocity of illusion of self-rotation, was measured by fixed modulus magnitude estimation continuously during the 30 min exposure. In other words, a subject was requested to report a new number as long as she felt any change of vection velocity. The individual latency of vection onset, vection build-up time and “average” vection velocity over the exposure time were measures of interest.

EOG signals recording horizontal and vertical eye movements were acquired continuously over the whole exposure period. Horizontal eye position time series was used to monitor whether OKN was fully suppressed over the whole exposure period. It was possible to check whether the eyes of the subject were open by monitoring the vertical eye position time series which recorded every eye blink. If a subject attempted to cheat by closing her eyes, her vertical eye position time series would be a flat line. No subject was found to close her eyes except for normal eye blinking.

Before and after each experimental session, the SSQ was completed by each participant. The total score and 3 sub-scores of pre and post SSQs were used to

quantify pre-exposure and post-exposure states of health. As discussed in Section 4.5.3.2, no subject is allowed to commence an experiment session if she reported any “moderate” symptoms.

5.2.6 Statistical analysis

ANOVA was performed to test the main effect of the rotation velocity of the optokinetic stimuli on vection velocity and parametric VIMS severity measures. Normality test (Anderson-Darling) was performed to check whether the normality assumption of ANOVA was satisfied. For normal distribution, Bartlett’s variance homogeneity test was performed to check whether equal variance assumption of ANOVA was satisfied. Levene’s variance homogeneity test without assumptions of normal distribution was used as the alternative to Bartlett’s test if data was non-normal. If applicable, the Box-Cox method was used to select a transformation parameter (λ) generating the minimum error sum of square ($SS_E(\lambda)$). If either assumption (or both) was not satisfied or the data were non-parametric, the Friedman Test (a nonparametric analysis of a randomized block experiment) was used as the alternative to ANOVA. Student-Newman-Keuls (SNK) post-hoc test and Wilcoxon sign-rank test were used to determine which of the means in the 4 conditions were different. The effects model of ANOVA (or Friedman test) is:

$$y_{ij} = \mu + \alpha_i + \tau_j + \varepsilon_{ij}$$

where $i=1, 2, 3, 4$ and $j=1, 2, \dots, 14$. The rotation velocity is the main factor α . The subject is random factor τ . The VIMS severity (7-point nausea rating, nausea ratio scale and SSQ scores) measures or the vection velocity is the dependent variable y . The model does not include an interaction term due to the lack of degree of freedom.

Pearson's (r) correlation was employed to test the significance of a linear relation between parametric and normal distributed measures. Spearman's (rho) correlation was used as the alternative to Pearson's correlation if the data were non-normal or non-parametric.

5.3 Results

The results for normally distributed variables are expressed as the mean \pm SD and continuous variables with non-normal distribution are presented as the median value (interquantile interval).

5.3.1 EOG recording data

In experiment one, OKN needed to be fully suppressed to investigate the effect of rotation velocity on VIMS in the presence of vection alone. The method used to

completely suppress OKN was presented in Section 4.3. Individual horizontal eye position time series in all 4 conditions were visually inspected. No repetitive OKN pattern is found to occur in all 4 conditions, indicating that OKN is fully suppressed across the 4 conditions.

5.3.2 Vection velocity (perceived self-rotation velocity)

Following the stimuli onset of experiment one, all participants reported certain levels of vection velocity during each of the 3 non-zero rotation velocity conditions (see Appendix 5-1 for individual time series of vection velocity). Figure 5.2 shows the median of the vection velocity time series for 14 subjects in 3 non-zero rotation velocity conditions. The “average” and individual vection velocity time series all show a noticeable fluctuation among the time axis, which is different from the quality pattern consisting of only three stages (onset, buildup, saturation), as reported by Brandt et al. (1973). The exposure duration in this study was 30 mins which is much longer than the 30 sec exposure duration used by Brandt et al. (1973). It is possible to explain this discrepancy between the results of Brandt et al. (1973) and this study by this exposure duration difference.

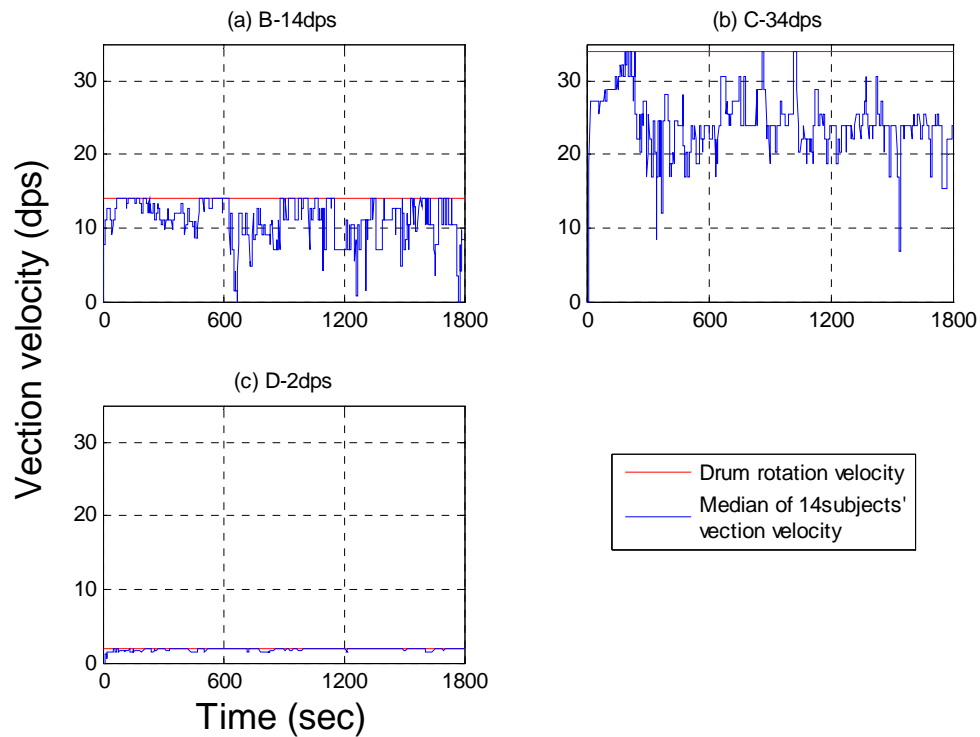


Figure 5.2 Vection velocity (median of 14 subjects) as function of exposure duration for 3 non-zero rotation velocity conditions: rotating at (a) 2 dps, (b) 14 dps, and (c) 34 dps.

First, individual data show that not all subjects can eventually reach vection saturation (a visual illusion where a subject felt that she was rotating and the optokinetic drum pattern was still) eventually over 30 min of exposure to the rotating optokinetic drum. Among the 14 subjects, 6 subjects did not reach vection saturation in one or more conditions while the other 8 subjects experienced vection saturation in all conditions. Secondly vection velocity could still drop after vection saturation, even back to zero, and sometimes increased back to vection saturation again. Therefore, vection onset is defined in this study as the first time interval from zero to the non-zero vection velocity. Latencies of vection onset in 2 dps, 14 dps, and 34 dps

rotation velocity conditions were 12.5 sec (7.5-25.5), 8 sec (4.25-20), and 11.5 sec (7.5-19.75), respectively. Thirdly, vection build-up time was originally defined as the time interval from first non-zero vection to the vection saturation (Brandt, et al., 1973). In this study, vection build-up time is defined as the time interval from the first non-zero vection velocity to the average level of vection velocity over exposure time since not all subjects reached vection saturation in the end. Vection build-up time in 2 dps, 14 dps and 34 dps rotation velocity conditions were 1 sec (1-1), 1 sec (1-1), and 5 sec (1-85.25), respectively.

The average level of vection velocity over 30 mins in 2 dps, 14 dps, and 34 dps rotation velocity conditions are 1.43 ± 0.53 dps, 8.91 ± 3.94 dps, 21.43 ± 6.47 dps (see Table 5.2), respectively. As illustrated in Figures 5.3 and 5.4, all vection velocity data are normal distributed (in each case $p > 0.05$) while the equal variance assumption is not satisfied. After the quarter-root transformation, the equal variance assumption is satisfied while sacrificing the normality of vection velocity in the 2 dps rotation velocity condition ($p < 0.05$). The Friedman test shows that the rotation velocity of the optokinetic stimuli has a significant main effect on the vection velocity ($p < 0.01$). Such results indicate that H1.1 should not be rejected. A post-hoc analysis of both transformed and non-transformed data shows that (i) vection velocity in the 34 dps

condition is significantly higher than in the other two conditions and (ii) vection velocity in the 14 dps condition is significantly higher than in the 2 dps condition ($p < 0.05$) (See Table 5.3).

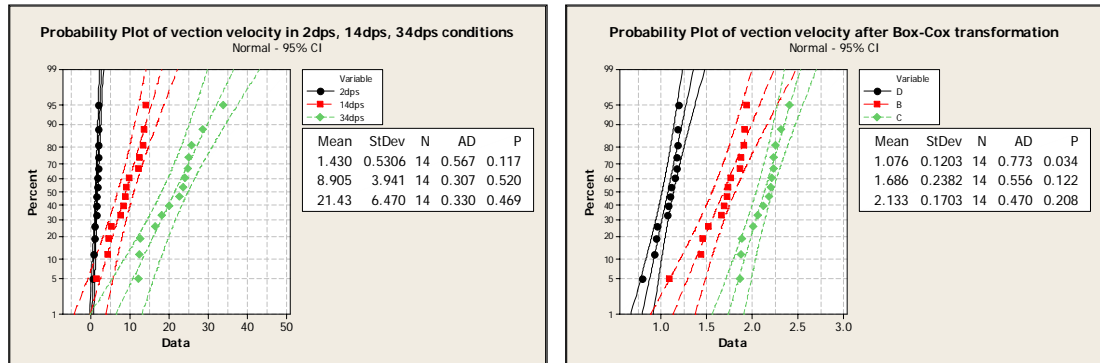


Figure 5.3 Normality test of vection velocity (average over 30 min) (a) before Box-Cox transformation ($\lambda=0.25$) (b) after Box-Cox transformation ($\lambda=0.25$) for rotation velocity condition of 2 dps, 14 dps and 34 dps

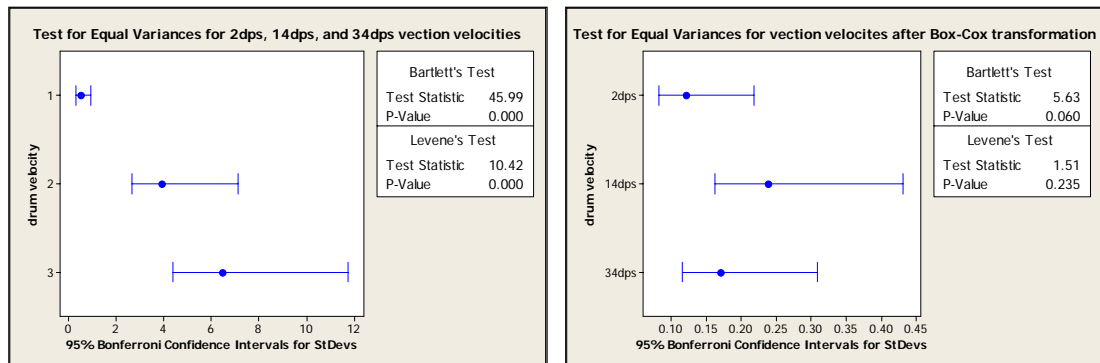


Figure 5.4 Variance homogeneity test of vection velocity (average over 30 min) (a) before Box-Cox transformation ($\lambda=0.25$) (b) after Box-Cox transformation ($\lambda=0.25$) for rotation velocity condition of 2 dps, 14 dps and 34 dps

Table 5.2 Vection velocity averaged over 30 min in 3 non-zero velocity conditions

Subject	2dps	14dps	34dps
1	1.7	9.8	24.1
2	1.9	5.3	24.7
3	1.3	12.1	25.8
4	0.8	13.6	20.1
5	1.5	4.6	12.1
6	0.4	4.3	12.4
7	0.9	8.9	23.5
8	2	13.4	22.7
9	2	1.4	28.6
10	1.4	9	16.4
11	1.9	7.7	18.2
12	2	14	25.1
13	0.8	8.2	12.6
14	1.5	12.4	33.8

Table 5.3 Student-Newman-Keuls (SNK) tests on the effects of rotation velocity on vection velocity (average over 30 min) (a) before Box-Cox transformation ($\lambda=0.25$) (b) after Box-Cox transformation ($\lambda=0.25$) for rotation velocity condition of 2 dps, 14 dps and 34 dps

drum velocity	N	Subset		
		1	2	3
2dps	14	1.429741	8.905321	21.42571
14dps	14			
34dps	14			
Sig.		1.000	1.000	1.000

(a) Dependent variable: vection velocity before transformation

drum velocity	N	Subset		
		1	2	3
2dps	14	1.08	1.69	2.13
14dps	14			
34dps	14			
Sig.		1.000	1.000	1.000

(b) Dependent variable: vection velocity after transformation

Consistent with the results of Kennedy et al. (1996), there exists a linear relationship between the vection velocity (y) and rotation velocity of the optokinetic stimuli (x).

Such linear relation is described by a first-order polynomial function:

$$\begin{aligned} y &= ax + b \\ a &= 0.63(p < 0.05) \\ b &= 0.09(p > 0.05) \end{aligned} \quad (5-1)$$

where R square and Adjusted R square = 0.84. Such result indicates that H2.2 should not be rejected (see Figure 5.5). The value of slope ($a=0.63$) is lower than what was reported by Kennedy et al. (1996) ($a=0.98$). It is worth pointing out that the velocity conditions of 2 dps and 14 dps were not investigated in Kennedy et al. (1996).

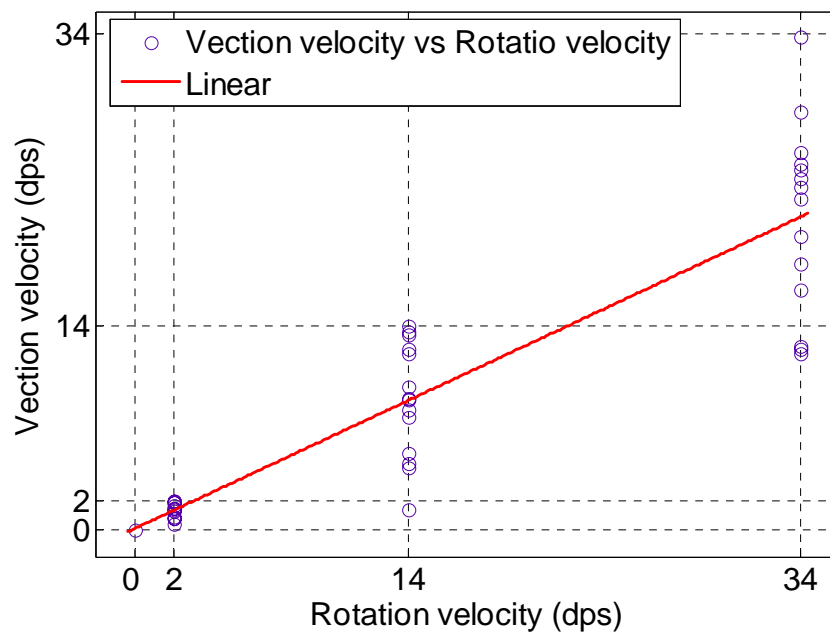


Figure 5.5 Linear relationships between the vection velocity and the rotation velocity of the optokinetic stimuli

5.3.3 7-point nausea rating

Individual data regarding the time course of nausea severity measured by the 7-point nausea rating are shown in Appendix 5-2. An experiment session was stopped at the moment when a subject reported G (i.e. 6 or “moderate nausea and want to stop”)

and a rating of 6 was assigned for the remaining period. In this study, a subject who reached a rating of 3 (“mild nausea”) or higher was considered as “sick” and considered as “not sick” if the maximum rating reached was 2 or lower. Three subjects out of the 14 subjects became sick in the 0 dps rotation velocity condition. It should be noted that 0 dps condition was the first repetition for all 3 subjects. Such results indicate that sickness is generated without any “motion” of visual stimuli. This phenomenon is initially suspected to be a type of photosensitivity (pattern sensitivity).

Pattern sensitive epilepsy consists of seizures triggered by viewing patterns, typically with equally wide black and white stripes with a spatial frequency in a range of 2 to 4 cycles per degree (cpd) and a flash rate in a range of 13 to 21 Hz. (Harding & Harding, 2007) However, neither the spatial frequency (0.067cpd) nor the flash rate (60Hz) of the static visual stimuli in experiment one was in such a photosensitive range. Moreover, the black (5.7 deg) and white (9.3 deg) stripes used in this study had unequal widths. Visual inspection of corresponding video clips of the 3 subjects did not find common seizure associated symptoms; i.e., convulsions, absences and brief myoclonic attacks (Binnie and Wilkins 1998). It was also noticed that the level of the 3 nausea rating time courses decreased after reaching a rating of 3 instead of

continuing to increase. All of these evidences indicate that the sickness provoked in the static condition was less likely to be a type of pattern sensitivity. Professor Graham Harding, one of the top researchers of photosensitive epileptic seizures, was consulted on this matter during the implementation of experiment one. The professor did not have an objection to recruiting the 3 subjects in the VIMS experiment who could be potentially photosensitive epilepsy patients. Blocking one eye after an exposure session was recommended in order to relief discomfort possibly caused by pattern sensitive epilepsy.

As shown in Figure 5.6, the time courses of the median 7-point nausea rating in 0 dps and 2 dps conditions never reach the rating of 3 while the one for the 14 dps and 34 dps conditions is able to do so. Both original nausea rating data (averaged over 30 mins) and transformed data ($\lambda=0.25$) fail to pass the normality test. The Friedman test shows that rotation velocity has a significant effect on the 7-point nausea rating ($p<0.01$). Such results indicate that H1.2 should not be rejected. A post-hoc test shows that (i) nausea rating in the 34 dps condition is significantly higher than the other 3 conditions (ii) nausea rating in the 14 dps condition is significantly higher than in the conditions of 0 dps and 2 dps. (See Table 5.4)

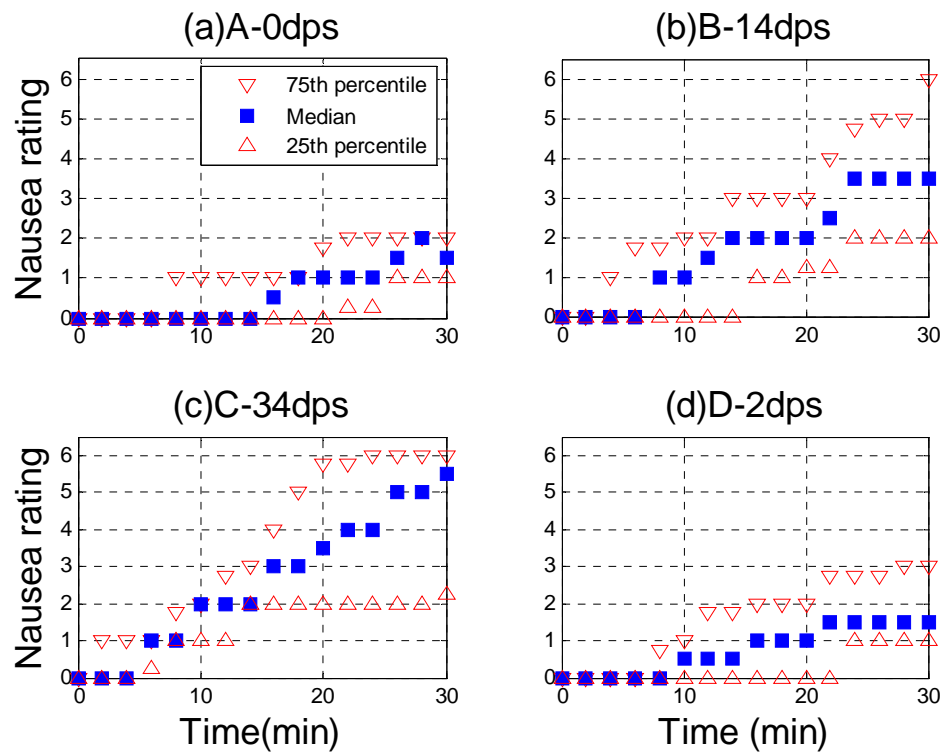


Figure 5.6 Median, 25th and 75th percentile of nausea rating as a function of exposure duration for 4 rotation velocity conditions: rotating at (a) 0 dps, (b) 14 dps, (c) 34 dps, (d) 2 dps

Table 5.4 Student-Newman-Keuls (SNK) test on the effect of rotation velocity on 7-point nausea rating data (average over 30 min)

drum velocity	N	Subset		
		1	2	3
0dps	14	.959821		
2dps	14	1.022321		
14dps	14		1.870536	
34dps	14			2.508929
Sig.		.798	1.000	1.000

Similar tests are used to analyze the nausea severity level at 30 min measured by the 7-point nausea rating. Both original nausea rating data (at 30 min) and transformed data ($\lambda=0.25$) fail to pass the normality test. The Friedman test shows that the rotation velocity has a significant effect on the nausea severity level at 30 min

measured by the 7-point nausea rating ($p<0.01$). Such results indicate that H1.2 should not be rejected. A post-hoc test shows (i) nausea severity at 30 min measured with the 7-point nausea rating in 14 dps and 34 dps condition is significantly higher than in 0 dps and 2 dps conditions.(ii) the nausea severity level in the 14 dps condition is not significantly different from the 34 dps condition (See Table 5.5). Such results are confirmed by results of Wilcoxon sign-rank test ($p<0.05$).

Table 5.5 Student-Newman-Keuls (SNK) test on the effects of rotation velocity on nausea severity at 30 min measured by 7-point nausea rating

drum velocity	N	Subset	
		1	2
0dps	14	1.71	
2dps	14	2.21	
14dps	14		3.71
34dps	14		4.36
Sig.		.278	.165

Spearman's correlation analysis shows that the nausea severity measured by 7-point nausea rating scale significantly correlates with the drum rotation velocity ($\rho=0.53$, $p<0.01$). Such Significant correlation and the observed linear increasing trend shown in Figure 5.7 indicate that the H2.1 should be rejected.

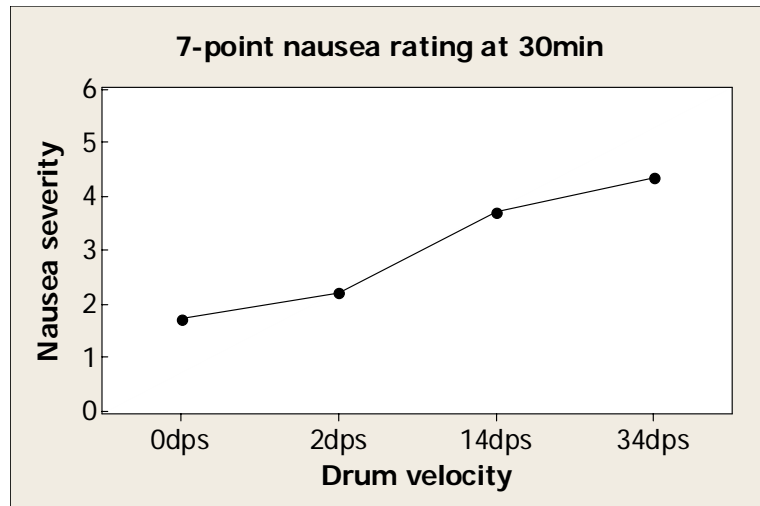


Figure 5.7 Observed linear increasing trend of 7-point nausea rating at 30min as a function of drum rotation velocity

5.3.4 Nausea ratio scale data

If an experimental session was stopped before 30 mins, the number of the last reported nausea ratio scale was assigned for the remaining period. Individual data regarding the time course of modulus equalized nausea ratio scale data are shown in Appendix 5-3. Four out of 14 subjects were “not sick” (reporting “zero” over the whole exposure duration) in all 4 rotation velocity conditions. Three out of the 14 subjects “got sick” in 0 dps rotation velocity conditions. Such results are consistent with the results of the 7-point nausea rating. As shown in Figure 5.8, median nausea ratio scale in 0 dps and 2 dps conditions is always zero along the time axis and those in the 14 dps and 34 dps conditions eventually reach a non-zero level.

Both the nausea ratio scale data before transformation (averaged over 30 mins) and

after transformation ($\lambda=0.25$) fail to pass the normality test as shown in Figure 5.9.

The Friedman test shows that rotation velocity has a significant effect on the nausea ratio scale data ($p<0.05$). Such results indicate that H1.2 should not be rejected. A post-hoc test shows that (i) a nausea ratio scale in the 34 dps condition is significantly higher than in the 0 dps and 2 dps conditions and (ii) the nausea severity in the 14 dps condition is not significantly different from the 34 dps condition (See Table 5.6).

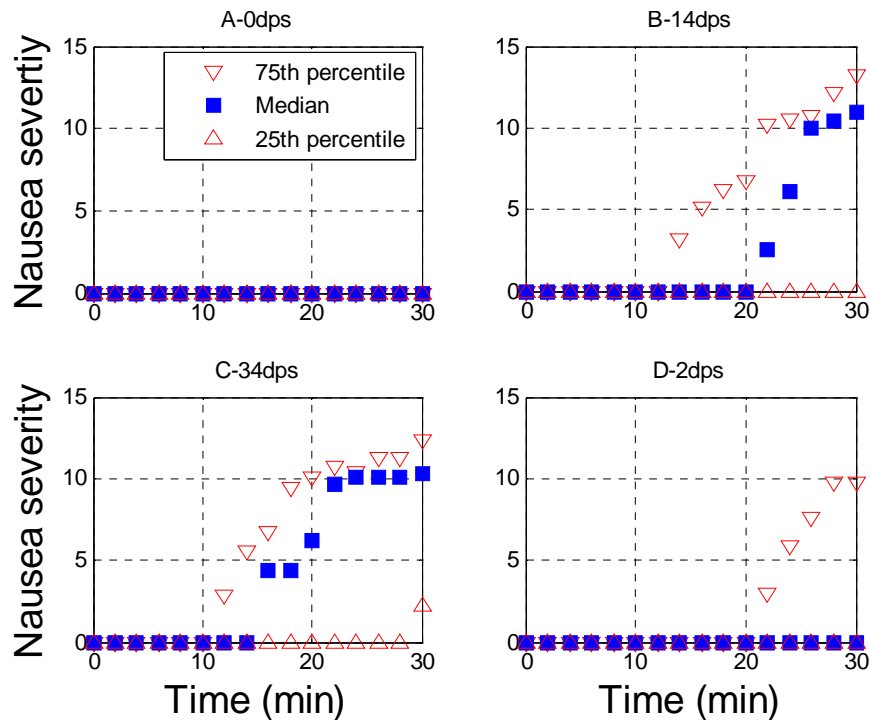


Figure 5.8 Median, 25th and 75th percentile of nausea ratio scale data as a function of exposure duration for 4 rotation velocity conditions: rotating at (a) 0 dps, (b) 14 dps, (c) 34 dps, (d) 2 dps

Based on comments of thesis examination committee, the raw nausea ratio scale data was re-normalized. A small positive constant was used to replace each zero value in a

row where there are both zero and non-zero data. Friedman test of the re-processed data shows the same results, i.e., rotation velocity has a significant effect on the nausea ratio scale data ($p < 0.05$). Wilcoxon sign-rank test re-confirmed the significant difference between the nausea severity in 34dps condition and in 0dps condition ($p < 0.05$).

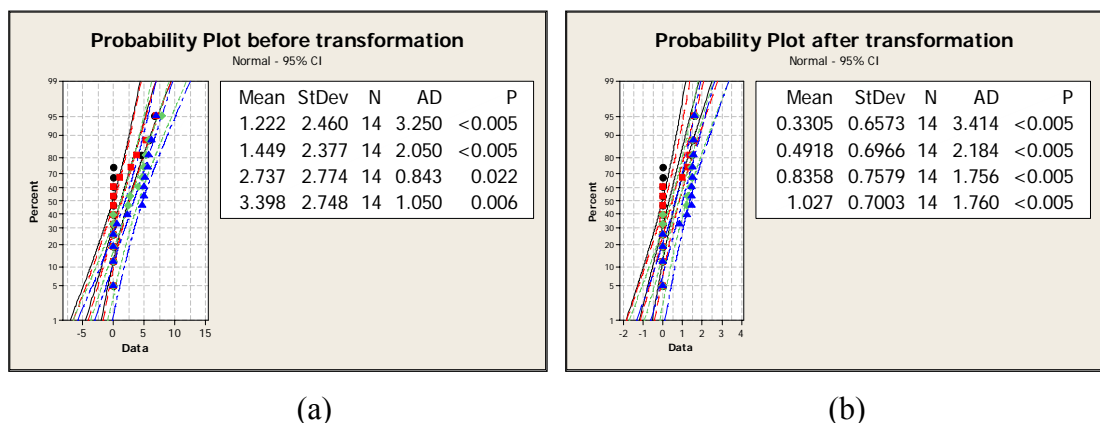


Figure 5.9 Normality test of (a) modulus equalized nausea ratio scale data before transformation ($\lambda=0.25$) and (b) after transformation ($\lambda=0.25$)

Table 5.6 Student-Newman-Keuls (SNK) test on the effect of rotation velocity on modulus equalized nausea ratio scale (average over 30 min)

Drum velocity	N	Subset	
		1	2
0dps	14	1.22	
2dps	14	1.45	
14dps	14	2.74	2.74
34dps	14		3.40
Sig.		.067	.320

Similar tests are used to analyze the nausea ratio scale data at 30 mins. Both modulus equalized nausea ratio scale data (at 30 min) before transformation and after transformation ($\lambda=0.25$) fail to pass the normality test as shown in Figure 5.10. The

Friedman test shows that rotation velocity has a significant effect on the nausea ratio scale data at 30 min ($p < 0.05$). Such results indicate that H1.2 should not be rejected.

A post-hoc test shows that the nausea rating in the 14 dps and 34 dps conditions is significantly higher than the 0 dps condition (See Table 5.7). Such results are confirmed by Wilcoxon sign-rank test.

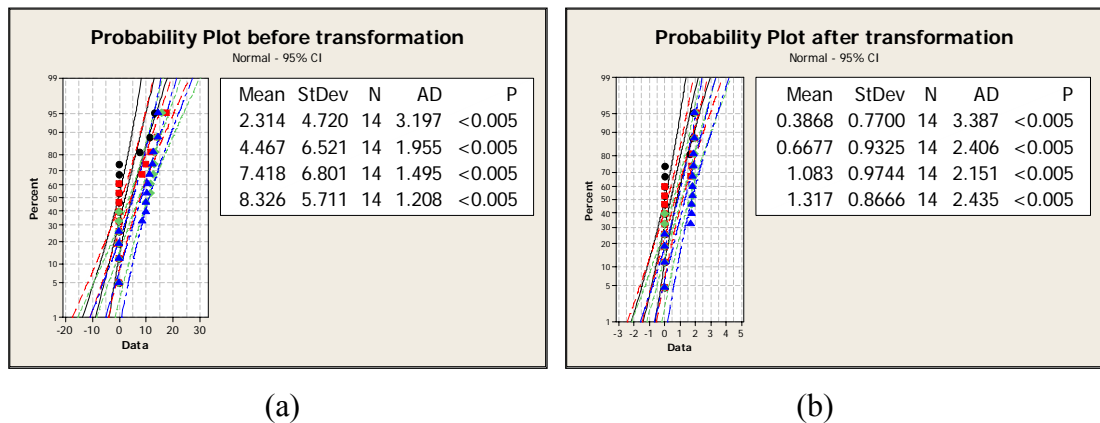


Figure 5.10 Normality test of (a) modulus equalized nausea ratio scale before transformation ($\lambda=0.25$) and (b) after transformation ($\lambda=0.25$) at 30 min

Table 5.7 Student-Newman-Keuls (SNK) test on the effects of rotation velocity on modulus equalized nausea ratio scale data at 30 min

Drum velocity	N	Subset	
		1	2
0dps	14	2.31	
2dps	14	4.47	4.47
14dps	14		7.42
34dps	14		8.33
Sig.		.205	.066

Spearman's correlation analysis shows that the nausea severity measured by nausea ratio scale significantly correlates with the drum rotation velocity ($\rho=0.36$, $p < 0.01$).

Such Significant correlation and the observed linear increasing trend shown in Figure

5.11 indicate that the H2.1 should be rejected.

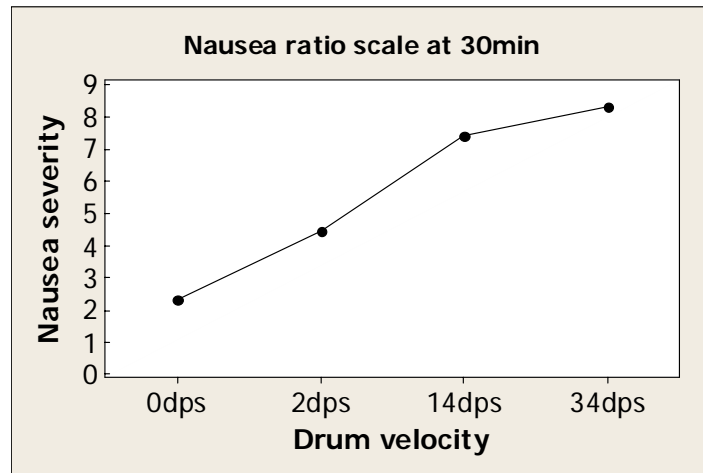


Figure 5.11 Observed linear increasing trend of the nausea ratio scale data at 30 min as a function of the rotation velocity of the optokinetic stimuli

5.3.5 Simulator Sickness Questionnaire Scores

Individual data regarding the pre and post-exposure SSQ total scores and sub-scores are shown in Appendix 5-4. The Wilcoxon signed-rank test is used to test the significance of differences between a pair of post and pre-scores in each condition since the SSQ data were of a non-parametric distribution. It is found that post-exposure scores of SSQ-N, SSQ-O, SSQ-D, and SSQ-TS are all significantly larger than corresponding pre-exposure scores in all velocity conditions (in each case $p < 0.01$). Such results indicate that the group of subjects became “sick” in all 4 conditions, including the 0 dps condition in which subjects viewed a static image pattern. As discussed in Section 5.3.3, this type of sickness is neither induced by any “motion” of visual stimuli nor by pattern sensitivity. Twelve out of the 14 subjects

reported eye strain in post-exposure SSQ after exposure to the 0 dps condition. Several subjects believed that it was caused by fixating their viewpoint on a small red dot (eye fixation point subtending 1 deg) while viewing a complete static image pattern of black and white striped pairs for a long time (30 mins).

Although the change from post to pre-exposure SSQ scores (see Figure 5.12) captures the change of a participant's state of health by viewing provocative stimuli under the experimental setup, the difference in scores of SSQ (post-pre scores) cannot quantify such change of state of health since SSQ employs an ordinal scale, but not a ratio scale (Kennedy et al., 1990). Therefore, pre-SSQ scores and post-SSQ scores are analyzed separately in this study.

The pre-exposure SSQ total scores in 0 dps, 2 dps, 14 dps and 34 dps are 7.48(3.74-7.48), 3.74(0-7.48), 3.74(2.805-9.35) and 0(0-3.74), respectively. Three out of the 14 subjects reported a pre-exposure SSQ total score higher than 10 in the 0 dps and 14 dps conditions. One out of the 14 subjects reported a pre-exposure SSQ total score higher than 10 in the 2 dps and 34 dps conditions. As mentioned in Section 4.5.3.2, a different control approach of pre-exposure health state was employed in this study from what was used by Kennedy et al. (1999) who excluded

any subject with a pre-exposure SSQ total score of more than 10 in their experiments.

Therefore, data analysis on pre-exposure SSQ scores is used to check whether the control approach adopted in this study is efficient enough.

Both original pre and post-SSQ data and transformed pre and post-SSQ data ($\lambda=0.25$) fail to pass the normality test. The Friedman test show that only the state of health measured by pre-exposure SSQ-O score, but not the other 3, has a significant fluctuation over 4 rotation velocity conditions conducted on different days ($p<0.05$).

A post-hoc test shows that (i) SSQ-O score in the 0 dps condition is significantly higher than in the 2 dps and 34 dps conditions. (ii) SSQ-O scores in the 3 non-zero velocity conditions are not significantly different from each other. (See Table 5.8)

This result indicates that the control approach adopted in this study is acceptable. It is acknowledged that the fluctuation of health state can be eliminated if the method in Kennedy et al. (1999) is adopted. Fortunately, only the discomfort level in the 0 dps condition is found to be higher than other conditions. Since the discomfort level measured by both the 7-point nausea rating and free modulus magnitude estimation in the 0 dps condition is found to be the least among all 4 conditions, such fluctuation of the state of health is less possible in obscuring the main effect of rotation velocity on pre-exposure SSQ scores.

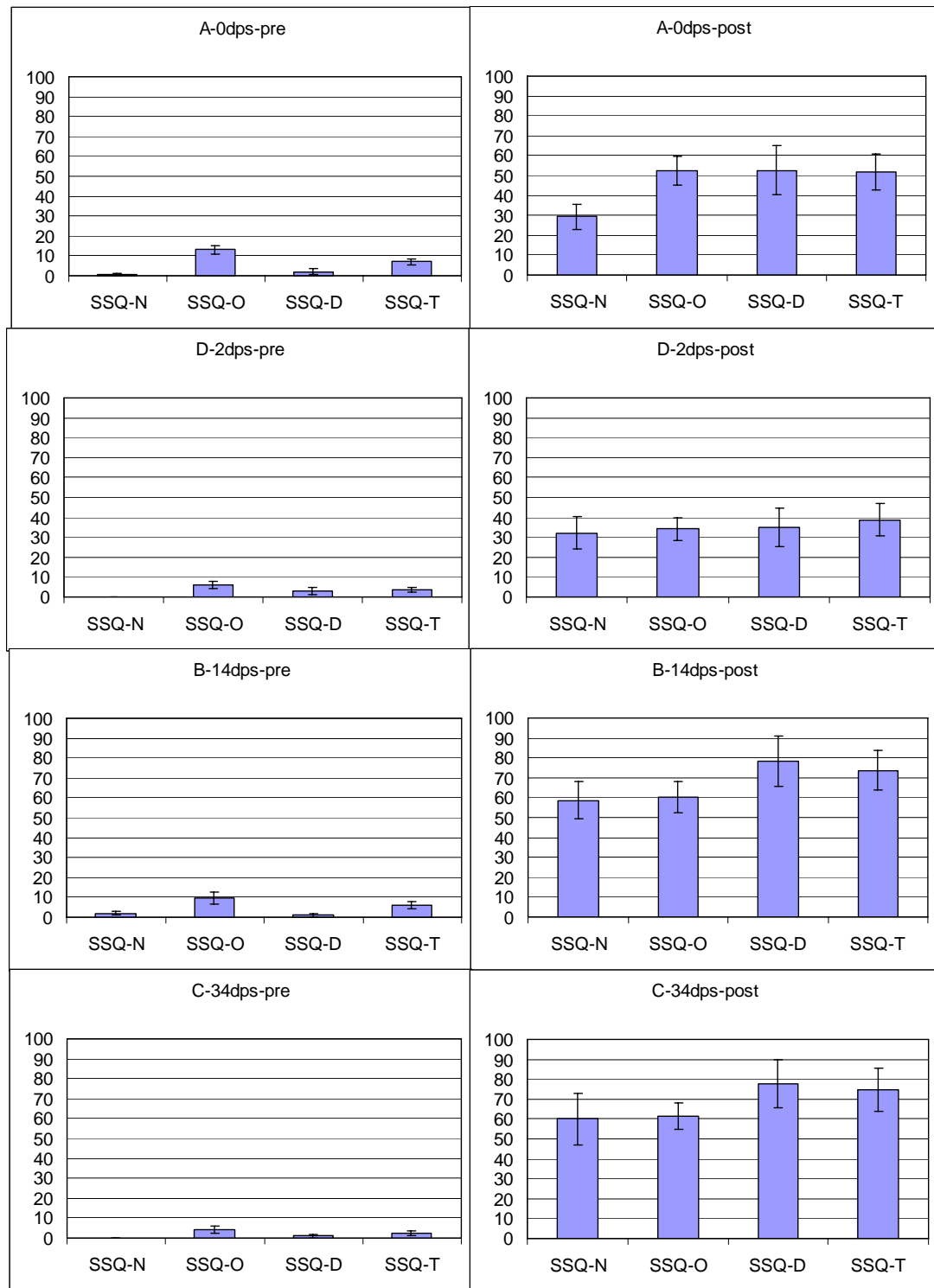


Figure 5.12 Mean and SE (standard error) of pre and post-exposure SSQ total scores and sub-scores for conditions of 0 dps, 2 dps, 14 dps and 34 dps.

Table 5.8 Student-Newman-Keuls (SNK) tests on significance of health state fluctuation measured by pre-exposure SSQ scores across 4 rotation velocity conditions

DRUMVEL	N	Subset
		1
2dps	14	.00
34dps	14	.00
0dps	14	.68
14dps	14	2.04
Sig.		.139

(a) Dependent variable: pre SSQ-N

DRUMVEL	N	Subset	
		1	2
34dps	14	4.33	
2dps	14	5.96	
14dps	14	9.75	9.75
0dps	14		12.99
Sig.		.149	.259

(b) Dependent variable: pre SSQ-O

DRUMVEL	N	Subset
		1
14dps	14	.99
34dps	14	.99
0dps	14	1.99
2dps	14	2.98
Sig.		.598

(c) Dependent variable: pre SSQ-D

DRUMVEL	N	Subset
		1
34dps	14	2.40
2dps	14	3.74
14dps	14	5.88
0dps	14	7.21
Sig.		.055

(d) Dependent variable: pre SSQ-T

The Friedman test shows rotation velocity has a significant effect on VIMS severity measured by post-exposure SSQ-N, SSQ-O, SSQ-D and SSQ-T (in each case $p < 0.05$). Such results indicate that H1.2 should not be rejected. A post-hoc test shows that (i) SSQ scores in 2 dps condition are significantly lower than 14 dps and 34 dps conditions. (ii) SSQ scores in the 14 dps condition are not significantly different than the 34 dps condition (See Table 5.9). Such results are confirmed by Wilcoxon sign-rank test.

Table 5.9 Student-Newman-Keuls (SNK) tests on the effects of rotation velocity on VIMS severity measured by post SSQ total score and 3 sub-scores

DRUMVEL	N	Subset	
		1	2
0dps	14	29.3014	
2dps	14	32.0271	
14dps	14		58.6029
34dps	14		59.9657
Sig.		.797	.898

(a) Dependent variable: post SSQ-N

DRUMVEL	N	Subset	
		1	2
2dps	14	34.110	
0dps	14		52.519
14dps	14		60.099
34dps	14		61.723
Sig.		1.000	.527

(b) Dependent variable: post SSQ-O

DRUMVEL	N	Subset	
		1	2
2dps	14	34.8000	
0dps	14	52.6971	52.6971
34dps	14		77.5543
14dps	14		78.5486
Sig.		.183	.136

(c) Dependent variable: post SSQ-D

DRUMVEL	N	Subset	
		1	2
2dps	14	38.7357	
0dps	14	51.5586	51.5586
14dps	14		73.7314
34dps	14		74.8000
Sig.		.248	.098

(d) Dependent variable: post SSQ-T

Spearman's correlation analysis shows that the nausea severity measured by post SSQ-Nausea subscore significantly correlates with the drum rotation velocity ($\rho=0.33$, $p<0.05$). Such Significant correlation and the observed linear increasing trend shown in Figure 5.13 indicate that the H2.1 should be rejected.

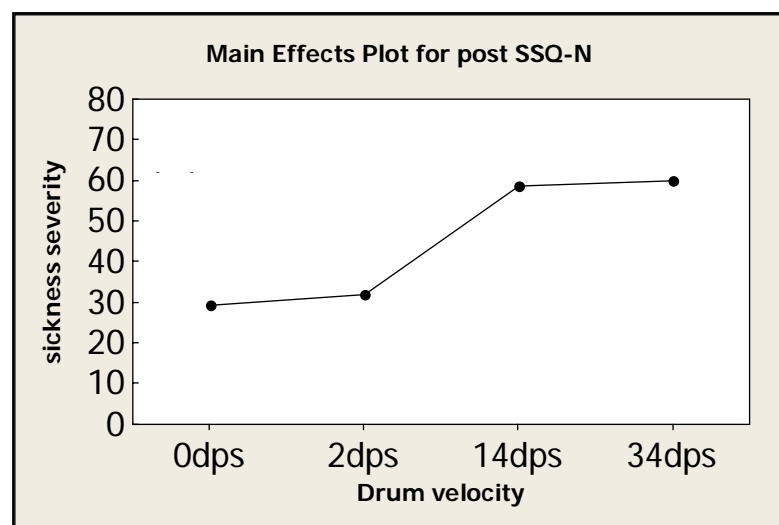


Figure 5.13 Observed linear increasing trend of post SSQ-N as a function of drum rotation velocity

As mentioned in Section 4.5.3.2, data analysis on post minus pre (post-pre) scores was documented only for comparison purposes (See Figure 5.14). Both original SSQ data and transformed SSQ data ($\lambda=0.25$) fail to pass the normality test. The Friedman test shows that the rotation velocity has a significant effect on difference scores of SSQ-N ($p<0.01$), SSQ-D ($p<0.01$) and SSQ-T ($p<0.05$). A post-hoc test shows that the (i) difference in SSQ scores in the 2 dps condition are significantly lower than in the 14 dps and 34 dps conditions and (ii) difference in SSQ scores in the 14 dps condition is not significantly different than the 34 dps condition. (See Table 5.10)

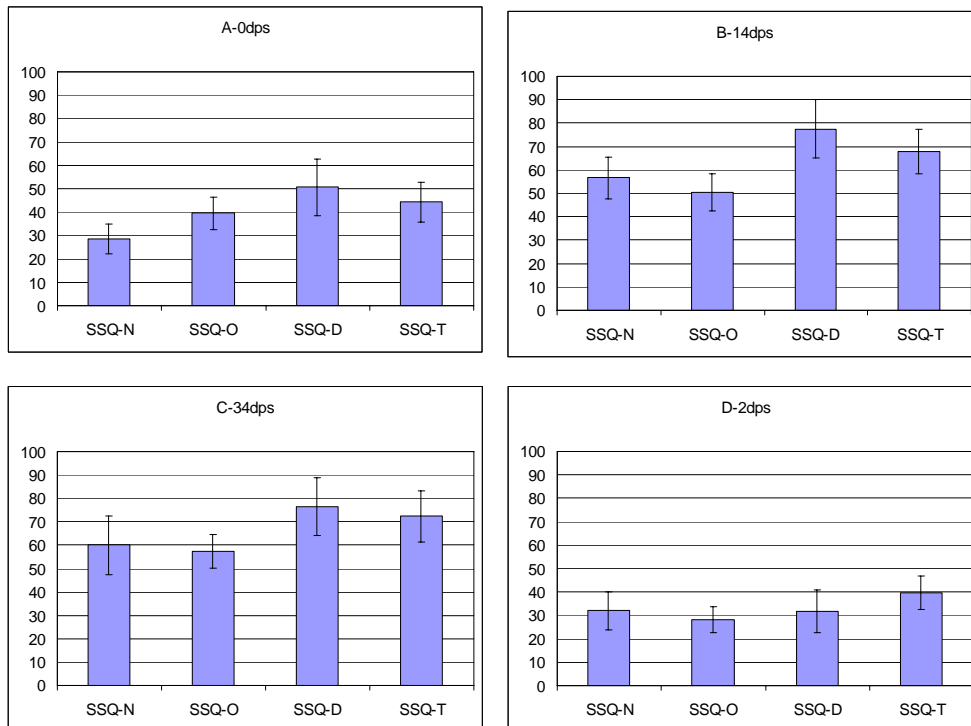


Figure 5.14 Difference (post-pre) SSQ total score and 3 sub-scores for rotation velocity of 0 dps, 2 dps, 14 dps and 34dps

Table 5.10 Student-Newman-Keuls (SNK) tests on the effect of rotation velocity on difference (post-pre) SSQ total score and 3 sub-scores at a rotation velocity of 0 dps, 2 dps, 14 dps and 34 dps

drum velocity	N	Subset	
		1	2
0dps	14	28.6200	
2dps	14	32.0271	
14dps	14		56.5586
34dps	14		59.9657
Sig.		.746	.746

(a) Dependent variable: SSQ-N

drum velocity	N	Subset	
		1	2
2dps	14	28.154	
0dps	14	39.524	39.524
14dps	14		50.353
34dps	14		57.391
Sig.		.198	.113

(b) Dependent variable: SSQ-O

drum velocity	N	Subset	
		1	2
2dps	14	31.8171	
0dps	14	50.7086	50.7086
34dps	14		76.5600
14dps	14		77.5543
Sig.		.155	.111

(c) Dependent variable: SSQ-D

drum velocity	N	Subset	
		1	2
2dps	14	34.9957	
0dps	14	44.3457	
14dps	14		67.8543
34dps	14		72.3957
Sig.		.398	.681

(d) Dependent variable: SSQ-T

5.3.6 Correlation analysis of vection related measures, 7-point nausea rating, nausea ratio scale data, and post SSQ-Nausea score

As shown in Figure 5.15, nausea severity measured by two nausea scales and post SSQ-N increases along with the increase of the rotation velocity. The vection velocity, as a function of the rotation velocity, has a similar increasing trend, consistent with the linear trend reported by Kennedy et al. (1996). Such results indicate a linear relation between vection velocity and nausea severity.

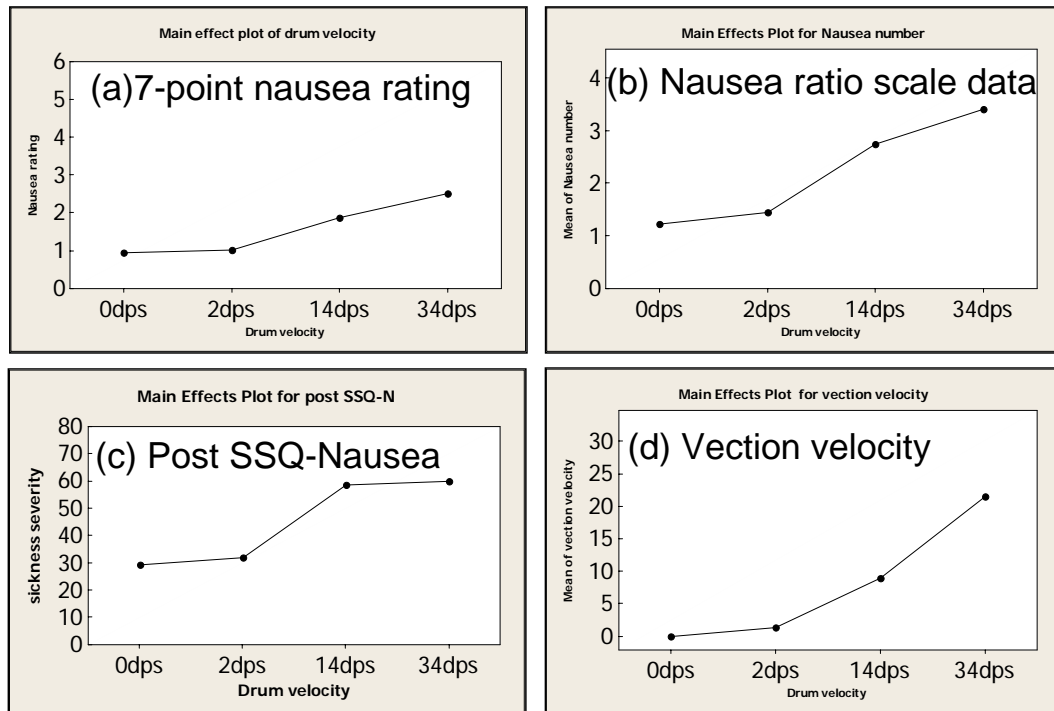


Figure 5.15 Main effect plots of rotation velocity on (a) 7-point nausea rating data, (b) nausea ratio scale data, (c) SSQ-N, and (d) vection velocity

Spearman's correlation analysis shows that the nausea severity measured by nausea ratio scale significantly correlates with the vection velocity ($\rho=0.3$, $p<0.05$). Such Significant correlation and the observed linear increasing trend shown in Figure 5.16 indicate that the H2.3 should be rejected.

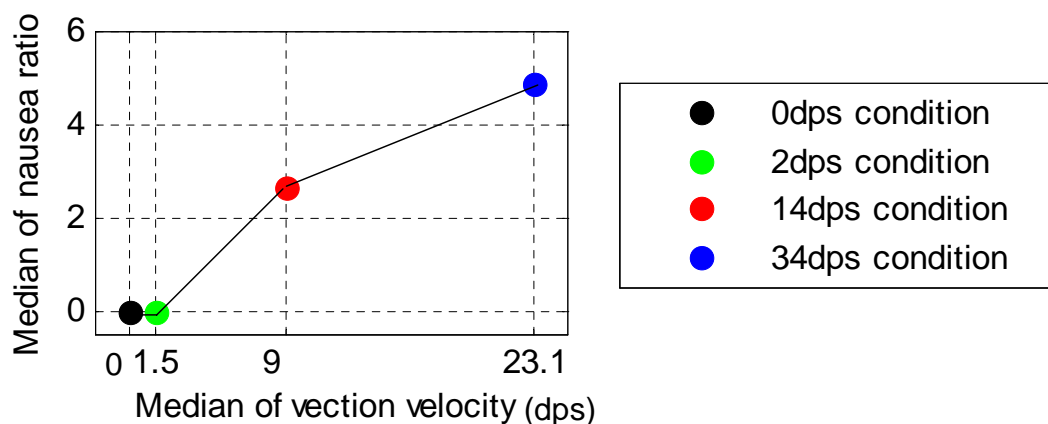


Figure 5.16 Observed linear increasing trend of nausea severity measured by nausea ratio scale (Median of 14 subjects) as a function of vection velocity (Median of 14 subjects)

The correlation results from Spearman indicate that the nausea ratio scale data from the free modulus magnitude estimation are significantly correlated with the 7-point nausea rating data ($\rho=0.907$, $p<0.01$) and post-exposure SSQ-nausea score ($\rho=0.871$, $p<0.01$) (see Figure 5.17). Such results indicate that the nausea ratio scale from the free modulus magnitude estimation can be considered as another valid measure of VIMS severity in future empirical studies, aside from the two commonly used measures, the 7-point nausea rating and SSQ scores. It is an important finding because most reported VIMS severity data has been collected using ordinal scales which make them unsuitable for modeling purposes. Free modulus magnitude estimation used as a supplement to ordinal sales can bring several benefits as discussed in Section 4.5.3.1.

Four measures related to vection perception are derived from vection velocity time series, i.e., maximum level of vection velocity, median level of vection velocity, latency of vection onset and vection build-up time. The maximum level of vection velocity (vection max in Figure 5.17) and the median level of vection velocity (vection median in Figure 5.17) significantly correlate with the 7-point nausea rating while both the latency of vection onset and vection build-up time does not correlate.

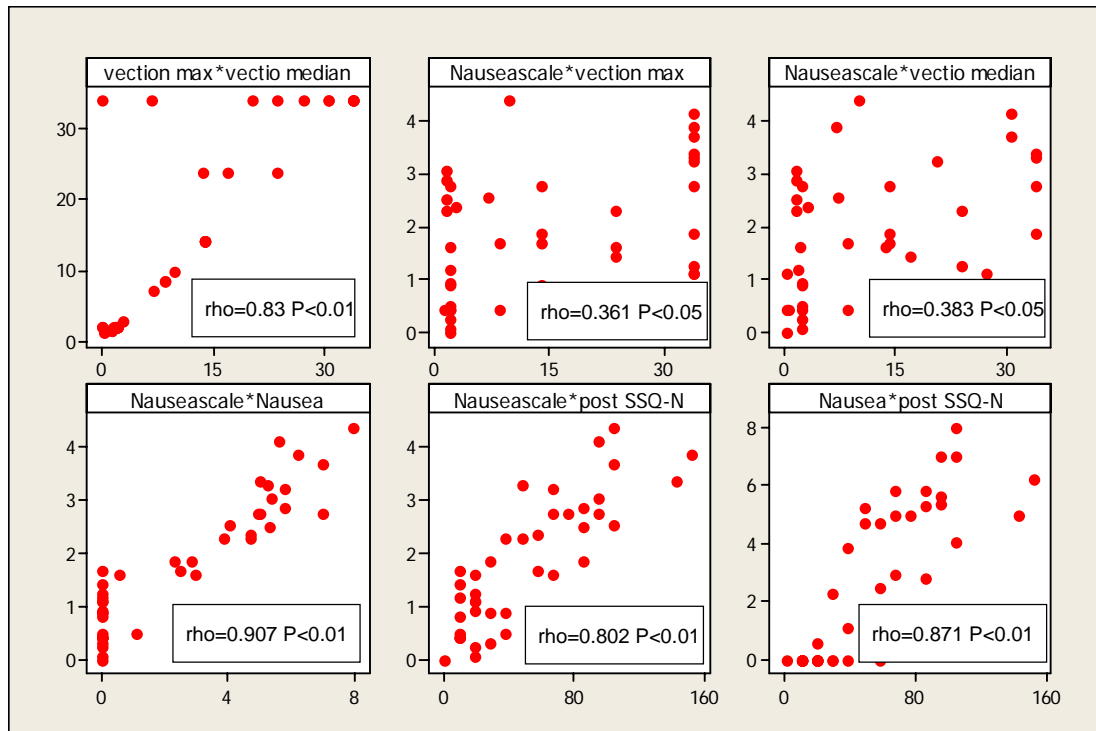


Figure 5.17 Scatter plots and correlation coefficients (Spearman's rho) summarized for correlation analysis of vection median, vection max, 7-point nausea rating data, nausea ratio scale data and post SSQ-N score. Results of vection onset latency and vection build-up time is not included since neither is found to be significantly correlated with VIMS severity

5.3.7 Visual acuity at near point and motion sickness susceptibility

Visual acuity at near point was 11.2 ± 1.7 . The MSSQ-short raw score was 19.5 ± 12.6 .

In the 0 dps and 2 dps conditions, neither visual acuity nor motion sickness susceptibility correlated with VIMS severity and vection velocity. As shown in Figure 5.18, visual acuity at near point significantly correlates with the 7-point nausea rating data in the 14 dps condition ($\rho=0.558$, $p<0.05$) and 34 dps condition ($\rho=0.57$, $p<0.05$).

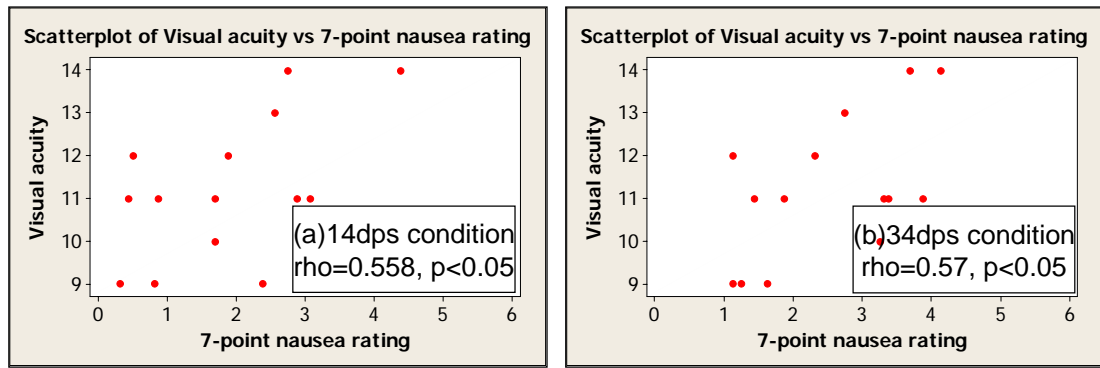


Figure 5.18 Scatter plots and correlation coefficients (Spearman's rho) of visual acuity at near point and 7-point nausea rating data in (a) 14 dps and (b) 34 dps condition.

5.4 Discussions

Consistent with expectations based on the neural mismatch theory, vection velocity is found to be significantly correlated with the 7-point nausea rating that is averaged over 30 min ($p<0.05$). Moreover, a significant linear relationship between vection velocity and nausea severity is identified. Such results disagree with Webb and Griffin (2002) who reported that rated vection intensity (ordinal data) and rated nausea data (ordinal data) while watching rotating striped patterns (also in yaw axis) with eye-fixation were not correlated. Such discrepancy in results can be explained by the different FOV size employed in these two studies. Vection and VIMS were provoked by a visual stimulus having restricted FOV (48 deg) in Webb and Griffin (2002) while they were provoked by a wide-angle (200 deg) visual stimulus in this study. Another support for the FOV explanation comes from the finding that a restricted FOV can also reduce levels of CV (e.g., Hettinger et al. 1990). Webb and

Griffin (2002) concluded thatvection is not a primary cause of sickness with optokinetic stimuli. The current finding proves otherwise when the visual stimuli has a wide FOV of 200 deg and OKN is fully suppressed.

The currently available VIMS theories suggest 4 factors as the potential causing factors of VIMS: (i)vection, (ii) optokinetic nystagmus (OKN), (iii) postural instability, and (iv) subjective-vertical conflict. In experiment one, OKN was completely suppressed by eye fixation and the effects of postural instability and subjective-vertical conflict were also controlled across different conditions by head fixation and careful head orientation alignment (see Chapter 4). Among the 4 factors,vection perception was the only one that was not controlled across different pattern rotating velocity conditions. Experiment one results show that the rotation velocity of the optokinetic stimuli has a significant main effect on both thevection velocity ($p<0.01$) and VIMS severity ($p<0.05$). Moreover, the ratio scalevection velocities reported at each non-zero pattern rotating velocity condition are found to be significantly different from each other. It indicates that the main effect of rotation velocity on VIMS severity is mediated by the main effect of rotation velocity onvection velocity. In other words, such results are consistent with the notion thatvection is a primary cause of VIMS.

Hu et al. (1989) reported a curvilinear relation (inverted U shape) between the velocity of the drum rotation and VIMS severity. Among the 4 velocity conditions (15 dps, 30 dps, 60 dps and 90 dps), the severity levels in the 60 dps and 90 dps conditions were reported to be significantly higher than the 15 dps condition, respectively. Bearing in mind that each of the 3 non-zero rotation velocity conditions; i.e., 2 dps, 14 dps and 34 dps, represented a retinal slip velocity level closer to that of Hu et al. (1989), consisting of 30 dps, 60 dps and 90 dps, an inverted U shape of sickness severity as a function of rotation velocity was not found in experiment one. Instead, a monotone increasing trend was identified. As shown in Tables 5.4, 5.5, 5.6, 5.7 and 5.9, the sickness severity as a function of rotation velocity increases from a 2 dps to 14 dps and 34dps condition. Among all types of measures, only the difference in sickness severity measured by the 7-point nausea rating (averaged over 30 min) in the 14 dps and 34 dps conditions is significant. For all sickness severity measures, there is a significant difference in the 34 dps and 2 dps condition.

Although such discrepancies in the results of the two studies are not statistically significant, some arguments are listed below for explanation purposes. First, the inverted U shape of the sickness severity, as a function of velocity of the drum

rotation in Hu et al. (1989), is found when both OKN andvection are present while the sickness severity in experiment one is provoked in the presence ofvection and in the absence of OKN. The effect of OKN contributes more for the drop of the sickness severity at the 60 dps condition than the effect ofvection. Actually, an inverted U shape of the sickness severity as a function of rotation velocity of an optokinetic stimulus was indeed found in experiment two in whichvection was suppressed and OKN was present. (See Chapter 6 for more details) Secondly, as mentioned in Section 5.2.3, the mapping between the levels of drum rotation velocity and retinal slip velocity is based on OKN gains reported by Koenig et al. (1978) since Hu et al. (1989) did not report related OKN gains. As indicated by the results of experiment two, humans have large individual differences in OKN gain given the same velocity level of rotation. Therefore, it is possible that the actual OKN gains in Hu et al.(1989) can be different from the OKN gains reported by Koenig et al.(1978) which was used to set 3 non-zero velocity levels of rotation in experiment one. Detailed argument will be presented in Section 9.3. Thirdly, the two studies used different methods to measure sickness severity. The Graybiel scale (Appendix 5-9) was used in Hu et al. (1989) while the 7-point nausea rating, nausea ratio scale from free-modulus magnitude estimation and post-exposure SSQ scores were used in experiment one. Therefore, it is hard to directly compare results of the two studies.

Hu et al. (1989) also reported a curvilinear relationship between the velocity of drum rotation and the strength of vection experience. In experiment one, vection velocity was monotonically increasing from a 2 dps condition to a 34 dps condition. The difference in vection velocity in each of the 2 non-zero rotation velocity conditions are found to be significant. Since levels of vection intensity in the two different experimental conditions can be different when corresponding levels of vection velocity are the same (Brandt, et al., 1973), it is hard to directly compare results of the two studies. Such results suggest that measuring both vection intensity and vection velocity in future empirical studies can be informative.

5.5 Conclusions

VIMS is provoked in the presence of vection and in the absence of OKN. Consistent to expectations on the basis of the neural mismatch theory, the vection velocity has a significant linear relationship with sickness severity indicating that vection and VIMS should not be separate phenomena. Furthermore, the significant main effect of rotation velocity on sickness severity is mediated by the significant main effect of rotation velocity on vection velocity given all other factors are controlled across conditions. Such results indicate that vection is the primary cause of VIMS in

experiment one. Last but not least, nausea severity as a function of rotation velocity is found to be monotone, increasing in a range from a rotation velocity of 2 dps to 34 dps, given full OKN suppression. A similar trend is found of vection velocity as a function of rotation velocity as well. In short, H2.2 should not be rejected, but H2.1 and H2.3 should be rejected.

CHAPTER 6

EXPERIMENT TWO: OKN AND VIMS AS A FUNCTION OF ROTATION VELOCITY OF AN OPTOKINETIC STIMULI IN THE ABSENCE OF VECTION

SUMMARY

As expected, on the basis of Ebenholtz's extraocular afference hypothesis, OKN and VIMS should not be separate phenomena. A review of literature indicates that the effect of rotation velocity of optokinetic stimuli on VIMS severity with OKN, but without vection perception has not been studied. To fill this gap and collect ratio scale data to validate model two, an experiment was conducted. Fourteen participants were exposed to optokinetic stimuli having a central visual field and peripheral visual field rotating in opposite directions along the earth-vertical axis at a constant velocity of 0 degree per second (dps), 30 dps, 60 dps and 90 dps. Such visual stimuli have been demonstrated in previous pilot tests to be capable of completely suppressing vection perception. Consistent with implications from the VIMS theory (see Chapter one) and related neural mechanisms (see Chapter three), results of experiment two indicate that the foveal retinal slip velocity mediates a significant

main effect on VIMS severity in the absence of vection. A quadratic function is identified to describe the nonlinear relation between the foveal retinal slip velocity and VIMS severity. Such results explain the inverted U-shape between the rotation velocity of optokinetic stimuli and VIMS severity as reported by Hu et al. (1989).

6.1 Objective and hypotheses

The objective of this experiment is to study the relation between OKN and VIMS severity in the absence of vection while watching wide FOV optokinetic stimuli with a central visual field and peripheral visual field rotating in opposite directions along the earth-vertical axis. It is hypothesized that the rotating velocity of the image pattern has a significant main effect on the foveal retinal slip velocity (H3.1) and VIMS severity level (H3.2) under the assumption that OKN is present and vection is absent. Based on implications from Hu et al. (1990), it is hypothesized that the relation between the rotation velocity of the optokinetic stimuli and the nausea ratio scale data (H4.1) can be described by a high-order polynomial function peaking at a rotation velocity of 60 dps. Based on the results of Koenig et al. (1978), the relation between the rotation velocity of the optokinetic stimuli and foveal retinal slip velocity is hypothesized to be described by a first-order polynomial (linear) function (H4.2). Last but not least, it is hypothesized that the relation between the foveal retinal slip velocity and the nausea ratio scale data can be described by a high-order

polynomial function (H4.3).

6.2 Methods

6.2.1 Participants

Fifteen Chinese females participated in experiment two. These subjects were university students ranging from 21 to 30 years old. Only 2 out of the 15 subjects were also involved in experiment one. For these 2 subjects, the time interval between the 2 experiments was at least 7 days. All of the participants were consenting volunteers who were healthy and free of medication or illness. Each subject was paid for her participation. The Human Subject and Research Ethics Committee at the Hong Kong University of Science and Technology approved the experiments. Fourteen out of the 15 subjects were involved in the whole experiment. One subject quit the experiment after experiencing only one condition due to high photosensitivity. In fact, this subject vomited after the exposure period. This subject had successfully passed a pilot test on the effect of the size of the central visual field on vection perception. Such a pilot test was implemented at least one day prior to experiment two. Each subject experienced 64 different trials with each lasting up to 90 sec with a maximum 3 min break between the two trials. Neither nausea nor vomiting was reported by the subject within and right after the pilot test. The

phenomenon of photosensitivity is discussed in detail in Section 6.3.3. Therefore, data from the 14 subjects were used in the data analysis. The mean MSSQ-Short raw score for the participants in experiment two was 14.6 (SD=7.6), indicating that a sample with only Chinese females are more susceptible to motion sickness than the average population (see Section 4.5.3.5).

6.2.2 Visual stimuli

The visual stimuli used to provoke OKN and VIMS and simultaneously suppress vection perception was a simulated wide FOV optokinetic drum pattern having a central visual field and peripheral visual field rotating in opposite directions at a constant velocity along the earth-vertical axis (see Figure 6.1). The diameter of the central visual field is technically adjustable in a range from 0 pixels to 1920 pixels.

6.2.3 Design of experiment (DOE)

As illustrated in Figure 6.1, experiment two has 4 conditions, each administrated in 30 min sessions: A) viewing static visual pattern; B) viewing visual pattern rotating at 60 dps; C) viewing visual pattern rotating at 90 dps; D) viewing visual pattern rotating at 30 dps. The suppression of vection perception in conditions B, C, D is achieved by fine tuning the size of the central visual field (Appendix 6-1) for each

subject before each condition based on the primary results of a previous pilot experiment. The size of the central visual field in condition A is fixed to 880 pixels (100 deg) since 100 deg was the size reported by Brandt et al. (1973) and can fully suppressvection perception.

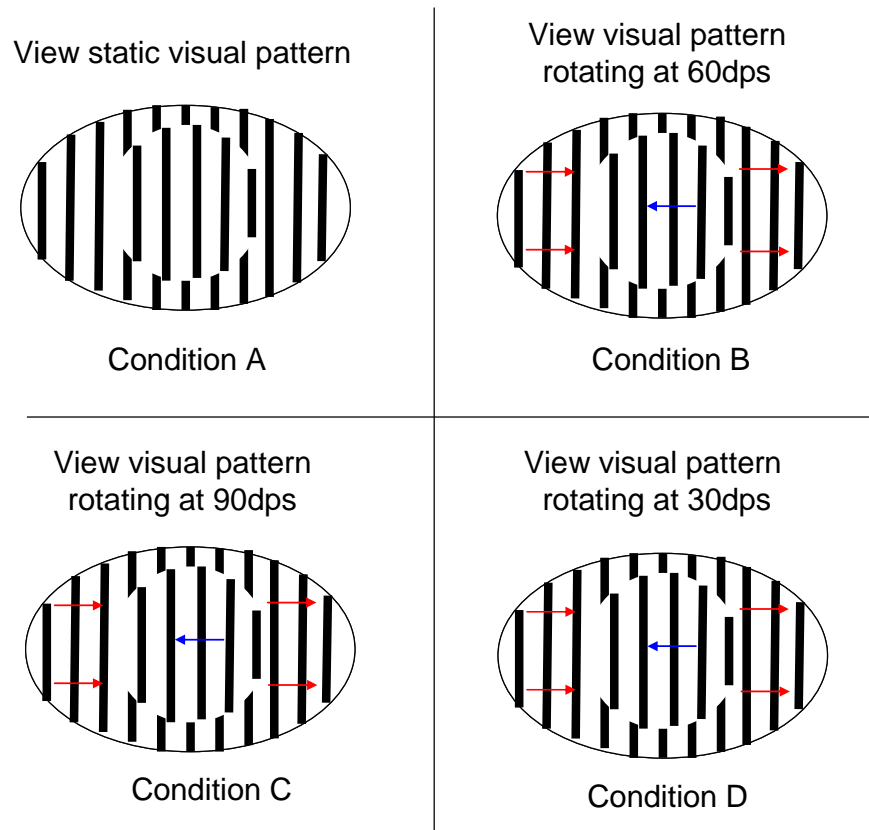


Figure 6.1 The 4 conditions of experiment two. The arrows are added in the figure to show the directions for the rotation of the visual patterns. The arrow in blue indicates the rotation direction in the central visual field. The arrow in red shows the rotation direction in the peripheral visual field.

The rotation velocity of 30 dps, 60 dps and 90 dps was selected on purpose so that the results of experiment two could be compared with findings in experiment one and Hu, et al. (1989). Designing experiment two in this way, the effect of rotation

velocity of optokinetic stimuli on VIMS in the absence of OKN and the effect of rotation velocity of optokinetic stimuli on VIMS in the absence ofvection can be investigated and compared under the same, or as close as possible, set of foveal retinal slip velocities projected on the foveal retina of humans. At the same time, their similarities and discrepancies to the effect of the rotation velocity of optokinetic stimuli on VIMS in the presence of bothvection and OKN as reported by Hu et al. (1989) can be discussed in detail.

Experiment two used a within-subject design in consideration of high inter-subject variations in OKN gain, OKN SPV, foveal retinal slip velocity and sickness severity. A balanced Latin square (4 levels) technique (Appendix 4-10) is used to counter-balance the order of the presentation of the 4 rotation velocities to each subject. Fourteen participants were randomly assigned a condition that had 4 possible sequences of orders. To dampen the effect of habituation, the time interval between the two experiment runs for each subject was at least 7 days.

6.2.4 Procedure

A pilot test was implemented for each subject at least one day ahead before experiment two to investigate the effect of the central visual field's size onvection

perception given opposite rotating central and peripheral visual fields. The size of the central visual field was varied from 80 pixels (9 degree) to 1580 pixels (180 deg) at a stepping size of 100 pixels. For each size of the central visual field, the subject was exposed to 4 different rotation velocities in sequence, i.e., 15 dps, 30 dps, 60 dps and 90 dps (after Hu et al., 1989). Therefore, each subject needed to experience 64 different trials. In each trial, the subject was instructed to report whether she experienced an illusion of self-rotation (vection) to the left or to the right. If no such illusion of self-rotation was reported, the trial continued for 90 sec and then ceased. There was a maximum 3 min break between the two trials to avoid provocation of VIMS symptoms, such as nausea. The results of the pilot test helped identify a specific range in which the vection perception was fully suppressed for 90 sec for each subject in each velocity condition. (See more details in Section 4.3.3)

The subject was then invited to participate in experiment two after at least 24 hours after the pilot test. First, participants were requested to read experiment two instructions (Appendix 6-2) and the experimenter answered their questions. Secondly, participants read and signed a consent form (Appendix 5-7). Thirdly, a line length estimation test including 20 line segments with different lengths was implemented to provide participants familiarity with the free modulus magnitude estimation method

(Stevens, 1971; McGee, 1998). Regression analysis was implemented immediately to obtain R square. If the R square value was smaller than 0.9, then the subject was requested to do the test again until her R square value was no less than 0.9. No subject was found to have difficulties in using the free modulus magnitude estimation method to estimate line lengths. Fourth, visual acuity at near point for both eyes and each individual eye was measured and recorded following the instructions of the vision tester menu (Appendix 5-8). Fifth, participants were requested to complete a motion sickness susceptibility survey questionnaire (So et al., 1999, Appendix 4-3) and a MSSQ-short questionnaire (Golding, 2006, Appendix 4-4) which was used to indicate her sensitivities to motion sickness. Sixth, participants were to complete a pre-exposure Simulation Sickness Questionnaire (SSQ, Appendix 4-1) after becoming familiar with the literal meanings of various VIMS symptoms. Seventh, before the commencement of conditions B, C or D, the subject first experienced a series of rotating visual patterns with different central visual field sizes, from the smallest to the largest. The size ranges were decided from the results of pilot test. The size condition in which the subject reported no vection perception during the 90 sec for the first time was used in the main test (Appendix 6-1). The diameter of the central visual field in the condition of 0 dps was fixed at 880 pixels (100 deg). Eighth, the subject wore five EOG electrodes. For each condition, eye

movements were calibrated by asking subjects to horizontally move her eyes across a pair of black and white stripes (subtending 15 deg) back and forth for three times (see Section 4.5.3.4). The horizontal and vertical eye positions were recorded. There was a 5 min break between the pre-test on the size of the central visual field and the eye calibration. Ninth, the subject was exposed to a particular condition for up to 30 mins. She was requested to report her subjective nausea severity level using the free modulus magnitude estimation (Stevens, 1971; McGee, 1998) and 7-point nausea rating (Golding & Kerguelen, 1992) as well as her vection intensity on a 4-point vection scale (Webb & Griffin, 2002) every 2 min. In the main test, the EOG recording started the moment that the subject was told to open her eyes and gaze directly at the rotating image pattern. The experimenter terminated the visual stimuli and EOG recording when it was 30 mins or a time point when the subject wanted to stop the exposure immediately (reporting a rating of 6 on the 7-point nausea scale). Finally, the subject completed a post-exposure SSQ (Appendix 4-1).

6.2.5 Measures

Visual acuity at the near point and previous susceptibility to motion sickness were measured before the first experiment session. These two measures were used to quantify characteristics of the participating group, but not used for subject screening.

EOG signals that recorded horizontal and vertical eye movements were acquired continuously over the whole exposure period. Horizontal eye position time series capture repetitive OKN movement cycles. Such data were processed by a matlab-based program to calculate the time series of OKN slow-phase velocity (SPV), OKN gain and the foveal retinal slip velocity. It was possible to check whether a subject's eyes were open by monitoring the vertical eye position time series which recorded every eye blink. If a subject attempted to cheat by closing her eyes and rotating her eye balls randomly, her vertical eye position time series could reveal the cheating. No subjects were found to close her eyes except for normal eye blinking.

During the 30 min exposure period, participants rated the severity of their motion sickness for every 2 minutes using free modulus magnitude estimation and 7-point nausea scale. The raw ratio scale data from the free modulus magnitude estimation was then transformed by modulus equalization so that the transformed ratio scale data was comparable across different subjects and experimental conditions.

Before and after each experimental session, the SSQ was completed by each

participant. The total score and 3 sub-scores of pre and post SSQ were used to quantify the pre-exposure and post-exposure states of health. As discussed in Section 4.5.3.2, no subject is allowed to commence an experiment session if she reported any “moderate” symptoms.

In consideration of model two’s assumption of completevection suppression over the whole exposure duration, thevection intensity was rated at 2 min intervals on a 4-point scale to check whether such an assumption was satisfied.

6.2.5 Statistical analysis

ANOVA was performed to test the main effect of rotation velocity of the optokinetic stimuli on the foveal retinal slip velocity and ratio scale data of VIMS severity measures. Normality test (Anderson-Darling) was performed to check whether normality assumption of ANOVA was satisfied. For normal distribution, Bartlett’s variance homogeneity test was performed to check whether equal variance assumption of ANOVA was satisfied. Levene’s variance homogeneity test which did not have assumptions of normal distribution was used as the alternative to Bartlett’s test if the data were non-normal. If applicable, the Box-Cox method was used to select a transformation parameter (λ) generating the minimum error sum of square

($SS_E(\lambda)$). If either assumption (or both) was not satisfied or data were non-parametric, the Friedman Test (a nonparametric analysis of a randomized block experiment) was used as the alternative to ANOVA. Student-Newman-Keuls (SNK) post-hoc test and Wilcoxon sign-rank test were used to determine which means in the 4 conditions were different. The effects model of ANOVA (or Friedman test) is:

$$y_{ij} = \mu + \alpha_i + \tau_j + \varepsilon_{ij}$$

where $i=1, 2, 3, 4$ and $j=1, 2, \dots, 14$. The rotation velocity of the image pattern is the main factor α . The subject is the random factor τ . Sickness severity (7-point nausea rating, nausea ratio scale and SSQ scores) measures or the foveal retinal slip velocity are the dependent variable y . The model does not include an interaction term due to the lack of degree of freedom.

Pearson's (r) correlation was employed to test the significance of a linear relation between parametric and normal distributed measures, e.g., the relations between 3 OKN measures and 3 VIMS severity measures. Spearman's (ρ) correlation was used as the alternative to Pearson's correlation if the data were non-normal or nonparametric.

6.3 Results

Results for normally distributed variables were expressed as the mean \pm SD and continuous variables with non-normal distribution were presented as the median value (interquartile interval).

6.3.1 Vection intensity

In experiment two, vection was required to be completely suppressed for investigating the effect of rotation velocity of the image pattern on VIMS and OKN in the absence of vection perception. A method presented in Section 4.4 is capable of fully suppressing vection perception for 90 sec in a range of rotation velocity of the image pattern from 15 dps to 90 dps. Results of experiment two show that such a method is also capable of fully suppressing vection perception for 30 min in the conditions of 60 dps and 90 dps since none of the 14 subjects reported any non-zero vection rating over the whole exposure duration. Vection perception was also fully suppressed in the condition of 30 dps up to 18 min. However, two subjects reported a vection rating of 1 (intermittent vection) at 20 mins and one subject reported a vection rating of 1 at 22 mins. Such results show that the effect of OKN is confounded with the effect of vection within some periods in the last 12 mins in the condition of 30 dps.

It is reported that the coupling of vection and OKN produces significantly higher levels of sickness severity (Stern et al., 1990; Flanagan et al., 2002). In this study, the data analysis on VIMS severity show that the sickness severity level in the 30 dps condition induced by a partial coupling of vection and OKN is the lowest along the 3 non-zero velocity conditions (see details from Sections 6.3.3 to 6.3.5). Moreover, it is found that the rotation velocity of the image pattern has a significant main effect on VIMS severity. Therefore, such partial coupling in the condition of 30 dps does not obscure the main effect of the rotation velocity of the image pattern on VIMS severity, assuming complete vection perception. However, it can be the cause of the non-significant difference of the level of sickness severity between the 30 dps condition and the other 2 non-zero velocity conditions, 60 dps and 90 dps (see details from Sections 6.3.3 to 6.3.5).

6.3.2 OKN slow-phase velocity (SPV), OKN gain, and foveal retinal slip velocity

An EOG unit mapping constant (in the unit of V) was calculated from the EOG recordings of eye calibration for each subject in each experimental session (see details in Section 4.5.3.4). As shown in Table 6.1, the value of the constant can be a

bit different across the 3 non-zero velocity conditions. Such a result is expected since the attachment positions of EOG electrodes in the 3 conditions conducted on a different day can be slightly different. According to a method presented in Section 4.5.3.4, to derive OKN SPV from raw eye position data, a lower and upper bound of OKN SPV in the unit of V per sample are calculated by Equations 4-1 and 4-2. The lower bounds in the unit of degree per second are calculated and listed in Table 6.1. Following the commencement of an optokinetic stimuli, the OKN SPV increases immediately to a level of 25 ± 2.7 dps, 30.9 ± 18.6 dps, and $19.0(9.8-39.6)$ in the conditions of 30 dps, 60 dps, and 90 dps, respectively.

Table 6.1 (a) EOG unit mapping constant calculated from horizontal eye position data recorded during eye calibration. Each number represents the voltage change of 15 deg eye rotation. (b) The lower bound of OKN SPV is in the unit of degree per second (dps)

Subject	(a)EOG unit mapping constant (V)			(b)OKN SPV lower bound(dps)		
	B	C	D	B	C	D
1	1.2	1.4	1.4	14.0	8.0	20.0
2	1	1	0.9	56.3	23.4	26.0
3	1.6	1.6	1.4	10.3	7.8	26.8
4	1.4	1.2	1	43.2	34.4	25.0
5	1.1	1.5	1.2	34.0	37.5	25.0
6	1	1	1	48.6	75.0	23.4
7	1	1	1	45.0	9.6	25.6
8	0.8	0.9	1.1	46.9	41.7	28.4
9	0.9	0.8	0.9	33.3	40.3	26.0
10	1.2	1	1.4	15.6	14.5	19.5
11	0.8	1	0.9	6.7	12.0	26.0
12	0.8	0.5	0.6	5.6	8.6	28.1
13	0.9	0.8	1	18.3	10.3	23.4
14	1.2	1.1	1.4	54.7	52.8	26.8

Given the lower and upper bounds (the rotation velocity of visual stimuli) of OKN SPV, EOG unit mapping constant as well as the sampling rate of EOG recording, OKN SPV time series can be derived in a way as defined by Equation 4-3. Appendix 6-3 lists all the individual plots of the OKN SPV time series. The average OKN SPV, OKN gain, and foveal retinal slip velocity are calculated and listed in Table 6.2. The OKN SPV that is averaged over time is 27.9dps (26.9-28.3), 47.8dps (23.6-52.3) and 41.5 ± 20.5 dps in the condition of 30 dps, 60 dps and 90 dps. The OKN gain is 0.93 dps (0.90-0.94), 0.8 dps (0.4-0.9), and 0.4 dps (0.3-0.6) in the 3 conditions, respectively. The foveal retinal slip velocity is 2.1(1.7-3.1), 12.2(7.7-36.4) and 48.6 ± 20.5 dps in the 3 conditions, respectively. Such results are consistent with reports by Koenig et al. (1978), which investigated the OKN SPV as a function of rotation velocity of visual stimuli under a similar experimental setting. As illustrated in Figure 6.2, the mean levels of OKN gain, OKN SPV and retinal slip velocity in the study by Koenig et al.(1978) are within the corresponding 25th -75th interquantile ranges of the OKN results in experiment 2.

Table 6.2 Average values of (a) OKN SPV calculated from Equation 4-3, (b) OKN gain defined as OKN SPV over the rotation velocity of image pattern, and (c) foveal retinal slip velocity defined as the rotation velocity of image pattern minus OKN SPV

Subject	(a)OKN SPV (dps)			(b)OKN gain			(c)Foveal retinal slip (dps)		
	B	C	D	B	C	D	B	C	D
1	22.6	15.5	24.8	0.4	0.2	0.8	37.4	74.5	5.2
2	58.1	44.1	28.0	1.0	0.5	0.9	1.9	45.9	2.0
3	17.8	26.8	28.4	0.3	0.3	0.9	42.2	63.2	1.6
4	49.4	47.9	27.6	0.8	0.5	0.9	10.6	42.1	2.4
5	48.2	51.4	27.8	0.8	0.6	0.9	11.8	38.6	2.2
6	54.0	81.8	26.7	0.9	0.9	0.9	6.0	8.2	3.3
7	51.9	24.0	27.7	0.9	0.3	0.9	8.1	66.0	2.3
8	52.4	57.8	29.2	0.9	0.6	1.0	7.6	32.2	0.8
9	47.4	64.4	28.0	0.8	0.7	0.9	12.6	25.6	2.0
10	26.7	26.6	23.8	0.4	0.3	0.8	33.3	63.4	6.2
11	19.3	26.9	28.0	0.3	0.3	0.9	40.7	63.1	2.0
12	15.8	23.1	29.1	0.3	0.3	1.0	44.2	66.9	0.9
13	28.7	23.4	26.7	0.5	0.3	0.9	31.3	66.6	3.3
14	57.2	66.6	28.4	1.0	0.7	0.9	2.8	23.4	1.6

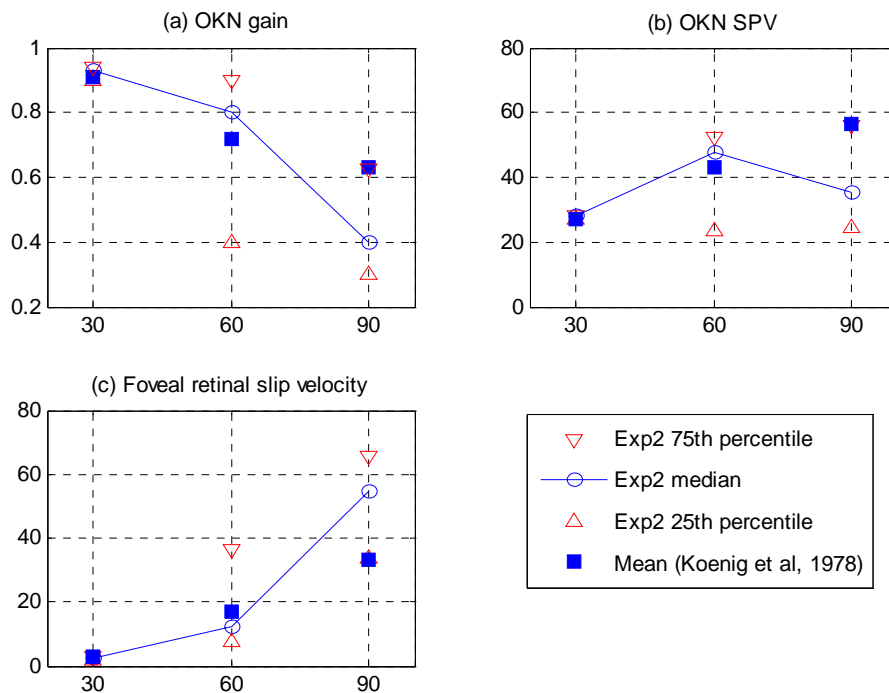


Figure 6.2 Comparing (a) OKN gain, (b) OKN SPV, and (c) foveal retinal slip velocity's median level of experiment two with results of Koenig et al., 1978

Both the original data of the 3 OKN related measures and transformed data ($\lambda=0.25$)

fail to pass the normality test. The Friedman test shows that the rotation velocity of

the image pattern has a significant main effect on OKN gain ($p < 0.01$) and the foveal retinal slip velocity ($p < 0.01$), but not on OKN SPV ($p > 0.05$). Such results indicate that H3.1 should not be rejected. A post-hoc test shows that (1) OKN SPV in the 30 dps condition is significantly lower than in the 60 dps and 90 dps conditions, and (2) OKN gain decreases significantly when the rotation velocity of the image pattern increases from 30 dps to 60 dps and from 60 dps to 90 dps, and (3) the foveal retinal slip velocity increases significantly when the rotation velocity of the image pattern increases from 30 dps to 60 dps and from 60 dps to 90 dps.

Table 6.3 Student-Newman-Keuls (SNK) tests on the effect of rotation velocity of image pattern on (a) OKN SPV, (b) OKN gain, and (c) the foveal retinal slip velocity for velocity condition of 2 dps, 14 dps, and 34 dps

DRUMVEL	N	Subset	
		1	2
30dps	14	27.443	
60dps	14		39.250
90dps	14		41.450
Sig.		1.000	.627

(a) Dependent variable: OKN SPV

DRUMVEL	N	Subset		
		1	2	3
90dps	14	.461		
60dps	14		.654	
30dps	14			.915
Sig.		1.000	1.000	1.000

(b) Dependent variable: OKN gain

DRUMVEL	N	Subset		
		1	2	3
30dps	14	2.557		
60dps	14		20.750	
90dps	14			48.550
Sig.		1.000	1.000	1.000

(c) Dependent variable: foveal retinal slip velocity

Consistent with the expectations based on the results from Koenig et al. (1978), the linear relationship between the foveal retinal slip velocity (y) and rotation velocity of the optokinetic stimuli (x) is described by a first-order polynomial function:

$$\begin{aligned} y &= ax + b \\ a &= 0.77(p < 0.05) \\ b &= -22.04(p < 0.05) \end{aligned} \quad (6-1)$$

where R square = 0.62 (adjusted R square = 0.61). Such a result indicates that H4.2 should not be rejected (see Figure 6.3).

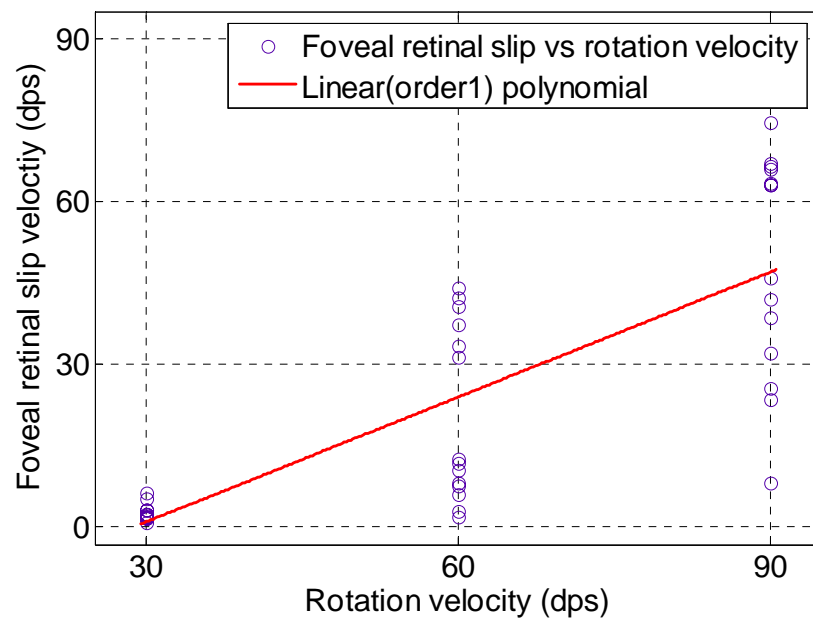


Figure 6.3 Linear relationships between the foveal retinal slip velocity and the rotation velocity of the optokinetic stimuli.

6.3.3 7-point nausea rating

Individual data regarding the time course of nausea severity measured by a 7-point nausea rating scale is shown in Appendix 6-4. An experiment session was terminated

at the moment when a subject reported G on the 7-point nausea scale (i.e., a rating of 6 or “moderate nausea and want to stop”). A rating of 6 was assigned for the remaining period. In this study, a subject who reached a rating of 3 (“mild nausea”) or higher was considered as “sick” while she was considered as “not sick” if the maximum rating that was reached was 2 or lower. One subject out of the 14 subjects became sick in the rotation velocity condition of 0 dps. For that subject, the 0 dps condition was her first experience. Such results indicate that VIMS is generated without any “motion” of visual stimuli for the particular subject. This phenomenon is initially suspected to be a type of photosensitivity (pattern sensitivity). As discussed in Section 5.3.3, neither the spatial frequency (0.134cpd) nor the flash rate (60Hz) of the static visual stimuli in experiment one is in the corresponding photosensitivity ranges (2-4 cpd spatial frequency and 13-21Hz flash rate). Visual inspection of a corresponding video clip did not find common seizure associated symptoms. It was also noticed that the rating level of the time course can decrease after reach a rating of 3 rather than continuing to increase. All the evidence made such sickness provoked in the static condition less possible as a type of pattern sensitivity.

As shown in Figure 6.4, time courses of the median 7-point nausea rating in 0 dps, 30 dps and 90 dps never reached a rating of 3 unlike 60 dps. The nausea rating data

(averaged over 30 min) passed the normality test ($p>0.05$), but not the variance homogeneity test ($p<0.01$). The transformed nausea rating data ($\lambda=0.25$) passed the variance homogeneity test ($p>0.1$), but not the normality test ($p<0.01$ in conditions A and D). The Friedman test shows that the rotation velocity of the image pattern has a significant main effect on the 7-point nausea rating ($p<0.01$). Such results indicate that H3.2 should not be rejected. A post-hoc test shows that (i) the nausea severity level in the 60 dps condition is the highest among the 3 non-zero velocity conditions, and (ii) the nausea severity level measured by the 7-point nausea rating in the 0 dps condition is significantly lower than the other 3 conditions; i.e., 30 dps, 60 dps and 90 dps, and (iii) the nausea severity levels measured by the 7-point nausea rating in the 3 non-zero velocity conditions are not significantly different from each other. Such results are confirmed by the data of the 7-point nausea rating at 30 min as shown in Table 6.4.

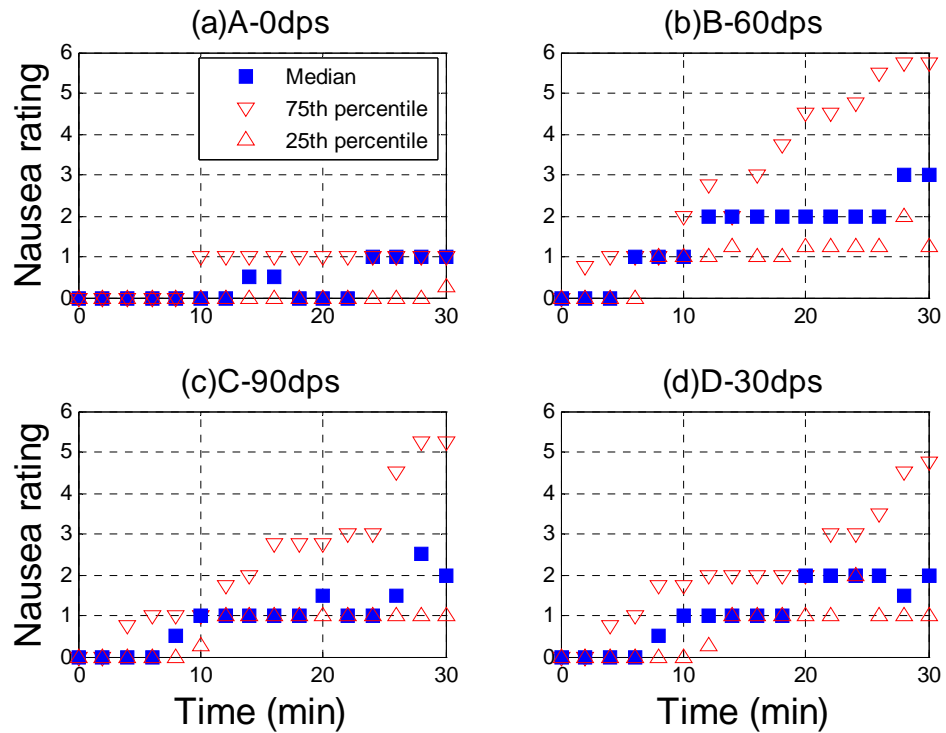


Figure 6.4 Median, 25th and 75th percentile nausea rating as a function of exposure duration for 4 velocity conditions: rotating at (a) 0 dps, (b) 60 dps, (c) 90 dps, and (d) 30 dps

Table 6.4 Student-Newman-Keuls (SNK) tests on the effect of rotation velocity of the image pattern on a 7-point nausea rating (a) averaged over 30 mins and (b) at 30 min

drum velocity	N	Subset	
		1	2
0dps	14	.424107	
30dps	14		1.428571
90dps	14		1.508929
60dps	14		2.053571
Sig.		1.000	.124

(a) Dependent variable: 7-point nausea rating averaged over 30min

drum velocity	N	Subset	
		1	2
0dps	14	.93	
30dps	14		2.79
90dps	14		2.93
60dps	14		3.36
Sig.		1.000	.619

(b) Dependent variable: 7-point nausea rating at 30min

Spearman's correlation analysis of data in condition 0dps and 60dps shows a piece-wise linear relationship between nausea severity and drum rotation velocity ($\rho=0.785$, $p<0.01$) while such relationship is not found from data of all 4 velocity conditions. Such results and the observed inverted-U shape shown in Figure 6.5 indicate that the H4.1 should not be rejected.

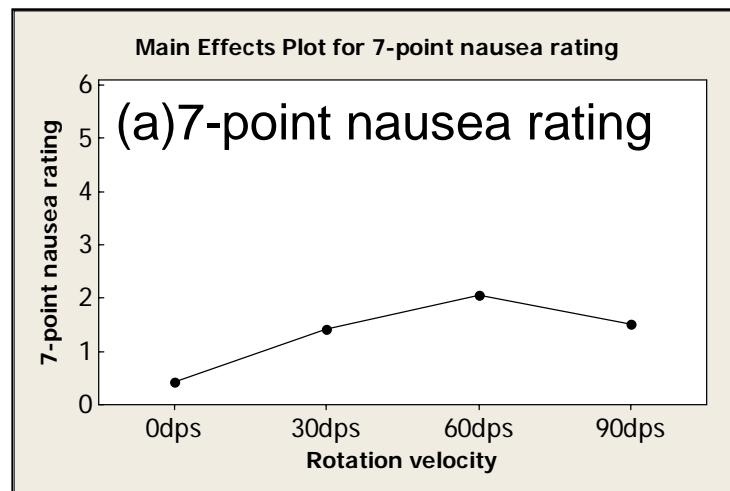


Figure 6.5 Observed inverted shape relationship between nausea severity measured by 7-point nausea rating and drum rotation velocity

As discussed in Section 6.3.1, the coupling of OKN and vection in the last 12 mins in the 30 dps condition can induce a higher sickness severity level than in the presence of OKN alone that is decoupled from vection perception. Therefore, if only the data from the first 18 mins are used in the data analysis, it is possible that a significant difference of VIMS severity among the 3 non-zero velocity conditions can be identified.

Both the original 7-point nausea rating data (averaged over or at 18 min) and the transformed data ($\lambda=0.25$) failed to pass the normality test (in each case $p>0.05$). The Friedman test shows that the rotation velocity of the image pattern has a significant main effect on the nausea severity measured by (i) the 7-point nausea rating at 18 min ($p<0.01$) and (ii) the 7-point nausea rating data that is averaged over 18 min ($p<0.01$). Such results indicate that H3.2 should not be rejected. A post-hoc test on the data of the 7-point nausea rating at 18 min shows that (i) the nausea severity in the 60 dps condition is the highest among the 4 velocity conditions, (ii) the nausea severity in the 60 dps condition is significantly higher than in the conditions of 30 dps and 0 dps, (iii) the nausea severity in the conditions of 30 dps and 90 dps is significantly higher than in the condition of 0 dps, and (iv) the nausea severity in the conditions of 60 dps and 90 dps is not significantly different from each other. A post-hoc test on the data of the 7-point nausea rating that is averaged over 18 mins shows that (i) the nausea severity in the 60 dps condition is the highest among the 4 velocity conditions, (ii) the nausea severity in the 60 dps condition is significantly higher than in the condition of 0 dps, and (iii) the nausea severity levels in the 3 non-zero velocity conditions are not significantly different from each other (See Table 6.5).

Table 6.5 Student-Newman-Keuls (SNK) tests on the effect of the rotation velocity on the nausea severity measured by 7-point nausea rating (a) averaged over the first 18 min (b) at 18 min. 0 dps, 30 dps, 60 dps and 90dps is labeled as 1, 2, 3, and 4, respectively

drum velocity	N	Subset	
		1	2
1	14	.314	
2	14	.871	.871
4	14	.879	.879
3	14		1.429
Sig.		.063	.067

(a) Dependent variable: 7-point nausea rating averaged over the first 18min

drum velocity	N	Subset		
		1	2	3
1	14	.43		
2	14		1.57	
4	14		1.86	1.86
3	14			2.71
Sig.		1.000	.527	.063

(b) Dependent variable: 7-point nausea rating at 18min

6.3.4 Nausea ratio scale data

If an experiment session stopped before the 30 mins, the number of the last reported nausea ratio scale data was assigned for the remaining period. Individual data regarding the time course of modulus equalized nausea ratio scale data are shown in Appendix 6-5. Three out of the 14 subjects were “not sick” in all 4 velocity conditions, consistent with revelations by the 7-point nausea rating. As shown in Figure 6.6, medians of nausea ratio scale data in the 0 dps and 30 dps conditions are always zero along the time axis and those in the 60 dps and 90 dps conditions eventually reach a non-zero level.

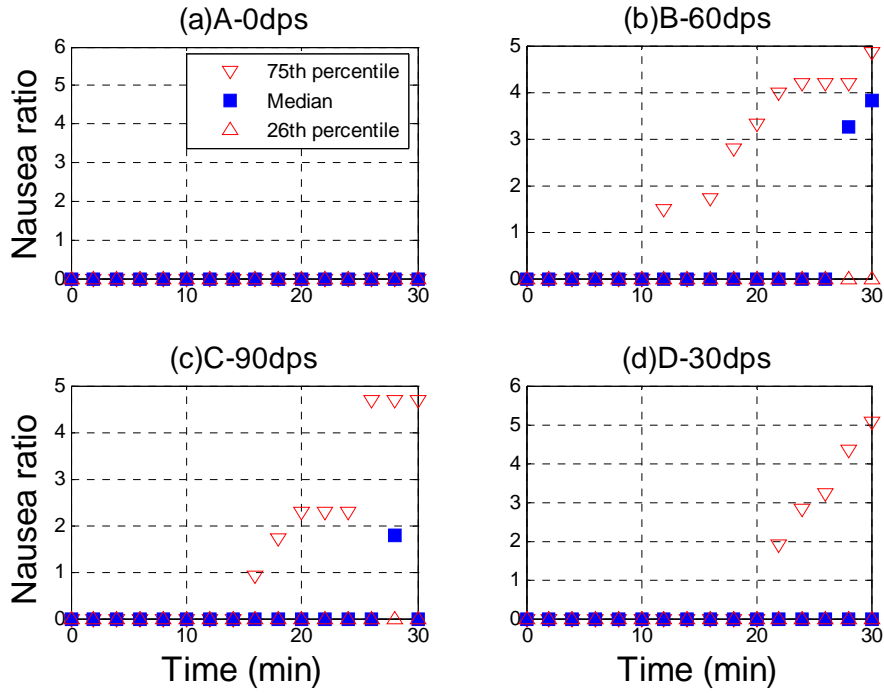


Figure 6.6 Median, 25th and 75th percentile of nausea ratio scale data as a function of exposure duration for the 4 velocity conditions: rotating at (a) 0 dps, (b) 60 dps, (c) 90 dps, and (d) 30 dps

Both the nausea ratio scale data (averaged over 30 mins) and transformed data ($\lambda=0.25$) failed to pass the normality test. The Friedman test shows that the rotation velocity of the image pattern has a significant main effect on the nausea ratio scale data that is averaged over 30 min ($p<0.05$). Such results indicate that H3.2 should not be rejected. A post-hoc test (see Table 6.6(a)) shows that (i) the nausea severity level in the 60 dps condition is the highest among the 3 non-zero velocity conditions, (ii) the nausea ratio scale data in 60 dps is significantly higher than in the condition of 0 dps, and (iii) the nausea ratio scale data in the 3 non-zero velocity conditions are not significantly different from each other. Such results are confirmed by a nausea severity measure of the nausea ratio scale data at 30 min as shown in Table 6.6(b).

Based on comments of thesis examination committee, the raw nausea ratio scale data was re-normalized. A small positive constant was used to replace each zero value in a row where there are both zero and non-zero data. Friedman test of the re-processed data shows the same results, i.e., rotation velocity has a significant effect on the nausea ratio scale data ($p<0.05$). Wilcoxon sign-rank test re-confirmed the significant difference between the nausea severity in 60dps condition and in 0dps condition ($p<0.05$).

Table 6.6 Student-Newman-Keuls (SNK) tests on the effect of rotation velocity of the image pattern on nausea ratio scale data (a) averaged over 30 mins and (b) at 30 min

drum velocity	N	Subset	
		1	2
0dps	14	.12	
30dps	14	.67	.67
90dps	14	.89	.89
60dps	14		1.12
Sig.		.060	.361

(a) Dependent variable: nausea ratio scale data averaged over 30min

drum velocity	N	Subset	
		1	2
0dps	14	.20	
30dps	14	2.07	2.07
90dps	14	2.23	2.23
60dps	14		2.85
Sig.		.070	.655

(b) Dependent variable: nausea ratio scale data at 30min

Spearman's correlation analysis of data in condition 0dps and 60dps shows a piece-wise linear relationship between nausea severity and drum rotation velocity

($\rho=0.583$, $p<0.01$) while such relationship is not found from data of all 4 velocity conditions. Such results and the observed inverted-U shape shown in Figure 6.7 indicate that the H4.1 should not be rejected.

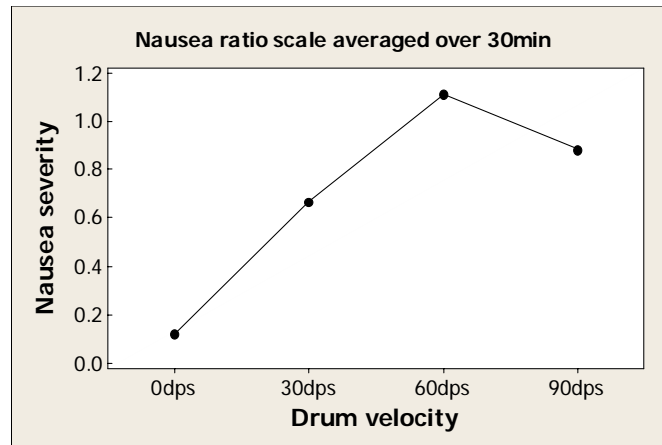


Figure 6.7 Observed inverted shape relationship between nausea severity measured by nausea ratio scale and drum rotation velocity

As observed from Figure 6.5, the median data from the first 18 mins does not show any differences among the 4 velocity conditions. Such an observation is confirmed by the Friedman test which shows that the rotation velocity of the image pattern has no significant main effect on the nausea severity measured by the nausea ratio scale data (averaged at or over 18 min) (in each case $p>0.05$).

6.3.5 Simulator Sickness Questionnaire Scores

Individual data regarding the pre and post-exposure SSQ total scores and sub-scores are shown in Appendix 6-6. The Wilcoxon signed-rank test was used to test the significance of the differences between a pair of post and pre-scores in each

condition since the SSQ data were of a non-parametric distribution. It was found that the post-exposure scores of SSQ-N, SSQ-O, SSQ-D and SSQ-TS are all significantly larger than the corresponding pre-exposure scores in all 4 velocity conditions (in each case $p < 0.05$). Such results indicate that the group of subjects becomes “sick” in all 4 conditions, including the 0 dps condition in which subjects viewed a static image pattern. As discussed in Section 6.3.3, this type of sickness is neither induced by any “motion” of visual stimuli nor by pattern sensitivity.

As shown in the instructions of experiment two (Appendix 6-2), the subjects were told to gaze directly at the static image pattern in front of them and maintain a position of viewpoint although no eye fixation point was presented in the 0 dps condition. As well, the subjects were requested to maintain their original aligned head orientation for as long as possible. During the 30 min exposure period, the subjects were told to refrain from moving the hand with the EOG electrode. Such constraints of eye, head and hand movements, and lengthy standing might be capable of inducing some level of discomfort related to body and eye fatigue. This deduction is supported by empirical data since 12 out of the 14 subjects reported “fatigue” and 10 out of the 14 subjects reported “eye strain” after exposure. Moreover, there were 11 subjects who reported “boredom”. It was understandable since the subjects were told to view the static image pattern without changes for 30 min.

Although the change from post to pre-exposure SSQ scores (see Figure 6.8) captured the change of a participant's state of health by viewing provocative stimuli under the experimental setup, the difference in scores of SSQ (post pre-scores) cannot quantify such change in the state of health since SSQ employed the ordinal scale, but not ratio scale (Kennedy et al., 1990). Therefore, pre-SSQ scores and post-SSQ scores are analyzed separately in this study.

The pre-SSQ total score in 0 dps, 30 dps, 60 dps and 90 dps was 0.0(0.0-6.5), 0.0(0.0-3.7), 1.9(0.0-7.5) and 1.9(0.0-7.5), respectively. Three out of the 14 subjects, two out of the 14 subjects and one out of the 14 subjects reported a pre-SSQ total score higher than 10 in 0 dps, 60 dps and 90 dps conditions, respectively. As mentioned in Section 4.5.3.2, a different control approach of pre-exposure health state is employed in this study from those used by Kennedy et al. (1999) who excluded any subject with a pre-exposure SSQ total score of more than 10 in their experiments. Therefore, data analysis on pre-exposure SSQ scores is used to check whether the control approach adopted in this study is efficient enough.

Both the original pre and post-SSQ data and transformed pre and post-SSQ data ($\lambda=0.25$) failed to pass the normality test (in each case $p<0.01$). The Friedman test shows that none of the 4 pre-SSQ scores measuring the pre-exposure state of health

has a significant fluctuation over the 4 velocity conditions conducted on different days (in each case $p>0.1$). Such results indicate that the control of the pre-exposure state of health in experiment two is good enough.

The Friedman test shows that the rotation velocity of the image pattern has a significant effect on sickness severity measured by post-exposure SSQ-N, SSQ-O, SSQ-D and SSQ-TS (in each case $p<0.05$). Such results indicate that H3.2 should not be rejected. A post-hoc test (see Table 6.7) shows that (i) SSQ scores in the 60 dps condition is the highest among all 4 velocity conditions, (ii) SSQ scores in the 0 dps condition are significantly lower than in the 60 dps condition, and (iii) SSQ scores in the 3 non-zero velocity conditions are not significantly different from each other.

Table 6.7 Student-Newman-Keuls (SNK) tests on the effects of the rotation velocity of the image pattern on sickness severity measured by post SSQ total score and 3 sub-scores

DRUMVEL	N	Subset	
		1	2
0dps	14	14.3100	
90dps	14	34.0714	34.0714
30dps	14	35.4343	35.4343
60dps	14		42.2486
Sig.		.090	.682

(a)Dependent variable: post SSQ-N

DRUMVEL	N	Subset	
		1	2
0dps	14	24.9057	
30dps	14		45.4800
90dps	14		49.2700
60dps	14		60.0986
Sig.		1.000	.172

(b)Dependent variable: post SSQ-O

DRUMVEL	N	Subset	
		1	2
0dps	14	13.92	
30dps	14		47.73
90dps	14		61.65
60dps	14		66.62
Sig.		1.000	.373

(c)Dependent variable: post SSQ-D

DRUMVEL	N	Subset	
		1	2
0dps	14	21.6386	
30dps	14		49.1543
90dps	14		54.2300
60dps	14		64.1143
Sig.		1.000	.308

(d)Dependent variable: post SSQ-T

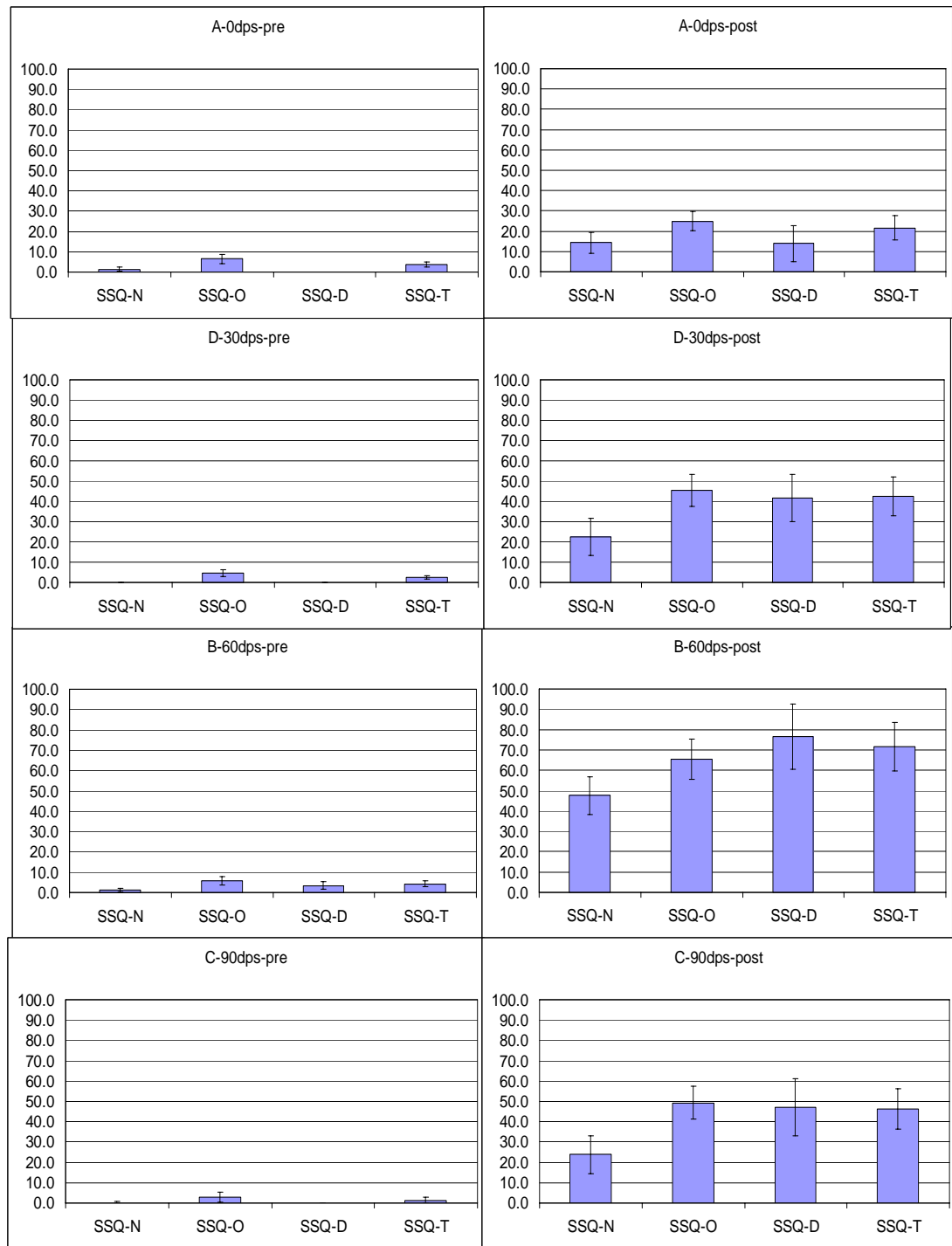


Figure 6.8 Mean and SE (standard error) of pre and post-exposure SSQ total scores and sub-scores for conditions of 0 dps, 30 dps, 60 dps and 90 dps.

Spearman's correlation analysis of data in condition 0dps and 60dps shows a piece-wise linear relationship between nausea severity and drum rotation velocity

($\rho=0.583$, $p<0.01$) while such relationship is not found from data of all 4 velocity conditions. Such results and the observed inverted-U shape shown in Figure 6.9 indicate that the H4.1 should not be rejected.

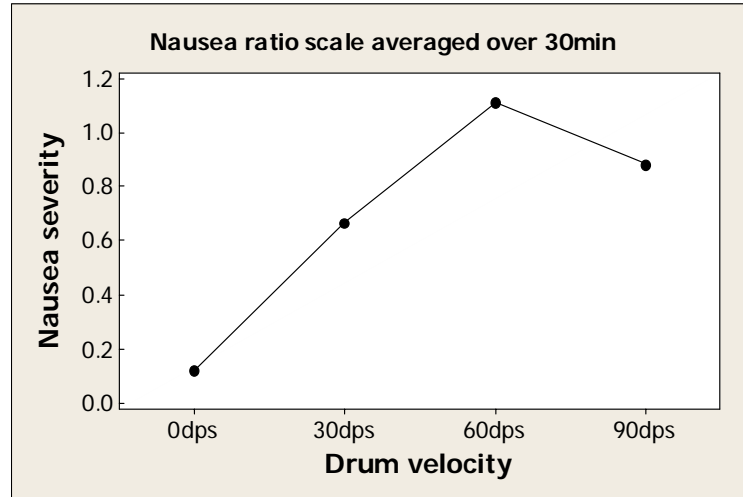


Figure 6.9 Observed inverted shape relationship between nausea severity measured by post SSQ-Nausea and drum rotation velocity

As mentioned in Section 4.5.3.2, data analysis on post minus pre (post-pre) different scores is documented for comparison purposes only (see Figure 6.10). The Friedman test shows that the rotation velocity of the image pattern has a significant effect on VIMS severity measured by difference in scores of SSQ-N ($p<0.05$), SSQ-O ($p<0.01$), SSQ-D ($p<0.01$) and SSQ-TS ($p<0.01$). Such results indicate that H2.2 should not be rejected. A post-hoc test (see Table 6.8) shows that (i) the difference in SSQ scores in the 60 dps condition is the highest among all 4 velocity conditions, (ii) the difference of the post-pre SSQ scores in the 3 non-zero velocity conditions is not significant, and (iii) the difference in the SSQ score in the 60 dps condition is

significantly higher than in the condition of 0 dps.

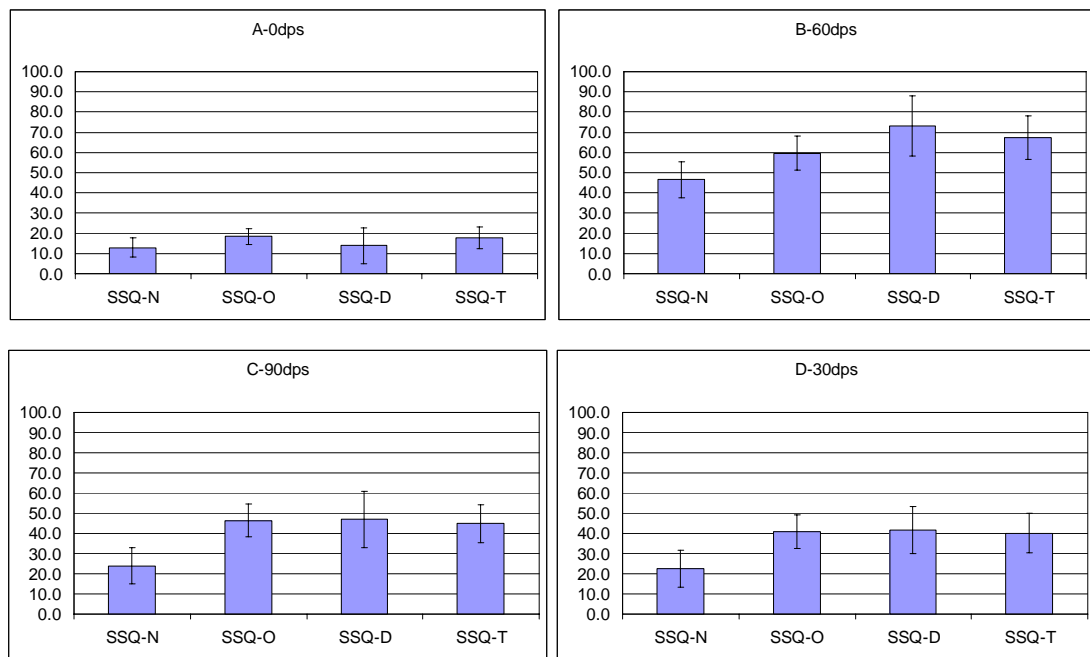


Figure 6.10 Post-Pre SSQ total scores and 3 sub-scores in the 4 conditions of rotation velocity of image pattern, i.e., 0 dps, 30 dps, 60 dps, and 90 dps

Table 6.8 Student-Newman-Keuls (SNK) tests on the effect of rotation velocity on differences (post-pre) SSQ total score and 3 sub-scores at a rotation velocity of 0 dps, 30 dps, 60 dps and 90 dps

DRUMVEL	N	Subset	
		1	2
0dps	14	14.3100	
90dps	14	34.0714	34.0714
30dps	14	35.4343	35.4343
60dps	14		42.2486
Sig.		.090	.682

(a)Dependent variable: post-pre SSQ-N

DRUMVEL	N	Subset	
		1	2
0dps	14	24.9057	
30dps	14		45.4800
90dps	14		49.2700
60dps	14		60.0986
Sig.		1.000	.172

(b)Dependent variable: post-pre SSQ-O

DRUMVEL	N	Subset	
		1	2
0dps	14	13.92	
30dps	14		47.73
90dps	14		61.65
60dps	14		66.62
Sig.		1.000	.373

(c)Dependent variable: post-pre SSQ-D

DRUMVEL	N	Subset	
		1	2
0dps	14	21.6386	
30dps	14		49.1543
90dps	14		54.2300
60dps	14		64.1143
Sig.		1.000	.308

(d)Dependent variable: post-pre SSQ-T

6.3.6 Correlation analysis of OKN related measures, 7-point nausea rating, nausea ratio scale data, and post SSQ-Nausea (SSQ-N)

As illustrated in Figure 6.11, there is an inverted-U shape relationship between the rotation velocity of the image pattern and the sickness severity measured by the 7-point nausea rating and nausea ratio scale data that are averaged over 30 min as well as the post-exposure SSQ-N score. The level of the three VIMS measures increases when the rotation velocity increases up to 60 dps and then drops down when the rotation velocity increases further up to 90 dps. The foveal retinal slip velocity and the OKN SPV are found to monotonically increase from a 30 dps condition up to 90 dps condition, consistent with the trend reported by Koenig et al. (1978) in the retinal slip velocity and OKN SPV (see Figure 6.2). The OKN gain is found to monotonically decrease from a 30 dps condition to 90 dps condition, also consist with the trend of OKN gain reported by Koenig et al. (1978). The foveal retinal slip velocity is significantly correlated with OKN SPV ($\rho=-0.38$, $p<0.05$) and OKN gain ($\rho=-0.973$, $p<0.01$). The OKN SPV and OKN gain are significantly correlated ($\rho=0.519$, $p<0.01$) (see Figure 6.12).

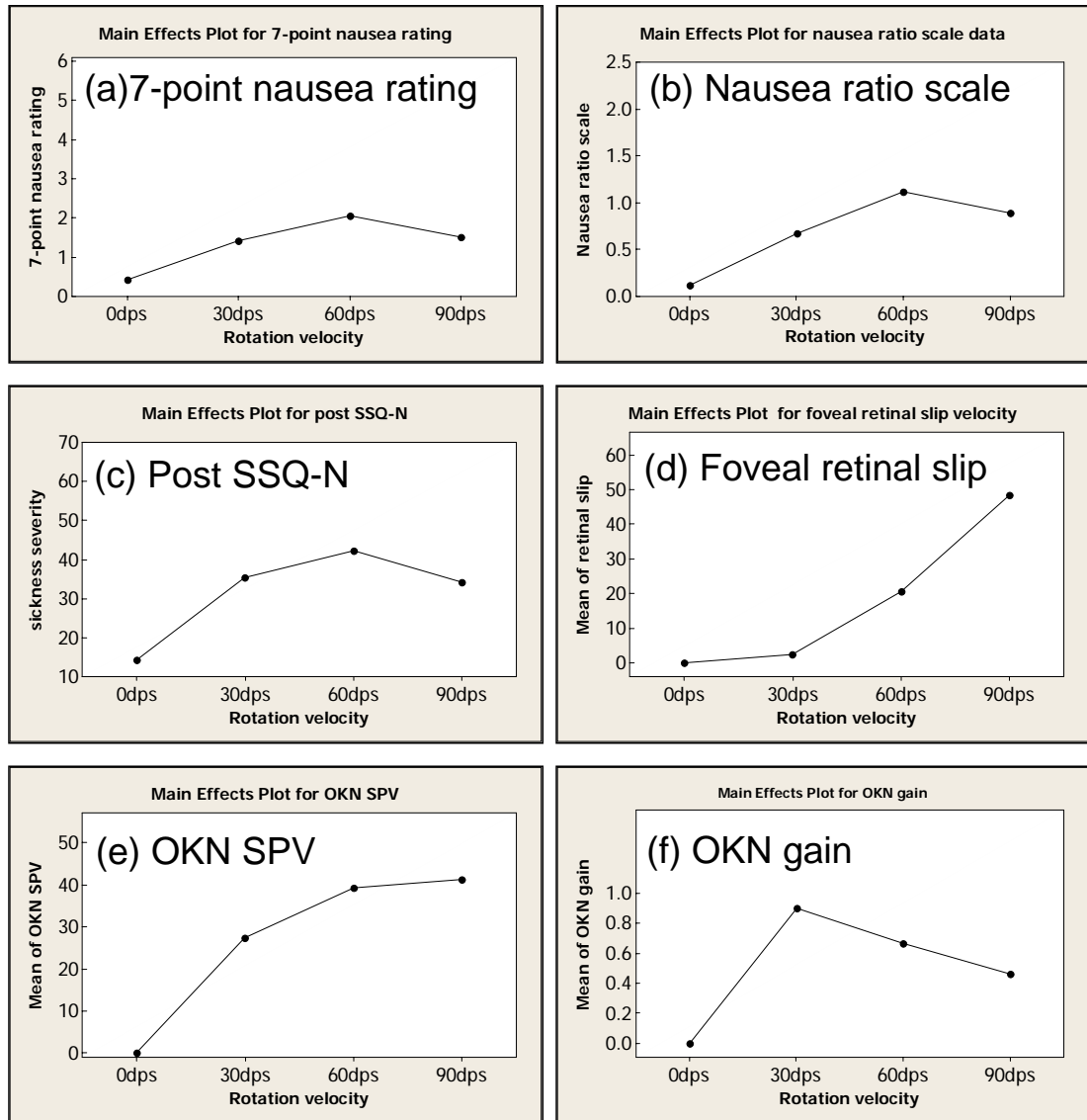


Figure 6.11 Main effect plots of the rotation velocity of the image pattern on (a) 7-point nausea rating averaged over 30 min, (b) nausea ratio scale data averaged over 30 min, (c) post SSQ-N score, (d) the foveal retinal slip velocity, (e) OKN slow-phase velocity (SPV), and (f) OKN gain

Similar to the reports in experiment one (see Section 5.3.6), the nausea ratio scale data from the free modulus magnitude estimation is significantly correlated with the 7-point nausea rating ($\rho=0.871$, $p<0.01$) and post-exposure SSQ-N score ($\rho=0.711$, $p<0.01$) (see Figure 6.10). Such results indicate that the nausea ratio

scale data collected by free modulus magnitude estimation can be considered as another valid measure of VIMS severity in future empirical studies, aside from the two commonly used measures; i.e., the 7-point nausea rating and SSQ scores.

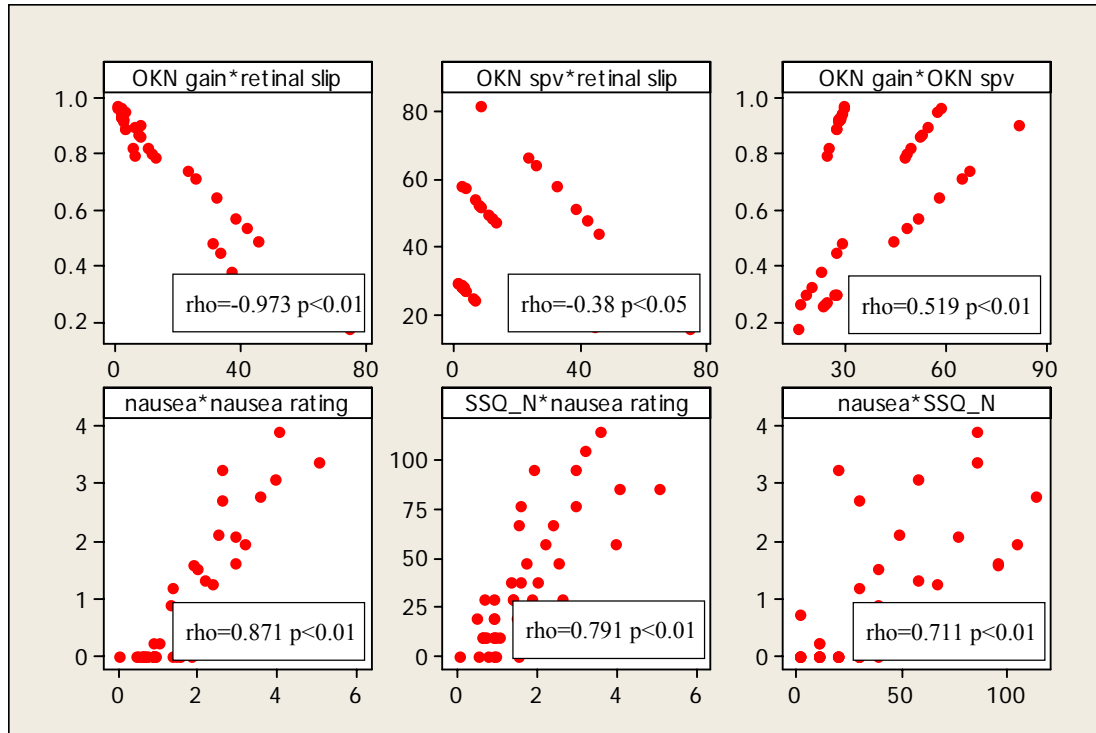


Figure 6.12 Scatter plots and correlation coefficients (Spearman's rho) summarized for correlation analysis of the foveal retinal slip velocity (labeled as retinal slip), OKN SPV, OKN gain, 7-point nausea rating that is averaged over 30 min (labeled as nausea rating), nausea ratio scale data that is averaged over 30 min (labeled as nausea) and post SSQ-N score (labeled as SSQ_N)

Spearman's correlation analysis of data in condition 0dps and 60dps shows a piece-wise linear relationship between nausea severity and the foveal retinal slip velocity ($\rho=0.574$, $p<0.01$) while such relationship is not found from data of all 4 velocity conditions. Such results and the observed inverted-U shape shown in Figure 6.13 indicate that the H4.3 should not be rejected.

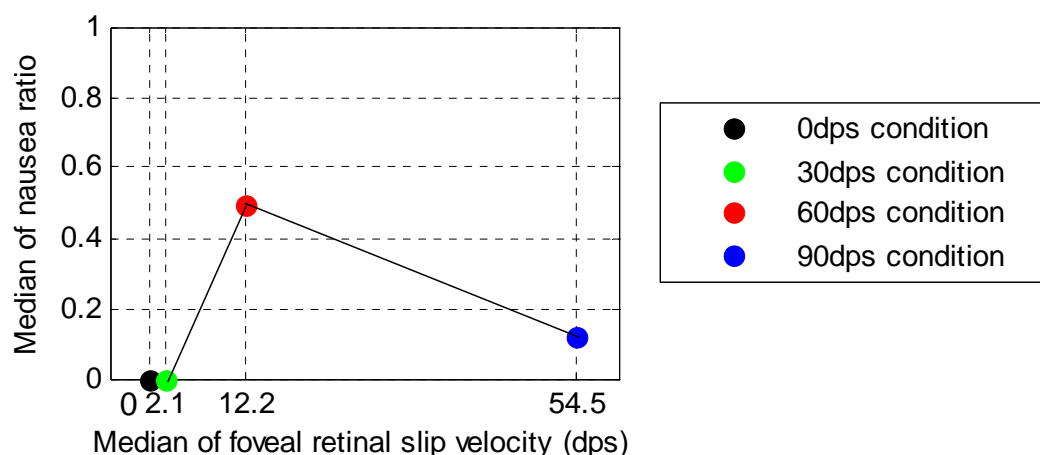


Figure 6.13 Observed linear increasing trend of nausea severity measured by nausea ratio scale (Median of 14 subjects) as a function of the foveal retinal slip velocity (Median of 14 subjects)

6.3.7 Visual acuity at near point and motion sickness susceptibility

Visual acuity at the near point was 11.6 ± 1.2 . MSSQ-short raw score was 14.6 ± 7.6 .

Neither the visual acuity at the near point nor the previous susceptibility to motion sickness are found to be significantly correlated with any VIMS measure in any velocity condition (in each case $p > 0.05$). It is reported that visual acuity at near point is significantly correlated with VIMS severity, which is provoked by a virtual optokinetic drum rotating at a speed of 30 dps without eye fixation (Webb & Griffin, 2002). Such a discrepancy in the results of the two studies might have resulted from the difference in their experiment design. In Webb and Griffin (2002), the visual acuity at the near point was measured when the subjects did not wear their glasses. However in experiment two, the visual acuity at the near point was measured when the subjects wore their glasses.

6.4 Discussions

The current available VIMS theories suggest 4 factors as the potential causing factor of VIMS: (i) vection, (ii) optokinetic nystagmus (OKN), (iii) postural instability, and (iv) subjective-vertical conflict. In experiment two, vection was completely suppressed by visual stimuli having a central visual field and peripheral visual field rotating in opposite directions within a time period of 18 min. At the same time, the effects of postural instability and subjective-vertical conflict were controlled across different velocity conditions by head fixation and head orientation aligning (see Chapter 4). Among the 4 factors, OKN (in particular, the foveal retinal slip velocity) was the only one that was not controlled across different velocity conditions. Experiment two results show that the rotation velocity of the optokinetic stimuli has a significant main effect on both the foveal retinal slip velocity ($p < 0.01$) and the VIMS severity ($p < 0.05$). Moreover, the foveal retinal slip velocity in each non-zero velocity condition is found to be significantly different from each other. Such results indicate that the main effect of the rotation velocity of the optokinetic stimuli on VIMS severity is mediated by its main effect on the foveal retinal slip velocity. In other words, such results are consistent with the notion that OKN is a primary cause of VIMS.

Consistent with reports by Koenig et al. (1978), the foveal retinal slip velocity is found to have a linear relation with the rotation velocity of the optokinetic stimuli in a range from 30 dps to 90 dps (Equation 6-1). When the rotation velocity increases from 30 dps to 60 dps and then to 90 dps, the foveal retinal slip velocity significantly increases as well.

Experiment one identified a linear relation between vection velocity and VIMS severity in the absence of OKN, and between rotation velocity of the optokinetic stimuli and VIMS severity in the absence of OKN. Experiment two identified an inverted-U shape relation between the foveal retinal slip velocity and VIMS severity in the absence of vection perception, and between rotation velocity of the optokinetic stimuli and VIMS severity in the absence of vection perception. Since experiments one and two were investigated under a similar set of retinal slip velocity levels (see Section 5.2.3), the results of these two studies can explain the inverted U-shape between the rotation velocity of an optokinetic stimuli and provoked sickness severity accompanied by both vection and OKN (Hu et al., 1989).

As discussed in Section 5.2.3, the three non-zero velocity conditions of experiment

one (i.e. 2dps, 14dps, 34dps) are different from in experiment two (i.e. 30dps, 60dps, 90dps), which are chosen on purpose to map the retinal slip velocity activating human's visual system in the two experiments. Such mapping was achieved by using SPV data reported by Koenig, et al (1978). However, Figure 6.2 indicates that the OKN SPV data collected in experiment two are a bit different from date reported by Koenig, et al (1978). As shown in Figure 6.14, 60dps and 90dps velocity condition in experiment two are corresponding to 12dps and 49dps retinal slip velocity levels, respectively. However, most likely such mapping mismatch will not affect the conclusions of experiment one with regards to the H2.1 as indicated by simulations of model one as shown in Figure 6.15.

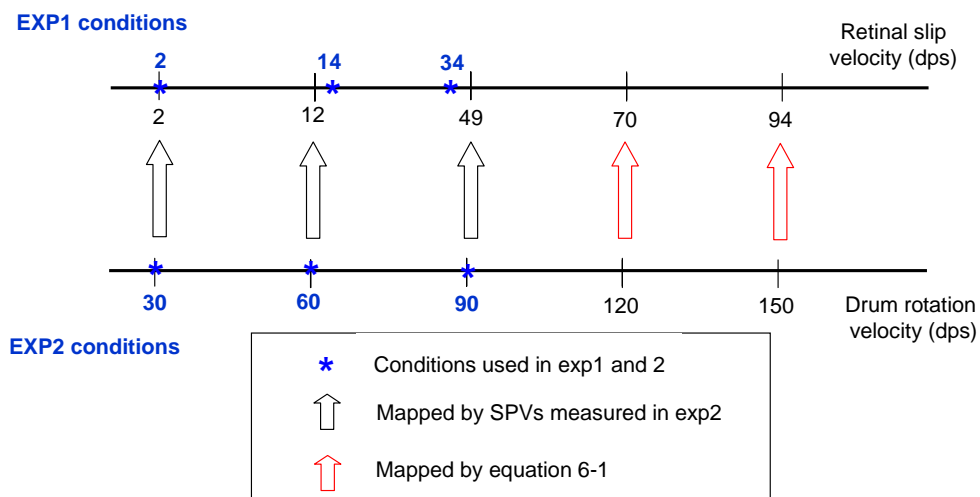


Figure 6.14 Mapping of retinal slip velocity levels between experiment one and two

The model simulated nausea severity monotonically increases along with the increase of drum rotation velocity (equal to drum rotation velocity in experiment one

and model one) within the range of 2dps to 70dps. Such results indicated that most likely the H2.1 will still be rejected if one extract condition at the drum rotation velocity of 49dps is run for experiment one. Furthermore, it is worth of pointing out that it is possible the linear relationship between nausea severity and drum rotation velocity will not exist anymore when the range of drum rotation velocity is further extended to 94dps. Such implication deserves further empirical investigations.

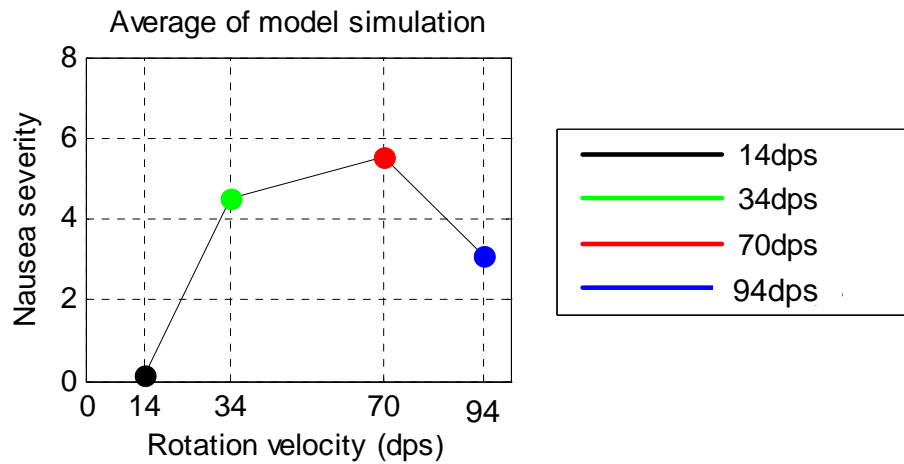


Figure 6.15 Model one simulated nausea severity at drum rotation velocity levels of 14dps, 34dps, 70dps, and 94dps.

6.5 Conclusions

VIMS is provoked in the presence of OKN and in the absence of vection perception.

Results indicate that all hypotheses (H3.1 to H3.2 and H4.1 to H4.3) of experiment two should not be rejected. Consistent to expectations on the basis of the extraocular afference hypothesis, the foveal retinal slip velocity is found to be the primary cause of VIMS provoked in experiment two. Moreover, an inverted U-shape between the

foveal retinal slip and the VIMS severity, and between the rotation velocity of the optokinetic stimuli and the VIMS severity, is identified. Results of the two experiments indicate that inverted U-shape between the drum rotation velocity and the VIMS severity reported by Hu et al. (1989) is mainly mediated by the effect of OKN on VIMS, which is confounded with the effect of vection on VIMS.

CHAPTER 7

MODEL VALIDATIONS

SUMMARY

This chapter presents model simulations used to validate model one (relating vection and VIMS) and model two (relating OKN and VIMS). The motivations behind the model validations are presented first. After a brief overview of the validating methods, the simulated (in the stage of “pre-validation”)/predicted (in the stage of “validation”) data of models one and two are compared with empirical data collected in experiments one and two, respectively. In short, both models one and two have satisfactory performances with regards to VISM severity predictions in different rotation velocity conditions.

7.1 Motivations

As demonstrated in Sections 2.5 and 3.5, model one relating vection and VIMS is capable of simulating rated VIMS severity as a function of exposure duration in Stern et al. (1990) and model two is capable of simulating the difference in rated levels of nausea severity with and without eye fixation as a function of exposure duration as reported in Webb & Griffin (2002). However, neither of the two studies

collected the ratio scale data of VIMS severity. Furthermore, each study involved only one drum rotation velocity condition: rotating at a speed of 60 dps in Stern et al. (1990) and 30 dps in Webb and Griffin (2002). Therefore, two experiments are conducted for model validation purposes: experiment one for validating model one and experiment two for validating model two (See Chapters 4, 5 and 6). In this chapter, models one and two are validated separately against the nausea ratio scale data at 3 non-zero rotation velocity conditions: 2 dps, 14 dps and 34 dps for model one, and 30 dps, 60 dps and 90 dps for model two. The following sections will first present a methodology overview of the model validations. This is followed by details of the comparison of model simulated/predicted data and empirically collected data for each model.

7.2 Methodology overview

Models one and two are defined by eight free parameters, respectively (see Sections 2.4.4 and 3.4.4). Before model validation, the eight free parameters were tuned to a set of values so that the model simulated data and empirical data in one rotation velocity condition were as close as possible. This stage was named “pre-validation”. After that, each model was validated against the data in the other two velocity conditions, given that the values of the model free parameters were unchanged, if

applicable. If the model predicted that the nausea severity level was within its corresponding empirical interquantile interval (25th-75th percentile) in each of the two velocity conditions, the model was verified as able to simulate VIMS elicitation. This stage was named “validation”.

In the pre-validation stage of model one, the first step was to tune the parameter Φ in weighting logic function K (in module 1) so that the steady state of the model simulated vection velocity was equal to an empirical benchmark (see Chapter 2). The ratio scale data of vection velocity (medians of the ratio scale data of the 14 subjects that were averaged over 30 min) in the rotation velocity condition of 34 dps was chosen as the empirical benchmark in this case. Defining the vection gain (G_v) as the median vection velocity over the rotation velocity of the optokinetic stimuli, Φ should be set to a value equal to $G_v/2$ (see Equation 2-2 and Figure 8.3) where Φ varies in a range of 0 to 0.5 and G_v varies in a range from 0 to 1. The parameter M (the number of components of input vector U in module 2), lr (the learning rate of the adaptive filter in module 2), and k (transfer function gain of fast and slow dynamic elements in module 3) was set to the same values used in simulating the results in Stern et al. (1990) ($M=5$, $lr=2^{-8}$, and $k=0.8$). The parameter c (in module 3) was set to 34 dps for normalization purposes. Finally, the parameter I (the threshold), a and b

(the constant and exponent of Stevens' power law function) was tuned to minimize the mean square error (MSE) measuring the difference between the model simulated nausea severity time course and an empirical nausea severity time course (medians of the ratio scale data from the 14 subjects) in the corresponding velocity condition.

In the validation stage of model one, all model free parameters were kept unchanged except for the parameter Φ . Φ is tuned to simulate different levels of the steady state of empirical vection velocity (measured by medians of the ratio scale data from the 14 subjects that was averaged over 30 mins) in different velocity conditions (see Table 8.2). Such corrections are indispensable for simulating nausea severity in an appropriate way since it has been reported empirically that vection velocity has a significant linear relation ($p < 0.05$) with nausea severity (see Section 5.3.6).

In the pre-validation stage for model two, the first step was to tune the sensory weighting parameter $W_{r,3}$ (in module 1) so that the model simulated foveal retinal slip velocity (or OKN slow-phase velocity) was equal to an empirical benchmark (see Chapter 3). The foveal retinal slip velocity (mean of the data from the 14 subjects) in the rotation velocity condition of 90 dps was chosen as the empirical benchmark in this case. Defining the OKN gain (G_o) as the mean OKN SPV over the

rotation velocity of the optokinetic stimuli, $W_{r,3}$ should be set to a value equal to $(0.98-G_0)/0.5$ (see Figure 8.9) where $W_{r,3}$ varies in a range of 0 to 1 and G_0 varies in a range from 0.48 to 0.98. Although $W_{r,3}$ is the only one found noticeably to affect the simulated foveal retinal slip velocity among the six sensory weighting parameters in module one (see Equations 3-7 and 3-8), $W_{r,1}$ is adjusted accordingly since Zupan et al. (2002) proposed that the summation of $W_{r,1}$, $W_{r,2}$ and $W_{r,3}$ should be equal to one. In model two, $W_{r,2}$ was set to zero for simplicity in consideration of some redundant information contained in Equation 3-7. The parameter M , l_r , and k was set to the same values used in simulating the results in Webb and Griffin (2002) ($M=5$, $l_r=2^{-8}$, and $k=0.8$). The parameter c (in module 3) was set to 90 dps for normalization purposes. Finally, the parameter I (the threshold), a and b (the constant and exponent of Stevens' power law function) was tuned to minimize the mean square error (MSE) measuring the difference between the model simulated nausea severity time course and an empirical nausea severity time course (medians of the ratio scale data from the 14 subjects) in the corresponding velocity condition.

In the validation stage of model two, all model free parameters were kept unchanged except for the parameter $W_{r,3}$ and c . $W_{r,3}$ is tuned to simulate different levels of empirical foveal retinal slip velocity (medians of the data from the 14 subjects were

averaged over 30 mins) in different velocity conditions (see Table 8.6). Such corrections are indispensable to simulate nausea severity in an appropriate way since it has been reported empirically that a nonlinear relation exists between the foveal retinal slip velocity and the nausea severity described by a quadratic function (see Figure 6.6). Preliminary simulation keeping c unchanged across different velocity conditions produced inappropriate model predictions. It was found that model two demonstrates a good prediction performance when c is set to a value equal to its corresponding rotation velocity of the optokinetic stimuli (magnitude of the visual input).

To further evaluate the prediction performances of models one and two, the empirical data of the 14 subjects in each experiment was divided into two groups. For model one, the 14 subjects were first ranked by their vection velocity level (median over 30 mins) in the condition 34 dps from the lowest to highest. The subjects ranked as No. 1, 4, 5, 8, 9, 12 and 13 were grouped into group I and the others (No. 2, 3, 6, 7, 10, 11 and 14) were grouped into group II. As shown in Appendix 7-1, groups I and II has the same median motion sickness susceptibility (MSS) score derived from the MSSQ-short questionnaire (equal to 18 for both groups I and II). Empirical data (vection velocity and nausea severity) of the 34 dps group II was used in the stage of

“pre-validation”. Empirical data of the 34 dps group I, 14 dps group I and II were used in the stage of “validation”. For model two, the 14 subjects were ranked by their OKN SPV levels (mean over 30 mins) in the condition 90 dps from the lowest to highest. Then the 14 subjects were grouped by the rule as described above. As shown in Appendix 7-2, the mean motion sickness susceptibility score of group I subjects is 14.8 and one of the group I subjects is 14.5. Empirical data (OKN SPV and nausea severity) in the 90 dps group II were used in the stage of “pre-validation”. Empirical data of the 90 dps group I, 60 dps group I and II were used in the stage of “validation”. In short, the model simulations described above are used to evaluate whether models one and two that are constructed respectively on the basis of the data of group II subjects can be used to predict the data of group I subjects.

7.3 Pre-validation stage of model one

Experiment one reported that the vection velocity (median of the data from the 14 subjects in Table 5.2) in the 34 dps rotation velocity condition is 23.1 dps. Therefore, the parameter Φ is set to 0.34 (one half of the vection gain). Following the methods described in Section 7.2, the other parameters are set as $M=5$, $l_r=2^{-8}$, $k=0.8$, $c=34$, $I=0.5$, $a=4.43$, $b=2.24$. The simulated nausea severity time course is compared with the empirical time course in Figure 7.1(a). The average of the simulated nausea

severity time course is compared with empirical data in Figure 7.3. The median vection velocity of group II subjects in the 34 dps velocity condition is 22.7dps. Therefore, the parameter Φ is set to 0.33. Following the methods described in Section 7.2, the other parameters are set as $M=5$, $lr=2^{-8}$, $k=0.8$, $c=34$, $I=0.5$, $a=4.43$, $b=2.24$. The simulated nausea severity time course is compared with the empirical time course in Figure 7.2 (c). The average of the simulated nausea severity time course is compared with empirical data in Figure 7.4 (b).

7.4 Validation stage of model one

This section presents model one predicted nausea severity as a function of exposure duration (time) and rotation velocity of the optokinetic stimuli (velocity) of all 14 subjects as well as of group I and II subjects. Each model prediction is compared with its corresponding empirical data.

7.4.1 Model predicted nausea severity as a function of time

Experiment one reports that the vection velocity (median of the data from the 14 subjects in Table 5.2) in the 2 dps and 14 dps rotation velocity condition is 1.5 dps and 9 dps, respectively. Therefore, the parameter Φ is set to 0.375, given an input of 2 dps rotation velocity and set to 0.32, given an input of 14 dps rotation velocity. As

illustrated in Figures 7.1(b) and (c), each model prediction (labeled as a black solid line) is enclosed in its corresponding 25th-75th percentile envelope (labeled as a series of red triangle pairs). Results of Spearman's correlation analysis indicate that model predicted time series in the 14dps is significant correlated with the corresponding empirical median time series ($\rho=0.879$, $p<0.01$). In consideration that the model prediction and empirical data in the 2dps rotation velocity condition are all zero, statistical analyses were not implemented.

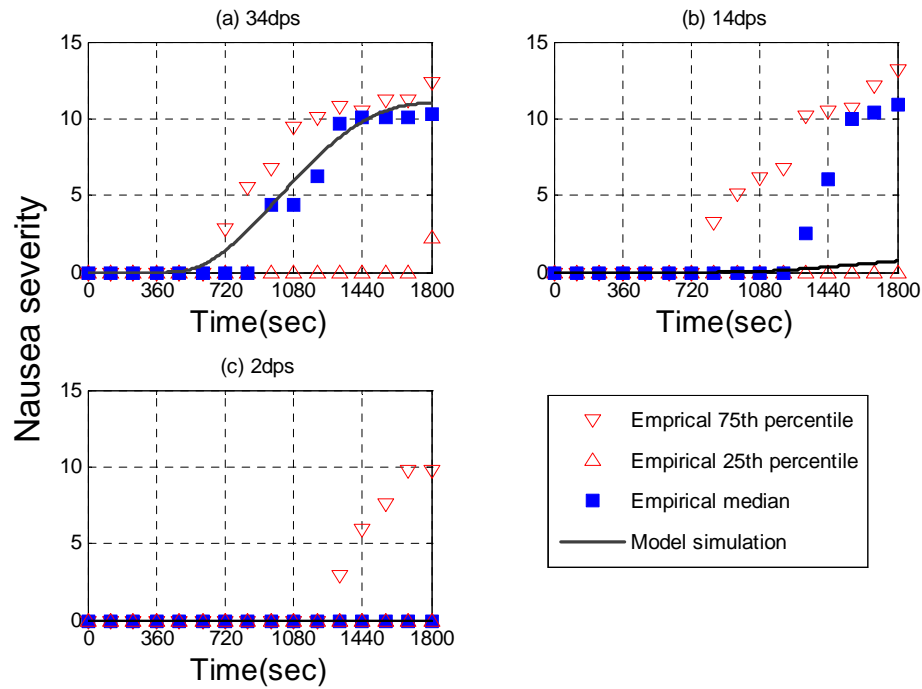


Figure 7.1 Comparison of model simulated/predicted nausea severity levels with empirical data as functions of time for 3 drum rotation velocity conditions: rotating at (a) 2, (b) 14, and (c) 34 degrees per second (dps). Data collected at the 34dps condition has been used to tune the model parameters.

The median vection velocity of the 34 dps group I, 14 dps group I and II is 23.5dps, 1.5 dps and 1.9 dps, respectively. Therefore, the parameter Φ is set to 0.35, 0.375 and

0.475, respectively. As illustrated in Figure 7.2, the model prediction of 14 dps group I is enclosed in its corresponding 25th-75th percentile envelope. Although the model prediction of the 34 dps group I exceeds the 75th percentile of nausea severity at 28 min, the value is still smaller than the maximum nausea level of that minute (labeled as a black cross). Likewise, although the model prediction of the 14 dps group II is below the 25th percentile of nausea severity at 24 min and after, the value is still larger than the minimum nausea level of that minute. Model simulations of the 2 dps velocity condition are not presented here since the empirical median nausea severity levels of the subjects of groups I and II are always zero within the 30 min exposure duration.

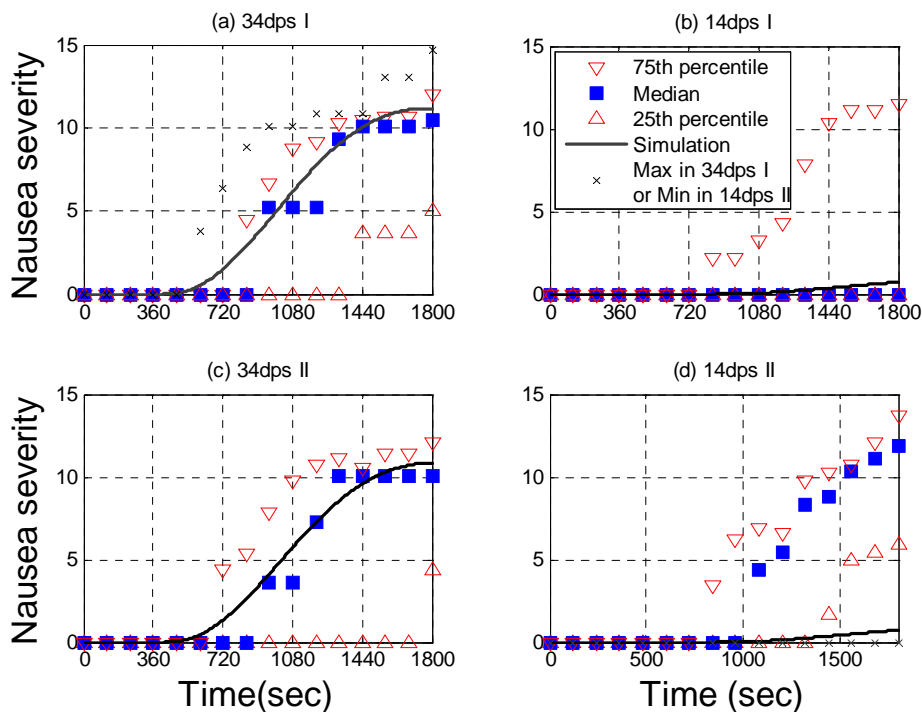


Figure 7.2 Comparison of model simulated/predicted nausea severity levels with empirical data as functions of time for the (a) 34 dps group I, and (c) group II as well as (b) 14 dps group I and (d) group II. Data of the 34 dps group II have been used to tune the model parameters.

7.4.2 Model predicted nausea severity as a function of velocity

The average of the model predicted time series data of all 14 subjects in the 3 non-zero velocity conditions is plotted in Figure 7.3. Each model prediction is enclosed in its corresponding interquantile interval. Model predictions increase with an increase of rotation velocity from 2 dps to 14 dps, and to 34 dps, following a similar trend with the empirical data of experiment one.

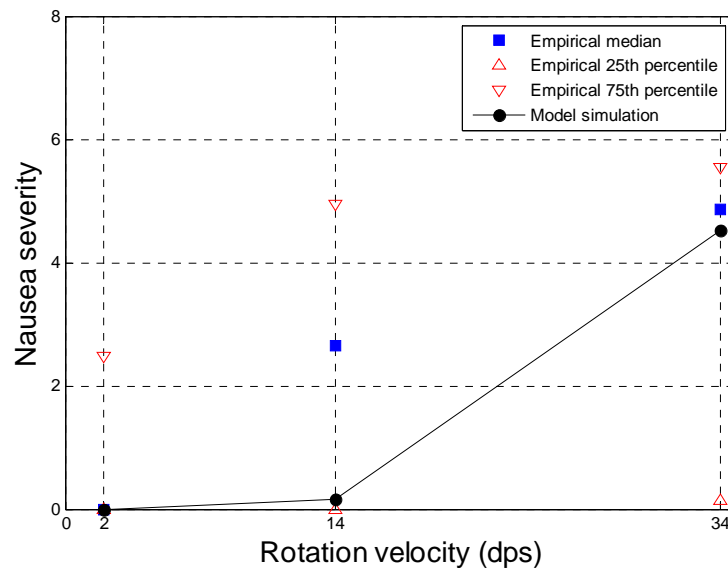


Figure 7.3 comparison of model simulated/predicted nausea severity levels with empirical data as functions of rotation velocity of the optokinetic stimuli from 2 dps, to 14 dps, then to 34 dps.

As shown in Figure 7.4, the empirical nausea severity (labeled as square) of group I subjects shows a similar increasing trend while the data of group II subjects reveal an inverted U-shape as reported by Hu et al. (1989). Statistical analysis indicate that nausea severity of 2 dps, 14 dps and 34 dps velocity conditions of group I subjects

are not significantly different from each other (SNK, $p>0.05$). Likewise, the nausea severity of the 2 dps condition is not significantly different from the 34 dps condition (SNK, $p>0.05$) while it is significantly different from the 14 dps condition (SNK, $p<0.05$). All model predictions are enclosed in their corresponding interquartile interval. The model predictions of groups I and II both increase with an increase of the rotation velocity.

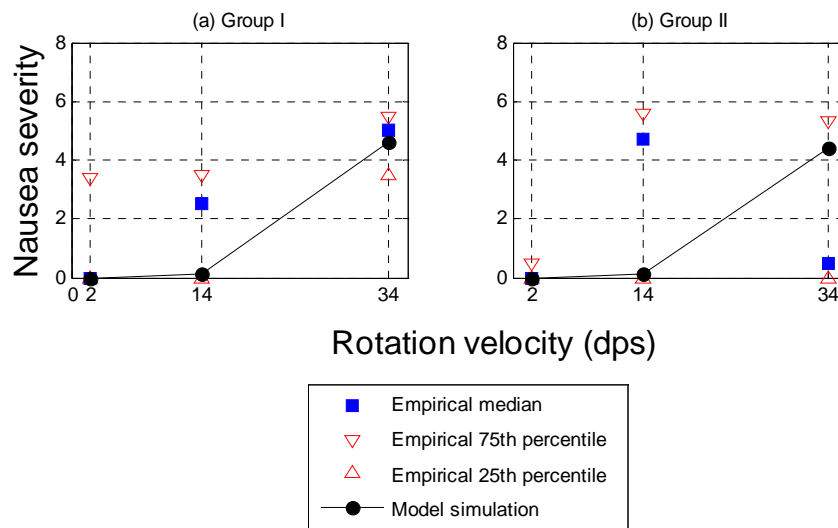


Figure 7.4 Comparison of model simulated/predicted nausea severity levels with empirical data as functions of rotation velocity of the optokinetic stimuli from 2 dps, to 14 dps, then to 34 dps of (a) group I subjects, and (b) group II subjects.

7.5 Pre-validation stage of model two

Experiment two reported that the OKN SPV (mean of the data from the 14 subjects in Table 6.2) in the 90 dps rotation velocity condition is 41.5 dps. Such a level of OKN SPV produces an OKN gain level equal to 0.46 which is outside the range that model two can simulate (a range from 0.48 to 0.98). Therefore, the parameter $W_{r,3}$ is

set to its upper bound (equal to 1) to produce a level of OKN SPV at its lower bound in the 90 dps condition (equal to 43.4 dps). A hypothetical nausea severity time series between the median time series and 75th percentile time series in the 90 dps velocity condition is chosen as the benchmark of the model simulated data. Its median time series is not chosen as the benchmark in this case since it has only one non-zero value over the 30 min exposure duration. Following the methods described in Section 7.2, the other parameters are set as $M=5$, $lr=2^{-8}$, $k=0.8$, $c=90$, $I=1.168$, $a=3.15$, $b=1.03$. The simulated nausea severity time course is compared with the empirical time course in Figure 7.5(b). The average of the simulated nausea severity time course is compared with empirical data in Figure 7.7. The mean OKN SPV of group II subjects in the 90 dps velocity condition is 40.4dps. Such a level of OKN SPV produces an OKN gain level equal to 0.45 which is outside the range that model two can simulate (a range from 0.48 to 0.98). Since the OKN SPV at its lower bound (43.3 dps) in the 90 dps condition is simulated in Figure 7.5(b), a constant retinal slip velocity time series at a level of 49.6 dps ($=90 \text{ dps}-40.4 \text{ dps}$) is directly inputted into module two to simulate the nausea severity time series produced when its corresponding OKN SPV is equal to 0.45. Such a model simulation is a hypothetical one since its OKN SPV is outside the feasible region of model two. Henceforth, such OKN SPV or foveal retinal slip as well as its corresponding hypothetical model

simulation are labeled with ‘*’ for clarity. Following the methods described in Section 7.2, the other parameters are set as $M=5$, $l_r=2^{-8}$, $k=0.8$, $c=90$, $I=1.168$, $a=3.15$, $b=1.03$. The simulated nausea severity time course * are compared with the empirical time course in Figure 7.6 (c). The average of the simulated nausea severity time course * are compared with empirical data in Figure 7.8 (b).

7.6 Validation stage of model two

This section presents model one predicted nausea severity as a function of exposure duration (time) and rotation velocity of the optokinetic stimuli (velocity) of all 14 subjects as well as subjects of groups I and II. Each model prediction is compared with its corresponding empirical data.

7.6.1 Model predicted nausea severity as a function of time

Experiment two reported that the OKN SPV (mean of the data for the 14 subjects in Table 6.2) in the 30 dps and 60 dps rotation velocity condition are 27.4 dps and 39.3 dps, respectively. Therefore the parameter $W_{r,3}$ is set to 0.14 and 0.66, respectively. As illustrated in Figures 7.5 (a) and (c), each model prediction (labeled as a black solid line) is enclosed in its corresponding 25th-75th percentile envelope (labeled as a series of red triangle pairs).

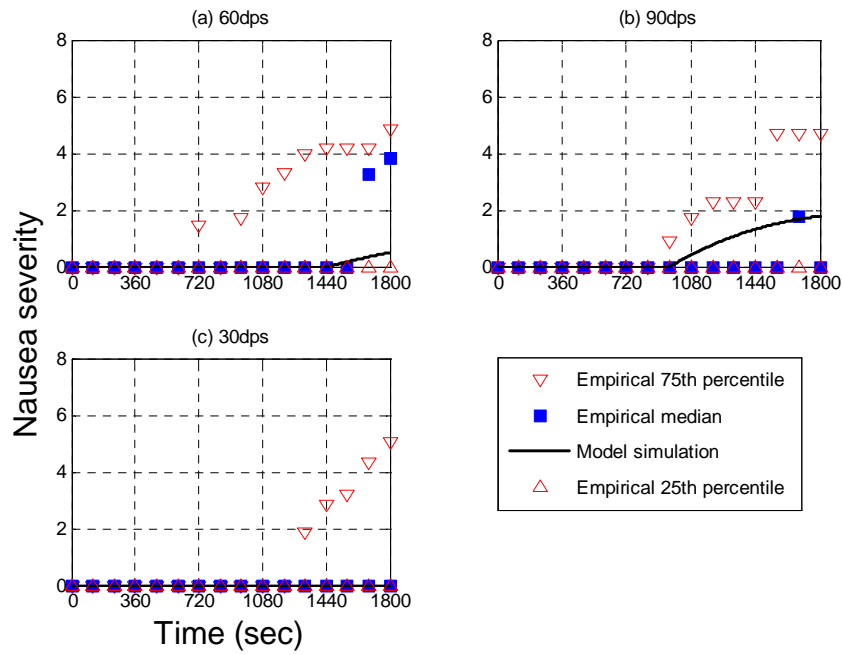


Figure 7.5 Comparison of model simulated/predicted nausea severity levels with empirical data as functions of exposure duration for 3 optokinetic stimuli rotation velocity conditions: rotating at (a) 60 dps, (b) 90 dps, and (c) 30 dps. Data collected at the 90 dps condition are used to tune the model parameters.

Results of Spearman's correlation analysis indicate that model predicted time series in the 60dps is significant correlated with the corresponding empirical median time series ($\rho=0.844$, $p<0.05$). Results of the Wilcoxon signed-rank test indicate that such model predictions are not significantly different from the empirical data ($p>0.05$). In consideration that the model prediction and empirical data in the 30dps rotation velocity condition are all zero, statistical analyses were not implemented.

The mean OKN velocity of the 90 dps group I, 60 dps groups I and II is 42.5dps*, 32.9dps and 45.6dps, respectively. The parameter $W_{r,3}$ is set to 0.86 and 0.44 for the 60 dps groups I and II, respectively. As illustrated in Figures 7.6 (b) and (d), the

model predictions of the 60 dps groups I and II are enclosed in its corresponding 25th-75th percentile envelope, although the model prediction of the 90 dps group I* exceeds the 75th percentile of nausea severity from 18 min to 24 min, and at 28min, the values are still smaller than their corresponding maximum nausea level (labeled as a black cross). Model simulations of the 30 dps velocity condition is not presented here since the empirical median nausea severity levels of the subjects of groups I and II are always zero within the 30 min exposure duration.

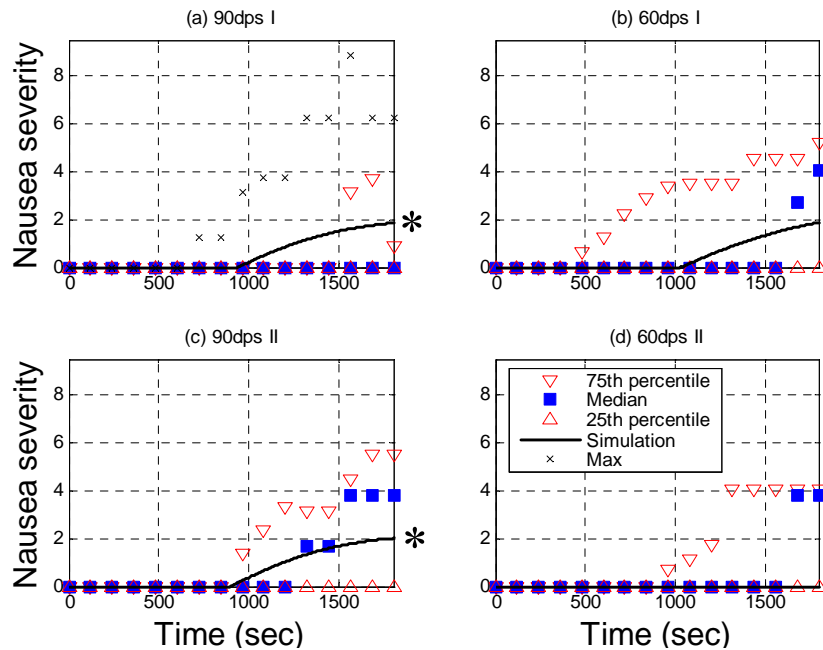


Figure 7.6 comparison of model simulated/predicted nausea severity levels with empirical data as functions of exposure duration for the (a) 90 dps group I and (c) group II as well as (b) 60 dps group I and (d) group II. The black lines represent the simulated/predicted data (a hypothetical one labeled as *).

7.6.2 Model predicted nausea severity as a function of velocity

The average of the model predicted time series data of all 14 subjects in the 3

non-zero velocity condition is plotted in Figure 7.7. Each model prediction is enclosed in its corresponding interquartile interval. Model prediction increases with an increase of rotation velocity from 30 dps to 60 dps, and to 90 dps, without following the inverted U-shape reported by experiment two. However, it is worth pointing out that the nausea severity levels of the 60 dps and 90 dps conditions are not significantly different from each other (SNK, $p>0.05$), consistent with reports from Hu et al. (1989).

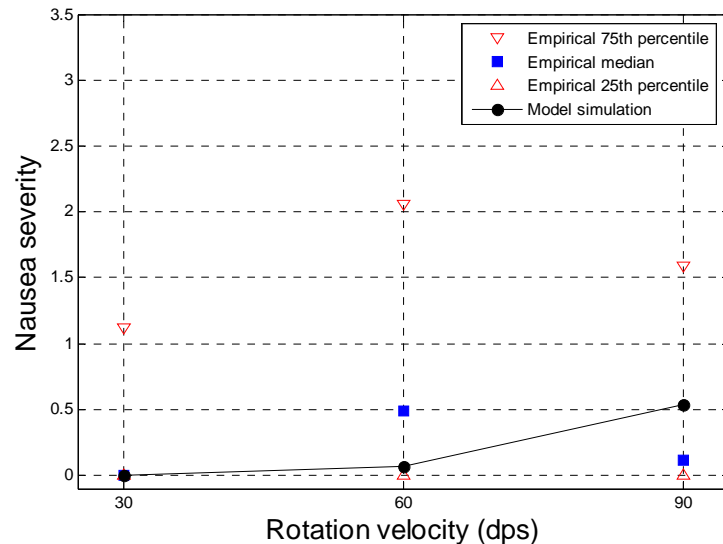


Figure 7.7 Comparison of model simulated/predicted nausea severity levels with empirical data as functions of rotation velocity of the optokinetic stimuli from 30 dps, to 60 dps, then to 90 dps. The black filled circles represent the average values of the model predicted/simulated time series data. The blue squares represent medians of empirical data collected from the 14 participants. The pairs of red triangles represent the 25th and 75th percentiles of the empirical data.

As shown in Figure 7.8, empirical nausea severity (labeled as square) of group I subjects reveals an inverted U-shape as reported by Hu et al. (1989) while data of

group II subjects increase with an increase of rotation velocity. Statistical analysis indicated that the nausea severity of 30 dps, 60 dps and 90 dps velocity conditions of both subjects from groups I and II are not significantly different from each other (SNK, in each case $p>0.05$). All model predictions are enclosed in their corresponding interquantile interval. Model predictions of groups I and II both increase with an increase of the rotation velocity.

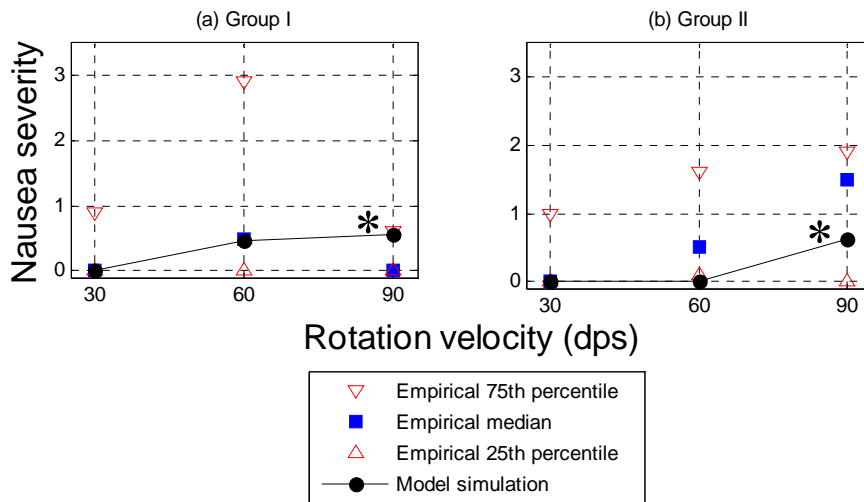


Figure 7.8 Comparison of model simulated/predicted nausea severity levels with empirical data as functions of rotation velocity of the optokinetic stimuli from 30 dps, to 60 dps, then to 90 dps of (a) group I subjects, and (b) group II subjects. The black lines represent the average values of the simulated/predicted time series data (a hypothetical one labeled as *). The blue squares represent medians of empirical data collected from group I and II subjects. The pairs of red triangles represent the 25th and 75th percentiles of empirical data.

7.7 Conclusions

Model one is demonstrated to have a good performance in terms of predicting nausea severity with known associated veciton velocity. Taking in the rotation velocity of

the optokinetic stimuli as the visual input, model one can predict the average sickness responses of a group of human participants as a function of time and rotation velocity in the absence of OKN. Likewise, model two is demonstrated to have a good performance in terms of prediction nausea severity with known foveal retinal slip velocity. Taking in the rotation velocity of the optokinetic stimuli as the visual input, model two can predict the average sickness responses of a group of human participants as a function of time and rotation velocity in the absence ofvection perception.

CHAPTER 8

MODEL SIMULATED INDIVIDUAL DIFFERENCES AND MODEL SENSITIVITY ANALYSIS

SUMMARY

In this chapter, motivations behind the simulations of individual differences and model sensitivity analysis are presented first. After a brief methodology overview, detailed motion simulations are used to demonstrate that model one can simulate inter-subject variation in three vection related measures reported in experiment one. Parameters τ_w , τ_{va} , and Φ are tuned separately to simulate various levels of vection onset latency, vection build-up time and vection velocity's steady state. Likewise, model two is demonstrated to be able to simulate inter-subject variation in three OKN related measures reported in experiment two. Parameters $W_{r,3}$ and $W_{r,1}$ are adjusted together to simulate various levels of OKN SPV, OKN gain and foveal retinal slip velocity. In addition, the results of the model sensitivity analysis indicate that model one simulated inter-subject variation in vection velocity can explain part of the variation of nausea severity reported in experiment one and model two simulated inter-subject variation in the foveal retinal slip velocity can explain part of the variation of nausea severity reported in experiment two.

8.1 Motivations

Experiment one reported large individual differences in the latencies of vection onset, vection build-up time and vection velocity's steady state (see Chapter 5). It was found that the vection velocity's steady state is the only one among the three having a significant linear relation with nausea severity. Likewise, experiment two reported large individual differences in the OKN SPV, OKN gain and foveal retina slip velocity (see Chapter 6). The three OKN related measures strongly associate with each other by definition. Such an observation was later confirmed by Spearman's correlation analysis (see Section 6.3.6). Furthermore, a quadratic function was found to describe the nonlinear relationship between the foveal retina slip velocity and the nausea ratio scale data at 30 min. As presented in Chapter 7, a parameter Φ in model one is tuned to simulate various levels of the vection velocity's steady state and a parameter $W_{r,3}$ in model two is tuned to simulate various levels of OKN SPV, OKN gain or foveal retinal slip velocity. Such results indicate that model one has the flexibility to simulate individual differences in vection perception and the same is for model two with regards to the simulation of individual differences in OKN related measures. Since the vection velocity is the sensory input directly contributing to VIMS generation in model one and the same is for the foveal retinal slip velocity in

model two, it is expected that the model simulated variation of nausea severity resulting from such model simulated individual differences in vection perception and OKN can account for at least part of the empirical variation of nausea severity reported in experiments one and two.

This study proposes to simulate individual differences in vection perception and OKN related measures reported empirically. Such model simulations are then used to study the ways that the variation in the nausea severity output of a model can be apportioned to different sources of variation in vection perception (model one) or in OKN related measures (model two).

The following sections will first present a methodology overview of individual differences in simulation and model sensitivity analysis. After detailed model simulations with regards to individual differences in vection perception or OKN related measures are presented, model simulated individual differences in nausea severity will be compared with its corresponding empirical data for each model.

8.2 Methodology overview

The parameters of model one affecting the simulated latency of vection onset,

vection build-up time and vection velocity's steady state are presented first. Then the 25th and 75th percentile of each vection related measure are simulated by tuning its corresponding parameters within its feasible region. Varying only one model simulated vection related measure at a time, the corresponding changes of the model output is the part of the nausea severity variation which can be explained by model one. Finally, the model simulated variation of nausea severity is compared with its corresponding empirical data. On the basis of the significant linear relation between the vection velocity and nausea severity reported in experiment one, it is expected that model one simulated individual differences in the vection velocity's steady state can account for part of the empirical variation of nausea severity in experiment one. This is not true for the other two vection related measures.

Similar methods are used to study the parameters of model two which affect the simulated OKN SPV, OKN gain and foveal retinal slip velocity. Likewise, the model simulated individual differences in the foveal retinal slip velocity can account for part of the empirical variation of nausea severity in experiment two, in consideration of the quadratic function between the foveal retinal slip velocity and the nausea severity identified in experiment two.

8.3 Model one simulated individual differences in latency of vection onset, vection build-up time, and vection velocity's steady state

The interquantile ranges of the vection onset latency in the rotation velocity conditions of 2 dps, 14 dps and 34 dps are 7.5-25.5 dps, 4.25-20 dps, and 7.5-19.75 dps, respectively. Model one can simulate such individual differences by tuning parameters τ_w and ξ . τ_w is the time constant of a transfer function T_{ao} which is a high pass filter used to wash out the high-frequency mismatch between visual input and vestibular input over time. ξ is a preset parameter in the weighting logic function K . It is defined to equal the mean yaw direction vestibular indifference motion threshold (1.6 deg) reported by Benson et al. (1989). As shown in Figure 8.1, the model simulated latency of vection onset is positively correlated with τ_w and negatively correlated with ξ . It was once reported that ξ varied in a range of 0.84 to 4.63 dps for a group of human individuals (Benson et al., 1989). However, model simulation shows that the change of vection onset latency caused by such variation of ξ is less than 0.5 sec. Therefore, an adjustable τ_w with a constant ξ (equal to 1.6 deg) is used in model one to account for the variation of vection onset latency for simplicity (see Figure 8.2(a)).

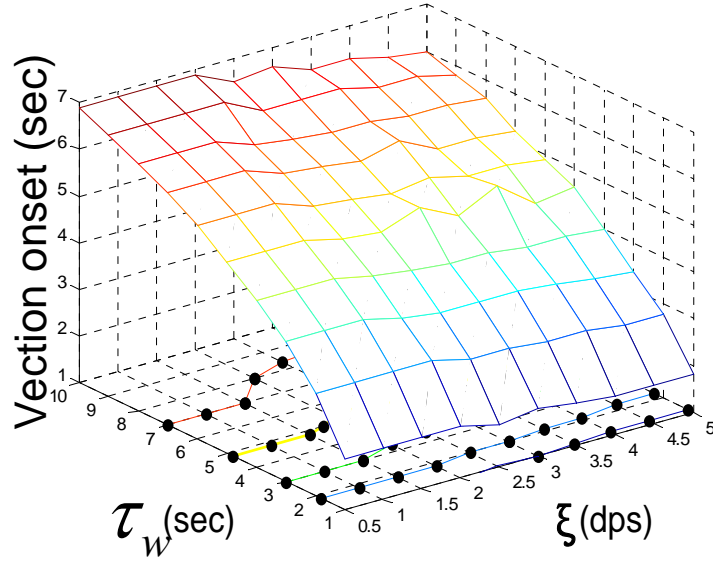


Figure 8.1 Model simulated latency of vection onset as a function of τ_w and ξ .

The interquantile ranges of the vection build-up time in the three non-zero velocity conditions are 1-1sec, 1-1sec and 1-85.25 sec, respectively. Model one can simulate such individual differences by tuning parameter τ_{va} . τ_{va} is the time constant of a transfer function T_{opto} accounting for the low pass frequency response of vection perception. As shown in Figure 8.2(b), the model simulated vection build-up time increases with an increase of τ_{va} .

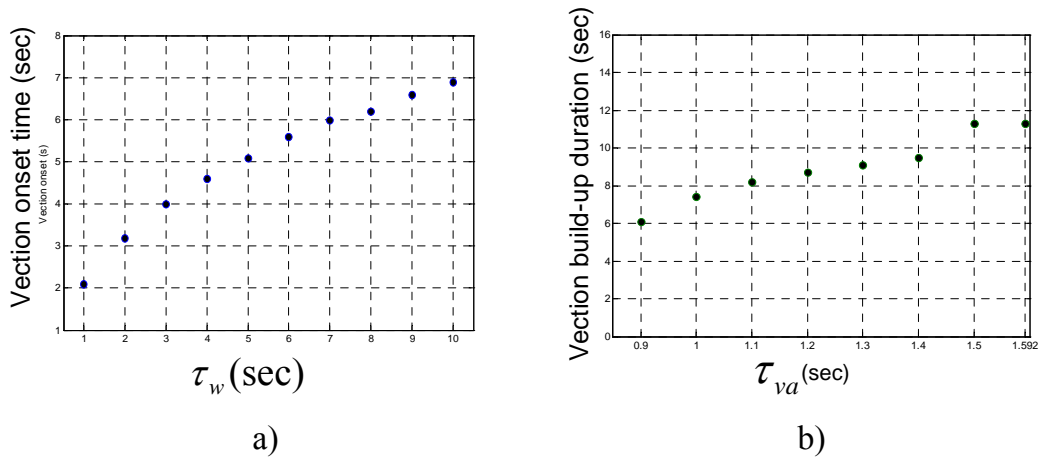


Figure 8.2 a) Model simulated vection onset time as function of τ_w given ξ equal to 1.6 dps as suggested by Telban & Cardullo (2001); b) Model simulated vection build-up time as a function of τ_{va}

The interquantile ranges of the vection velocity's steady state level (measured by the average value of vection velocity time series data) in the three non-zero velocity conditions are 1-1.9dps, 5.9-12.3dps, and 16.9-25dps (see Table 8.1), respectively.

The vection gain (G_v), defined as the vection velocity's steady state level over the rotation velocity, varies in a range of 0.42 to 0.95. Model one can simulate such individual differences by tuning parameter Φ in a range of 0.21 to 0.475. As shown in Figure 8.3 (d), the linear relation between models simulated G_v (Gain) and the parameter Φ (Phi) is described by a linear function $G_v = 2\Phi$, where Φ varies in a range of 0 to 0.5.

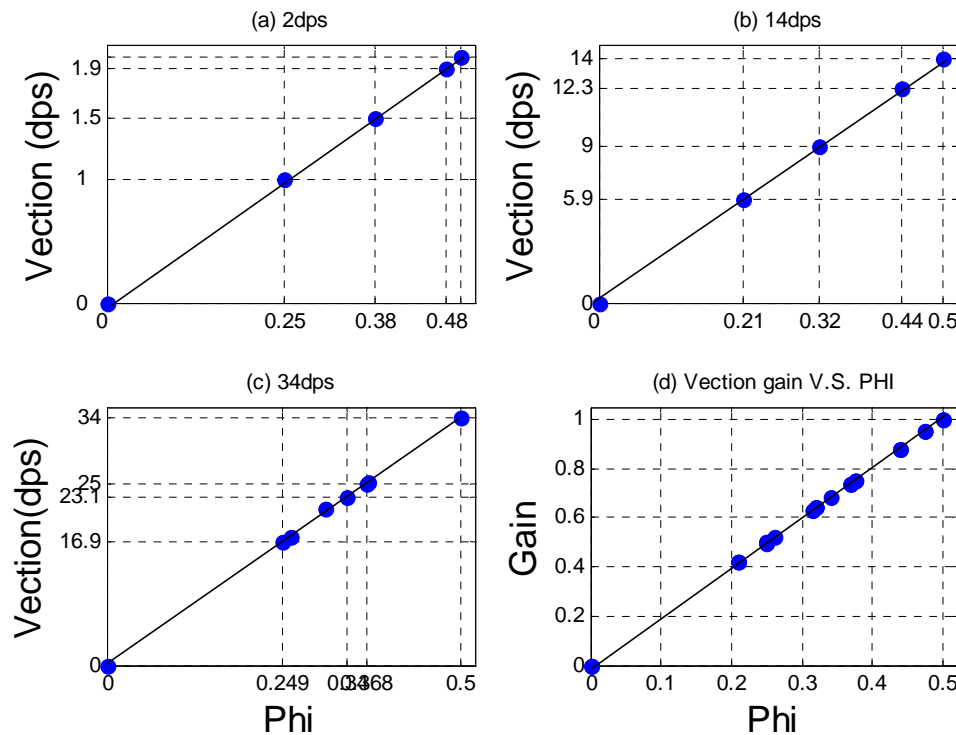


Figure 8.3 Model simulated vection velocity's steady state varied in its empirical interquantile range in the velocity condition of (a) 2 dps, (b) 14 dps, and (c) 34 dps and (d) model simulated vection gain as a function of parameter Φ .

Table 8.1 Model simulated vection velocity's steady state levels and their corresponding parameter Φ plotted in Figure 8.3

Vection velocity					
2dps	0	1	1.5	1.9	2
14dps	0	5.9	9	12.3	14
34dps	0	16.9	23.1	25	34
PHI					
2dps	0	0.25	0.375	0.475	0.5
14dps	0	0.21	0.32	0.44	0.5
34dps	0	0.249	0.34	0.368	0.5

8.4 Model one's sensitivity analysis and model one simulated individual differences in nausea severity

When the model simulated vection onset latency or vection build-up time is varied in its empirical interquantile range given the other two vection related measures remain unchanged, the model simulated nausea severity time series does not change. As shown in Figure 8.4, the change of nausea severity time series bounded by a pair of blue solid lines in each velocity condition results from varying the model simulated vection velocity's steady state in its empirical interquantile range (upper line for 75th percentile and lower line for 25th percentile, values listed in Table 8.2). All model parameters used in the model sensitivity analysis are the same with the ones used in the model validation aside from the necessary correction of parameter Φ . In the velocity condition of 14 dps, all model simulations (nausea severity time series data) are enclosed in their corresponding 25th-75th percentile intervals as reported in

experiment one. In the velocity condition of 34 dps, the upper blue line (where Φ is tuned to simulate the 75th percentile of the vection velocity's steady state) does not exceed the maximum values of empirical nausea severity although it is higher than the 75th percentiles from 24 min to 28 min. In the velocity condition of 2 dps, no changes of model simulation are produced by varying the model simulated vection velocity's steady state in its interquantile range. Such results indicate that the individual differences in the vection velocity's steady state are the only ones among the three vection perception related individual differences that can explain part of the variation of nausea severity in model one. Bearing in mind that experiment one, which reported nausea severity, has a significant linear relation with the vection velocity, but not with the latency of vection onset and vection build-up time, the results of model one's sensitivity analysis and experiment one are consistent.

Each set of model simulated time series data is averaged over 30 mins. The nausea severity is plotted against the rotation velocity in Figure 8.5. The part of the nausea severity variation explained by the model simulated individual differences in the vection velocity in each velocity condition is represented by the distance between a pair of open and filled circles which is about 50% of empirical inter-subject variation of nausea severity at 34dps velocity condition. All model simulated nausea severity

variations are enclosed in their corresponding 25th to 75th percentile intervals of the empirical data.

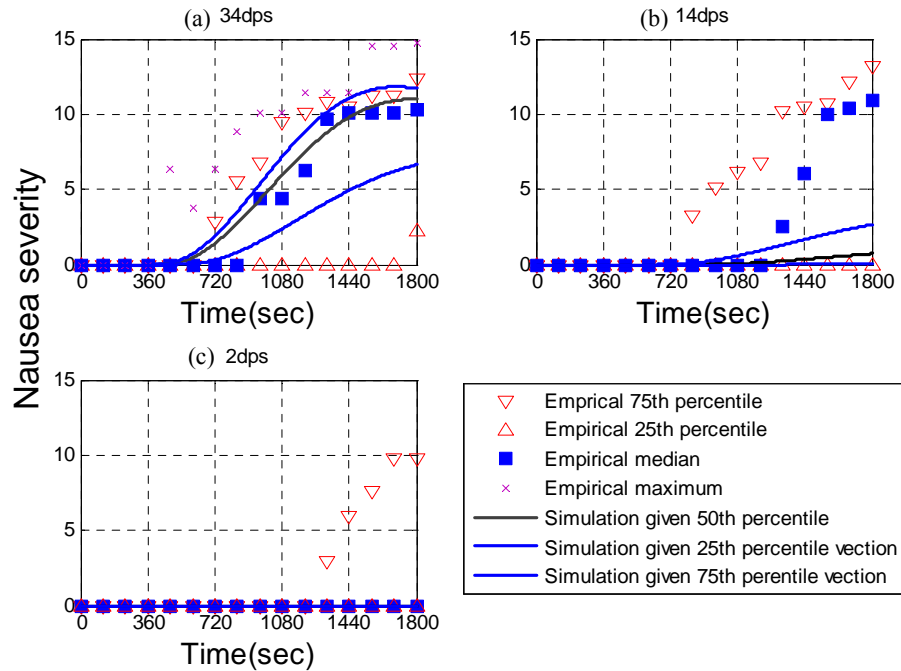


Figure 8.4 comparison of model simulated/predicted nausea severity levels with empirical data as functions of exposure duration for three optokinetic stimuli velocity conditions: rotating at (a) 2 dps, (b) 14 dps, and (c) 34 dps.

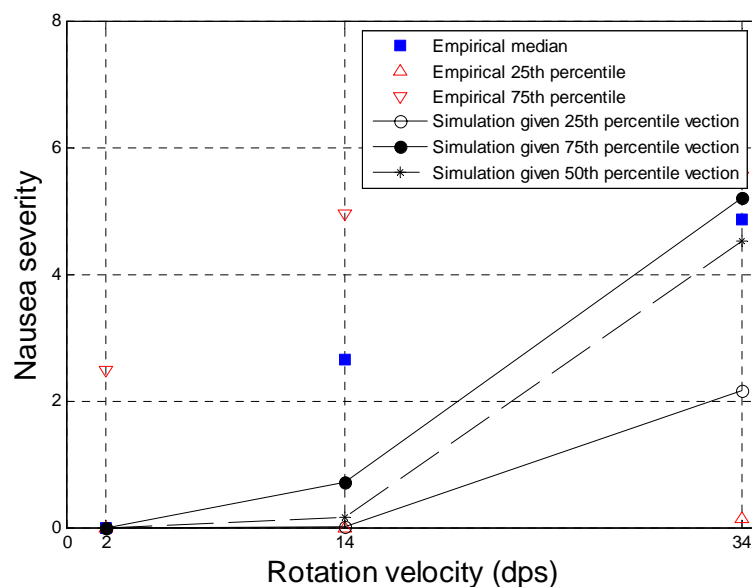


Figure 8.5 Comparison of model simulated/predicted nausea severity levels with empirical data as functions of rotation velocity from 2 dps, to 14 dps, and to 34 dps.

Table 8.2 25th percentile, 50th percentile and 75th percentile of vection velocity reported in experiment one

	25th percentile	Median	75th percentile
2dps	1	1.5	1.9
14dps	5.9	9	12.3
34dps	16.9	23.1	25

Parameter Φ was then tuned to simulate the steady state level of vection velocity of each subject (listed in Table 5.2). Each corresponding model output is a model simulated individual nausea severity time series. Such model simulations make it possible that statistical analysis can be implemented to test the significance of the difference between the distributions of model simulated nausea severity and empirical data. Results of the Wilcoxon signed-rank test show that the difference is not statistically significant ($p>0.05$) in the 34dps rotation velocity condition but is marginal significant ($p=0.05$) in the 14dps rotation velocity condition and significant in the 2dps rotation velocity condition ($p<0.05$). Such results indicate that model one explains the empirical variation better in the 34dps condition than in the 2dps and 14dps conditions. Such results are consistent with the observations on Figure 8.4. As shown in Figure 8.6, the model simulated nausea severity in 14dps and 34dps are significantly higher than in 0dps condition (one sample Wilcoxon, $p<0.05$). Such result is the same with empirical results reported in experiment one.

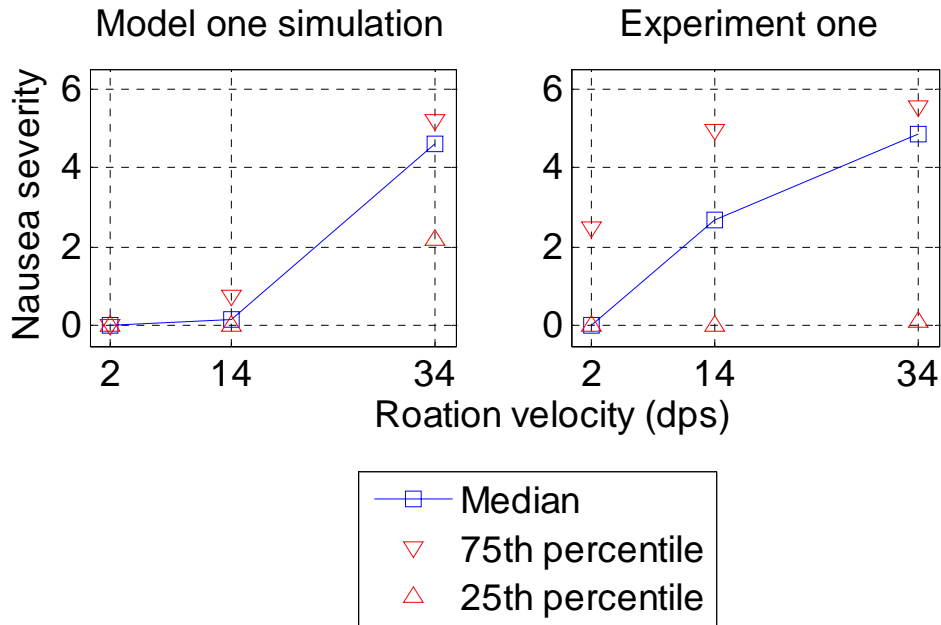


Figure 8.6 Comparing model one simulated data distribution with empirical data distribution collected from experiment one

To further evaluate the capability of model one to simulate nausea severity variation, model simulated nausea severity, given that the model simulated vection velocity's steady state is equal to the average values of the top and bottom three in the empirical data (listed in Table 8.3), is plotted in Figure 8.7. None of model simulations exceed the corresponding variation intervals bounded by the maximum and minimum values of the empirical data with regards to nausea severity.

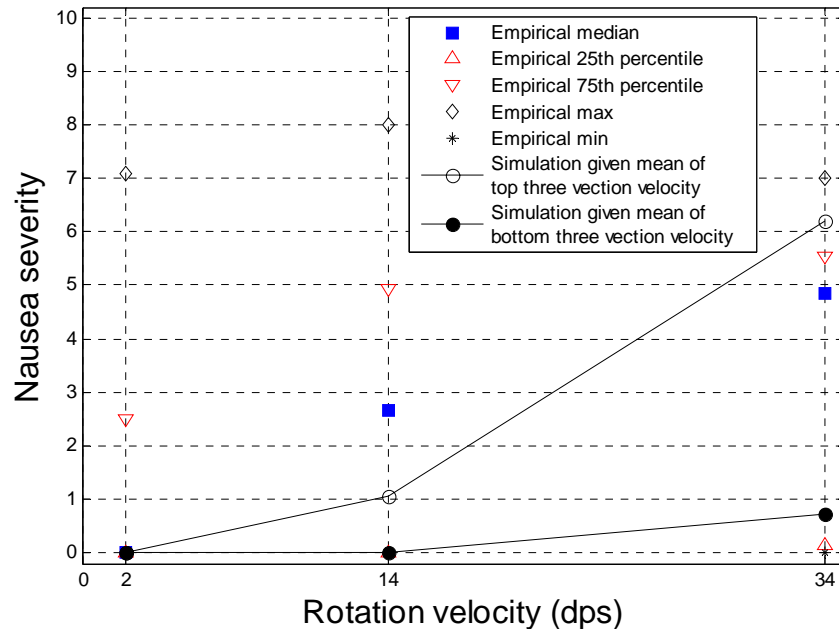


Figure 8.7 Comparison of model simulated/predicted nausea severity levels with empirical data as a function of rotation velocity from 2 dps to 14 dps, and to 34 dps.

Table 8.3 Top three and bottom three vection velocity levels in 2 dps, 14 dps and 34 dps rotation velocity conditions

	2dps	14dps	34dps
Top three	2.0	13.6	28.6
	2.0	13.4	25.8
	2.0	14.0	33.8
Average	2.0	13.7	29.4
Bottom three	0.8	4.6	12.1
	0.4	1.4	12.6
	0.8	4.3	12.4
Average	0.7	3.4	12.4

Model sensitivity analyses are separately implemented for subjects in groups I and group II. As illustrated in Figures 8.8 and 8.9, all model simulations, as a function of time or velocity, are enclosed in their corresponding max-min nausea severity intervals. All model parameters are the same with the ones used in the model validation except for necessary adjustments of parameter Φ (see Table 8.4).

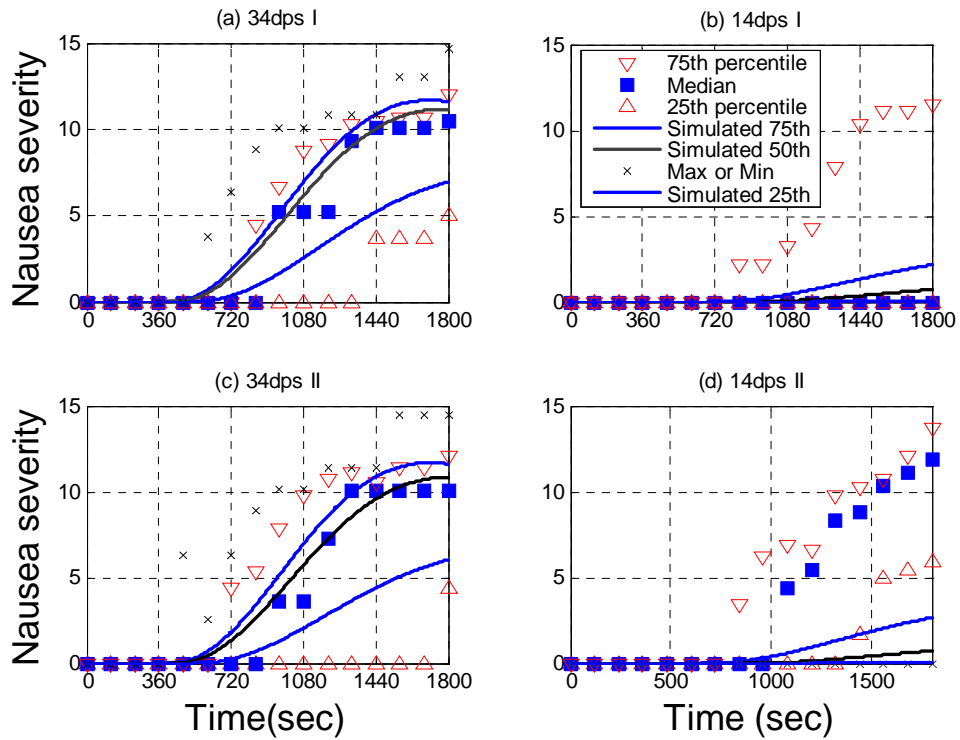


Figure 8.8 Comparison of model simulated nausea severity levels with empirical data as functions of exposure duration for the (a) 34 dps group I and (c) II as well as (b) 14 dps group I and (d) group II.

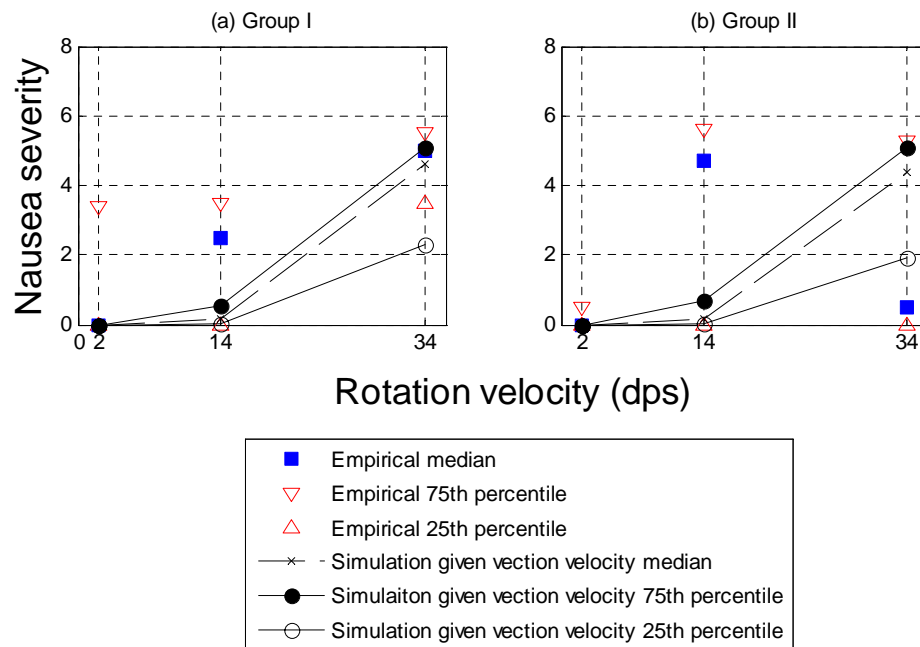


Figure 8.9 Comparison of model simulated/predicted nausea severity levels with empirical data as functions of rotation velocity from 2 dps to 14dps, and to 34 dps for (a) group I subjects and (b) group II subjects.

Table 8.4 vection velocity medians, 75th percentile, and 25th percentiles of 2 dps, 14 dps, and 34 dps drum velocity condition for subjects in groups I and II

		Vection velocity		
		2dps	14dps	34dps
Group I	Median	1.5	8.9	23.5
	75th percentile	1.6	11.6	24.9
	25th percentile	1.1	6.4	17.3
		Vection velocity		
		2dps	14dps	34dps
Group II	Median	1.9	9.0	22.7
	75th percentile	2.0	12.3	24.9
	25th percentile	1.1	6.5	16.3

8.5 Model two simulated individual differences in OKN SPV, OKN gain, and foveal retinal slip velocity

The 95% confidence interval (CI) of the OKN SPV in the rotation velocity conditions of 30 dps, 60 dps and 90 dps are 26.6-28.3 dps, 29.9-48.6 dps, and 29.6-53.3 dps, respectively. The 95% CI of the foveal retinal slip velocity in the three non-zero velocity conditions are 1.7-3.4 dps, 11.4-30.1 dps, and 36.7-60.4 dps, respectively. In each of the three velocity conditions, OKN gain varies in its 95% CI from 0.329 to 0.943. Model two can only simulate an OKN gain above or equal to 0.48 where the parameter $W_{r,3}$ is set as the maximum value 1. As shown in Figure 8.10, the linear relation between the model simulated OKN gain (G_o) and the

parameter $W_{r,3}$ is described by a linear function $G_o = -0.5W_{r,3} + 0.98$, where $W_{r,3}$

varies in a range of 0 to 1 as suggested by Zupan et al. (2002).

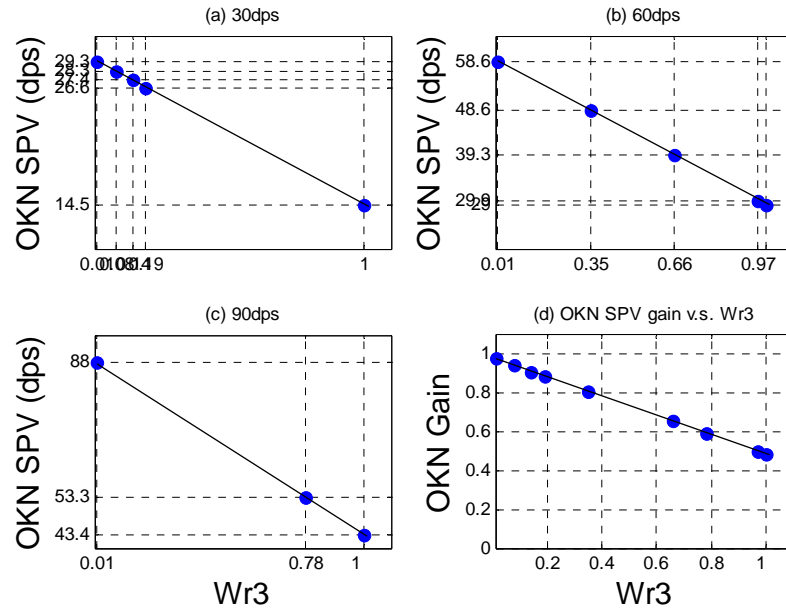


Figure 8.10 Model simulated OKN SPV in (a) 30 (b) 60 and (c) 90 dps velocity condition, and (d) model simulated individual differences in OKN gain as a function of parameter $W_{r,3}$.

Table 8.5 Model simulated OKN SPVs and their corresponding parameter $W_{r,3}$ plotted in Figure 8.9

OKN SPV					
30dps	29.3	28.3	27.4	26.6	14.5
60dps	58.6	48.6	39.3	29.9	29
90dps	88	53.3	43.4		
$W_{r,3}$					
30dps	0.01	0.08	0.14	0.19	1
60dps	0.01	0.35	0.66	0.97	1
90dps	0.01	0.78	1		

8.6 Model two's sensitivity analysis and model two simulated individual differences in nausea severity

As shown in Figure 8.11, the change of nausea severity time series bounded by a pair

of blue solid lines in each velocity condition results from varying model simulated foveal retinal slip velocity in its 95% CI (upper line for the upper bound of 95% CI and lower line for the lower bound). Bearing in mind that model two can only simulate a range of OKN gain from 0.48 to 0.98, the upper blue solid line is simulated by tuning $W_{r,3}$ to its maximum value 1 when the empirical OKN gain is lower than 0.48. All model parameters used in the model sensitivity analysis are the same with those used in the model validation aside from the necessary correction of parameter $W_{r,3}$. All model simulations are enclosed in their corresponding 25th to 75th percentile intervals of nausea severity collected in experiment two.

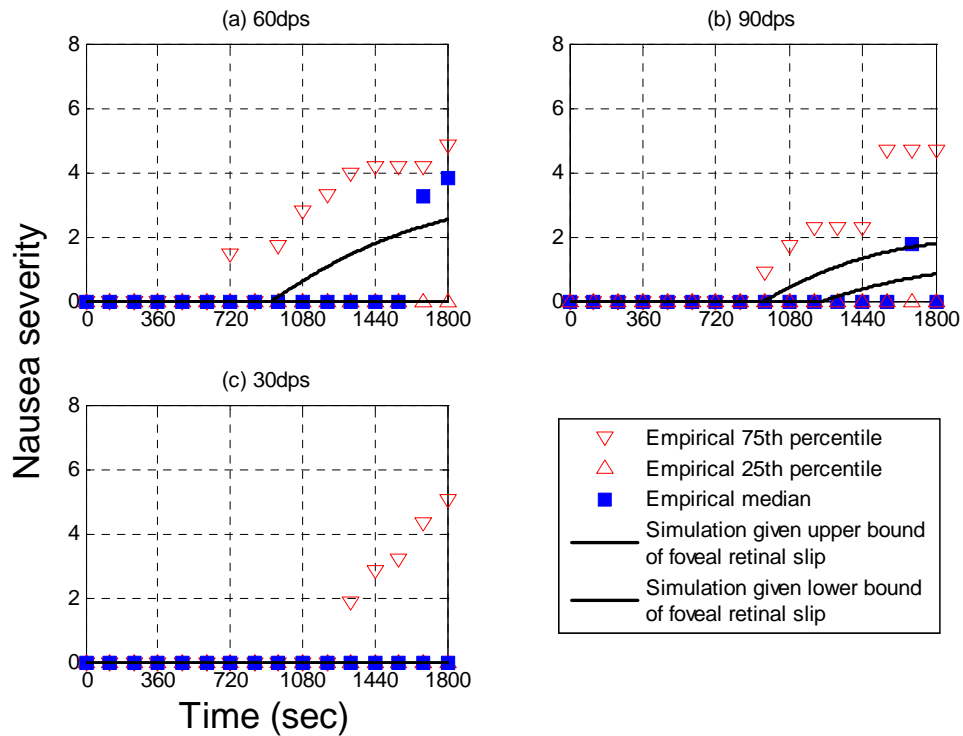


Figure 8.11 comparison of model simulated/predicted nausea severity levels with empirical data as functions of exposure duration for three optokinetic stimuli velocity conditions: rotating at (a) 30 dps, (b) 60 dps and (c) 90 dps. If a foveal retinal slip velocity is outside the range that model two can simulate, $W_{r,3}$ is set to its maximum value 1.

Each set of model simulated time series data is averaged over 30 mins. The nausea severity is plotted against the rotation velocity in Figure 8.12. The part of the nausea severity variation explained by the model simulated individual differences in foveal retinal slip velocity in each velocity condition are represented by the distance between a pair of open and filled circles which is about 40% of empirical inter-subject variation of nausea severity at 60dps velocity condition. All model simulated nausea severity variations are enclosed in their corresponding empirical 25th to 75th percentile intervals.

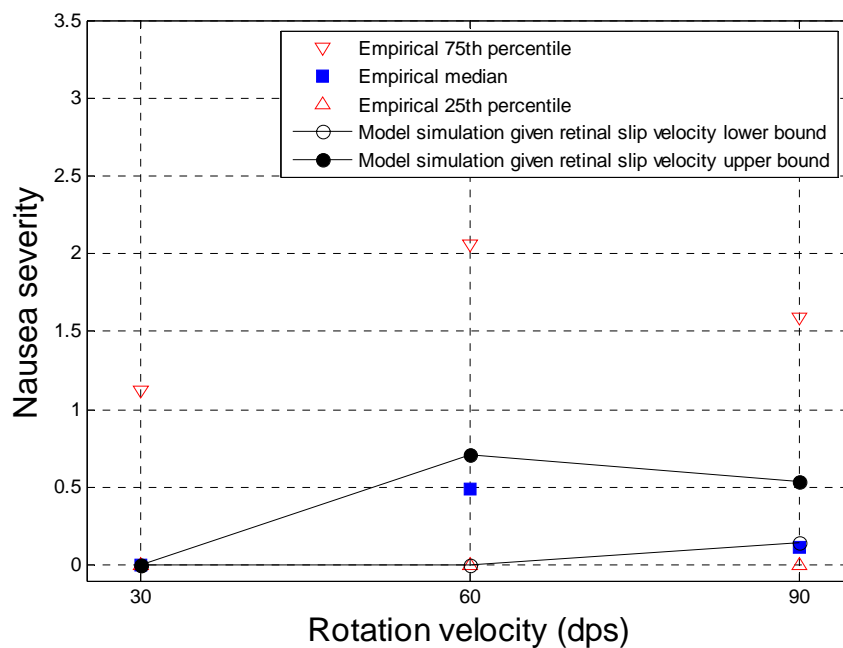


Figure 8.12 Comparison of model simulated/predicted nausea severity levels with empirical data as functions of rotation velocity from 30 dps to 60 dps, and to 90 dps..

As in Chapter 7, ‘*’ is used to label a hypothetical model simulation when its

corresponding OKN gain is lower than 0.48 which is outside the range of OKN gain that model two is able to simulate. Such a model simulation is produced by using a constant foveal retinal slip velocity time series as the input of module two. For example, 46.6 dps is the highest foveal retinal slip velocity that model two can simulate in the 90 dps velocity condition (where $W_{r,3}=1$). The mean (48.6 dps) and the upper bound of 95% CI (60.4 dps) of the empirical data with regards to the foveal retinal slip velocity are both higher than 46.6dps (see Table 8.6). Their corresponding model simulated time series are labeled by ‘*’ as shown in Figures 8.13 and 8.14. It is expected that model two can account for a larger percentage of nausea severity variation in the 90 dps velocity condition if such a modeling limitation is eliminated.

Table 8.6 Means and 95% confidence intervals of OKN SPV and foveal retina slip velocity levels reported by experiment two. * labels the OKN SPV or foveal retinal slip that velocity levels cannot be simulated by the OKN model from Zupan et al. (2002)

	OKN SPV				OKN retinal slip		
	30dps	60dps	90dps		30dps	60dps	90dps
Mean	27.4	39.3	41.5* 43.4	Mean	2.6	20.8	48.6* 46.6
Upper Bound of 95%CI	28.3	48.6	53.3	Lower Bound of 95%CI	1.7	11.4	36.7
Lower Bound of 95%CI	26.6	29.9	29.6* 43.4	Upper Bound of 95%CI	3.4	30.1	60.4* 46.6

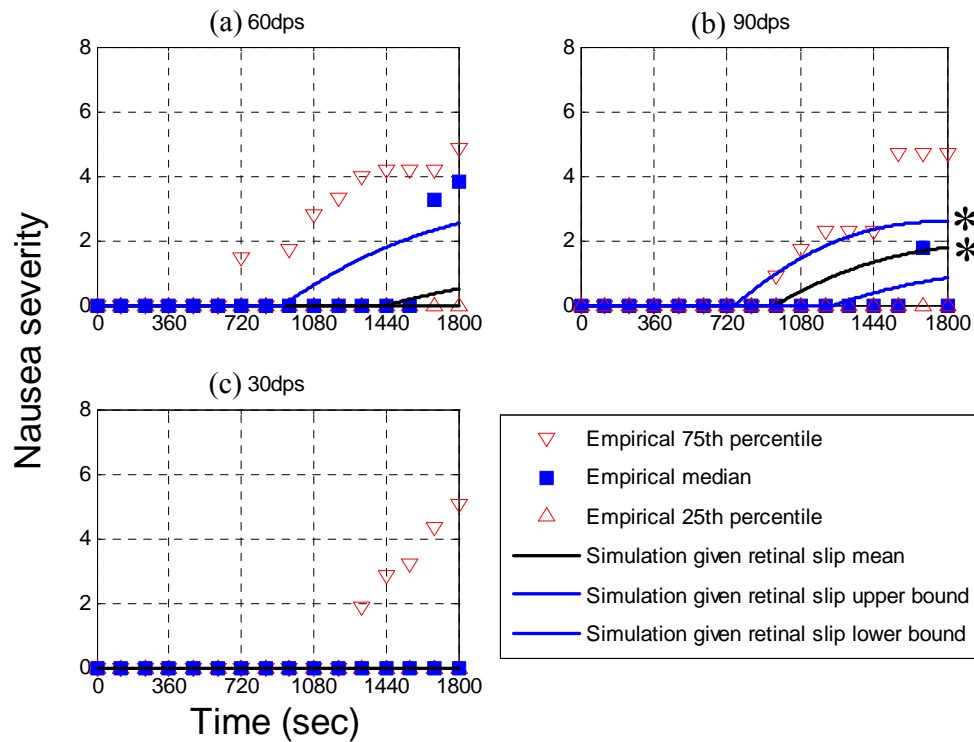


Figure 8.13 comparison of model simulated/predicted nausea severity levels with empirical data as functions of exposure duration at (a) 30 dps, (b) 60 dps and (c) 90 dps velocity condition. Hypothetical model simulations are labeled by *.

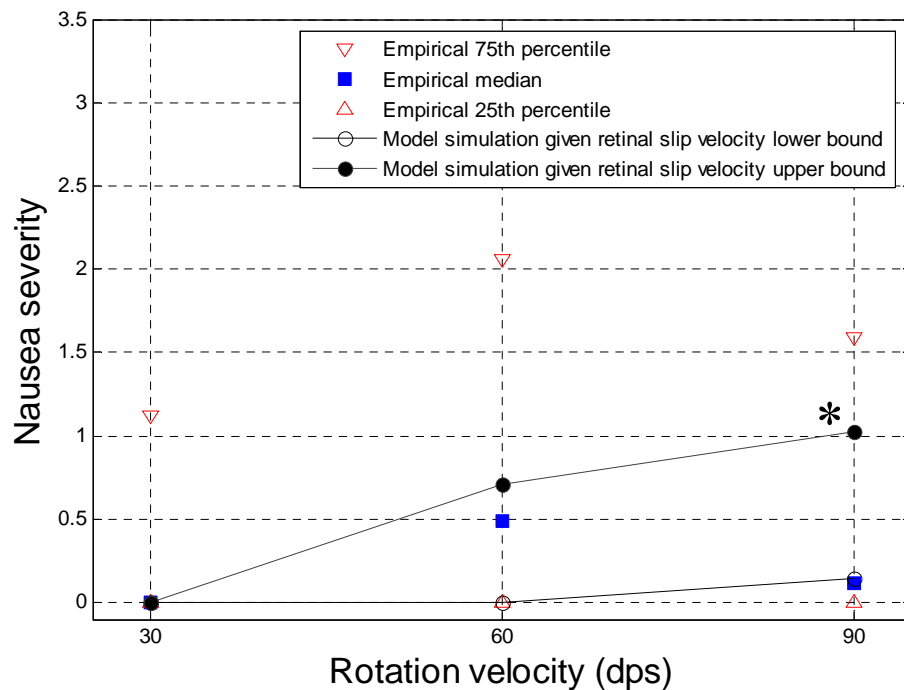


Figure 8.14 Comparison of model simulated/predicted nausea severity levels with empirical data as functions of rotation velocity from 30 dps to 60dps, and to 90 dps. The hypothetical model simulation is labeled by *.

Parameter $W_{r,3}$ and $W_{r,1}$ were then tuned to simulate the OKN gain level of each subject (listed in Table 6.2). Each corresponding model output is a model simulated individual nausea severity time series. Such model simulations make it possible that statistical analysis can be implemented to test the significance of the difference between the distributions of model simulated nausea severity and empirical data. Results of the Wilcoxon signed-rank test show that the difference is not statistically significant in all three non-zero velocity conditions (in each case, $p > 0.05$). As shown in Figure 8.15, the model simulated nausea severity in 60dps are significantly higher than in 0dps condition (one sample Wilcoxon, $p < 0.05$). Such result is the same with empirical results reported in experiment two.

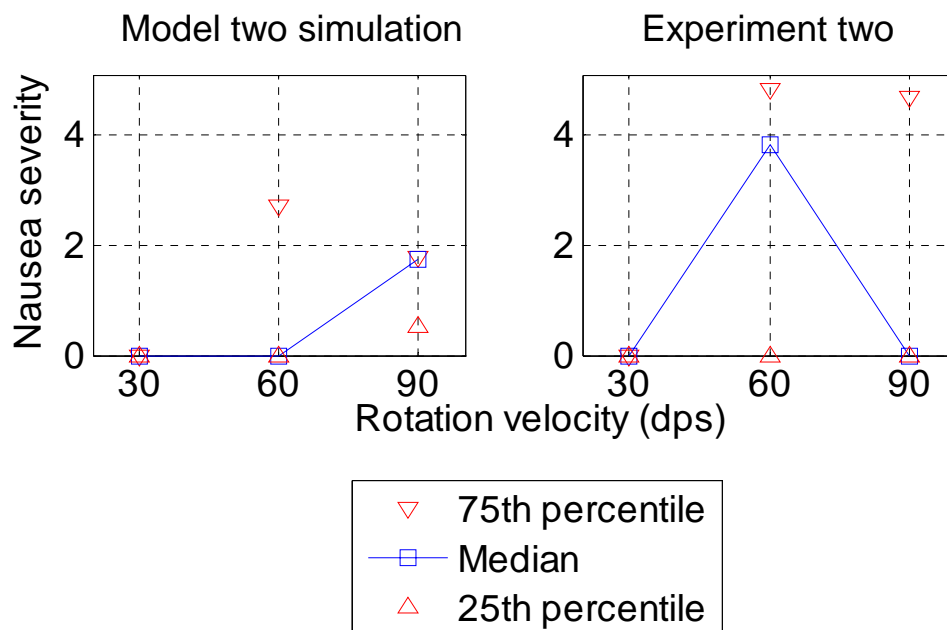


Figure 8.15 Comparing model two simulated data distribution with empirical data distribution collected from experiment two

To further evaluate the capability of model two of simulating nausea severity variation, model simulated nausea severity, given the model simulated foveal retinal slip velocity is equal to the average values of the top and bottom three of the empirical data (listed in Table 8.7), is plotted in Figures 8.16 and 8.17. None of the model simulations exceed the corresponding variation intervals bounded by the maximum and minimum values of the empirical data with regards to nausea severity.

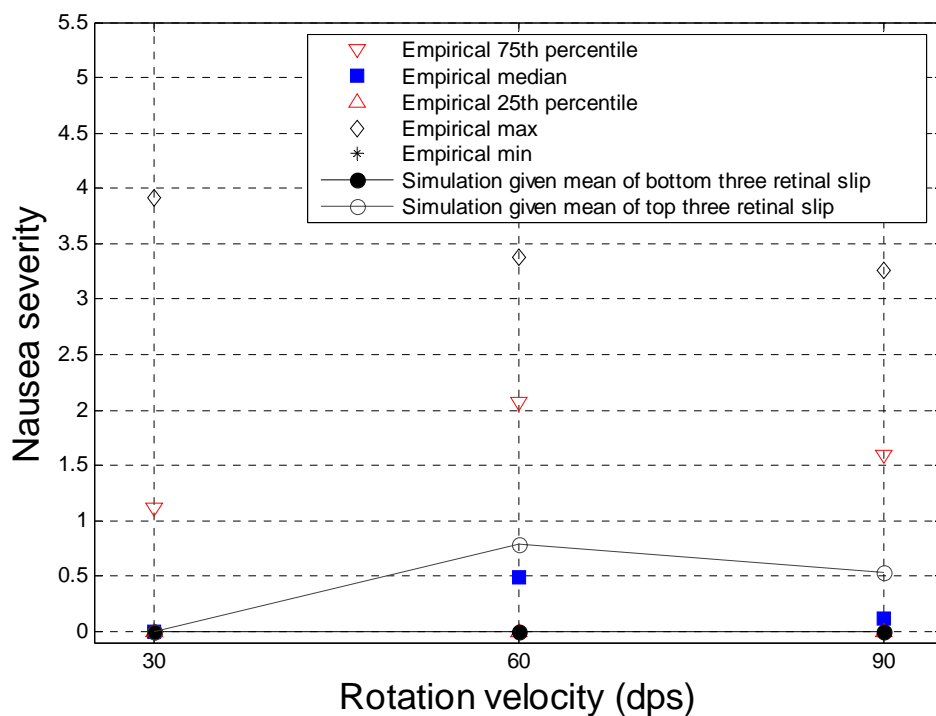


Figure 8.16 Comparison of model simulated/predicted nausea severity levels with empirical data as a function of rotation velocity from 30 dps to 60 dps, and to 90 dps. The blue squares and pairs of red triangles represent the 50th percentile, 25th percentile and 75th percentile of the empirical data with regards to nausea severity, respectively. The diamonds and crosses represent the maximum and minimum values of the empirical data with regards to nausea severity, respectively. The open and filled circles represent the model simulated nausea severity given that the model simulated foveal retinal slip velocity is equal to the average values of the top three and bottom three of the empirical data, respectively.

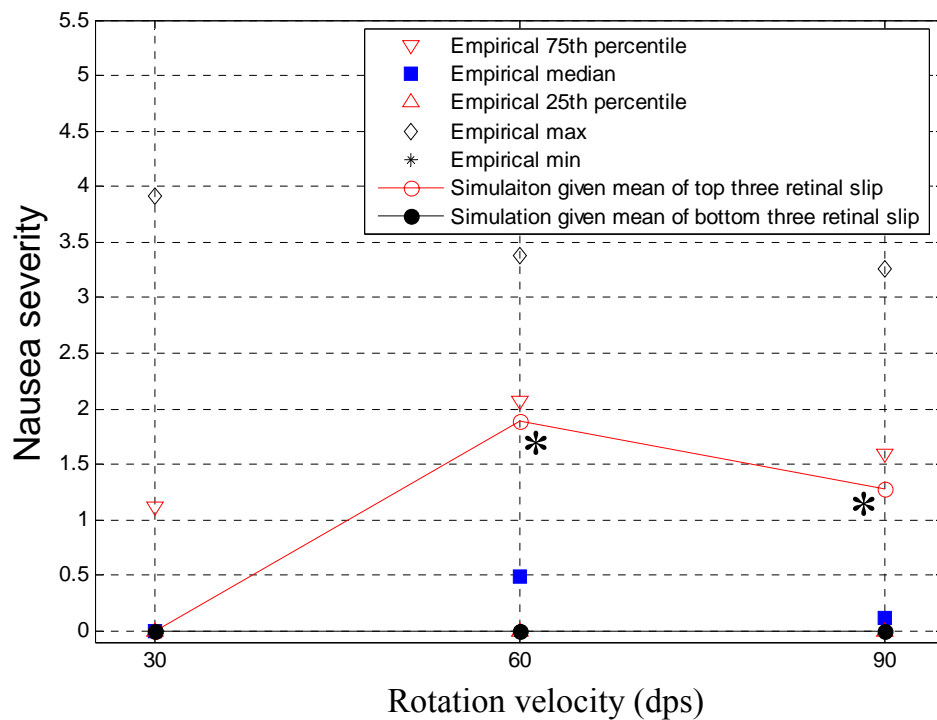


Figure 8.17 Model simulated nausea severity levels as a function of drum velocity given the average of the top three and average of bottom three vection velocity levels listed in Table 6.7 (*The two nausea severity levels are simulated by using constant OKN retinal slip velocity time series, i.e., 42.4 dps in 60 dps drum velocity condition and 69.3 dps in 90 dps drum velocity condition, as inputs of module two)

Table 8.7 The top three and bottom three retinal slip velocity levels reported by experiment two. * labels the average retinal slip velocity level larger than the maximum level that can be simulated by the OKN model from Zupan et al.(2002)

	30dps	60dps	90dps
Top three	6.2	44.2	74.5
	5.2	42.2	66.6
	3.3	40.7	66.9
Average	4.9	42.4 *	69.3 *
	4.9	31.0	46.6
Bottom three	0.8	1.9	8.2
	0.9	6.0	25.6
	1.6	2.8	23.4
Average	1.1	3.6	19.1

Model sensitivity analyses are separately implemented for subjects in groups I and group II. As illustrated in Figures 8.18 and 8.19, all model simulations, as a function of time or velocity, are enclosed in their corresponding max-min nausea severity intervals. All model parameters are the same with those used in the model validation except for necessary adjustments of parameter $W_{r,3}$ (see Table 8.8).

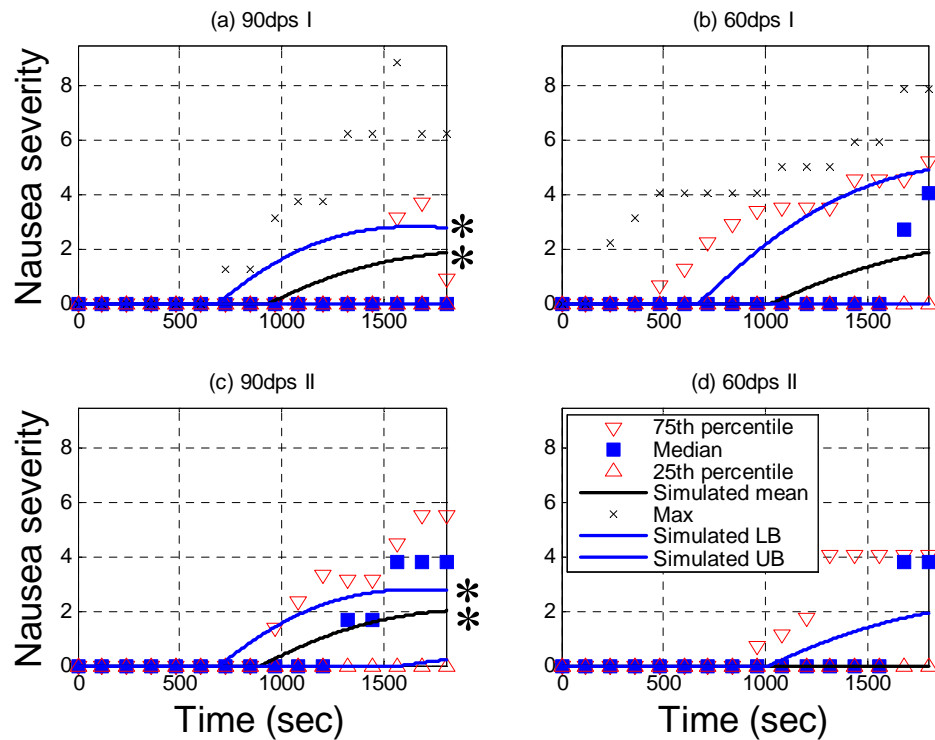


Figure 8.18 Comparison of model simulated nausea severity levels with empirical data as functions of exposure duration for the (a) 90 dps group I and (c) II as well as (b) 60 dps group I and (d) group II. * labels all hypothetical model simulations.

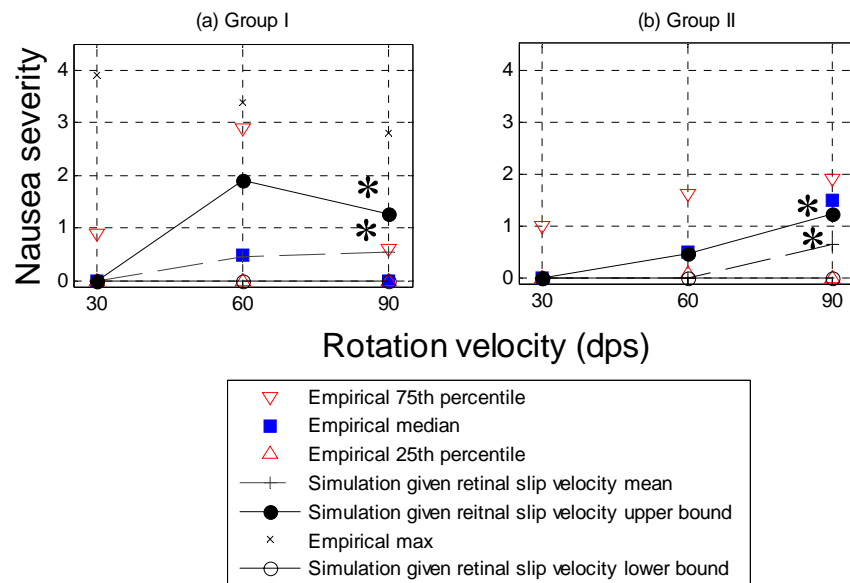


Figure 8.19 Comparison of model simulated/predicted nausea severity levels with empirical data as functions of rotation velocity of (a) group I subjects and (b) group II subjects. * labels all hypothetical model simulations.

Table 8.8 Means and 95% confidence intervals of the foveal retinal slip velocity of 30 dps, 60 dps and 90 dps velocity conditions for subjects in groups I and II

		OKN SPV				OKN retinal slip		
		30dps	60dps	90dps		30dps	60dps	90dps
Group I	Mean	27.4	32.9	42.5*	Mean	2.6	27.1	47.5*
	Upper Bound of 95%CI			43.4	Lower Bound of 95%CI			46.6
	Lower Bound of 95%CI	29.0	48.4	63.8	Upper Bound of 95%CI	1.0	11.6	26.2
		25.8	17.5	21.2*		4.2	42.5	68.8*
Group II				43.4				46.6
	Mean	27.5	45.6	40.4*	Mean	2.5	14.4	49.6*
	Upper Bound of 95%CI			43.4	Lower Bound of 95%CI			46.6
	Lower Bound of 95%CI	28.8	58.7	58.5	Upper Bound of 95%CI	1.2	1.3	31.5
		26.2	32.5	22.3*		3.8	27.5	67.7*
				43.4				46.6

8.7 Discussions

The accuracy of EOG measures in experiment two and its effect on the conclusions of model two deserves detailed discussion. For the purpose to map the unit of EOG records from volt to degree, EOG eye calibration was conducted to calculate the EOG unit mapping constant (EUMC) for each subject in each experimental session.

The experiment two used a within-subject design and the different experimental sessions for each subject were conducted in different days separated by a time interval of at least 7 days. As shown in Table 6.1, the EUMCs in different experimental conditions could be different for the same human participant. This variation may be caused by the fact that the attachment positions of EOG electrodes in each EOG calibration session conducted in different days can be slightly different. Further data analysis was conducted to investigate the effects of such variation in EOG measures.

First, the maximum and minimum of EUMC of each subject were identified. Second, the OKN SPV data of 14 participants for each velocity condition in Table 6.2 were reprocessed to generate one column of OKN SPV data given max EUMC and the other column given min EUMC as defined in the following two equations:

$$\text{OKN SPV}_{\text{max EUMC in condition x}} = \text{OKN SPV in condition x} * \text{EUMC in condition x} / \text{min EUMC}$$

$$\text{OKN SPV}_{\min} \text{ EUMC in condition } x = \text{OKN SPV in condition } x * \text{EUMC in condition } x / \text{max EUMC}$$

Third, the median of each column of OKN SPV for each velocity condition was calculated. As illustrated in Figure 8.20, the variation of EUMC across three different EOG calibration sessions results in a variation of OKN SPV levels in experiment two, representing by the distances between pairs of squares and circles. However, such variation originated from inaccuracy of EOG measures does not exceed the bounds of inter-subject variation of empirical OKN SPV used to evaluate model two in Chapter 8. Therefore, logically such variation of EUMC across different EOG calibration session in different days for the same human participants would not affect our conclusions on model two.

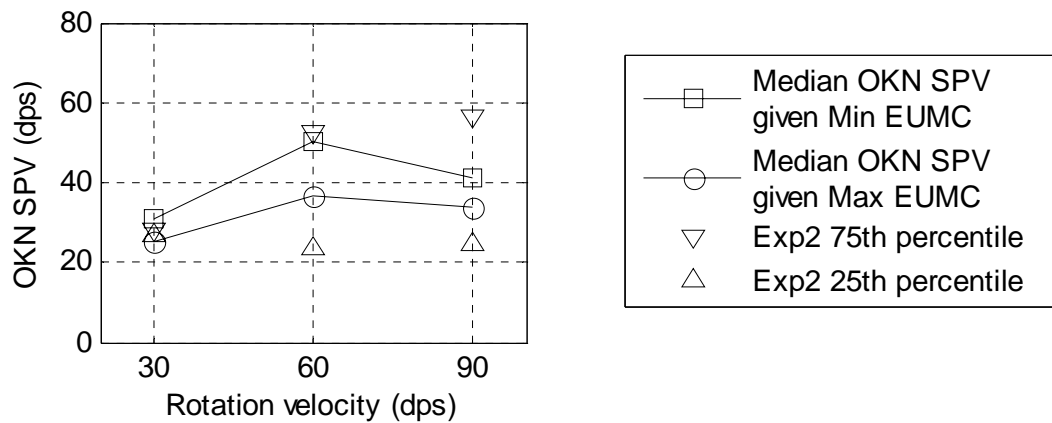


Figure 8.20 Variation of OKN SPV results of experiment two given a range of EOG unit mapping constants (* EUMC) measured in EOG calibration session. The squares and circle represent the medians of individual OKN SPV calculated by minimum and maximum EUMC across three rotation velocity conditions, respectively. The pairs of triangles represent the 75th and 25th percentiles of OKN SPV shown in Figure 6.2

The author also would like to emphasize that the two computational models presented in this study only serves the purpose to explain and simulate the strong association between veciton response and VIMS severity (model one) as well as between OKN response and VIMS severity (model two). The two models can only portray part of the mechanisms underlying the generation of VIMS, but not all. As illustrated in Figure 8.4 and Figure 8.11, the two models only explain part of the inter-subject variation of nausea severity captured by empirical studies. The part of individual difference in VIMS severity which can not be explained by the two models could be resulted from other factors such as the individual difference in motion sickness susceptibility. Although both of the two models have a free model parameter—the threshold I which makes the model itself has the potential to account for inter-subject variation originated from the motion sickness susceptibility, the threshold I was tuned to a fixed level in both model one and two currently. The author acknowledges such imperfection of model one and two and hope this research question can be solved in future studies.

8.8 Conclusions

In conclusion, model one has the flexibility to simulate inter-subject variations of vection perception (vection onset latency, vection build-up time, and vection

velocity's steady state) and nausea severity in 2, 14 and 34dps velocity conditions.

By tuning the parameter Φ , model simulated variations of vection velocity can explain part of the nausea variations reported in experiment one. Likewise, model two has the flexibility to simulate inter-subject variation of OKN SPV, OKN gain, foveal retinal slip velocity and nausea severity in 30, 60 and 90dps velocity conditions. By tuning the parameter $W_{r,3}$, model simulated variations of the foveal retinal slip velocity can explain part of the nausea variations reported in exp two.

CHAPTER 9

CONCLUSIONS

SUMMARY

This chapter concludes the thesis with a summary of the major contributions of this research and an outlook of future research directions.

9.1 Conclusions

A new and original biologically inspired computational model (model one) is developed to simulate the generation of nausea symptoms in viewers watching circularvection provoking visual stimuli with eye-fixation. This model successfully simulates the effects of (i) exposure duration, (ii) stimuli rotating velocity, and (iii) individual variations invection generation on ratio scale data of nausea severity levels. If baseline data on linear relationship betweenvection velocity and stimuli rotation velocity are known, model one can also predict the above effects on ratio scale nausea severity levels.

The predicted average time series nausea severity data by model one significantly

correlates with the measured average time series data collected in experiment one ($p < 0.01$). Consistent with empirical results collected in experiment one, the model predicted nausea severity in 14dps and 34dps are significantly higher than that in 0dps condition ($p < 0.05$).

A new and original biologically inspired computational model (model two) is developed to simulate the generation of nausea symptoms in viewers watching OKN provoking visual stimuli with vection suppression. This model successfully simulates the effects of (i) exposure duration, (ii) stimuli rotating velocity, and (iii) individual variations in OKN generation on ratio scale data of nausea severity levels. If baseline data on the linear relationship between foveal retinal slip velocity and rotation velocity are known, model two can also predict the above effects on ratio scale nausea severity levels.

The predicted average time series nausea severity levels by model two significantly correlate with the 75th percentile time series nausea severity levels, empirically collected in experiment two ($p < 0.01$). This indicates that although model two can predict the empirical result, the model over estimates the data magnitudes. Consistent with empirical results collected in experiment two, the model predicted nausea

severity for 60dps condition are significantly higher than that for the in 0dps condition ($p < 0.05$).

Model one has been demonstrated to be able to simulate how individual differences in three vection related measures (vection onset latency, vection build-up time, and vection velocity's steady state) can lead to individual variations in nausea severity levels. Likewise, model two can also simulate how individual differences in three OKN related measures (OKN SPV, OKN gain, foveal retinal slip velocity) can lead to individual variations in nausea severity levels. In particular, result of model simulation indicate that inter-subject variations of vection velocity's steady state (or vection gain) and OKN gain are able to account for about 50% and 40% of the inter-subject variations of VIMS severity reported by experiments one and two, respectively.

For the first time, both stimuli rotation velocity time course data (visual input) and head rotation velocity time course data are taken in by a mathematical model to simulate the subjective nausea severity as a function of time. The closest published mathematical model to my work is Oman's mathematical implementation of Reason's neural mismatch notion. Oman's model simulates the nausea severity by

taking in a hypothetical neural mismatch signal. However, detailed mathematical computations to transform visual and vestibular inputs into the neural mismatch signal are not within the scope of Oman's work. In addition, the testing conditions of Oman's work and my work are very different. The former focuses on vestibular input while my work focuses on visual inputs.

For the first time, both ratio scale data and ordinal scale data with regards to vection and nausea (i.e., the commonly used 7-point nausea rating and SSQ) are collected in the same VIMS experiment. Results of both experiments indicate that the ratio scale data and the ordinal scale data significantly correlate with each other ($p < 0.01$). Considering that ordinal scale data are not suitable for mathematical modeling and additional advantages of employing ordinal scale data and ratio scale data together, the free modulus magnitude estimation is suggested to be a supplement to ordinal scales for measuring VIMS severity in future VIMS empirical studies.

Experiment one not only confirms the linear relationship between stimuli rotation velocity of an optokinetic stimuli (drum rotation velocity) and vection velocity reported by Kennedy et al. (1996), but also reports a new finding. In contrary to Hu *et al.* (1989)'s study, the relationship between the optokinetic drum (or visual stimuli)

rotation velocity and VIMS severity is found to be linear with eye fixation (the range of velocity studied is from 2 dps to 34 dps in terms of retinal slip velocity, approximate to a range from 30 dps to 90 dps in terms of the optokinetic drum rotation velocity if viewed without eye-fixation). Hu *et al.* (1989) reported an inverted U shape relationship. Moreover, experiment one also identifies a linear relationship between the vection velocity and VIMS severity.

Results of Experiment two not only confirms the linear relationship between the optokinetic drum rotation velocity and the foveal retinal slip velocity reported by Koenig *et al.* (1978), but also confirms the inverted U-shape (in a range of 30 dps to 90 dps in terms of drum rotation velocity, peaking at 60 dps) relationship between the optokinetic drum rotation velocity and VIMS severity reported in Hu *et al.* (1989). Explanations of the differences in findings between Hu's work and mine can be found in Chapters 5 and 6.

In summary, this research study furthers the understanding of VIMS generation by developing two mathematical models to relate the two major hypothetical causes of VIMS: (i) vection, and (ii) OKN. Both models have modular structures that are consistent with the current neuroscience knowledge concerning VIMS. Both models

successfully simulate and predict the nausea data collected in two validation experiments. In consideration that the models will be made open-sourced after the findings are published, it is the hope of the author that the models can stimulate future modeling work on VIMS generation. In other words, future researchers can conduct other validation experiments to test the models and if needed, revise the open-sourced models.

9.2 Limitations and future research areas

The conceptual model of model one, built on the basis of a corresponding neural basis roadmap, provides a general framework for linkingvection to VIMS. The same is for the conceptual model of model two, for linking OKN to VIMS. Models one and two proposed in Chapters 2 and 3 are just one version of computational implementation of such theoretical frameworks. Some issues related to the current research may deserve further investigation and are listed as follows.

Models one and two were constructed to simulate VIMS provoked by a rotating optokinetic image pattern (or optokinetic drum) at a constant velocity along the earth-vertical axis. Although such a type of visual stimuli was commonly employed worldwide to provokevection, OKN and VIMS, the movements of visual stimuli

were limited to yaw-direction. It should be noted that vection model of Telban and Cardullo (2001) was not limited to yaw direction: the vection model has a parameter ξ to account for differences in circular vection perception along yaw, pitch and roll axis. In addition, Telban and Cardullo also model linear vection by replacing the semi-circular canal dynamics element with an otolith dynamics element which took in head acceleration information. It is noticed that the Telban and Cardullo model does not aim to simulate vection perception during dual axis or multi-axis motion. Therefore, the current version of model one cannot be directly applied to simulate VIMS provoked by a visual stimuli containing complex multi-axis movements, such as the VIMS generated inside the fix-based flight simulator of Hettinger et al.(1990). It has been reported that human participants exposed to a dual-axis (roll + fore-and-aft) moving visual stimuli perceived a corkscrew-like feeling of self-motion. Therefore, a mathematical model simulating vection perception along multi-axes and their associated VIMS severity deserves further attention.

Likewise, model two can be extended to simulate vertical eye movements and their associated VIMS severity data since the visual input of the OKN model from Zupan et al. (2002) was defined as a 3D vector. However, current VIMS studies have only investigated the effect of horizontal OKN on VIMS severity. The effect of vertical

OKN on VIMS severity is unknown.

Theoretically, involuntary eye movements provoked by translational visual disturbances can also contribute to VIMS generation as suggested by the extraocular afference hypothesis. However, the effect of reflexive eye movements induced by translational disturbance has not been studied. It is partially because these types of eye movements have a more complex position and velocity pattern than OKN provoked by rotational disturbance. Moreover, involuntary eye movements induced by translational disturbance are governed by multiple visual decoding mechanisms and their neural mechanisms are less known (see review paper of Miles, 1998). Insofar as I can see, it is still premature to expand model two to simulate involuntary eye movements provoked by translational visual disturbance and associated VIMS unless further empirical and neurobiological evidence are provided.

It is well-known that the effect ofvection and OKN on VIMS severity has a synergistic interaction. It was reported that VIMS severity level in the presence of both OKN andvection is significantly higher than the one in the presence ofvection only (Stern et al., 1990; Flanagan et al., 2002). Since models one and model two have been constructed to explain the isolated relationship betweenvection and VIMS,

and the isolated relationship between OKN and VIMS, respectively, neither can simulate the interactions between the effects ofvection and OKN on VIMS severity. Therefore, a mathematical model aiming to explain such synergistic interaction deserves further attention. Before such a model expansion, several research questions have to be answered:

- (i) How does the human central nervous system transform two types of information with different physical meanings (vection velocity and foveal retinal slip velocity) into a common representation?
- (ii) Does such integration of information happen before or after the process of adaptation network?
- (iii) Assuming the integration is processed in a form of linear combination, are there some related weightings and how are the weights being determined?

For readers who would like to follow this line of work, a hypothetical solution is proposed here. Wolpert et al. (1998) proposed that a modular strategy governs the computations in cerebellar neural circuitry. They claimed that the cerebellum is

composed of multiple modules and each individual module contains a relative independent neural circuit. The interactions among modules are controlled by a single “responsibility estimator” which calculates a corresponding signal for each module representing the degree to which the module captures the current context and should therefore, contribute to motor control. Logically, such a modular structure and the associated computations can be used to realize the integration of the signal processing of vection velocity and foveal retinal slip velocity. If the adaptation network in the cerebellum can process the vection velocity and foveal retinal slip velocity in parallel, the neural mismatch signal of each individual module can be easily integrated by a simple linear combination controlled by a central “responsibility estimator”. It is certain that a huge amount of effort is required to transform such a hypothetical solution into a feasible implementation.

Both models one and two take in the velocity information of the visual stimuli. Therefore, it is assumed that the velocity information of a provocative visual stimulus is known. To further expand the application scope of the two models, a velocity detecting front-end module can be added as a pre-processing module to extract velocity information from optical flow vectors calculated from an inputted image sequence. A primitive solution has been proposed and presented at the 2004’s

Human Factors and Ergonomics Society's Annual Conference (Ji et al., 2004).

It is worth pointing out that the two models proposed in this study take in only the temporal information without any spatial information of visual stimuli. In the current work, the average spatial frequency across the entire field-of-view is assumed to be fixed. In practice, changes of rotation velocity usually couple with changes of spatial frequency. For example, human subjects reported “individual stripes appeared as a blur” when the drum rotation velocity increased to 90 dps (Hu et al., 1989). It is expected that subjects would not be able to perceive the sharply striped pattern any more when the drum rotation velocity increases to an extremely high level. In that case, the dramatically reduced spatial frequency would in return, suppress the perceived drum rotation velocity as well as thevection velocity and the foveal retinal slip velocity. The critical role of spatial frequency should be taken into account in future model expansion. Practitioners can consider using a 3D Gabor filter to extract spatial and temporal information of visual stimuli simultaneously. As a matter of fact, the 3D Gabor filter, found to simulate the function of simple cells in the human visual cortex, has already been widely employed by researchers in computer vision in image processing and robot control (Heeger, 1987; Tsang and Shi, 2007).

In summary, the two conceptual frameworks and their mathematical implementations are still open for further enrichment. The mathematical modeling work aiming to explain the relationships amongvection, OKN and VIMS in this work has just been started.

Appendix 2-1: Transfer functions of M1 in model one

1) Semicircular canal dynamics are modeled by a transfer function T_{scc} which is a high pass filter with a low cut-off frequency at 0.033 Hz.

$$T_{scc} = \frac{\tau_1 \tau_a s^2}{(\tau_1 s + 1)(\tau_a s + 1)} \quad (\text{A2-1-1})$$

where $\tau_1 = 5.73s$ and $\tau_a = 80s$ are the dominant and adaptation time constants, respectively. (Fernandez and Goldberg, 1970)

2) Visual receptors dynamics are modeled by a transfer function T_{vis} which is a pure time delay to account for the time needed for neural transmissions from the rod-filled peripheral of the retina to the visual cortex and for signal processing during motion perception.

$$T_{vis} = -e^{-\tau_d s} \quad (\text{A2-1-2})$$

where $\tau_d = 0.09s$ as reported by Hosman & Van der Vaart, 1983. Negative sign is used to reflect the fact that visual surround rotating to one direction induces perceived self-rotating to the opposite direction.

3) A first-order low pass filter T_{opto} is added after K weighted visual input to account for vection's low pass frequency response. It was reported that visual input dominates the perception of self-motion below a frequency of 0.1Hz. Beyond the cut-off frequency, its response magnitude decreases at least as rapidly as a first-order filter. (Young, 1977) Meanwhile T_{opto} is used to model the gradual build-up of perceived self-rotating velocity after onset lasting for about 10 seconds as reported by Brandt, et al., 1973.

$$T_{opto} = \frac{1}{\tau_{va} s + 1} \quad (\text{A2-1-3})$$

where $\tau_{va} = 1.592s$ is the time constant for modeling a first-order low pass filter with a cut-off frequency at 0.1Hz and for modeling a 10-second gradual build-up time interval. Larger τ_{va} results in larger build-up duration and smaller cut-off frequency, and vice versa.

4) T_{ao} is a high pass filter used to wash out the high-frequency mismatch between visual input and vestibular input over time.

$$T_{ao} = \frac{\tau_w s}{\tau_w s + 1} \quad (\text{A2-1-4})$$

Where $\tau_w = 8s$ is used to control the wash-out at certain speed which eventually results in certain level of vection onset. The wash-out speed increases with smaller τ_w and vice versa.

Appendix 2-2: Transfer functions of M3 in model one and two

T_{fast} and T_{slow} are both second-order low pass filters used to simulate the leaky integrator dynamic of subjective discomfort observed in Bock & Oman, 1982.

$$T_{fast} = \frac{k}{(\tau_{fast}s + 1)^2} \quad (A2-2-1)$$

$$T_{slow} = \frac{5k}{(\tau_{slow}s + 1)^2} \quad (A2-2-2)$$

where $\tau_{fast} = 60s$ and $\tau_{slow} = 600s$ used to simulate a relative short response time for fast pathway and a relative long one for slow pathway, respectively. Moreover, the slow path transfer function has a larger gain than the fast path by a factor 5 as originally proposed by Oman. k is a positive constant free parameter.

Appendix 3-1: Transfer functions of M1 in model two

1) The part of the visual system that extracts angular information from foveal retinal slip is modeled by a 3×3 diagonal transfer function matrix T_{rs} , the diagonal elements of which are first-order low pass filter with a cut-off frequency at 1.06Hz.

$$T_{rs} = \frac{1}{\tau_r s + 1} I \quad (A3-1-1)$$

where $\tau_r = 0.15s$. This time constant has been chosen to fit eye movements in response to visual surround rotation (Cohen et al., 1981;Jell, et al., 1984) The transfer function \hat{T}_{rs} is referred to as the internal model of T_{rs} , which is chosen that

$T_{rs} = \hat{T}_{rs}$ to account for a perfect match of eye plant dynamics. The transfer

function $I - \hat{T}_{rs}$ is referred to as a complementary dynamics of internal model \hat{T}_{rs} ,

the diagonal elements of which are first-order high pass filter with a cut-off frequency at 1.06Hz. Consequentially the corresponding feedback loop for the processing of sensory estimate of eye angular velocity in space \tilde{r} is an algebraic loop. Therefore a first order low-pass filter with a cutoff frequency of 160Hz is chosen to break the algebraic loop.

$$I - \hat{T}_{rs} = \frac{\tau_r s}{\tau_r s + 1} \frac{1}{\varepsilon s + 1} I \quad (A3-1-2)$$

where $\varepsilon = 0.001s$. Its diagonal elements are band-pass filter with a frequency range from 0.95 to 159 Hz.

2) The dynamics of eye plant and its internal model are modeled by 3×3 diagonal transfer function matrix T_{eye} and \hat{T}_{eye} , respectively. The internal model \hat{T}_{eye} is chosen that $T_{eye} = \hat{T}_{eye}$, the diagonal elements of which are first-order low pass filter with a cut-off frequency at 53.1Hz.

$$T_{eye} = \frac{1}{\tau_e s + 1} I \quad (A3-1-3)$$

where $\tau_e = 0.003s$. This time constant is the smallest time constant characterizing the eye plant. (Fuchs, et al., 1988)

3) T_{OKNe} is a 3×3 diagonal transfer function matrix modeling the OKN_e motor control dynamics transforming central estimate of external visual disturbance into OKN_e motor command. Its diagonal elements have two components:

$$T_{OKNe} = T_{OKNe1} T_{OKNe2} = \frac{A}{Ts + 1} e^{\tau_d s} I \quad (A3-1-4)$$

where component 1 is a first-order low pass filter (cut-off frequency at 1.19 Hz) with time constant $T = 0.134s$ and gain $A = 0.95$ to fit the initial rise rate of OKN_e eye command e_p and pursuit gain. Component 2 is a pure delay unit ($\tau_d = 130ms$) enclosing a 50ms delay for the processing in the retinal and visual cortex, a 30ms delay for the processing from the cerebellum to final formation of eye motor command in eye motoneurons and another 50ms accounting for the processing in between. (Robinson, et al., 1986)

4) Semicircular canal dynamics are modeled by a 3×3 diagonal transfer function matrix T_{scc} , the diagonal elements of which are second-order high pass filter with a cut-off frequency at 0.027 Hz.

$$T_{scc} = \frac{\tau_1 \tau_a s^2}{(\tau_1 s + 1)(\tau_a s + 1)} I \quad (A3-1-5)$$

where $\tau_1 = 5.73s$ and $\tau_a = 80s$ are the dominant and adaptation time constants, respectively. (Fernandez & Goldberg, 1970) The transfer function \hat{T}_{scc} is referred to as the internal model of T_{scc} .

$$\hat{T}_{scc} = \frac{\tau_1 s}{\tau_1 s + 1} I \quad (A3-1-6)$$

where \hat{T}_{scc} is a first-order high pass filter with a cutoff frequency at 0.027Hz. It is not a perfect match of the semicircular canal dynamics for simplicity. The transfer function $I - \hat{T}_{scc}$ is referred to as a complementary dynamics of internal model \hat{T}_{scc} . Its diagonal elements are first-order low pass filter with a cutoff frequency at 0.027Hz.

$$I - \hat{T}_{scc} = \frac{1}{\tau_1 s + 1} I \quad (\text{A3-1-7})$$

Appendix 4-1 Pre-exposure and Post-exposure Simulator Sickness Questionnaires (Kennedy *et al.*, 1993)

SYMPTOM CHECKLIST (Pre-exposure) confidential

Pre-exposure instructions: please fill in this questionnaire. Circle below if any of the symptoms apply to you now. You will be asked to fill this again after the experiment.

一般不適	1. General discomfort	None	Slight	Moderate	Severe
疲 倦	2. Fatigue	None	Slight	Moderate	Severe
沉 悶	3. Boredom	None	Slight	Moderate	Severe
想 睡	4. Drowsiness	None	Slight	Moderate	Severe
頭 痛	5. Headache	None	Slight	Moderate	Severe
眼 痛	6. Eyestrain	None	Slight	Moderate	Severe
很難集中視力	7. Difficulty focusing	None	Slight	Moderate	Severe
口水分泌增加	8. Salivation increase	None	Slight	Moderate	Severe
口水分泌減少	Salivation decrease	None	Slight	Moderate	Severe
出 汗	9. Sweating	None	Slight	Moderate	Severe
作 嘔	10. Nausea	None	Slight	Moderate	Severe
很難集中精神	11. Difficulty concentrating	None	Slight	Moderate	Severe
精神的壓抑	12. Mental depression	No	Yes (Slight	Moderate	Severe)
頭 脹	13. "Fullness of the head"	No	Yes (Slight	Moderate	Severe)
視野模糊	14. Blurred vision	No	Yes (Slight	Moderate	Severe)
眼 花 (開)	15. Dizziness eyes open	No	Yes (Slight	Moderate	Severe)
眼 花 (合)	Dizziness eyes close	No	Yes (Slight	Moderate	Severe)
眩 暈	16. Vertigo	No	Yes (Slight	Moderate	Severe)
幻 覺	17. Visual flashbacks*	No	Yes (Slight	Moderate	Severe)
昏 厥	18. Faintness	No	Yes (Slight	Moderate	Severe)
呼吸異樣	19. Aware of breathing	No	Yes (Slight	Moderate	Severe)
胃感覺異樣	20. Stomach awareness	No	Yes (Slight	Moderate	Severe)
沒有胃口	21. Loss of appetite	No	Yes (Slight	Moderate	Severe)
胃口增加	22. Increased appetite	No	Yes (Slight	Moderate	Severe)
想去洗手間	23. Desire to move bowels	No	Yes (Slight	Moderate	Severe)
迷 惘	24. Confusion	No	Yes (Slight	Moderate	Severe)
打 嗝	25. Burping	No	Yes (Slight	Moderate	Severe)
嘔 吐	26. Vomiting	No	Yes (Slight	Moderate	Severe)
其 他	27. Other	No	Yes (Slight	Moderate	Severe)

SYMPTOM CHECKLIST (Post-exposure)
confidential

Post-exposure instruction: please fill in this questionnaire once more. Circle below if any of the symptoms apply to you now.

一般不適	1. General discomfort	None	Slight	Moderate	Severe
疲 倦	2. Fatigue	None	Slight	Moderate	Severe
沉 悶	3. Boredom	None	Slight	Moderate	Severe
想 睡	4. Drowsiness	None	Slight	Moderate	Severe
頭 痛	5. Headache	None	Slight	Moderate	Severe
眼 痛	6. Eyestrain	None	Slight	Moderate	Severe
很難集中視力	7. Difficulty focusing	None	Slight	Moderate	Severe
口水分泌增加	8. Salivation increase	None	Slight	Moderate	Severe
口水分泌減少	Salivation decrease	None	Slight	Moderate	Severe
出 汗	9. Sweating	None	Slight	Moderate	Severe
作 嘔	10. Nausea	None	Slight	Moderate	Severe
很難集中精神	11. Difficulty concentrating	None	Slight	Moderate	Severe
精神的壓抑	12. Mental depression	No	Yes (Slight	Moderate	Severe)
頭 脹	13. "Fullness of the head"	No	Yes (Slight	Moderate	Severe)
視野模糊	14. Blurred vision	No	Yes (Slight	Moderate	Severe)
眼 花 (開)	15. Dizziness eyes open	No	Yes (Slight	Moderate	Severe)
眼 花 (合)	Dizziness eyes close	No	Yes (Slight	Moderate	Severe)
眩 暈	16. Vertigo	No	Yes (Slight	Moderate	Severe)
幻 覺	17. Visual flashbacks*	No	Yes (Slight	Moderate	Severe)
昏 厥	18. Faintness	No	Yes (Slight	Moderate	Severe)
呼吸異樣	19. Aware of breathing	No	Yes (Slight	Moderate	Severe)
胃感覺異樣	20. Stomach awareness	No	Yes (Slight	Moderate	Severe)
沒有胃口	21. Loss of appetite	No	Yes (Slight	Moderate	Severe)
胃口增加	22. Increased appetite	No	Yes (Slight	Moderate	Severe)
想去洗手間	23. Desire to move bowels	No	Yes (Slight	Moderate	Severe)
迷 惘	24. Confusion	No	Yes (Slight	Moderate	Severe)
打 嗝	25. Burping	No	Yes (Slight	Moderate	Severe)
嘔 吐	26. Vomiting	No	Yes (Slight	Moderate	Severe)
其 他	27. Other	No	Yes (Slight	Moderate	Severe)

**Appendix 4-2 Calculations of SSQ total scores and three sub-scores
(Kennedy *et al.*, 1993)**

None = 0

Slight = 1

Moderate = 2

Severe = 3

Weights for Symptoms

Symptoms	Nausea	Oculomotor	Disorientation
General discomfort	1	1	
Fatigue		1	
Headache		1	
Eye strain		1	
Difficulty focusing		1	1
Increased salivation	1		
Sweating	1		
Nausea	1		1
Difficulty concentrating	1	1	
Fullness of head			1
Blurred vision		1	1
Dizzy (eyes open)			1
Dizzy (eyes closed)			1
Vertigo			1
Stomach awareness	1		
Burping	1		
Total*	[1]	[2]	[3]

Score

Nausea = [1] × 9.54

Oculomotor = [2] × 7.58

Disorientation = [3] × 13.92

Total Score = ([1] + [2] + [3]) × 3.74

* Total is the sum obtained by adding the symptoms scores. Omitted scores are zero

Appendix 4-3 A motion sickness susceptibility survey questionnaire (So et al., 1999)

Motion Sickness Susceptibility Survey

暈浪敏感調查

This survey is being conducted to examine the motion sickness susceptibility of the Hong Kong Chinese population. All information in this survey will be kept confidential. This survey is not a requirement of this course and participation is to be done on a voluntary basis.

這是一個有關中國人對暈浪的敏感性調查，所有調查所得的資料將會被保密。

Instructions: Please fill in this survey. Circle the answer which most closely corresponds to your own experience. Feel free to add any comments you would like to make at the end of the survey.

請圈出你的答案。

Name _____ Student ID _____

Email address _____ Age _____ Sex M F

School 學院 : BusinessEngineering Humanities Science

The term motion sickness is a refers to symptoms, such as dizziness, fatigue, nausea, headache, sweating, and vomiting, which can be evoked in susceptible individuals by the perception of various kinds of periodic motion,

暈浪的定義就是一種病徵，例流汗，作嘔，頭暈，頭痛或嘔吐。

1. In the pass 12 months how often have you experienced motion sickness while travelling as a passenger in the following situations? (E.g. If you travel by bus 300 times a year and experience motion sickness 30 times, that would be 10% of the time)

Car/Taxi	0%	1%-10%	11%-40%	41%-74%	75%-100%
----------	----	--------	---------	---------	----------

私家車/的士

Buses	0%	1%-10%	11%-40%	41%-74%	75%-100%
-------	----	--------	---------	---------	----------

巴士

Cross-Ferry	0%	1%-10%	11%-40%	41%-74%	75%-100%
-------------	----	--------	---------	---------	----------

渡輪

Jet-Foil	0%	1%-10%	11%-40%	41%-74%	75%-100%
----------	----	--------	---------	---------	----------

飛翔船

Trains (MTR/KCR)	0%	1%-10%	11%-40%	41%-74%	75%-100%
------------------	----	--------	---------	---------	----------

火車

Elevators	0%	1%-10%	11%-40%	41%-74%	75%-100%
-----------	----	--------	---------	---------	----------

升降機

2. Please circle the symptoms experienced while in the following situations:

請圈出在暈浪的病徵：

Car/Taxi	Sweating	Nausea	Dizziness	Headache	Vomiting
----------	----------	--------	-----------	----------	----------

私家車/的士	流汗	作嘔	頭暈	頭痛	嘔吐
--------	----	----	----	----	----

Buses	Sweating	Nausea	Dizziness	Headache	Vomiting
-------	----------	--------	-----------	----------	----------

巴士	流汗	作嘔	頭暈	頭痛	嘔吐
----	----	----	----	----	----

Cross-Ferry	Sweating	Nausea	Dizziness	Headache	Vomiting
渡輪	流汗	作嘔	頭暈	頭痛	嘔吐
Jet-Foil	Sweating	Nausea	Dizziness	Headache	Vomiting
飛翔船	流汗	作嘔	頭暈	頭痛	嘔吐
Trains (MTR/KCR)	Sweating	Nausea	Dizziness	Headache	Vomiting
火車	流汗	作嘔	頭暈	頭痛	嘔吐
Elevators	Sweating	Nausea	Dizziness	Headache	Vomiting
升降機	流汗	作嘔	頭暈	頭痛	嘔吐

3. In general, how susceptible to motion sickness are you?

通常，你對暈浪的敏感程度有幾大？

Not at all	Slightly	Moderately	Very	Extremely
從不	很少	一般	非常	極端

4. How many hours do you spend on computer in a week?

0-5 6-10 11-15 16-20 21-25 over 25

5. Did you use virtual reality in the past week? Yes/No

Appendix 4-4: Motion sickness susceptibility questionnaire (MSSQ)-Short (Golding, 2006)

Your childhood experience only (before 12 years of age), for each of the following types of transport or entertainment please indicate

1. As a child (before age 12), how often you felt sick or nauseated (tick boxes)

	Not Applicable - Never Traveled	Never Felt Sick	Rarely Felt Sick	Sometimes Felt Sick	Frequently Felt Sick
Cars					
Buses or Coaches					
Trains					
Aircraft					
Small Boats					
Ships, e.g. Channel Ferries					
Swings in playgrounds					
Roundabouts in playgrounds					
Big Dippers, Funfair Rides					

t 0 1 2 3

Your experience over the last 10 years (approximately), for each of the following types of transport or entertainment please indicate

2. Over the last 10 years, how often you felt sick or nauseated (tick boxes)

	Not Applicable - Never Traveled	Never Felt Sick	Rarely Felt Sick	Sometimes Felt Sick	Frequently Felt Sick
Cars					
Buses or Coaches					
Trains					
Aircraft					
Small Boats					
Ships, e.g. Channel Ferries					
Swings in playgrounds					
Roundabouts in playgrounds					
Big Dippers, Funfair Rides					

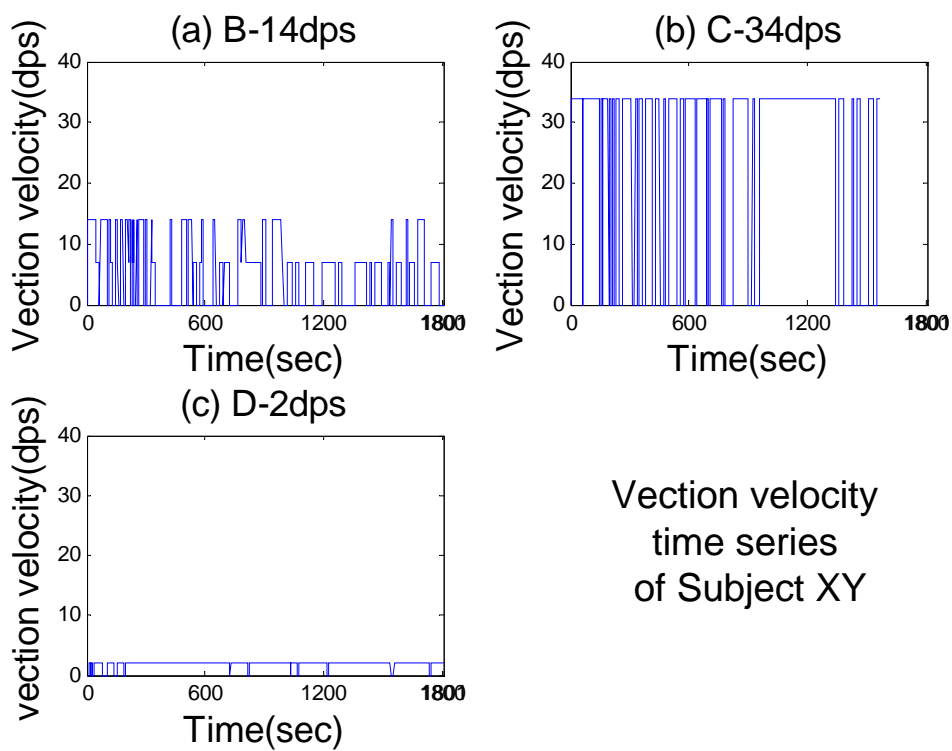
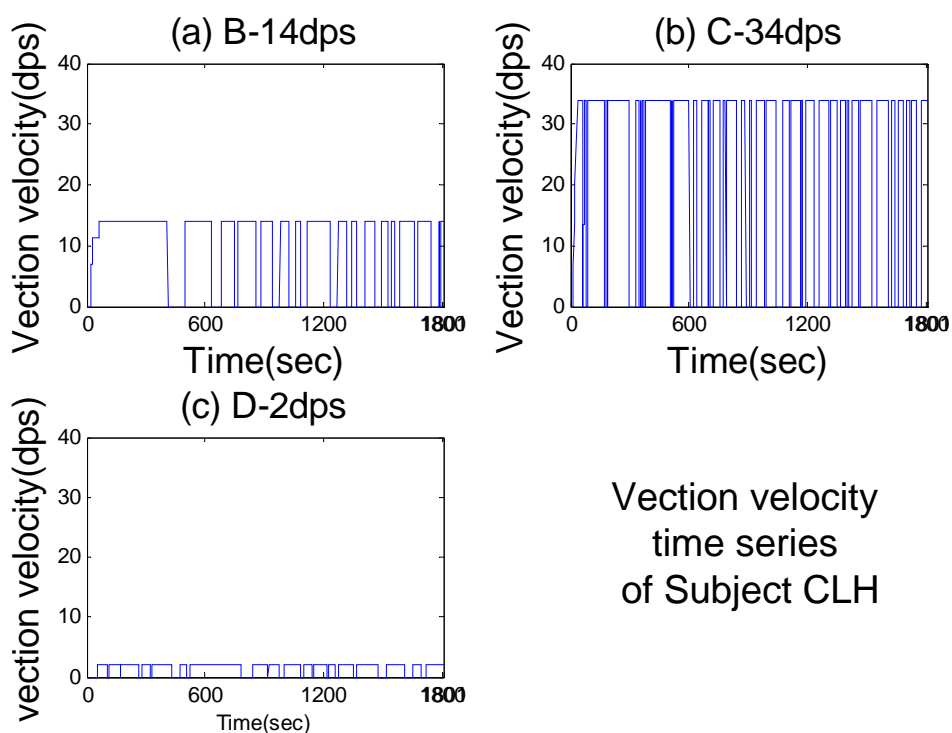
t 0 1 2 3

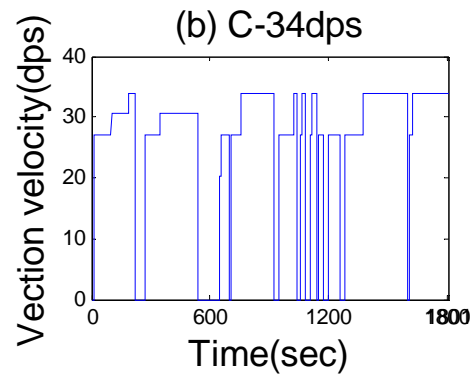
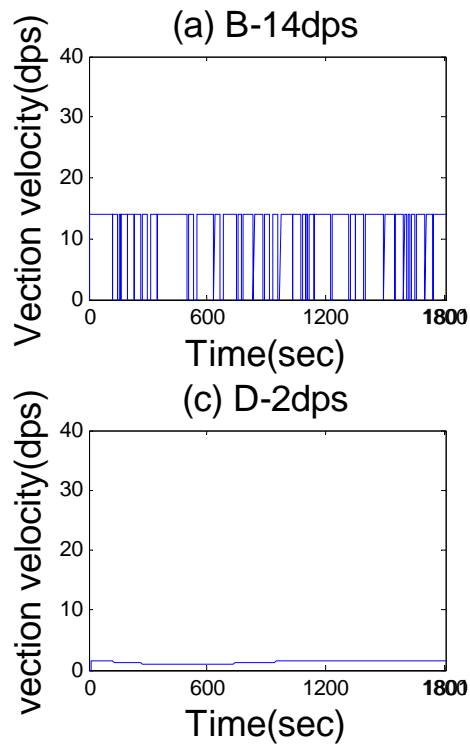
MSSQ-Short raw score = MSA+MSB

MSA = (total sickness score as a child)×(9)/(9-number of types not experienced as a child)

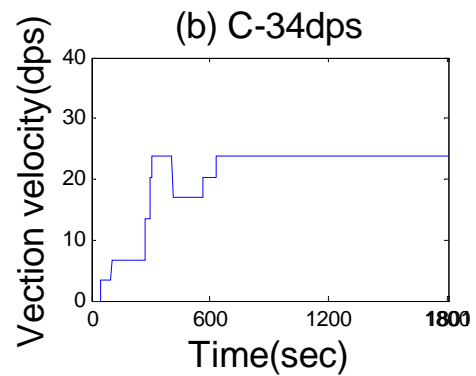
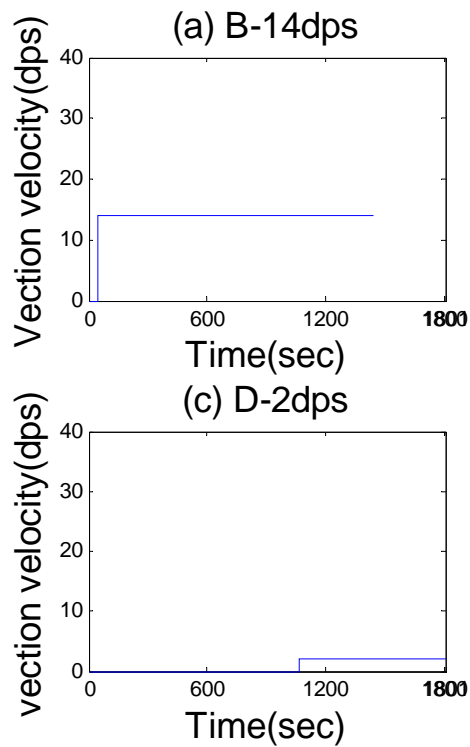
MSB = (total sickness score in past 10years)×(9)/(9-number of types not experience in past 10years)

Appendix 5-1 Individual vection velocity time series

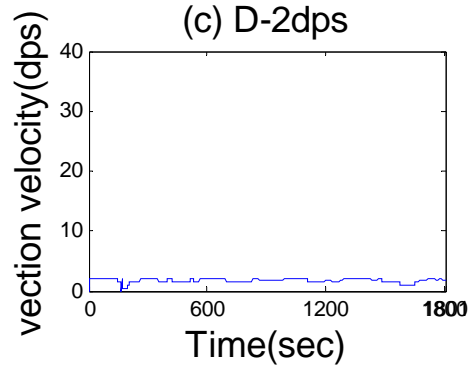
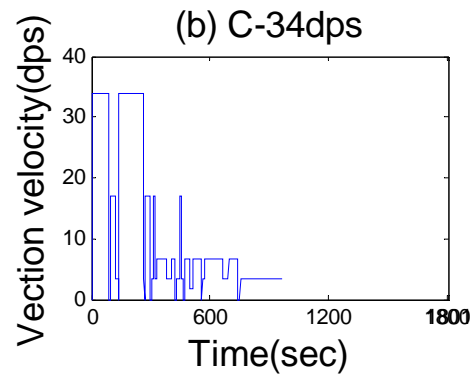
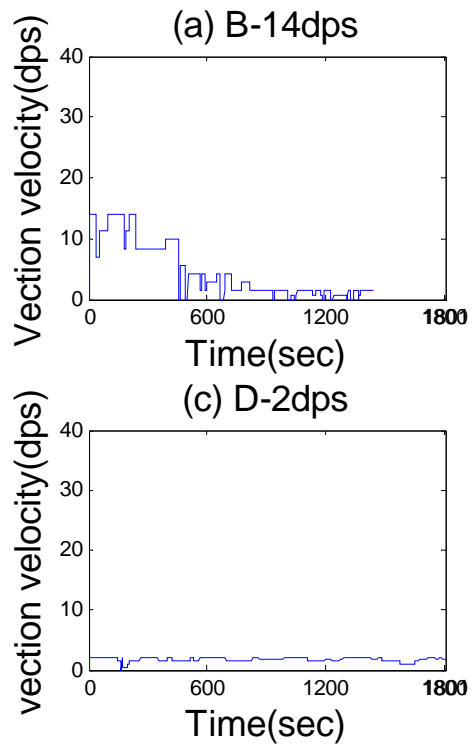




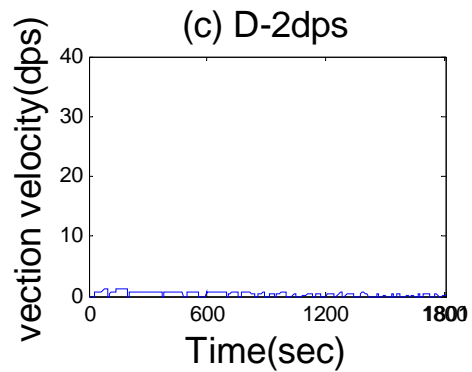
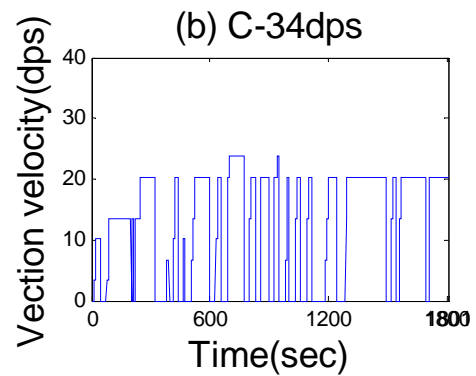
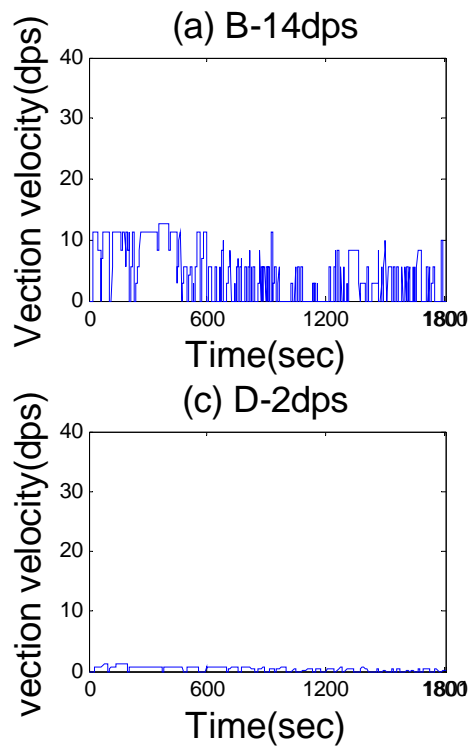
Vection velocity
time series
of Subject PBQ



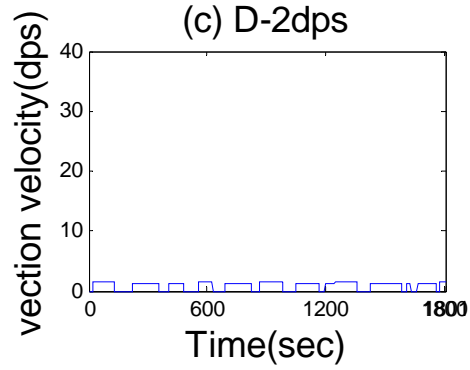
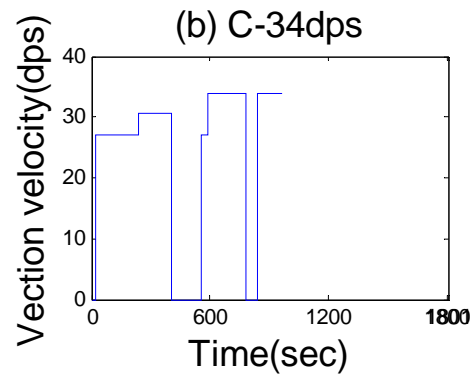
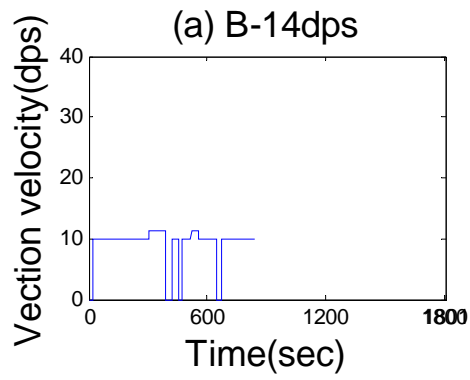
Vection velocity
time series
of Subject TYW



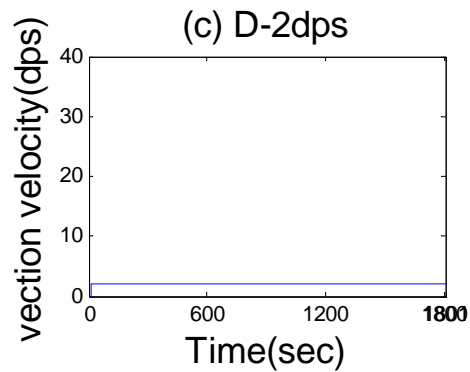
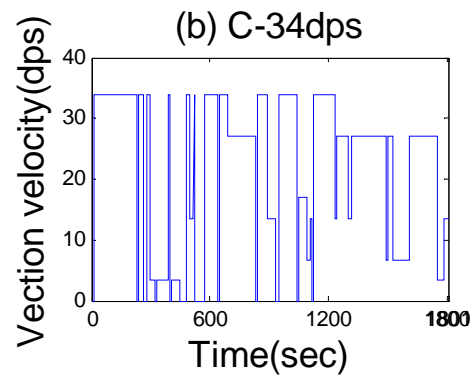
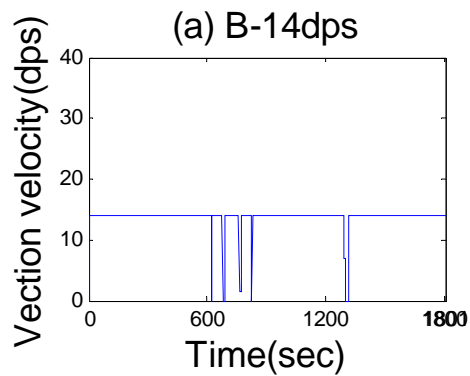
Vection velocity
time series
of Subject WXL



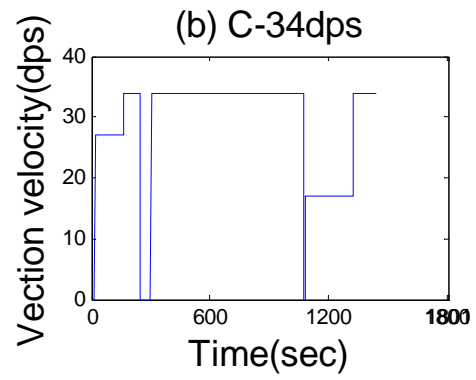
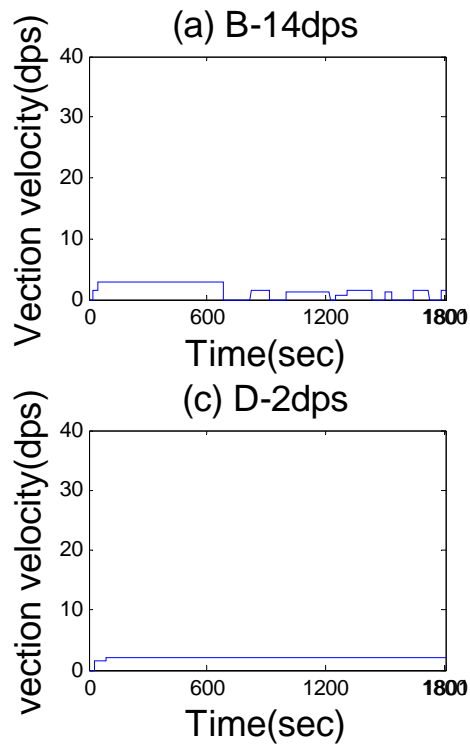
Vection velocity
time series
of Subject XJ



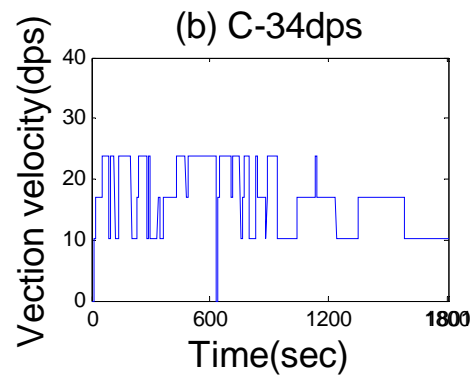
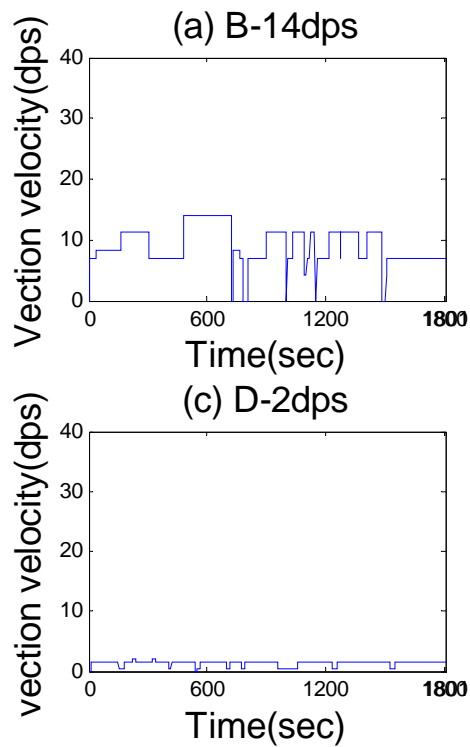
Vection velocity
time series
of Subject NXH



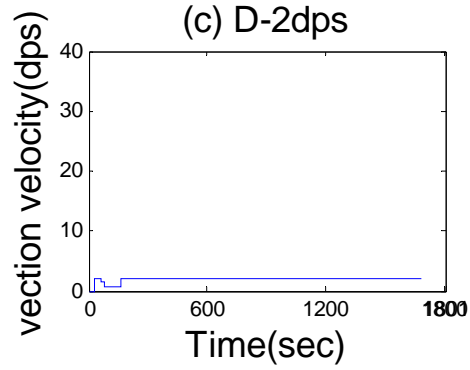
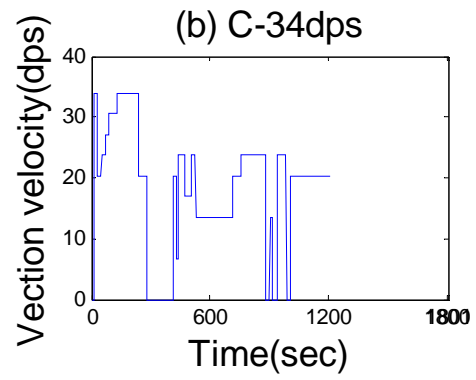
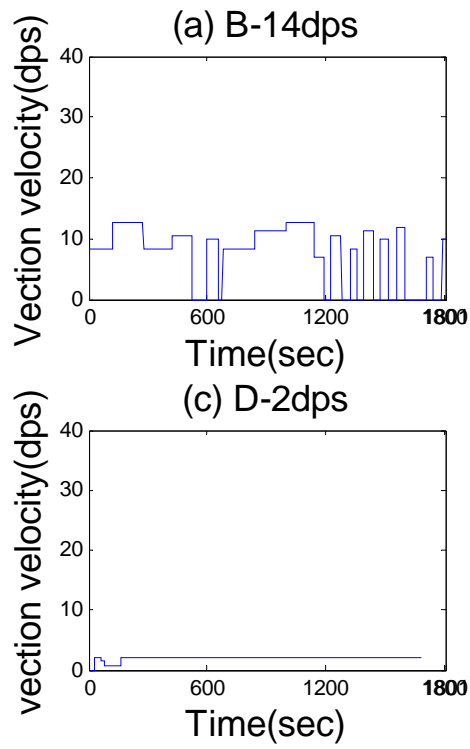
Vection velocity
time series
of Subject CX



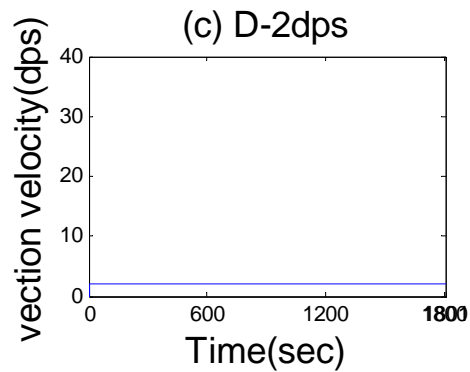
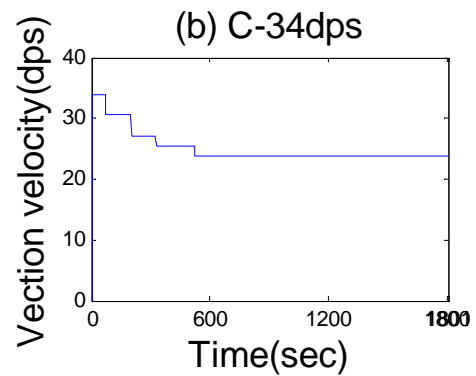
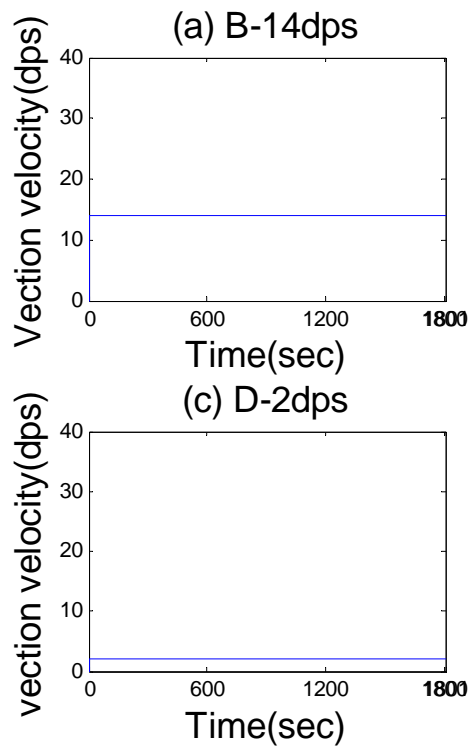
Vection velocity
time series
of Subject LD



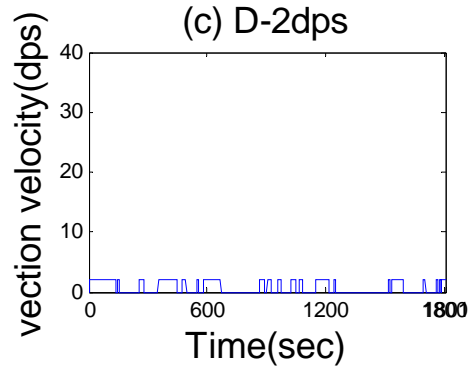
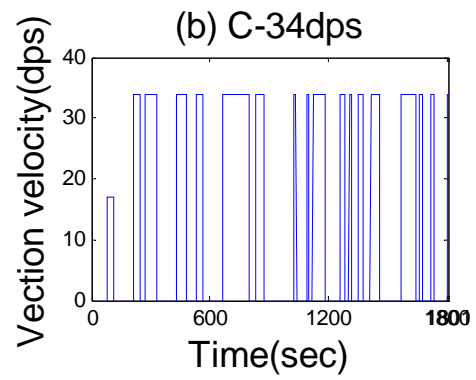
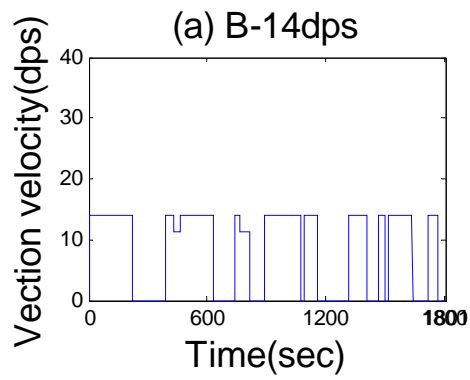
Vection velocity
time series
of Subject ZWT



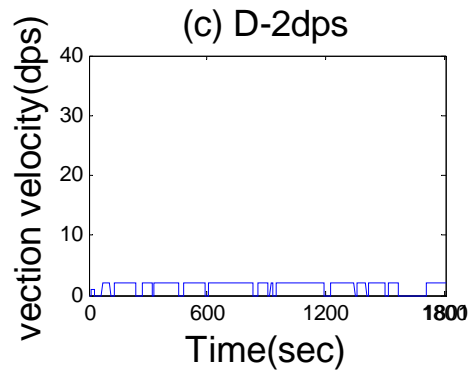
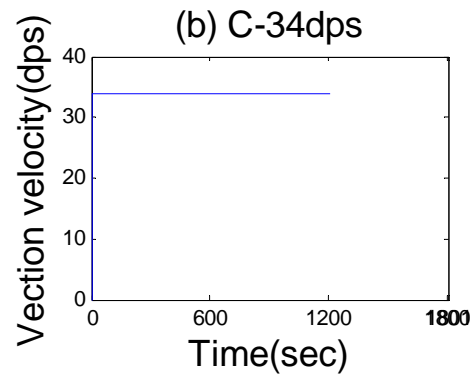
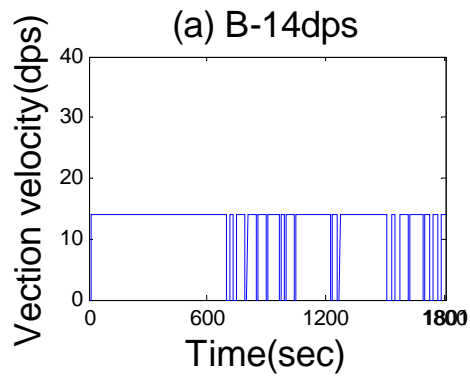
Vection velocity
time series
of Subject NYS



Vection velocity
time series
of Subject YXX



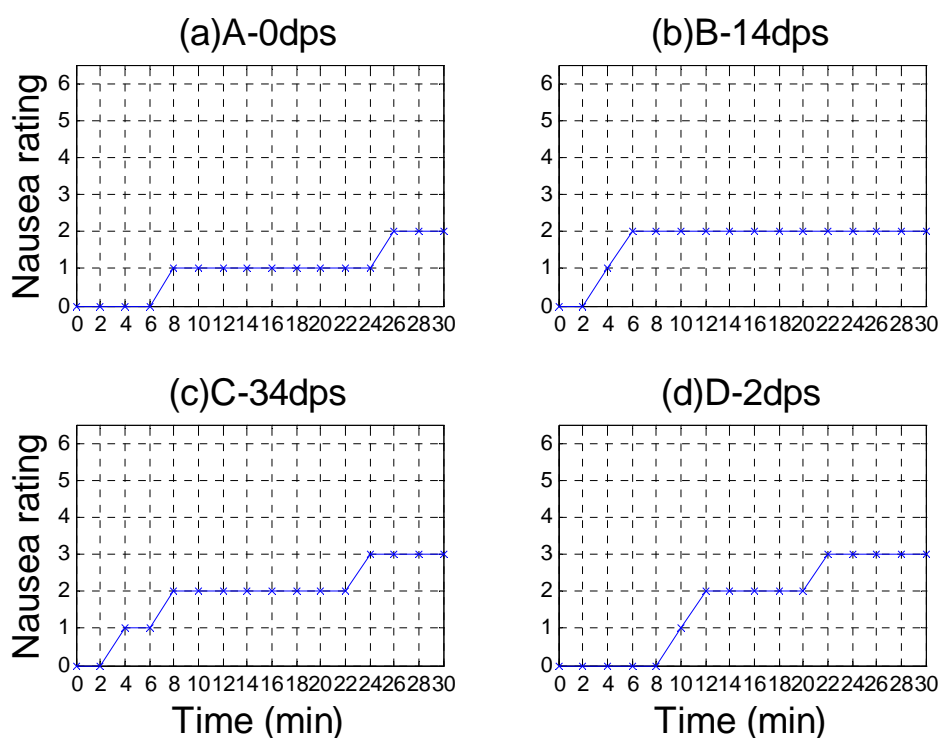
Vection velocity
time series
of Subject SLH



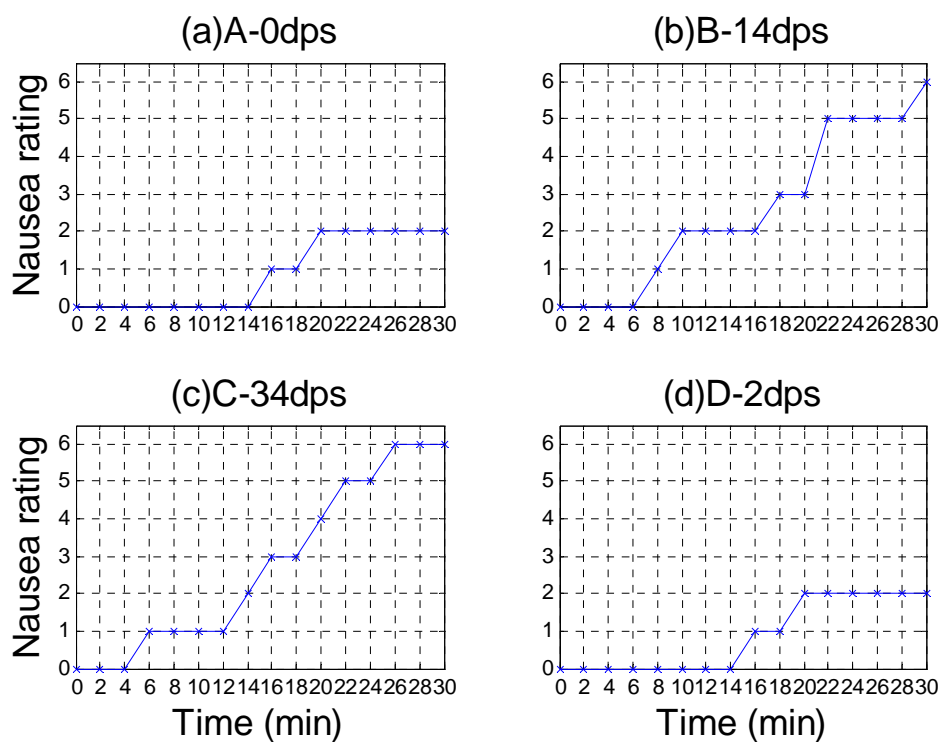
Vection velocity
time series
of Subject SYF

Appendix 5-2 Individual 7-point nausea rating time series

7-point nausea rating time series of Subject CLH

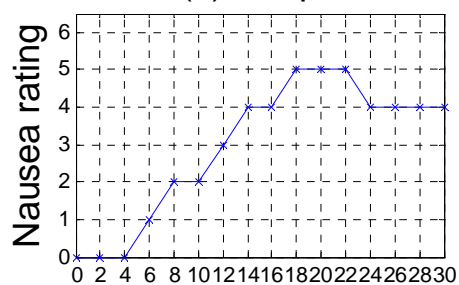


7-point nausea rating time series of Subject XY

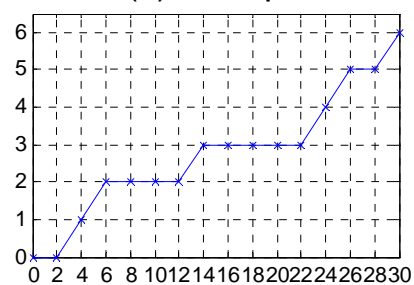


7-point nausea rating time series of Subject PBQ

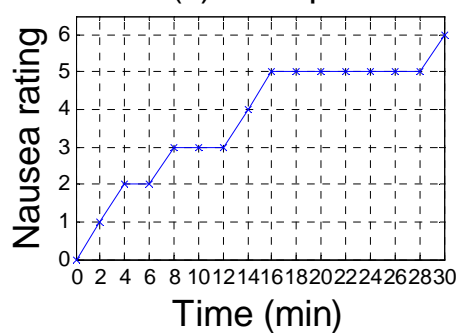
(a)A-0dps



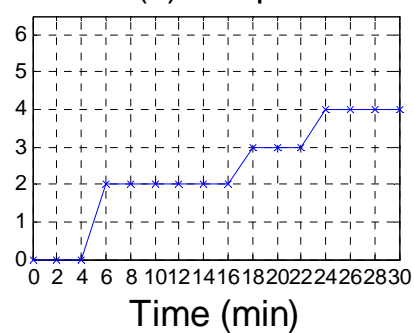
(b)B-14dps



(c)C-34dps

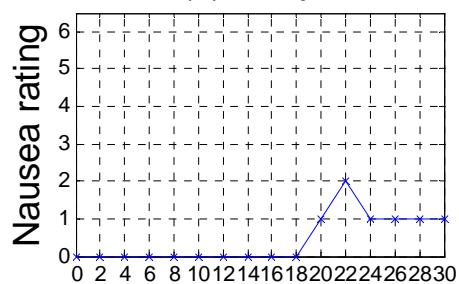


(d)D-2dps

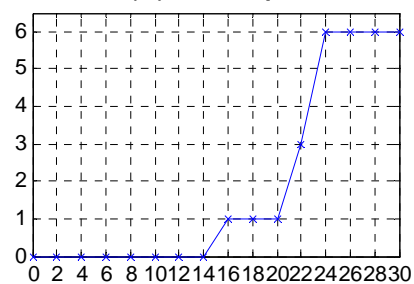


7-point nausea rating time series of Subject TYW

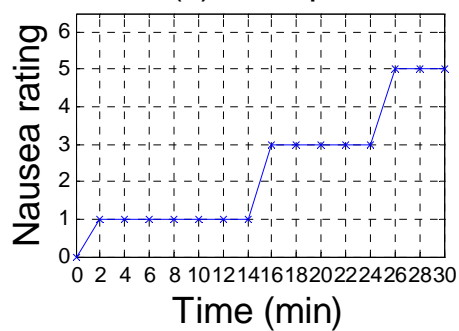
(a)A-0dps



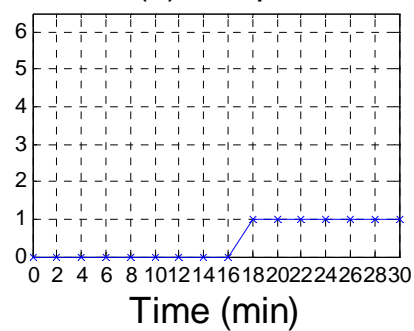
(b)B-14dps



(c)C-34dps

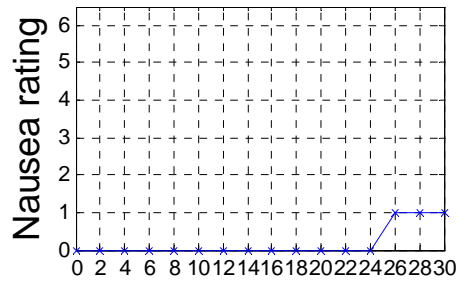


(d)D-2dps

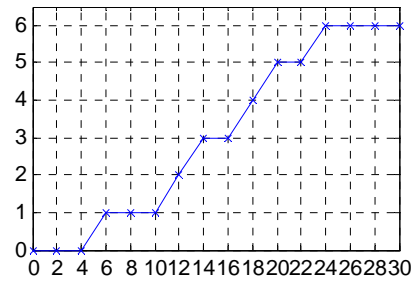


7-point nausea rating time series of Subject WXL

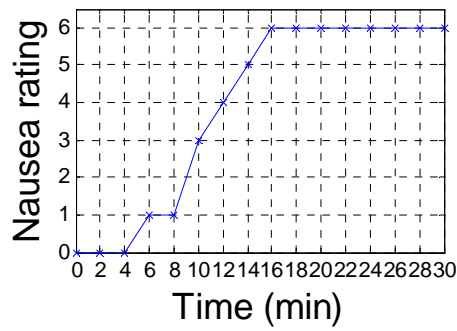
(a)A-0dps



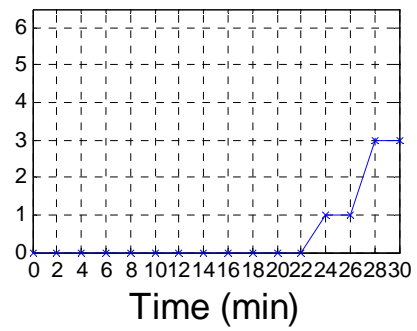
(b)B-14dps



(c)C-34dps

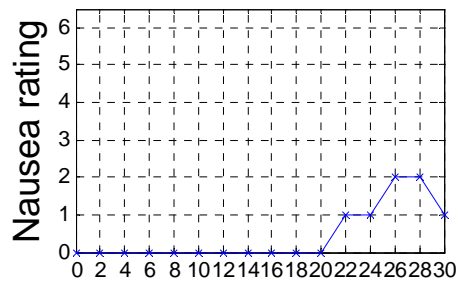


(d)D-2dps

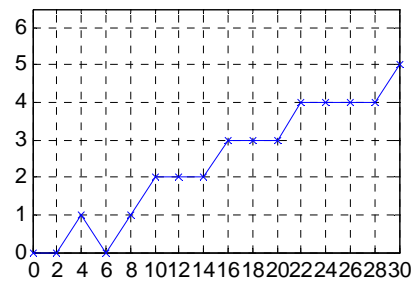


7-point nausea rating time series of Subject XJ

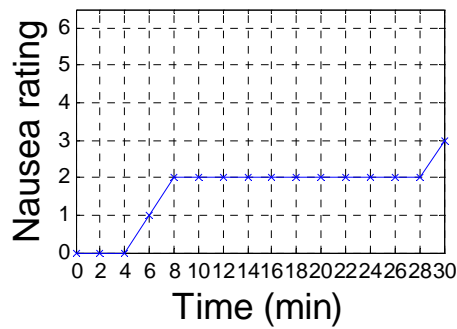
(a)A-0dps



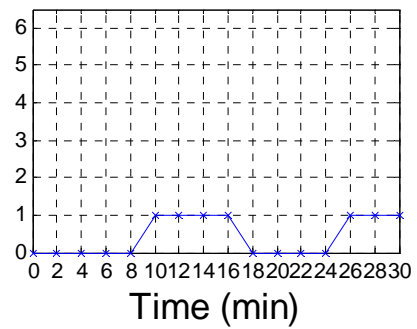
(b)B-14dps



(c)C-34dps

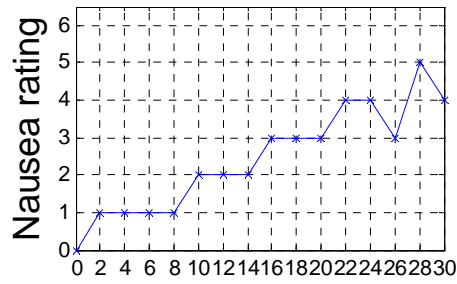


(d)D-2dps

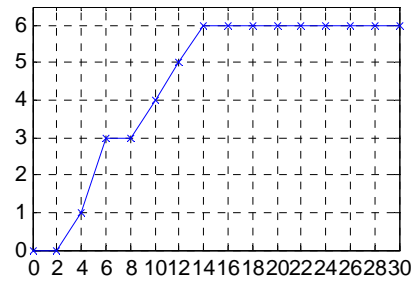


7-point nausea rating time series of Subject NXH

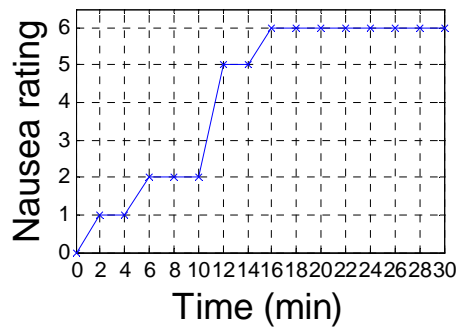
(a)A-0dps



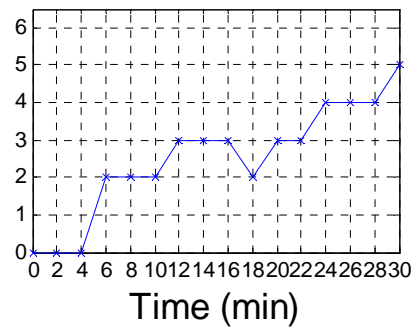
(b)B-14dps



(c)C-34dps

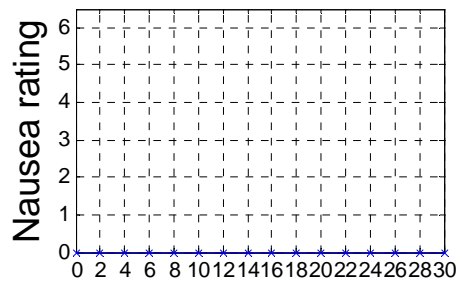


(d)D-2dps

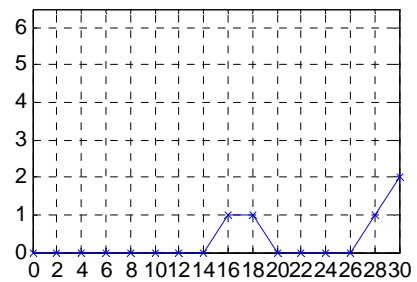


7-point nausea rating time series of Subject CX

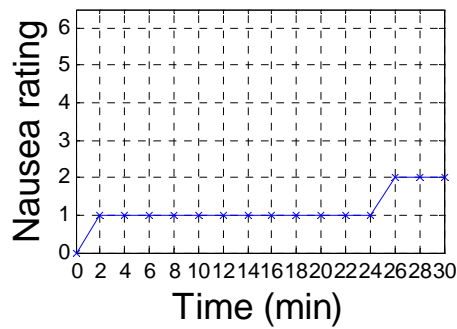
(a)A-0dps



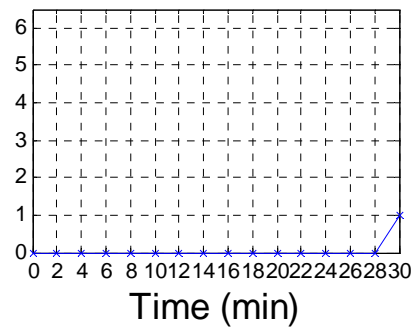
(b)B-14dps



(c)C-34dps

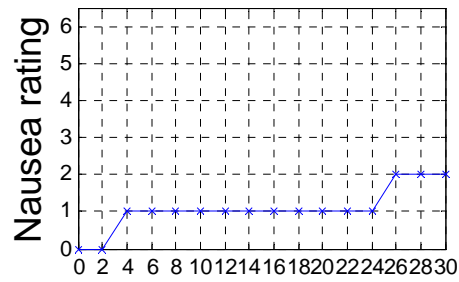


(d)D-2dps

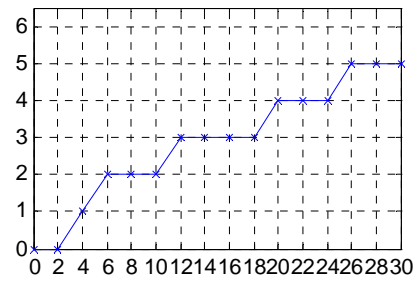


7-point nausea rating time series of Subject LD

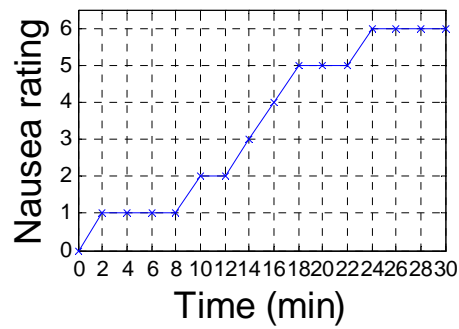
(a)A-0dps



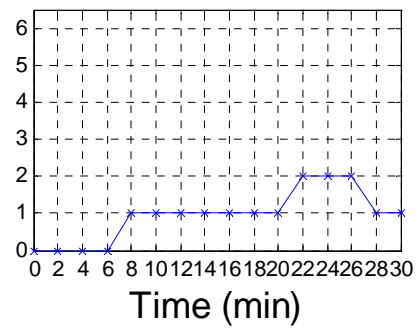
(b)B-14dps



(c)C-34dps

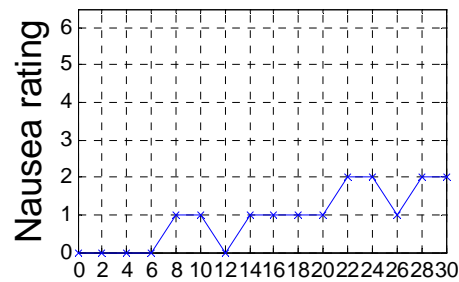


(d)D-2dps

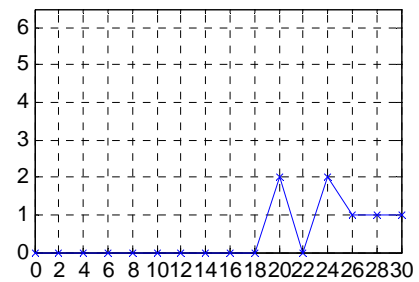


7-point nausea rating time series of Subject ZWT

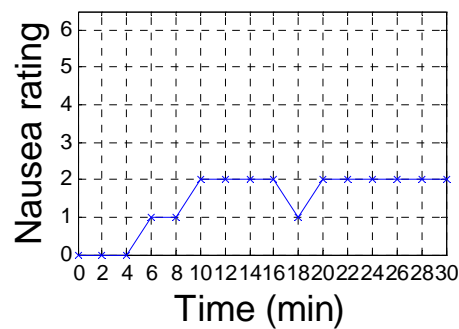
(a)A-0dps



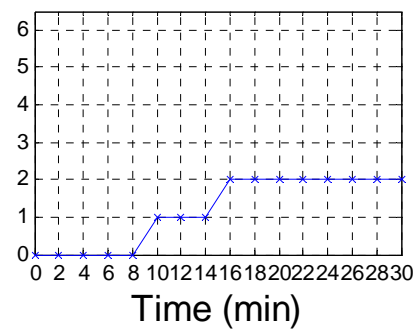
(b)B-14dps



(c)C-34dps

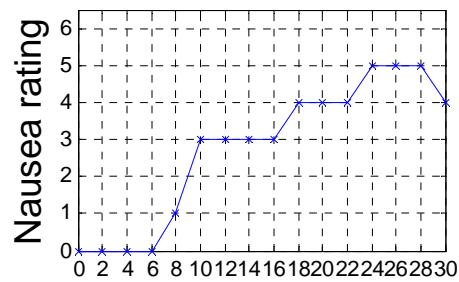


(d)D-2dps

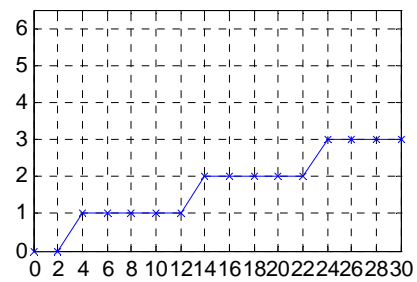


7-point nausea rating time series of Subject NYS

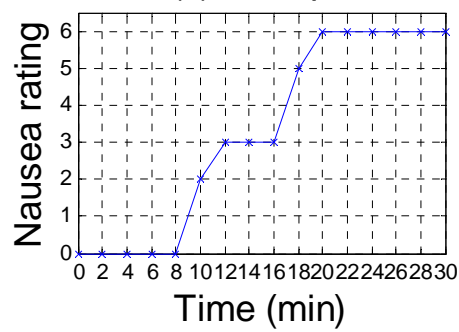
(a)A-0dps



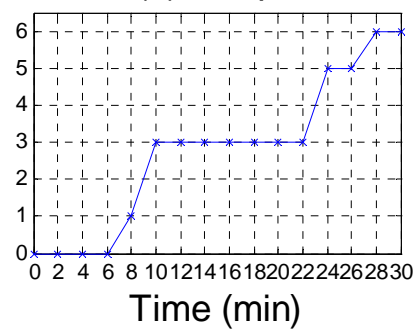
(b)B-14dps



(c)C-34dps

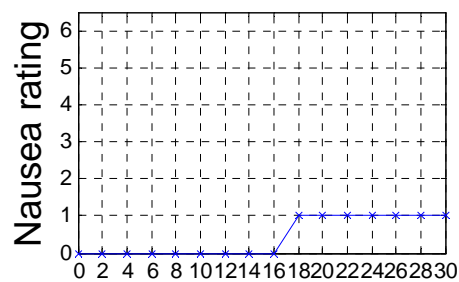


(d)D-2dps

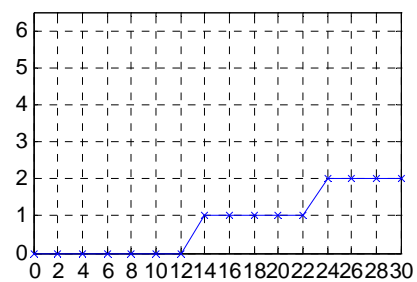


7-point nausea rating time series of Subject YXX

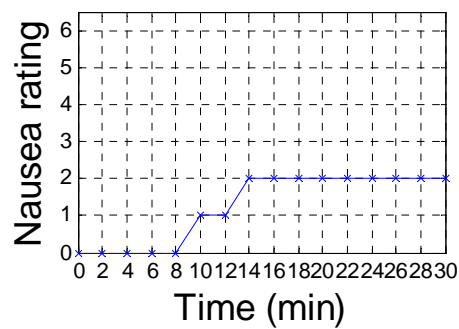
(a)A-0dps



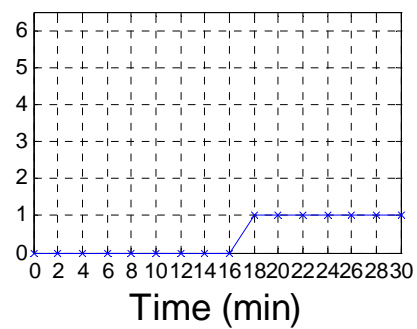
(b)B-14dps



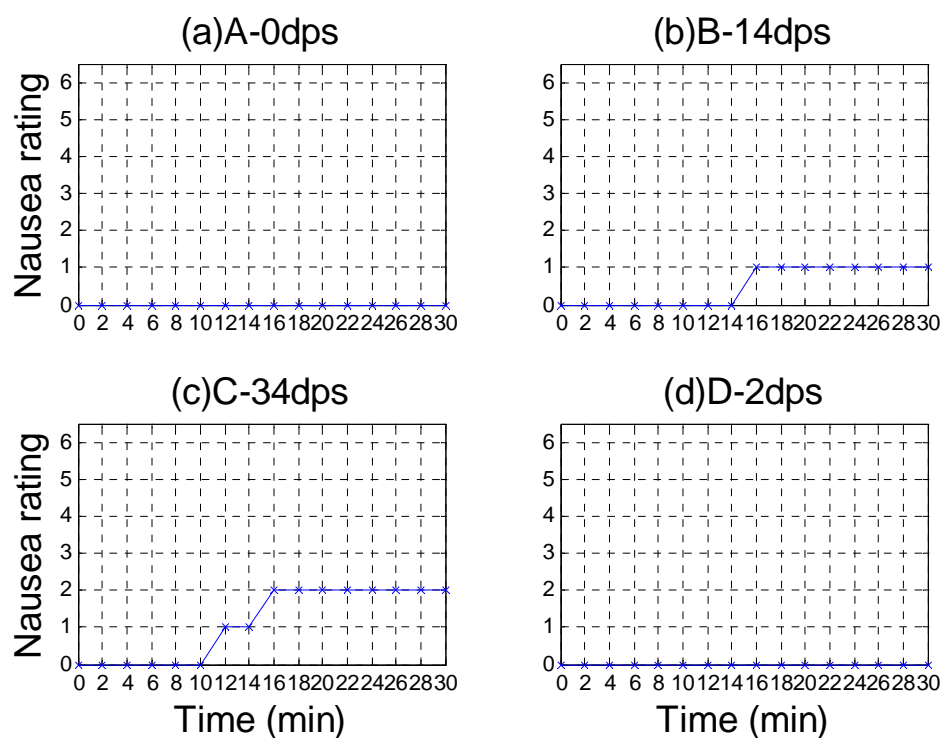
(c)C-34dps



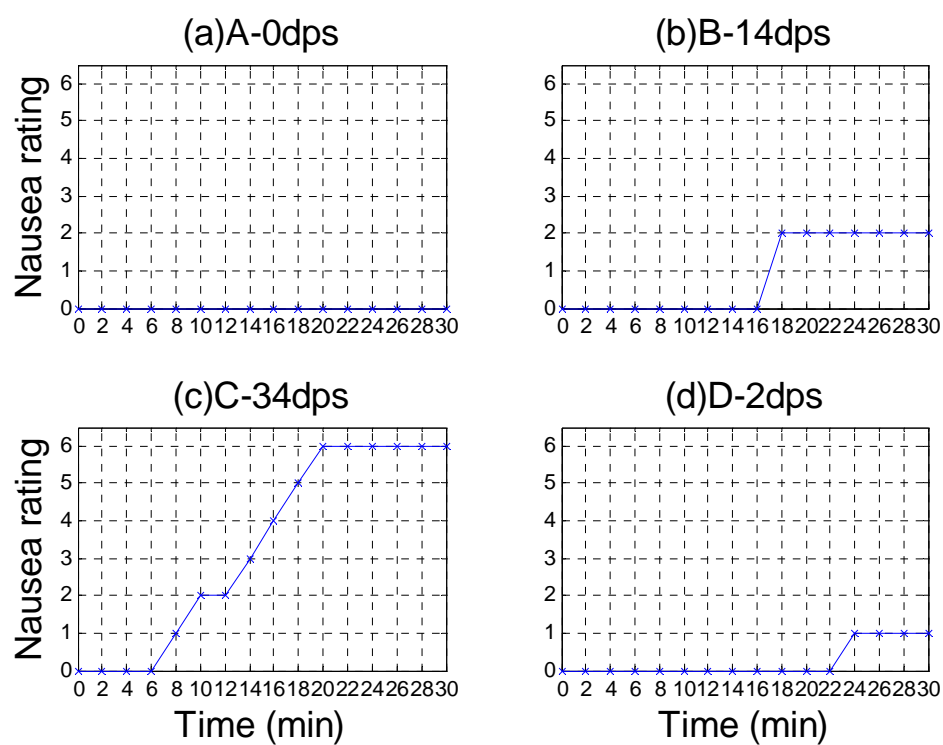
(d)D-2dps



7-point nausea rating time series of Subject SLH

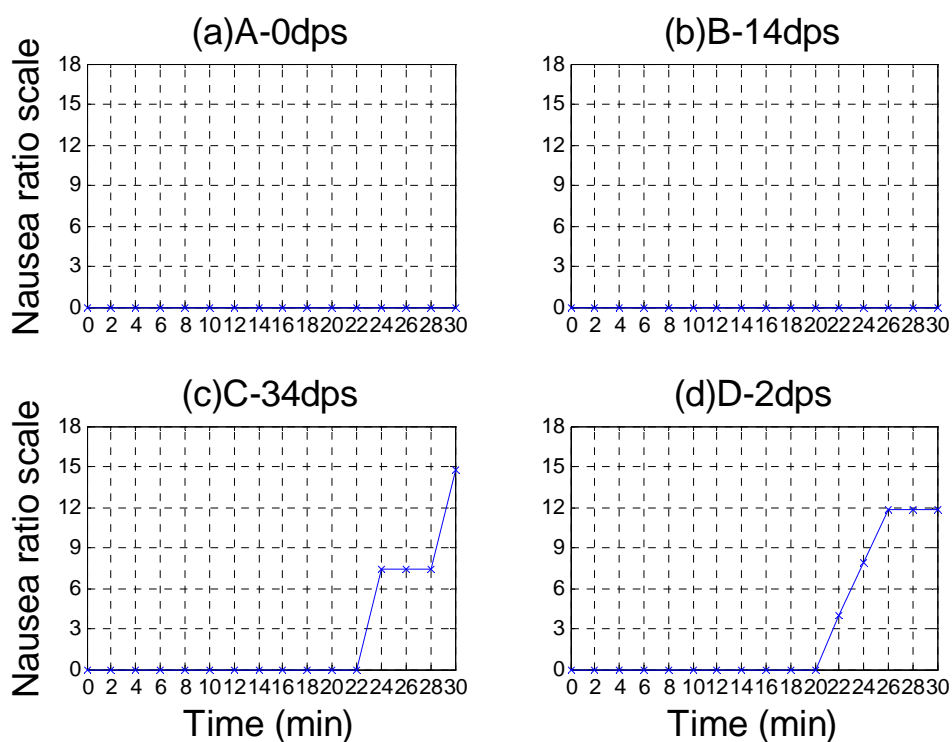


7-point nausea rating time series of Subject SYF

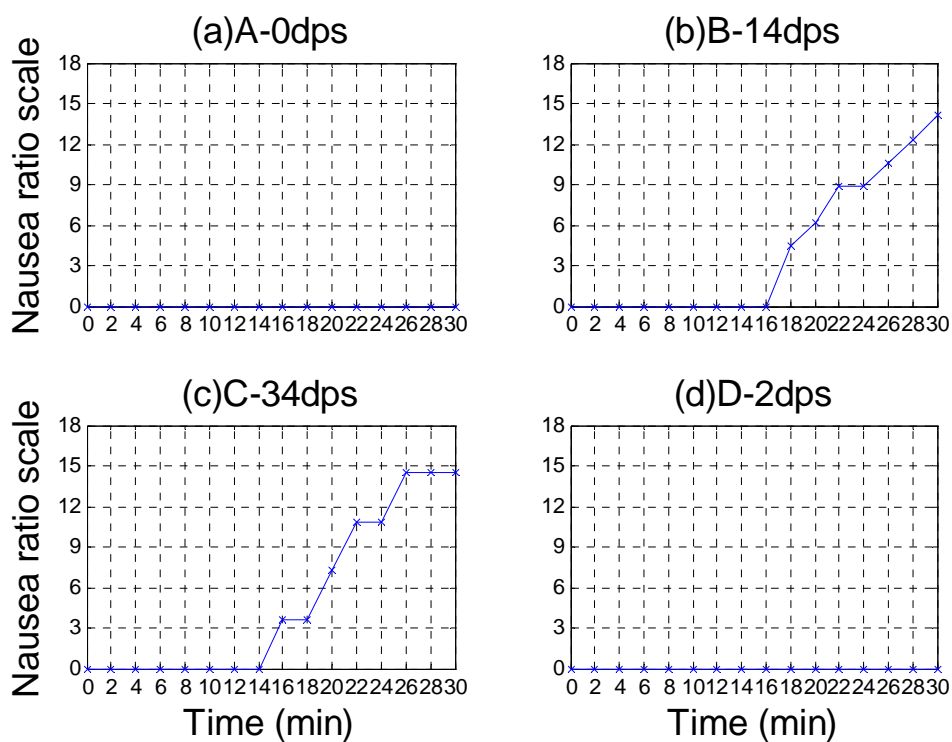


Appendix 5-3 Individual nausea ratio scale time series

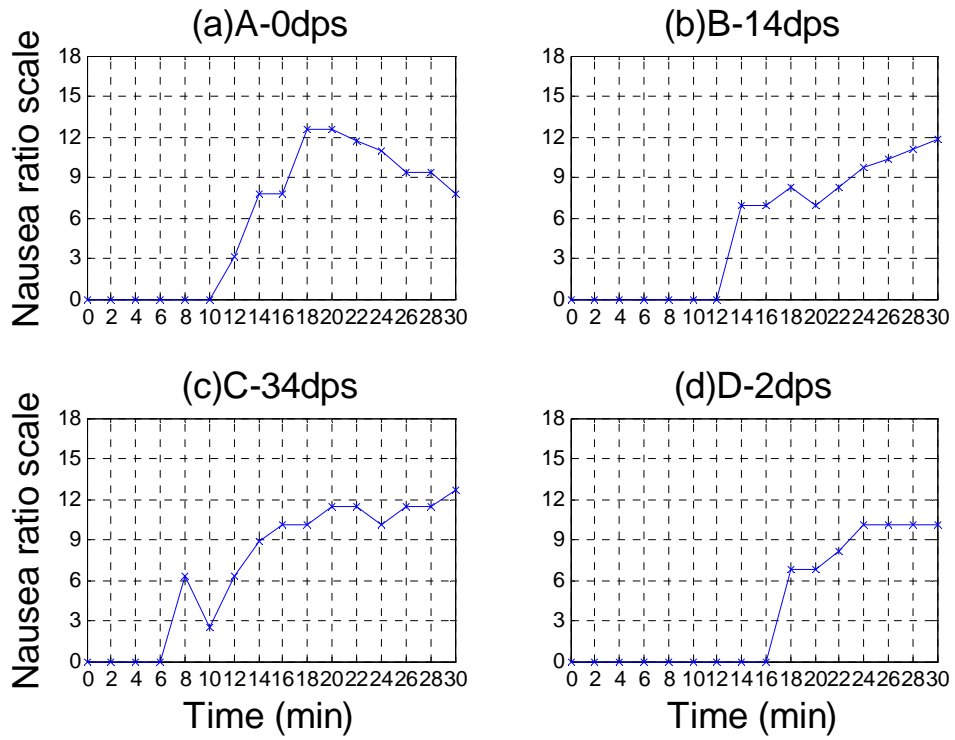
Nausea ratio scale time series of Subject CLH



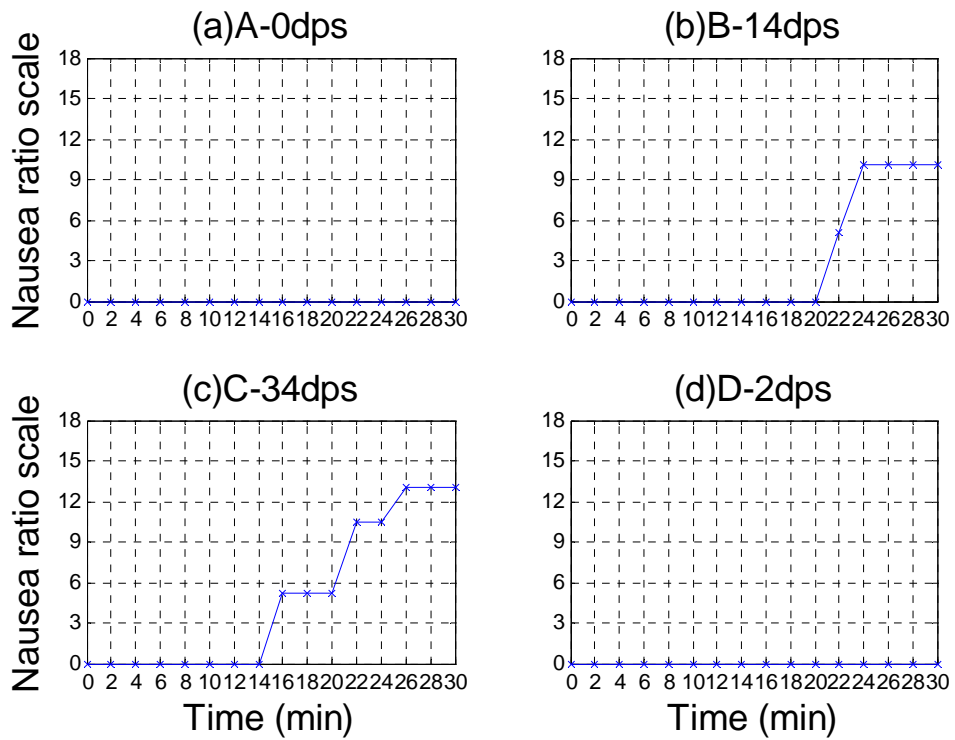
Nausea ratio scale time series of Subject XY



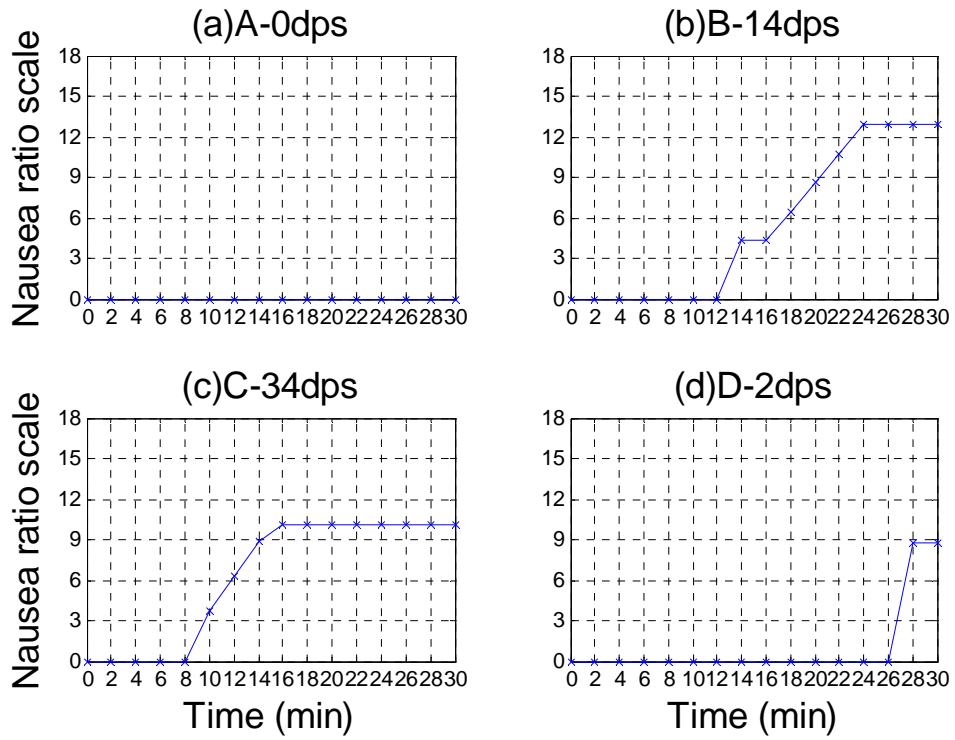
Nausea ratio scale time series of Subject PBQ



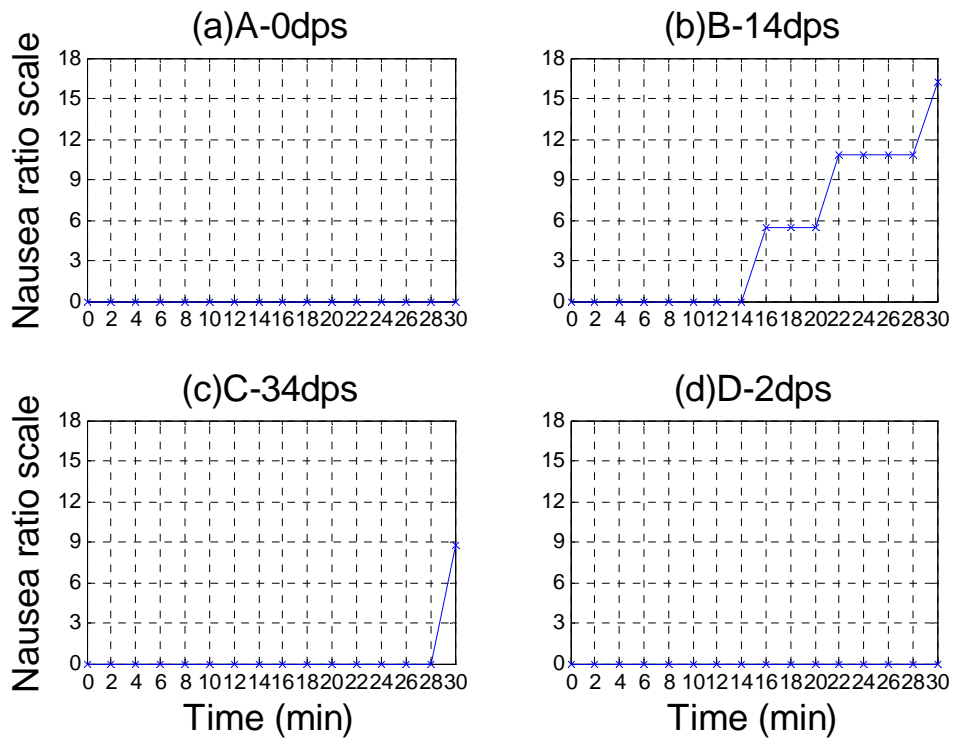
Nausea ratio scale time series of Subject TYW



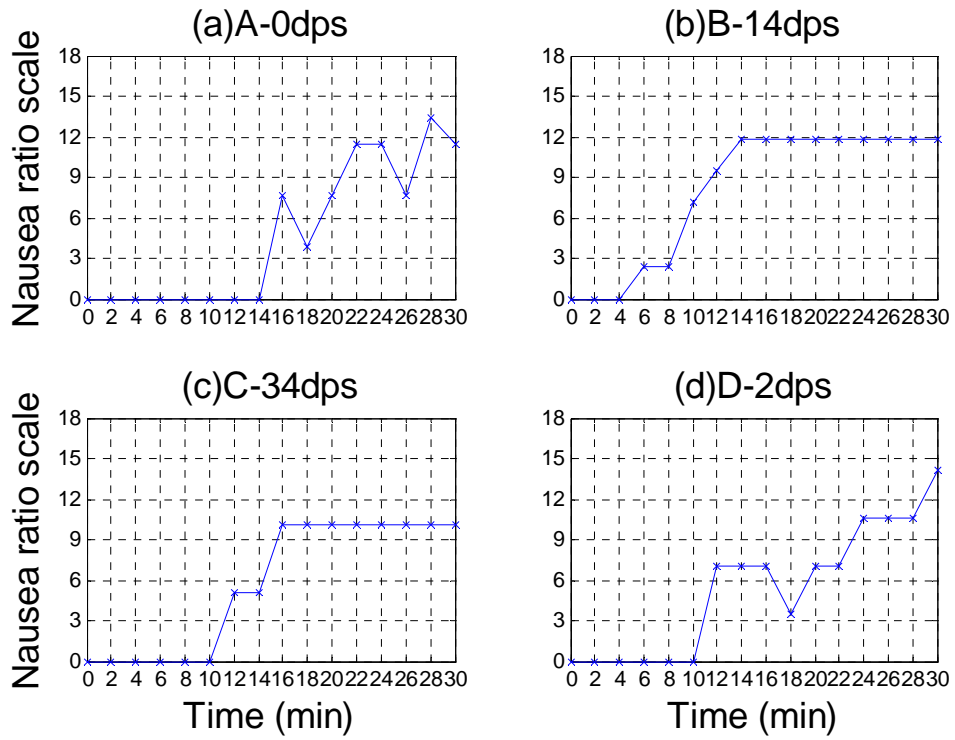
Nausea ratio scale time series of Subject WXL



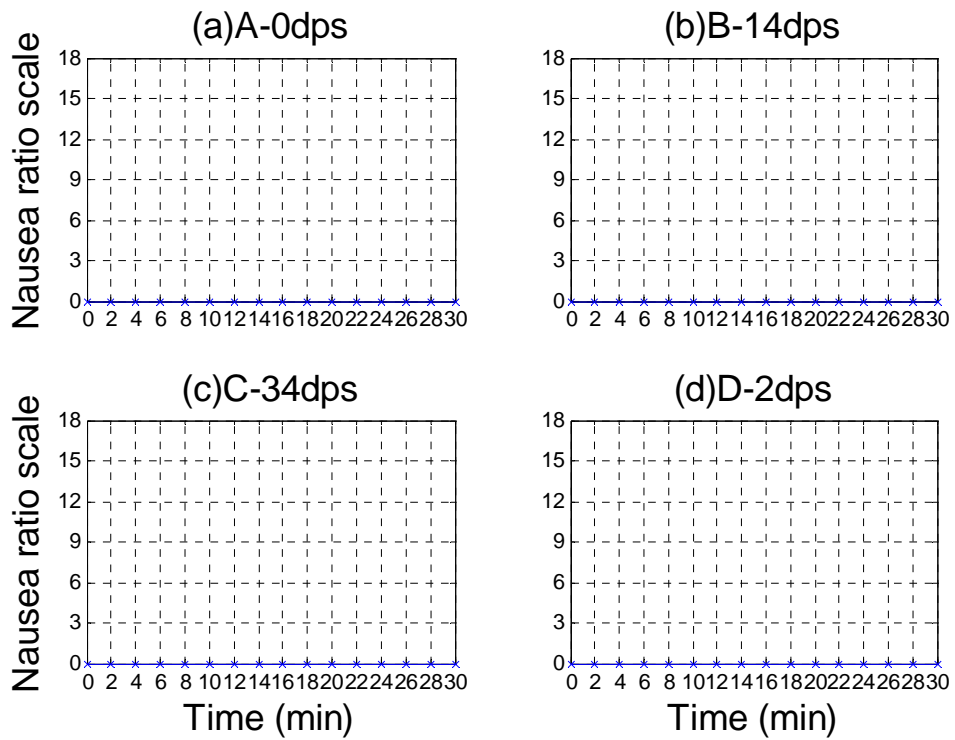
Nausea ratio scale time series of Subject XJ



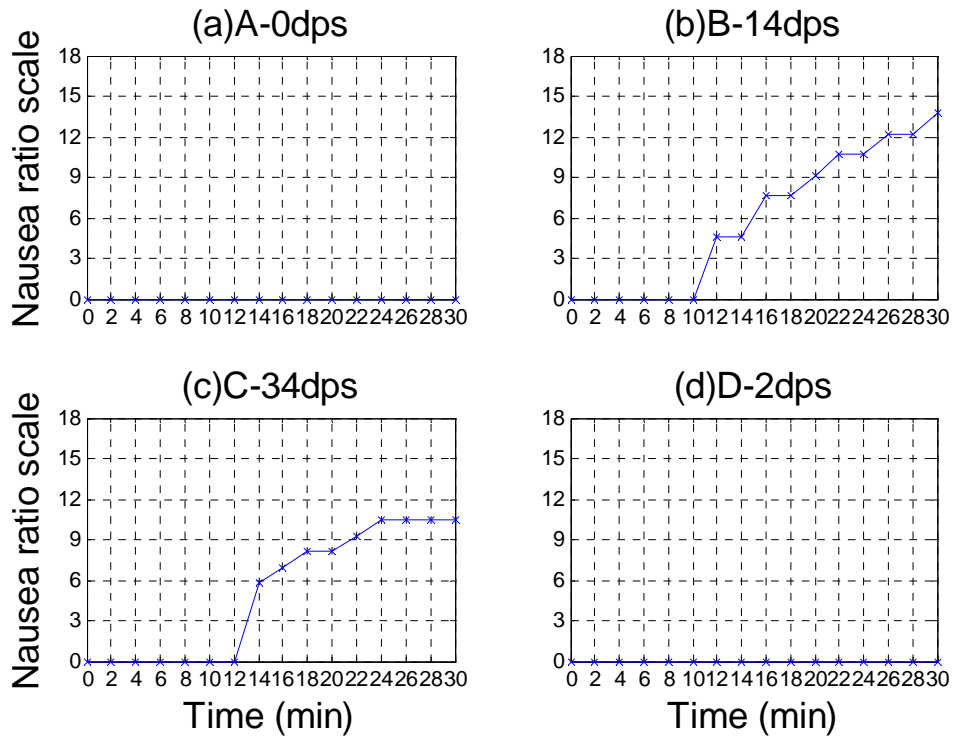
Nausea ratio scale time series of Subject NXH



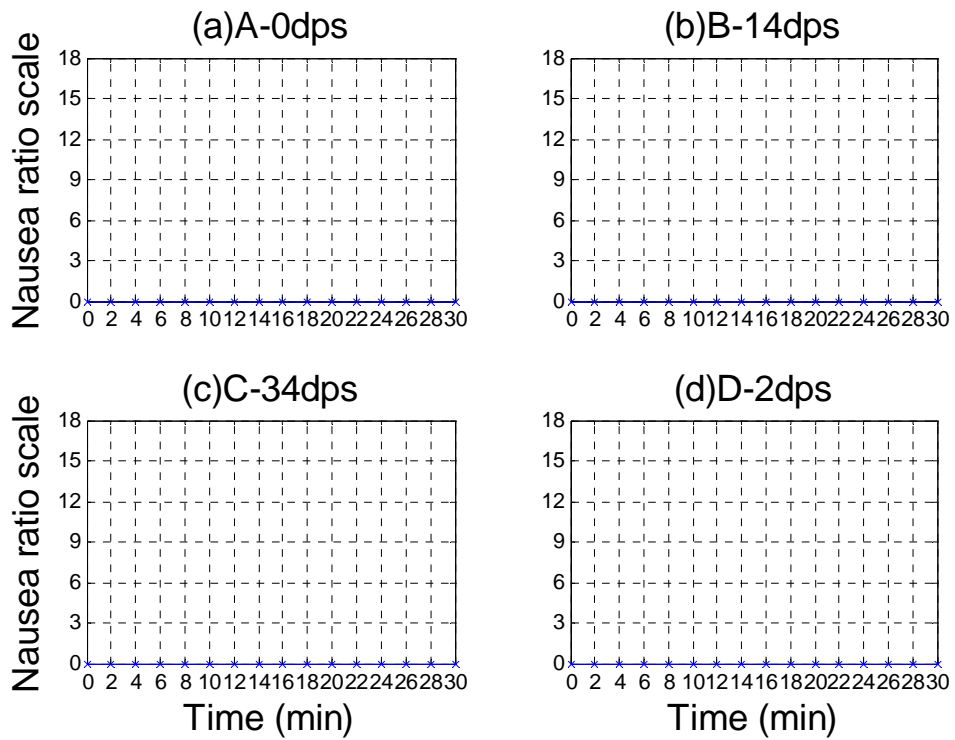
Nausea ratio scale time series of Subject CX



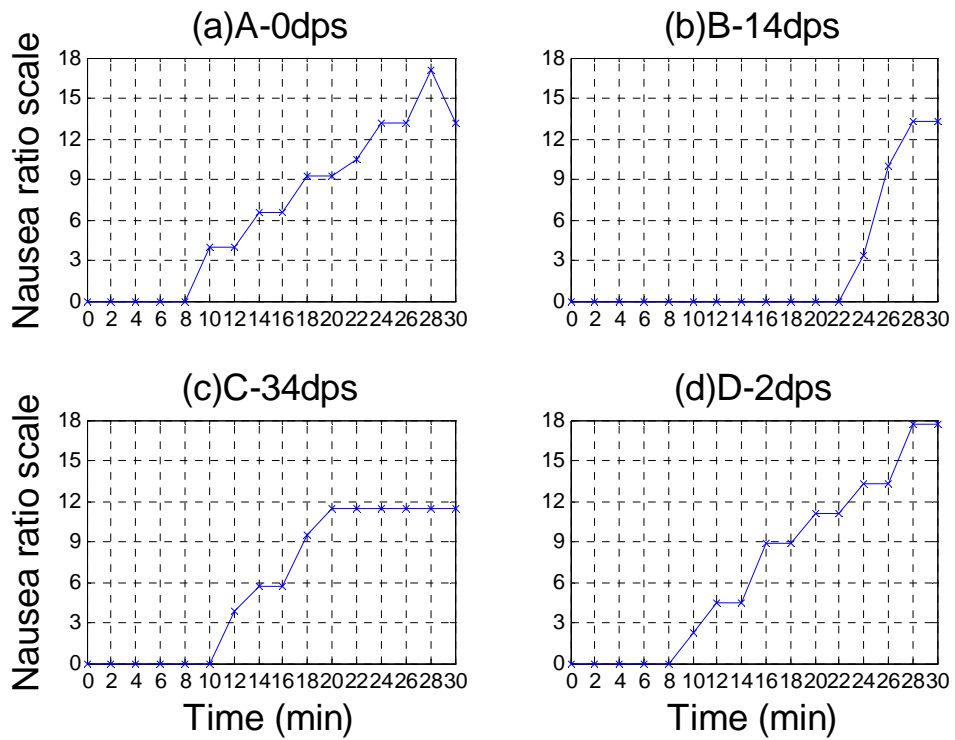
Nausea ratio scale time series of Subject LD



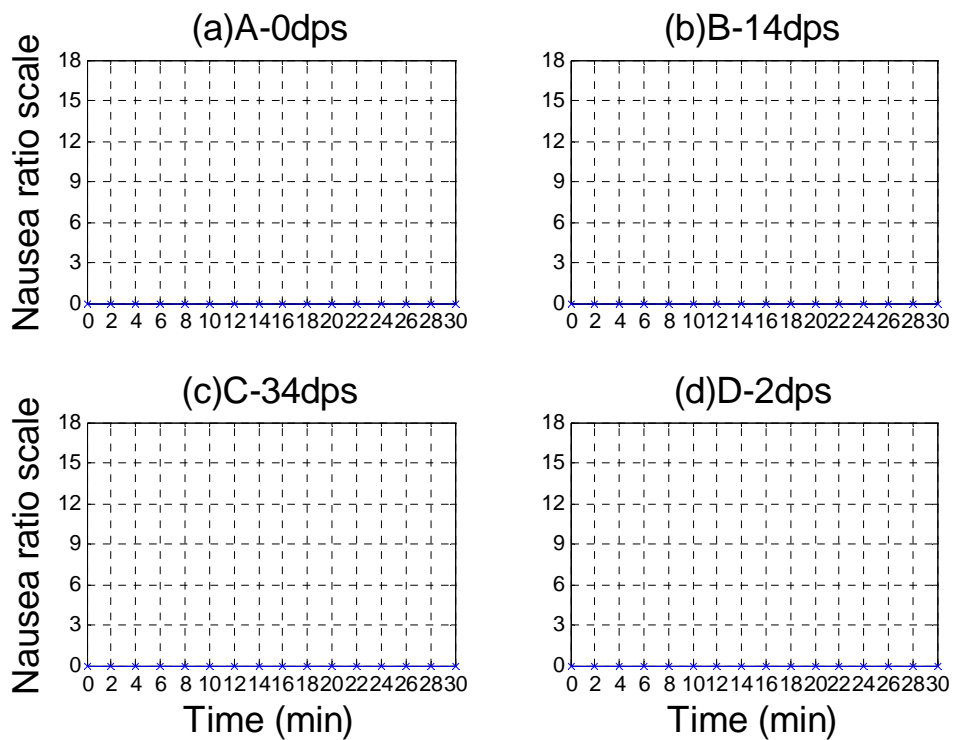
Nausea ratio scale time series of Subject ZWT



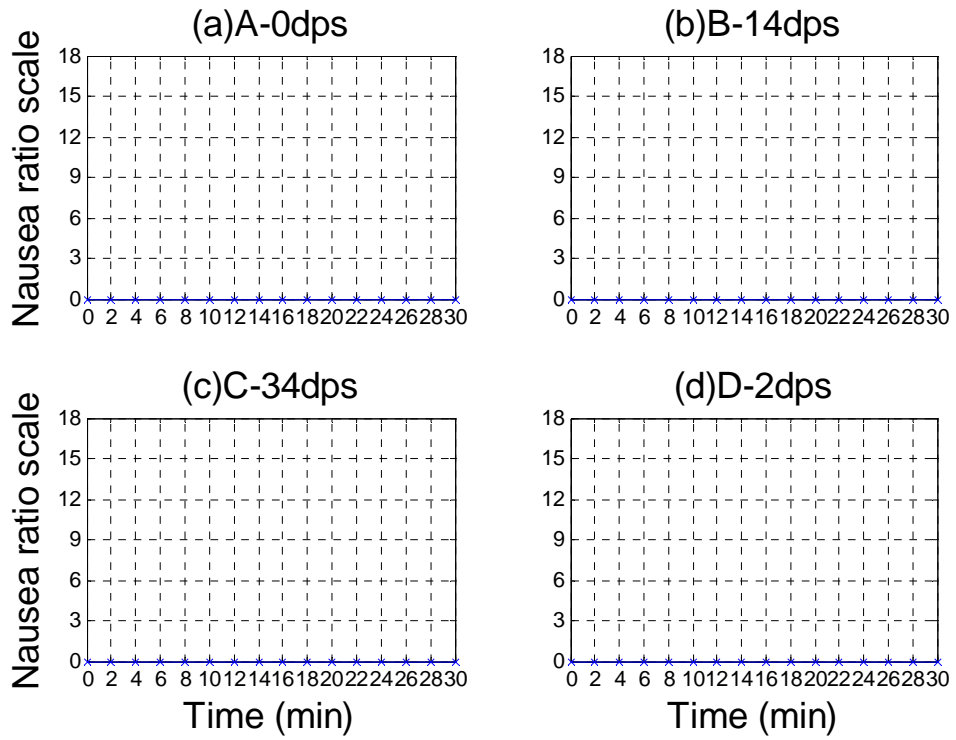
Nausea ratio scale time series of Subject NYS



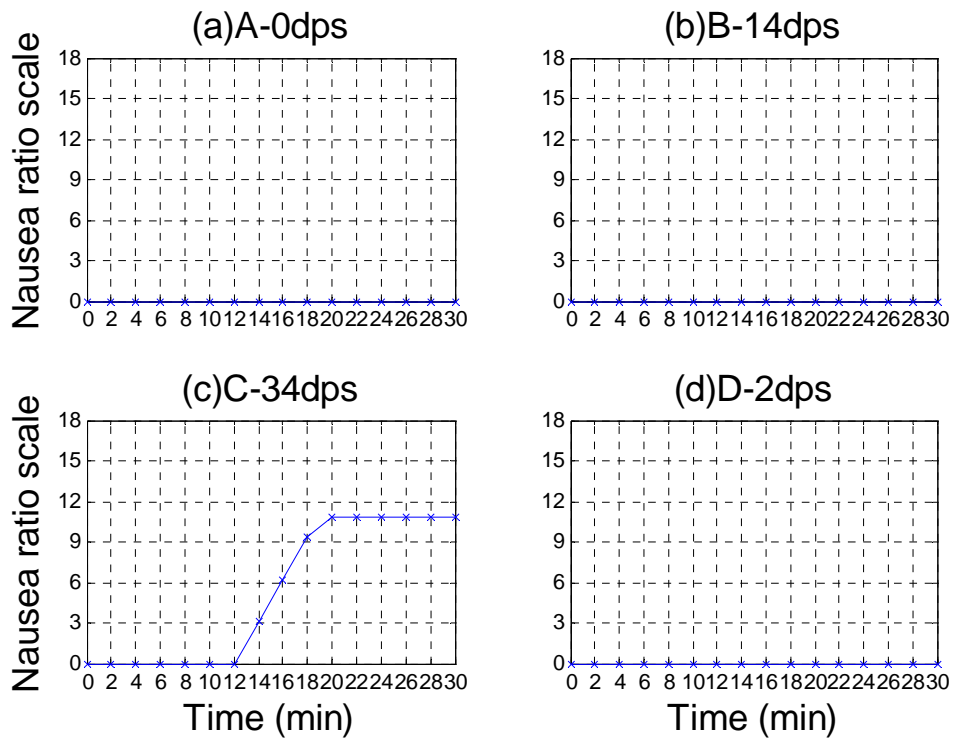
Nausea ratio scale time series of Subject YXX



Nausea ratio scale time series of Subject SLH

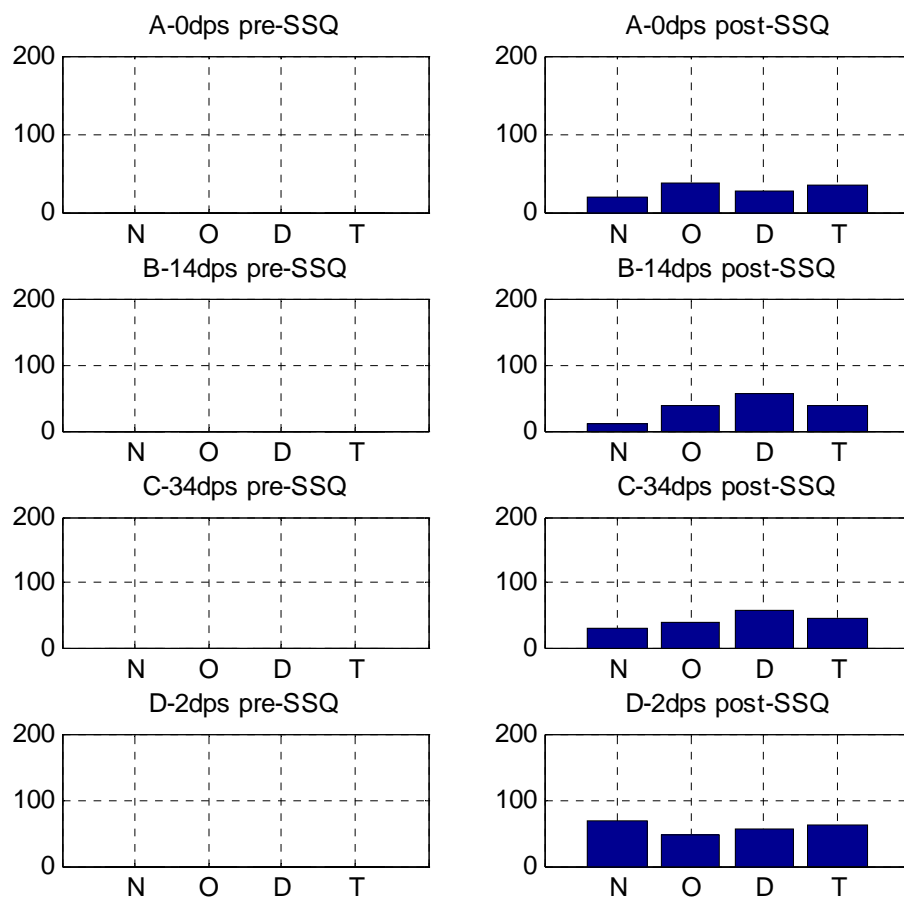


Nausea ratio scale time series of Subject SYF

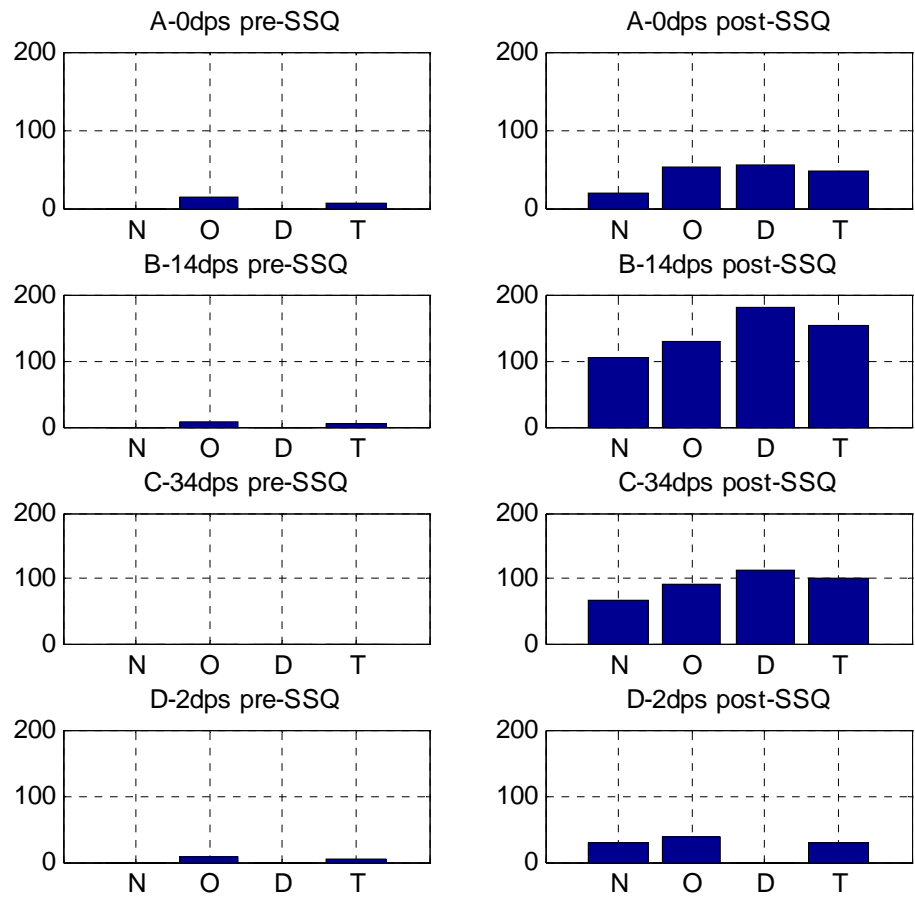


Appendix 5-4 individual plots of pre-& post-exposure SSQ scores

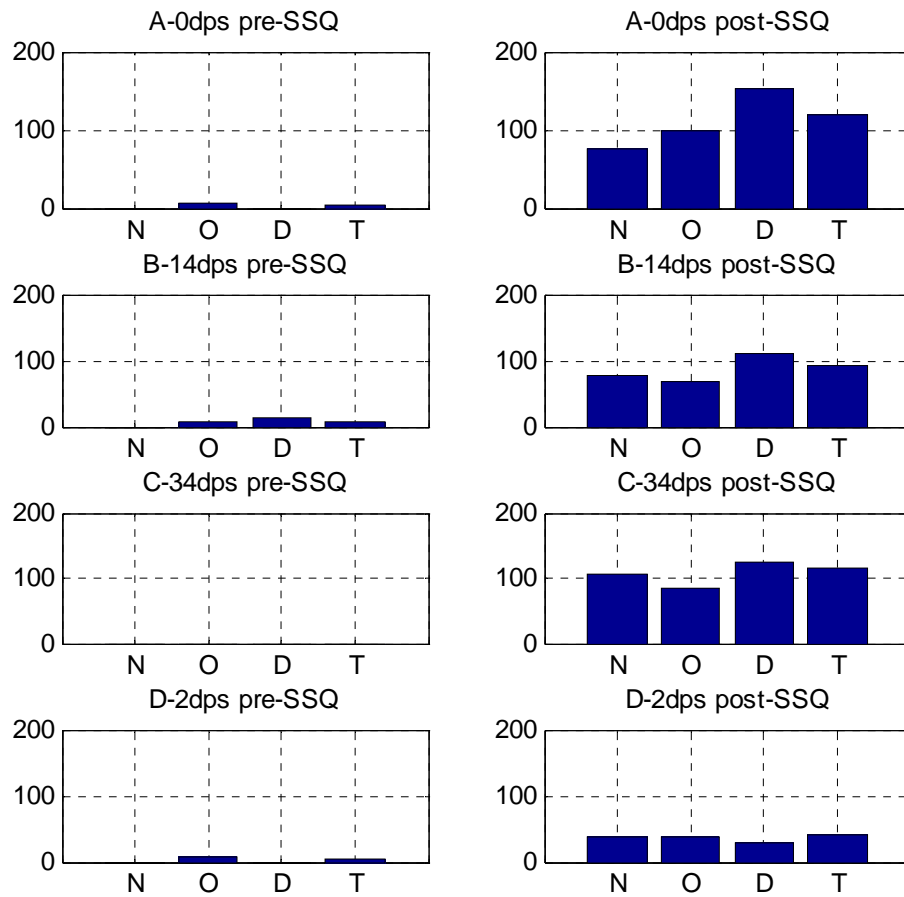
Pre- & Post- SSQ scores of subject CLH



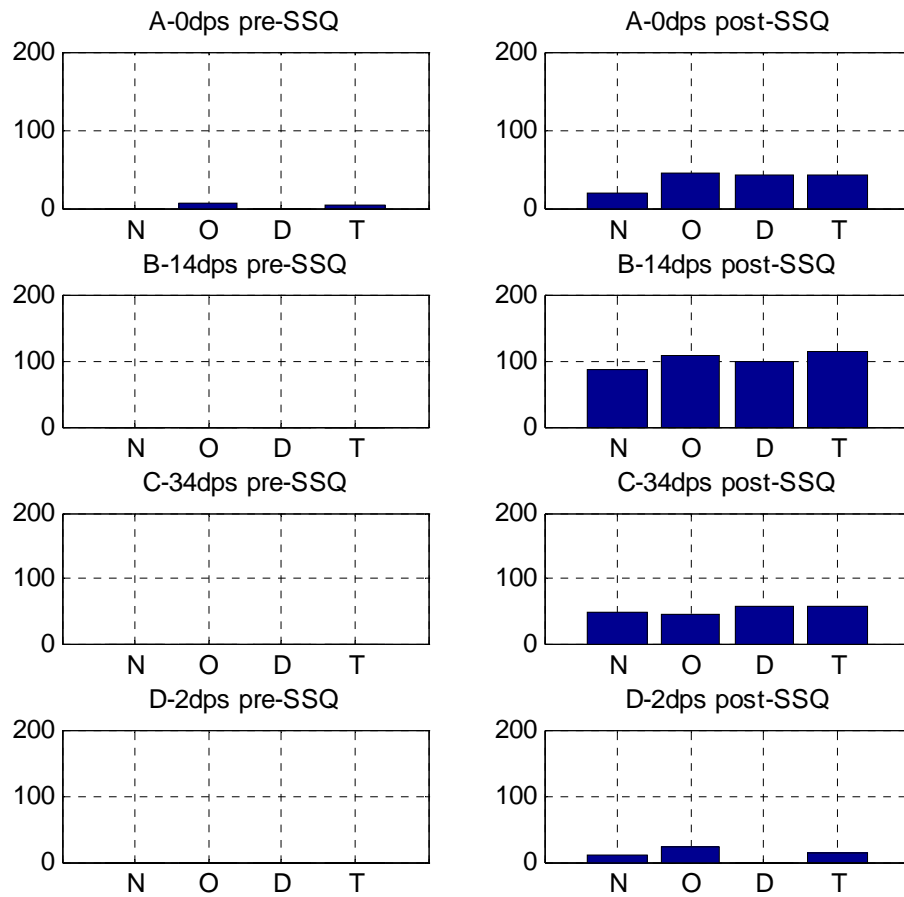
Pre- & Post- SSQ scores of subject XY



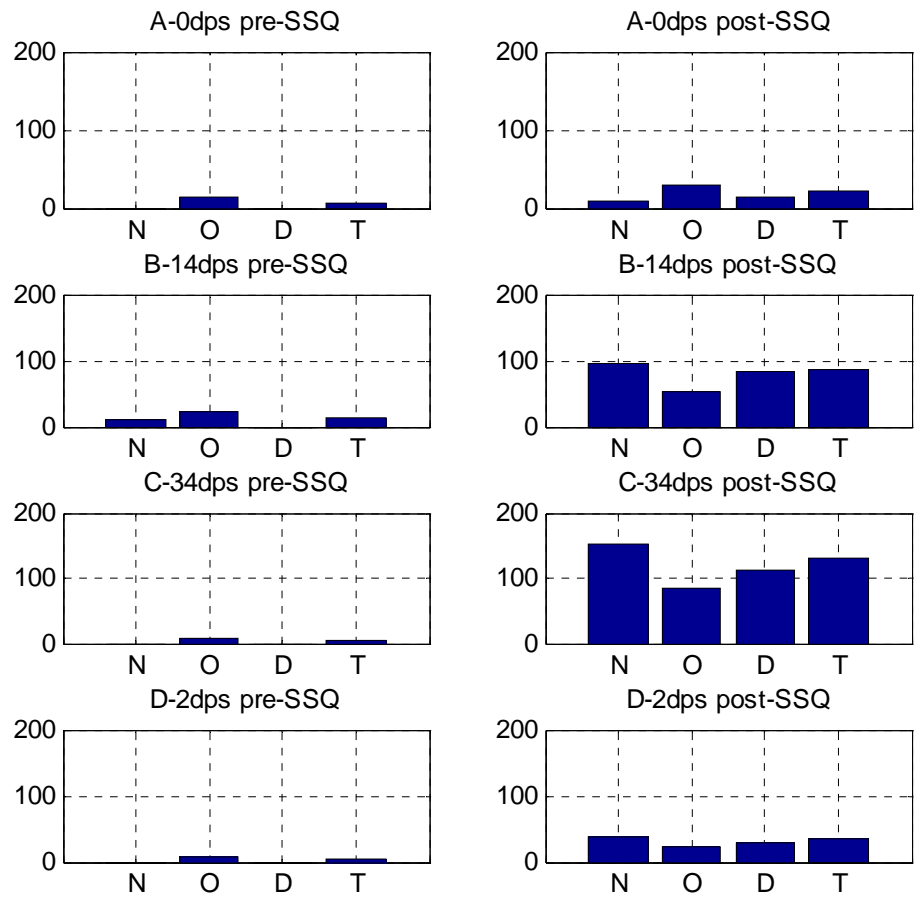
Pre- & Post- SSQ scores of subject PBQ



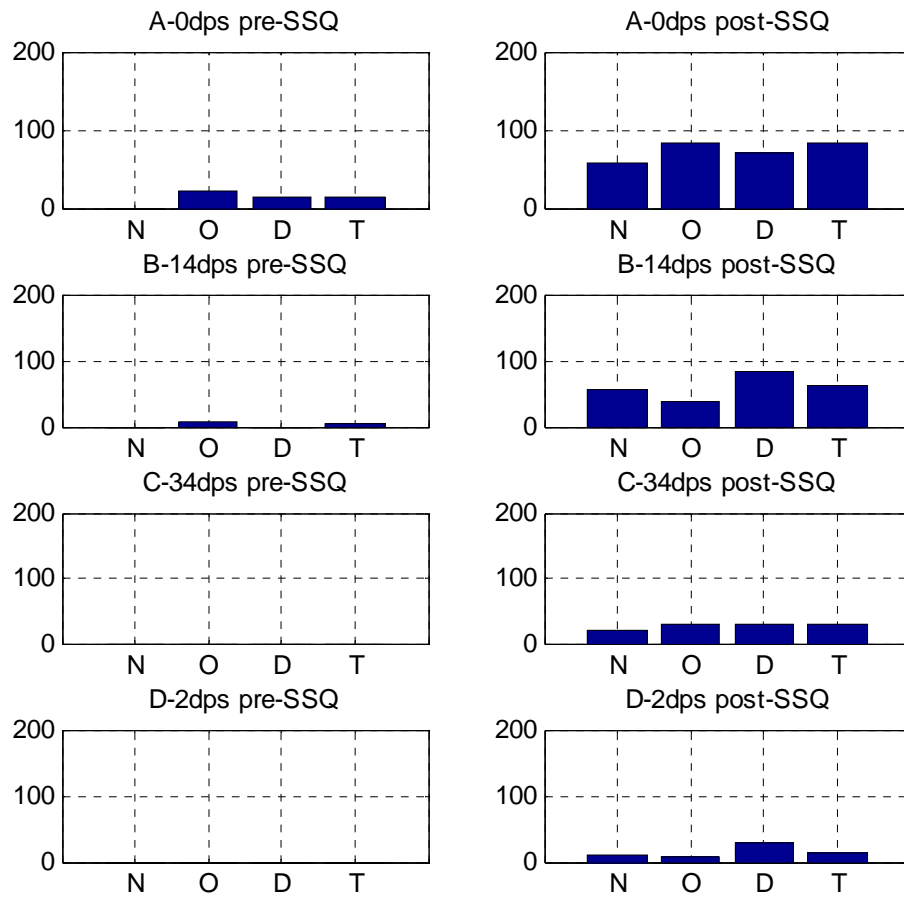
Pre- & Post- SSQ scores of subject TYW



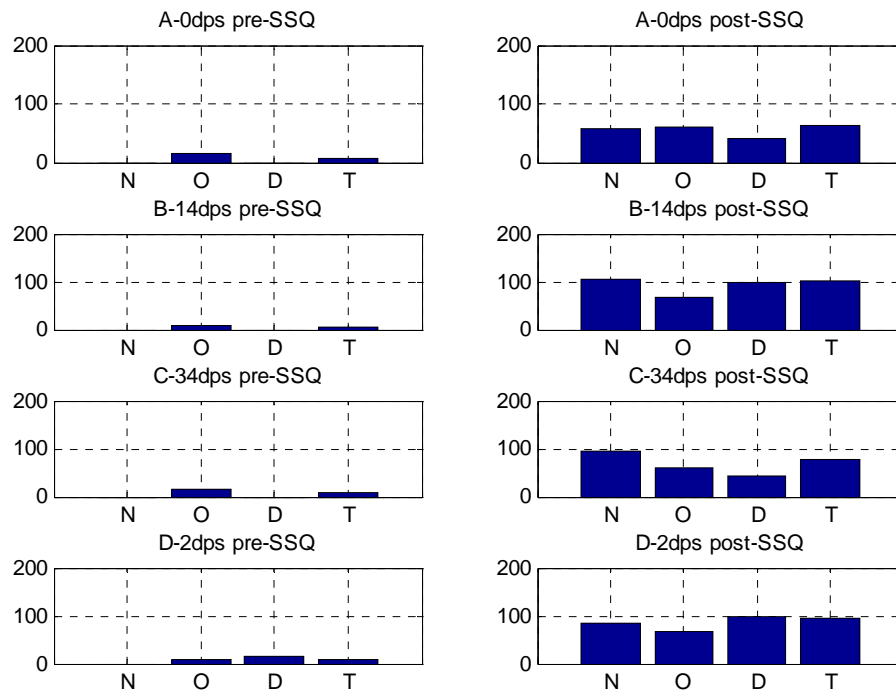
Pre- & Post- SSQ scores of subject WXL



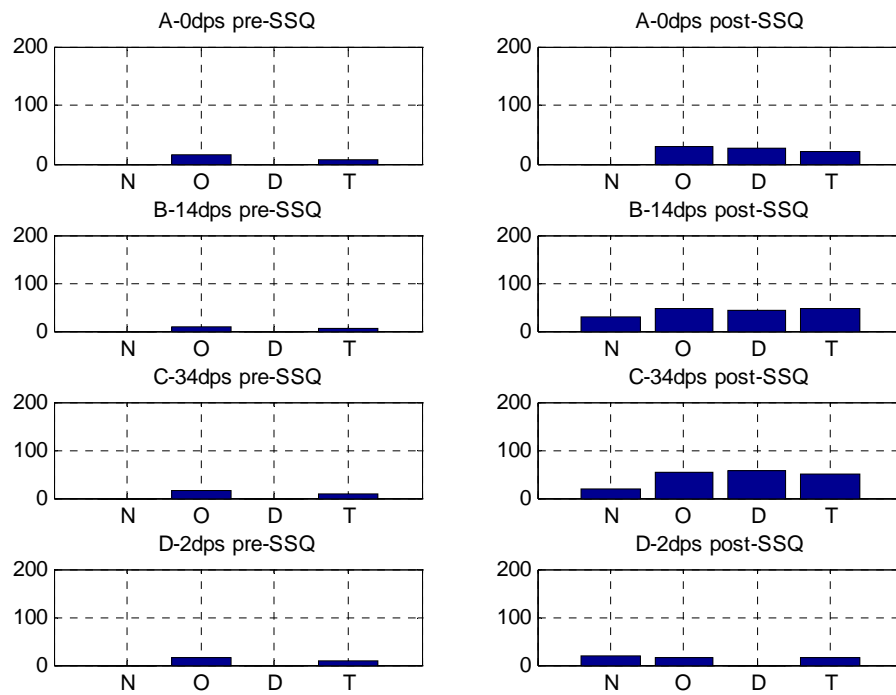
Pre- & Post- SSQ scores of subject NXH



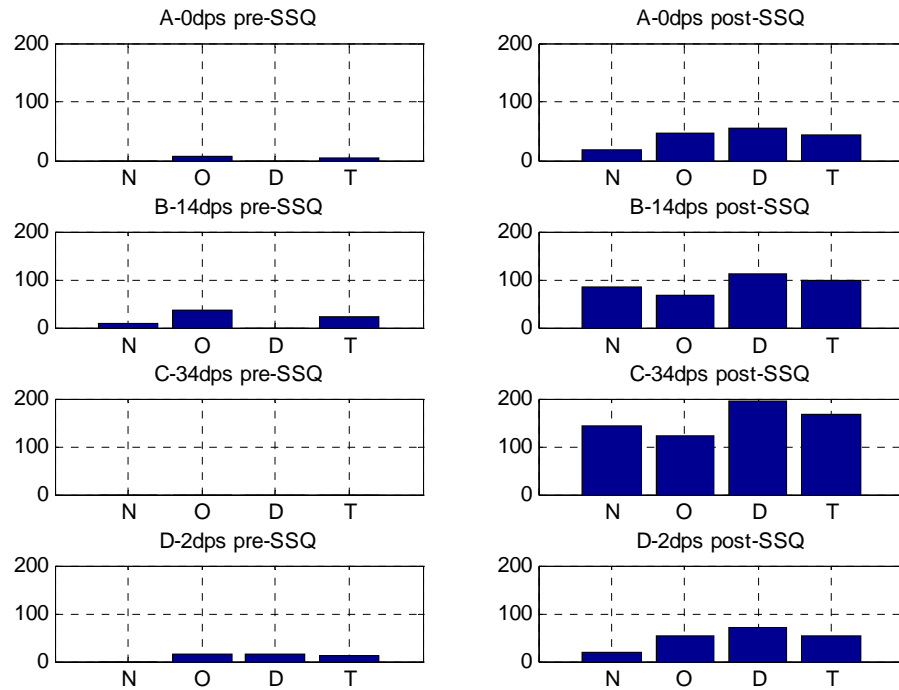
Pre- & Post- SSQ scores of subject XJ



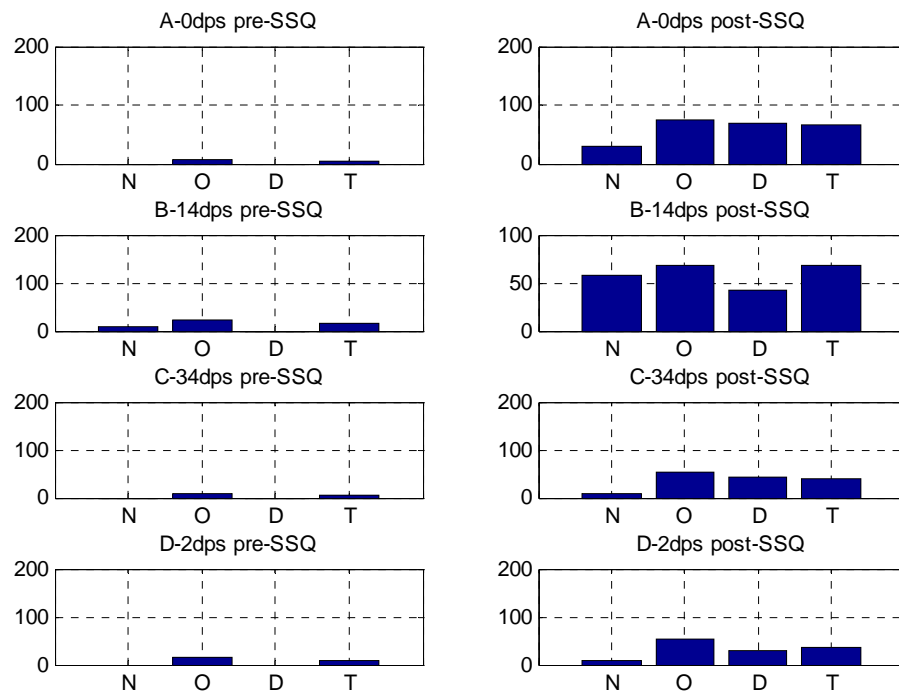
Pre- & Post- SSQ scores of subject CX



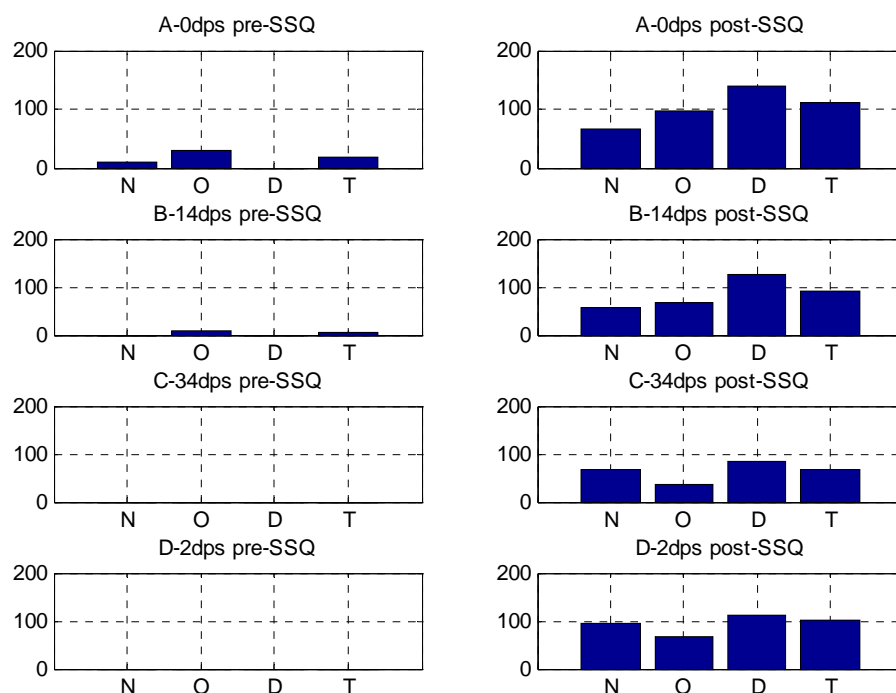
Pre- & Post- SSQ scores of subject LD



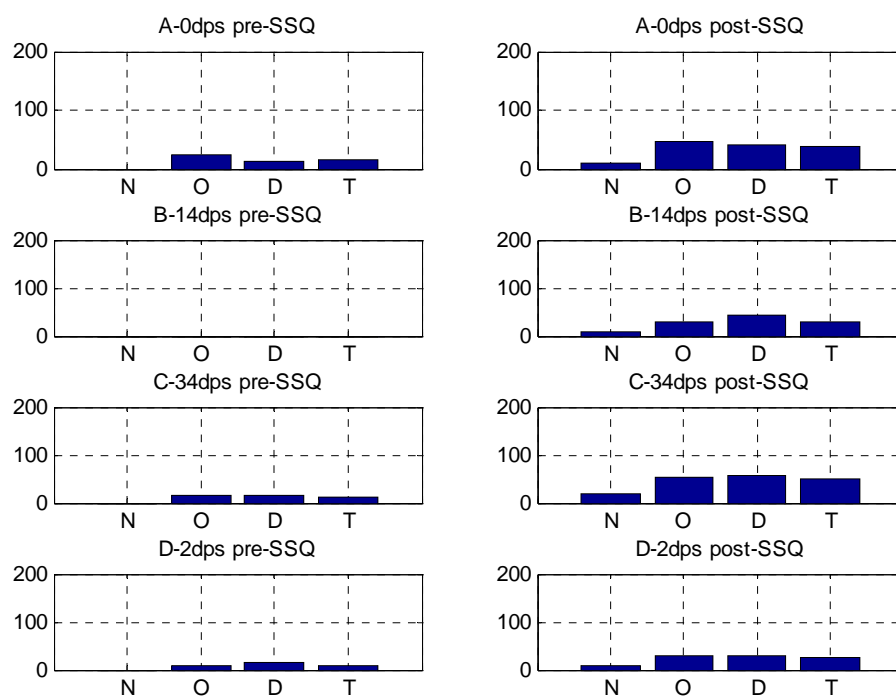
Pre- & Post- SSQ scores of subject ZWT



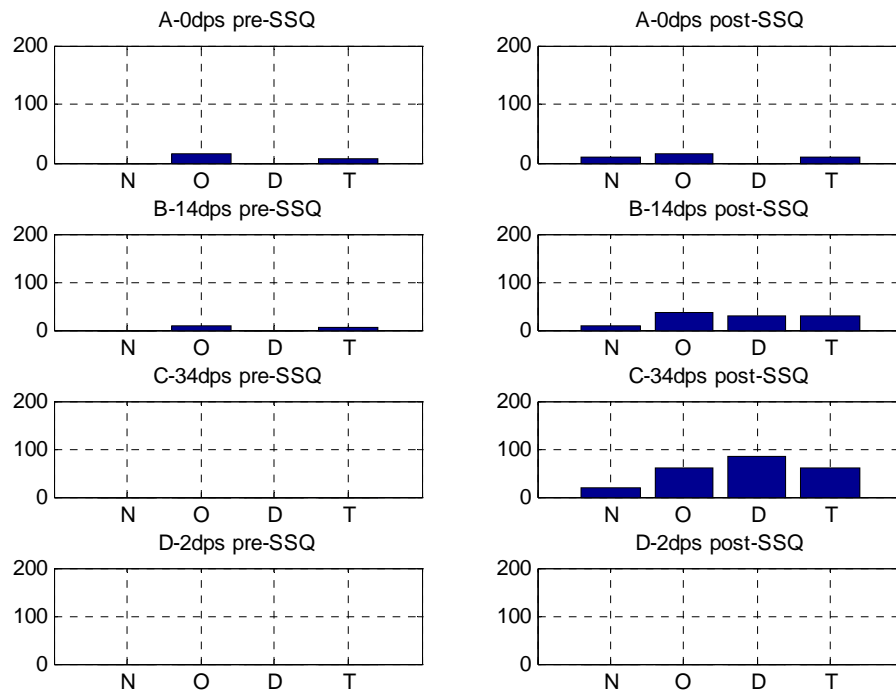
Pre- & Post- SSQ scores of subject NYS



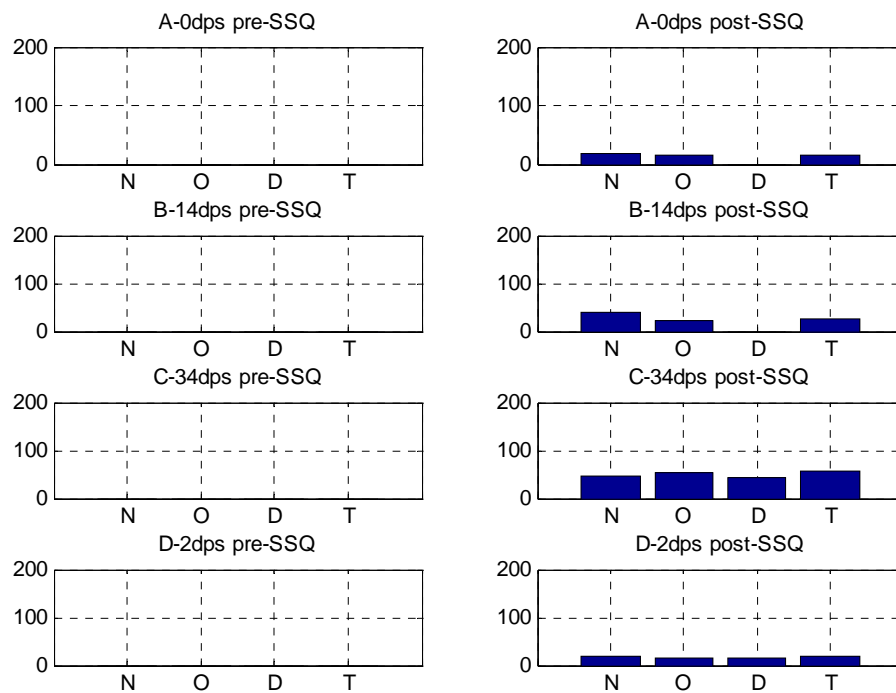
Pre- & Post- SSQ scores of subject YXX



Pre- & Post- SSQ scores of subject SLH



Pre- & Post- SSQ scores of subject SYF



Appendix 5-5 four-level balanced Latin Square technique

A	B	C	D
B	D	A	C
D	C	B	A
C	A	D	B
A	B	C	D
B	D	A	C
D	C	B	A
C	A	D	B
A	B	C	D
B	D	A	C
D	C	B	A
C	A	D	B
A	B	C	D
B	D	A	C

Appendix 5-6 Instruction of experiment one

- 1) The objective of this experiment is to measure how well you can maintain eye fixation given a disturbing visual stimulus and investigate how you respond to this visual stimuli. Therefore please do your best to fix your viewpoint on the eye fixation point and hold your line of sight for 30mins. (you can blink but please do not close your eyes too long) Your eye movements will be monitored by our equipment EOG to see how well you can maintain eye fixation.
- 2) Please keep your eyes open during the whole experiment except experimenter asks you to close eyes (please do not close your eyes except for normal blinking).
- 3) Please maintain your head position on the chin rest (don't move your head) during the whole experiment
- 4) Please try not to move the hand with EOG electrode attachment during the experiment
- 5) During the experiment, you will be asked to rate your various responses to this visual stimuli using 3 different methods. Please read the following instructions for each methods carefully and make sure you have fully understanding on all of them:
 - A. Measurement 1 (M1): rate your strength level of perceived nausea using a number (Now, please tell the experimenter what is the meaning of “nausea” in your native language)

Instruction of M1:

I am going to present to you an image pattern rotating at constant velocity for 30 mins. Your task is to tell me how much your sensation of nausea is induced and how the strength of nausea changes within the 30mins by assigning numbers. When you are asked to open your eyes and view the rotating pattern with eye fixation on the red fixation point, give a number to represent the current nausea severity level you perceive.

Notes: *At the moment when you open your eye, If you have no sensation of nausea, just give zero and if you feel nausea, just give any number that you think appropriate.*

After that, at 2 mins interval, I will ask you to give your current nausea severity level a number. Let high numbers represent high nausea level and low numbers represent low nausea level. Try to make the ratios between the numbers that you assign correspond to the ratio between the nausea levels you felt at different time. In other words, double your reported non-zero number when you felt your nausea level is doubled and halve your reported non-zero number when you felt your nausea level is half reduced, and so on. Remember that you can assign any number. There is no limit to the number that you may assign. There is no right or wrong answer. I just want to know how you judge your perceived nausea level over time. When I ask you to assign a number to your current level of nausea, I will remind you about your last assigned number 2 min ago. Any question?

B. Measurement 2 (M2): rate your strength level of perceived nausea by scale A to G.

Instruction of M2:

I am going to present you an image pattern rotating at constant velocity for 30 mins. Your task is to tell me how much nausea is induced and how its strength changes within the 30mins by assigning A-G according to the following scale:

Rating	Definition
A	No symptoms
B	Any unpleasant symptoms, however slight
C	Mild unpleasant symptoms, e.g. stomach awareness, sweating but no nausea
D	Mild nausea
E	Mild to moderate nausea
F	Moderate nausea but can continue
G	Moderate nausea, want to stop

In summary, when you are asked to open your eyes and view the rotating pattern with eye fixation on the red fixation point, give your current nausea severity rating based on the above scale. During the experiment, at 2 mins interval, I will ask you to give your current rating from time to time. Any question?

- C. Measurement 3 (M3): rate your perceived self-rotating velocity continuously (Now please verbally report your understanding of “self-rotating velocity” to the experimenter)

Instruction of M3:

Right before the experiment session, I am going to present you a pre-test session, i.e. a drum rotating at certain constant velocity for 90seconds. You could experience one of the following three types of responses in this pre-test session:

T1. Have feeling of self-rotating (vection) and the feeling will increase to a saturation point when the rotating pattern is stationary and you are rotating in the opposite direction instead

T2. Have feeling of self-rotating (vection) and your feeling never increases to a saturation point, i.e., you can perceive both you and the pattern are rotating but the pattern never stop.

T3. No feeling of self-rotating (vection)

If you are T1 person

In the pre-test session, report to me the first moment when you feel that the pattern appears stationary and only you are rotating. Please indicate your rotating direction, i.e., to right or to left. At that moment, you should rate your perceived self-rotating velocity as 100 and report to me image is static. Remember that feeling of self rotating during the pre-test session.

After up to 5mins rest when you are free from sustained self rotating perception

or other side-effect, I will present to you the rotating pattern again for 30mins. Your task is to estimate the angular velocity at which you perceive yourself to be rotating within the 30 mins using velocity “100” as reference. If you perceive you are rotating while the visual pattern is static, just report to me “100”. If you perceive you are rotating at half of the velocity “100” just report to me “50”.Also, the experimenter will ask you to indicate whether the image is appearing to be stationary or not.

If you are T2 person

In the pre-test session, report to me the first moment when you feel you start to rotate and indicate your rotating direction, i.e., to right or to left. Try to compare this speed with the initially perceived speed of the rotating pattern. In other words, if you are asked to give a number 100 to represent the speed of initially perceived rotating pattern, please practice to estimate your perceived self-rotating speed using “100” as reference. In other words, the initial perceived speed of the rotating pattern before you develop any feeling of self-rotating is the “100” reference.

After up to 5mins rest when you are free from sustained self rotating perception and other side-effect, I will present to you the rotating pattern again for 30mins. Your task is to estimate the angular velocity at which you perceive yourself to be rotating within the 30 mins using the initial perceived speed of the rotating pattern (100) as reference. If you feel you are rotating at the same speed of initial perceived rotating pattern, just report to me” 100”. If you perceive you are rotating at half of the velocity “100” just report to me”50”. If you feel that the rotating pattern appear to be stationary at any time, please report to me immediately

Notes: *If you are T1 or T2 person, after you are asked to open your eyes and view the rotating drum, Please report changes of your perceived rotating velocity*

continuously using reference 100. Report higher velocity when you perceive you are rotating faster and report lower velocity when you perceive you are rotating slower. Try to double your reported velocities when you feel you are rotating 2 times faster and halve your reported velocity when you feel you are rotating 2 times slower, and so on. Any question?

If you are T3 person

Please follow the instruction for T2 person. In theory, you will report zero but don't feel embarrassing to give non-zero number in main test session because it is normal for T3 person to become T2 or T1 after certain period of viewing the rotating pattern

Appendix 5-7 Consent form

1. Name _____
2. Are you feeling ill in any way? Yes/No
3. Do you suffer from diabetics (糖尿病) or epilepsy (癲癇症)? Yes/No
4. Are you under medical treatment or suffering disability which affects your daily life? Yes/No

If your answer is “Yes” to question (2), (3), (4) or (5), please give details to the Experimenter.

DECLARATION

I consent to take part in the experiment. My replies to the above questions are correct to the best of my belief, and I understand that they will be treated as confidential by the experimenter.

I understand that I may at any time withdraw from the experiment and that I am under no obligation to give reasons for withdraw declared above.

I undertake to obey the regulations of the laboratory and instructions of the experimenter regarding safety only to my right to withdraw declared above.

The purpose and methods of the experiment have been explained to me and I have had the opportunity to ask questions.

Signature of Subject _____ Date _____

This experiment conforms to the requirement of the University Research Ethic Committee.

Signature of Experimenter _____ Date _____

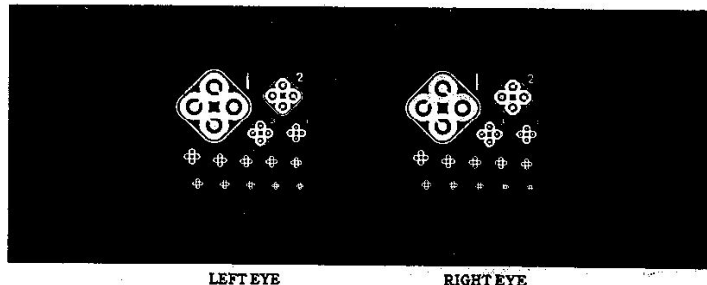
Appendix 5-8 Instruction of measuring visual acuity at near point by an "OPTEC® 2000" visual tester

TEST NO. 9 ACUITY BOTH EYES "NEAR"

1. NEAR/FAR Point Switch in the Down position
2. Right and Left eye Switches in the Down position
3. Dial #9 at Blue Indicator (Near)

This test stimulates near vision at a 14 inch distance. Both eyes see the same targets which are fused into a single target when viewed binocularly.

QUESTION: "Look at the #1 target. Is the ring at the RIGHT broken like the other rings or is it unbroken? Where is the unbroken ring in target #4—at the top, bottom, right or left? #5? #6? Score these tests the same as FAR acuity tests. Record last correct answer after two consecutive misses.



SCORE	1	2	3	4	5	6	7	8	9	10	11	12	13	14
KEY	R	L	T	R	B	R	T	L	T	L	B	R	B	L
	20	20	20	20	20	20	20	20	20	20	20	20	20	20
	200	100	70	50	40	35	30	25	22	20	18	17	15	13

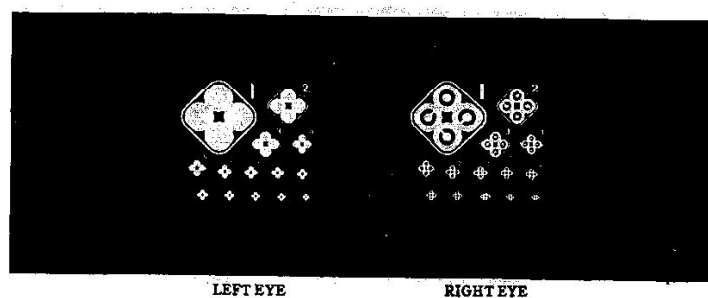
Left = ←, Right = →, Top = ↑, Bottom = ↓

TEST NO. 10 ACUITY RIGHT EYE "NEAR"

1. NEAR/FAR Point Switch in the Down position
2. Right and Left eye Switches in the Down position
3. Dial#10 at Blue Indicator (Near)

As with the FAR test, the right eye sees the target and the left eye sees only the background pattern. Together they fuse the slide into one picture. Therefore, both eyes are used for this test. Occluding the left eye may help subjects having difficulty at the low score level. To do this, push the left occluder switch off. Both occluded and unoccluded scores should be recorded.

Direct the subject as in previous acuity test.



SCORE	1	2	3	4	5	6	7	8	9	10	11	12	13	14
KEY	T	B	T	B	R	T	R	L	B	L	R	R	L	T
	20	20	20	20	20	20	20	20	20	20	20	20	20	20
	200	100	70	50	40	35	30	25	22	20	18	17	15	13

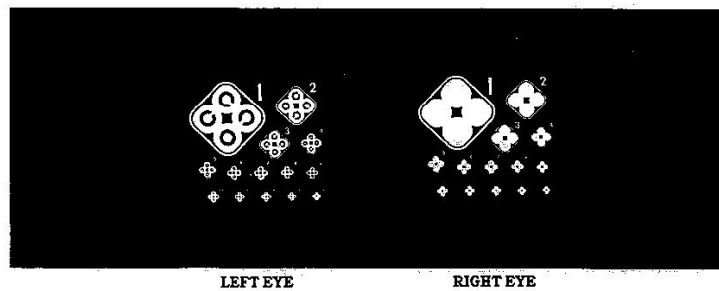
Left = ←, Right = →, Top = ↑, Bottom = ↓

TEST NO. 11 ACUITY LEFT EYE "NEAR"

1. NEAR/FAR Point Switch in the Down position
2. Right and Left eye Switches in the Down position
3. Dial #11 at Blue Indicator (Near)

Both eyes are used for this test. The left eye sees the target while the right eye sees only the background pattern. As with the right eye test, if the subject experiences difficulties at a low score level, occlude the right eye and retest, recording both scores.

Direct the subject as in previous acuity test.



SCORE	1	2	3	4	5	6	7	8	9	10	11	12	13	14
KEY	B	L	B	R	T	L	T	B	R	R	L	R	T	L
	20	20	20	20	20	20	20	20	20	20	20	20	20	20
	200	100	70	50	40	35	30	25	22	20	18	17	15	13

Left = ←, Right = →, Top = ↑, Bottom = ↓

Appendix 5-9 Graybiel scale (Graybiel *et al.*, 1968) used in Hu et al., 1989

<i>Category</i>	<i>Additional qualifying symptoms 1 point</i>	<i>Minimal 2 points</i>	<i>Minor 4 points</i>	<i>Major 8 points</i>	<i>Pathognomonic 16 points</i>
Nausea syndrome	Epigastric awareness	Epigastric discomfort	Nausea I	Nausea II, III	Vomiting or retching
Skin colour	Flushing	Pallor I	Pallor II	Pallor III	-
Cold sweating	-	I	II	III	-
Increased salivation	-	I	II	III	-
Drowsiness	-	I	II	III	-
Pain	Headache	-	-	-	-
Central nervous system	Dizziness: Eyes closed \geq II, Eyes open III	-	-	-	-

Remarks: I = slight, II = moderate and III = severe or marked

Max:50=16+8+8+8+8+1+1

Min:0

Appendix 6-1 The diameter (in the unit of degree) of central visual field used in experiment two fine tuned for each subject across three non-zero velocity conditions to fully suppress vection perception

subject	30dps	60dps	90dps
1	135	123	135
2	146	180	146
3	100	100	100
4	169	146	146
5	146	112	135
6	157	135	135
7	146	112	112
8	157	123	135
9	123	123	135
10	146	135	169
11	100	100	112
12	169	123	146
13	112	123	169
14	169	146	169

Appendix 6-2 Instruction

- 6) The objective of this experiment is to measure your involuntary eye movements triggered by a visual stimuli. You may experience certain level of negative side effects, e.g., eye fatigue and nausea, during 30mins exposure period.
- 7) Please keep your eyes open and look straight ahead at the blank/white stripes (you can blink but please do not close your eyes too long) during the whole experiment except experimenter asks you to close eyes.
- 8) Please maintain your head position on the chin rest (don't move your head) during the whole experiment
- 9) Please try not to move the hand with EOG electrode attachment (this equipment is used to measure your eye movements magnitude) during the experiment
- 10) In the pre-test section, I will show you a series of rotating image patterns with opposite rotating direction for central and peripheral visual field.(view each for 90sec) You need to report whether you perceive self-rotation and your rotating direction.

After that, I will help you to wear EOG electrodes, which is used to capture your eye movements. You are requested to move your eye balls from one point to the other according to my instructions. Then you have a 5min break.

- 11) During the experiment, you will be asked to rate your various responses to this visual stimuli using different methods. Please read the following instructions for each methods carefully and make sure you have fully understanding on all of them:

D. Measurement 1 (M1): rate your strength level of perceived nausea using a number (Now, please tell the experimenter what is the meaning of “nausea” in your native language)

Instruction of M1:

I am going to present to you an image pattern rotating at constant velocity for 30 mins. Your task is to tell me how much your sensation of nausea is induced and how the strength of nausea changes within the 30mins by assigning numbers.

When you are asked to open your eyes and look straight ahead at the black/white stripes, give a number to represent the current nausea severity level you perceive.

Notes: At the moment when you open your eye, If you have no sensation of nausea, just give zero and if you feel nausea, just give any number that you think appropriate.

After that, at 2 mins interval, I will ask you to give your current nausea severity level a number. Let high numbers represent high nausea level and low numbers represent low nausea level. Try to make the ratios between the numbers that you assign correspond to the ratio between the nausea levels you felt at different time. In other words, double your reported non-zero number when you felt your nausea level is doubled and halve your reported non-zero number when you felt your nausea level is half reduced, and so on. Remember that you can assign any number. There is no limit to the number that you may assign. There is no right or wrong answer. I just want to know how you judge your perceived nausea level over time. When I ask you to assign a number to your current level of nausea, I will remind you about your last assigned number 2 min ago. Any question?

E. Measurement 2 (M2): rate your strength level of perceived nausea by scale A to G.

Instruction of M2:

I am going to present you an image pattern rotating at constant velocity for 30 mins. Your task is to tell me how much nausea is induced and how its strength changes within the 30mins by assigning A-G according to the following scale:

Rating	Definition
A	No symptoms
B	Any unpleasant symptoms, however slight
C	Mild unpleasant symptoms, e.g. stomach awareness, sweating but no nausea
D	Mild nausea
E	Mild to moderate nausea
F	Moderate nausea but can continue
G	Moderate nausea, want to stop

In summary, when you are asked to open your eyes and look straight ahead at the black/white stripes, give your current nausea severity rating based on the above scale. During the experiment, at 2 mins interval, I will ask you to give your current rating from time to time. Any question?

***Notes:** please report to me the strength of your vection perception on the following scale at 2min interval:*

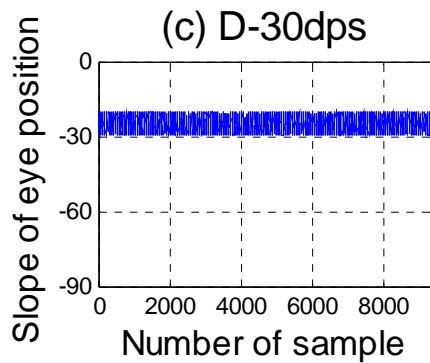
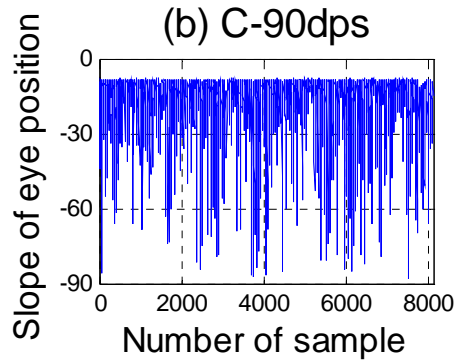
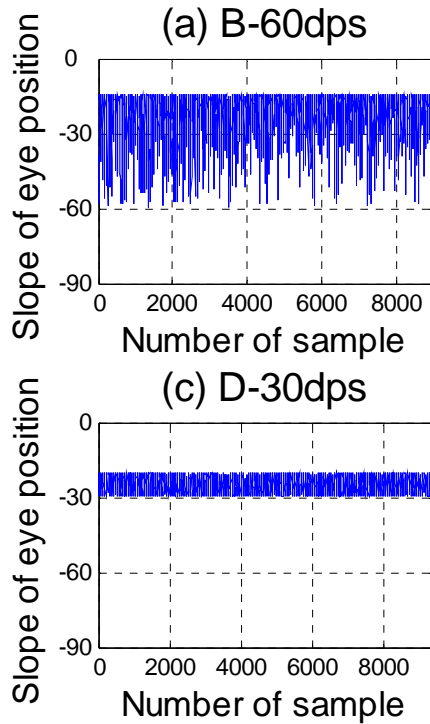
Drum only: you perceive that the only thing moving is the b/w stripes

Drum and self (intermittent): you perceive the b/w stripes to be moving but also experience periods of self rotating

Drum and self (continuously) you perceive the b/w stripes to be moving and simultaneously experience continuous self rotating

Self only: you perceive the b/w stripes to be stationary and experience continuous self rotating

Appendix 6-3 Individual plots of OKN SPV calculated from eye position data of EOG recording (negative value since OKN slow-phase had negative slope). Mean and SD of time series was listed

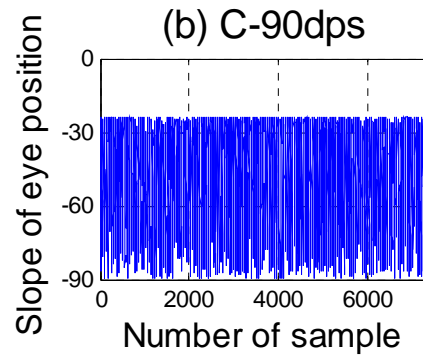
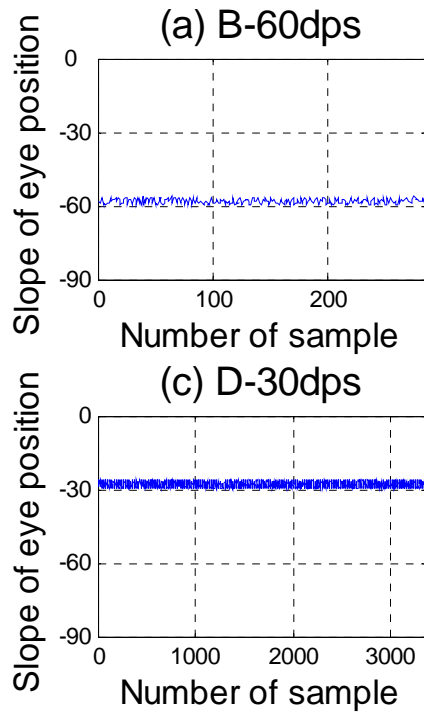


OKN eye position's
slope time series
of Subject CLH

Mean_30dps=-24.8dps±2.9

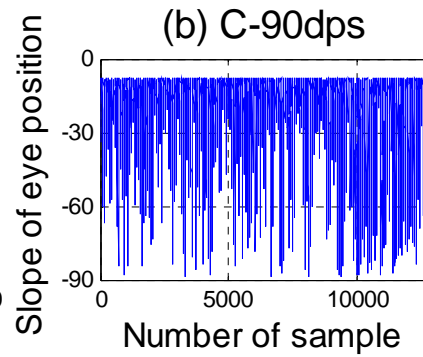
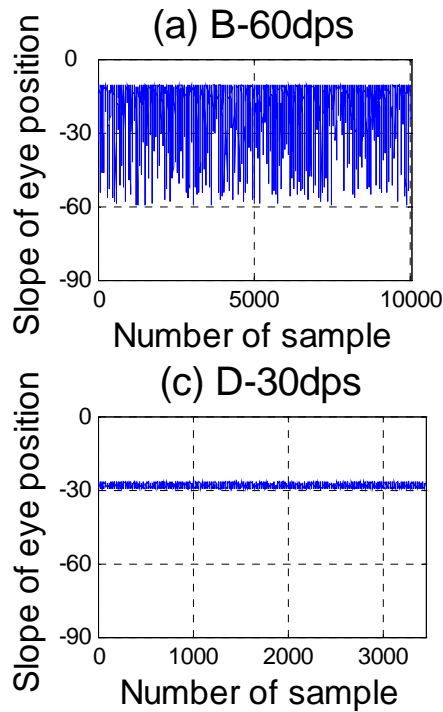
Mean_60dps=-22.6dps±8.2

Mean_90dps=-15.5dps±9.7



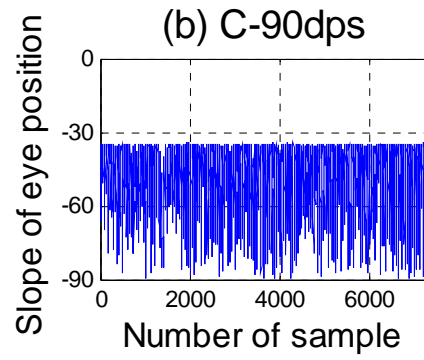
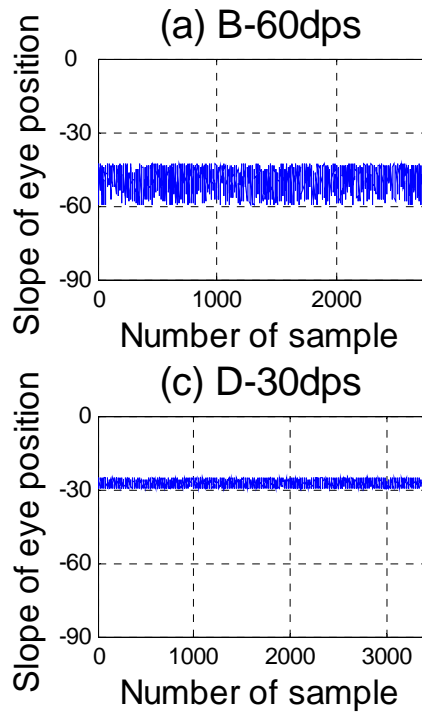
OKN eye position's
slope time series
of Subject LZM

Mean_30dps=-28.0dps±1.1
Mean_60dps=-58.1dps±1.1
Mean_90dps=-44.1dps±18.0



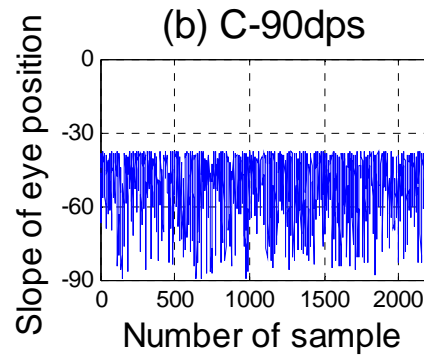
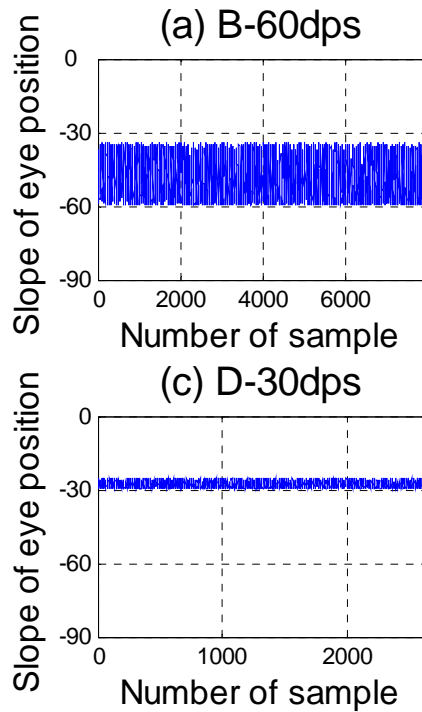
OKN eye position's
slope time series
of Subject YTC

Mean_30dps=-28.4dps±0.9
Mean_60dps=-17.8dps±8.9
Mean_90dps=-26.8dps±11.9



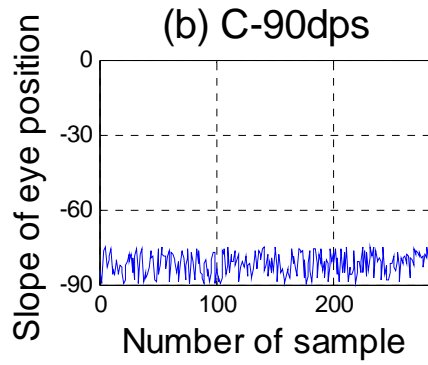
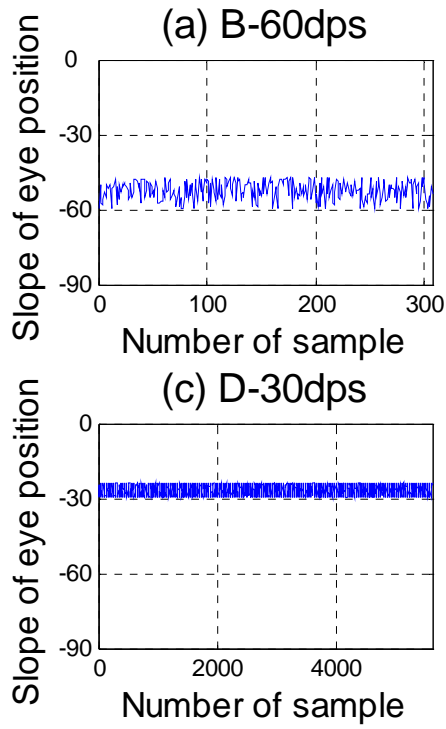
OKN eye position's
slope time series
of Subject ZJ(1)

Mean_30dps=-27.6dps±1.4
Mean_60dps=-49.4dps±4.5
Mean_90dps=-47.9dps±11.4



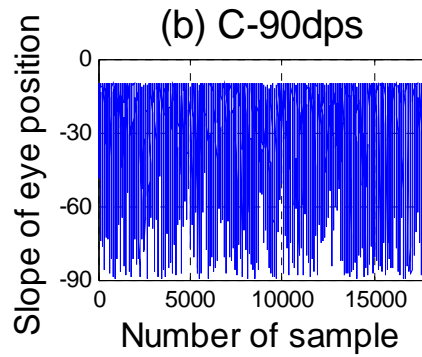
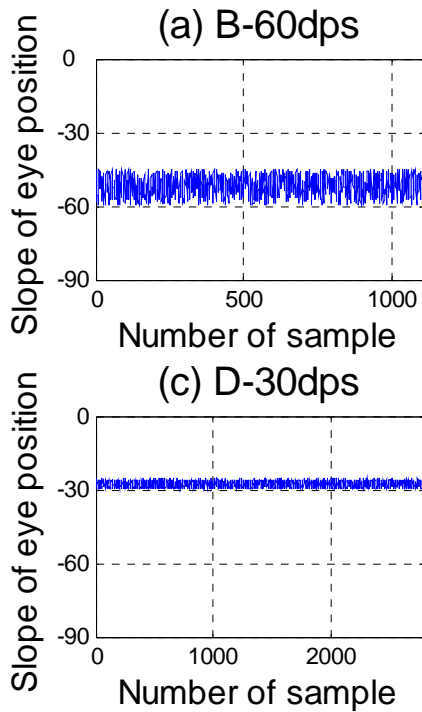
OKN eye position's
slope time series
of Subject SYF

Mean_30dps=-27.8dps±1.4
Mean_60dps=-48.2dps±7.5
Mean_90dps=-51.4dps±12.0



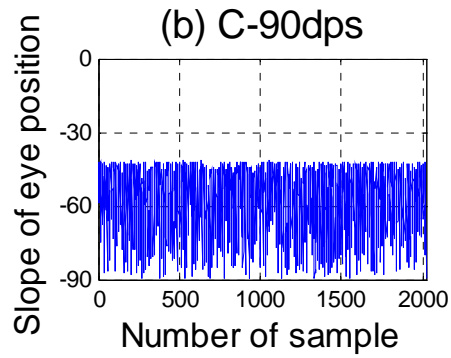
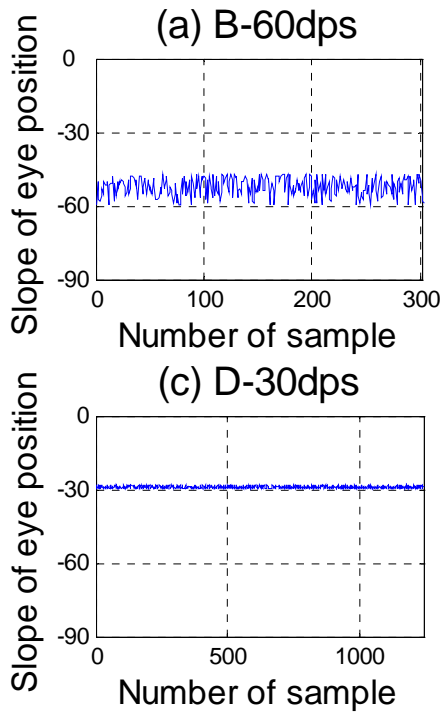
OKN eye position's
slope time series
of Subject CP

Mean_30dps=-26.7dps \pm 1.9
Mean_60dps=-54.0dps \pm 6.7
Mean_90dps=-81.8dps \pm 4.4



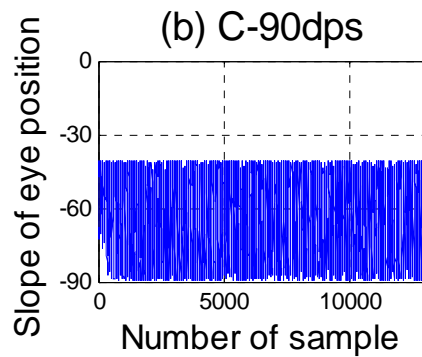
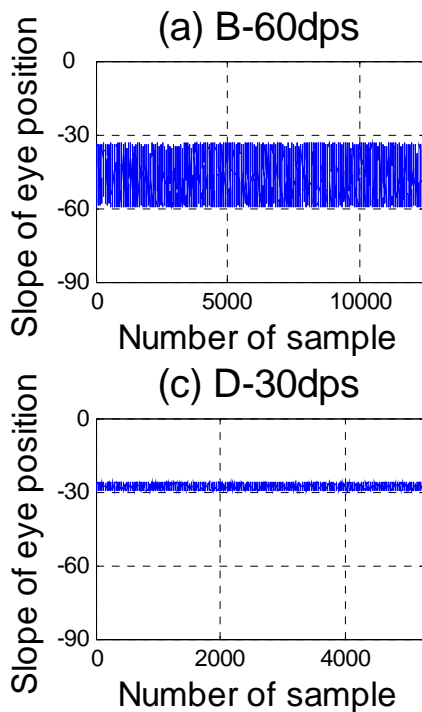
OKN eye position's
slope time series
of Subject FQ

Mean_30dps=-27.7dps \pm 1.3
Mean_60dps=-51.9dps \pm 4.3
Mean_90dps=-24.0dps \pm 15.6



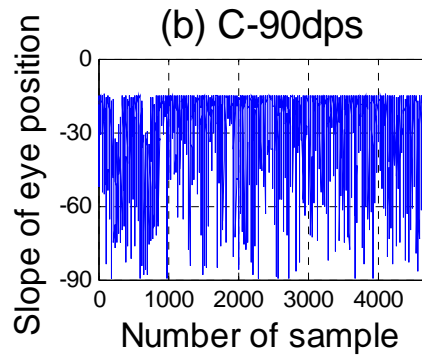
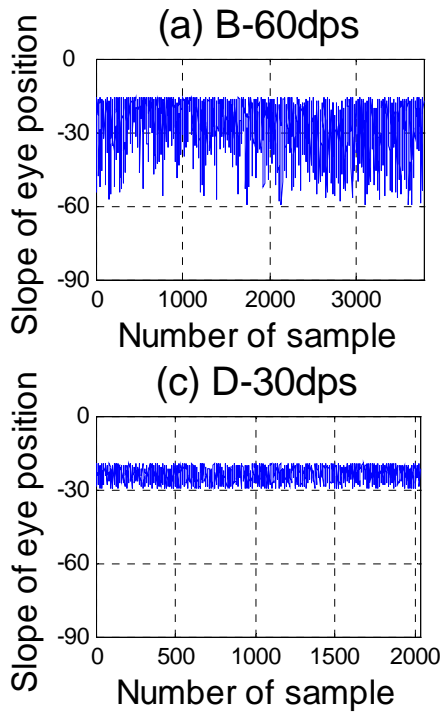
OKN eye position's
slope time series
of Subject LZY

Mean_30dps=-29.2dps±0.5
Mean_60dps=-52.4dps±3.8
Mean_90dps=-57.8dps±12.8



OKN eye position's
slope time series
of Subject ZMZ

Mean_30dps=-28.0dps±1.1
Mean_60dps=-47.4dps±7.6
Mean_90dps=-64.4dps±14.3

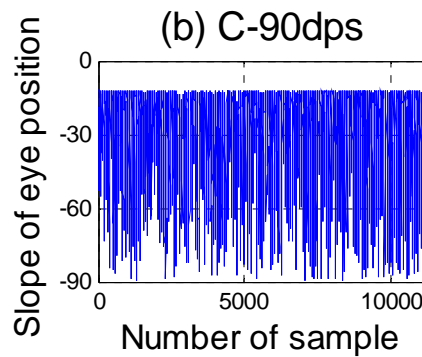
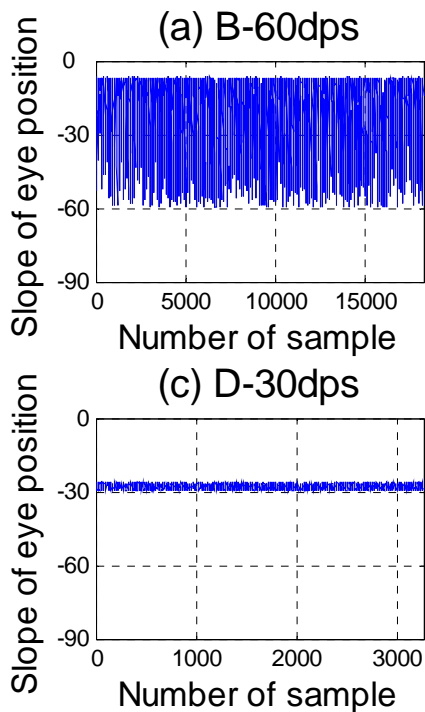


OKN eye position's
slope time series
of Subject YYY

Mean_30dps=-23.8dps \pm 3.0

Mean_60dps=-26.7dps \pm 9.3

Mean_90dps=-26.6dps \pm 14.9

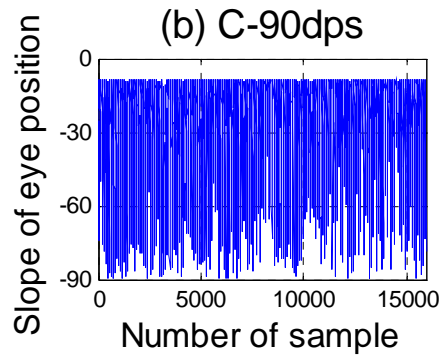
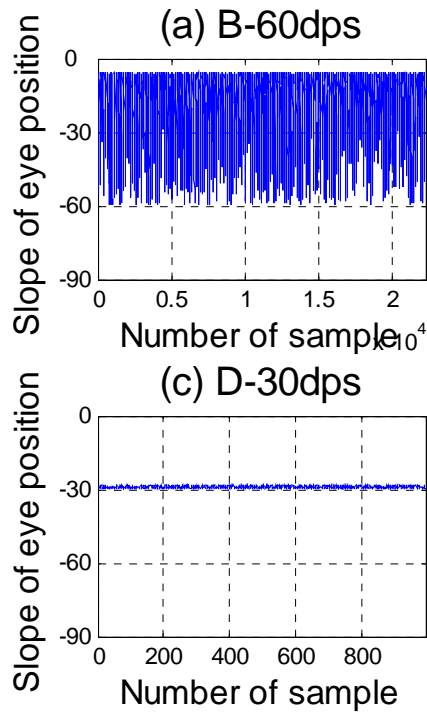


OKN eye position's
slope time series
of Subject MHM

Mean_30dps=-28.0dps \pm 1.1

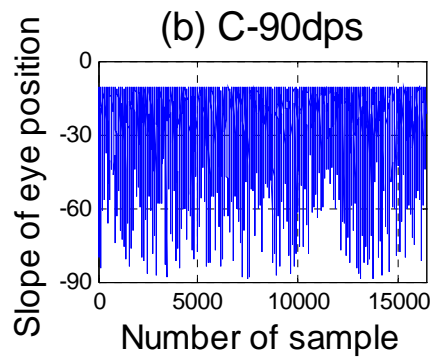
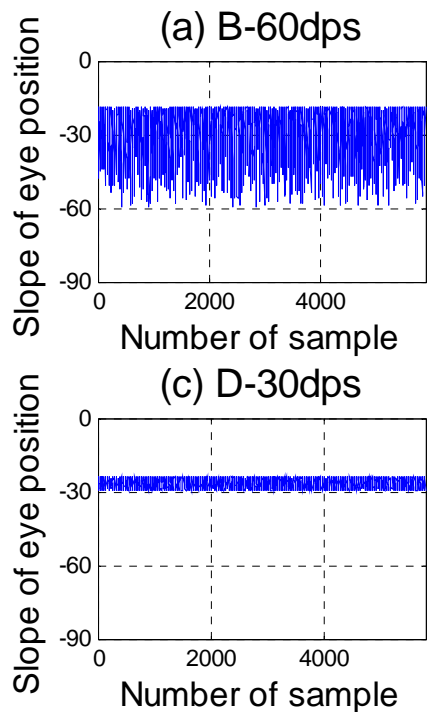
Mean_60dps=-19.3dps \pm 11.8

Mean_90dps=-26.9dps \pm 15.4



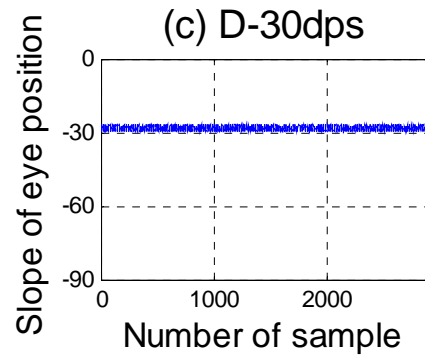
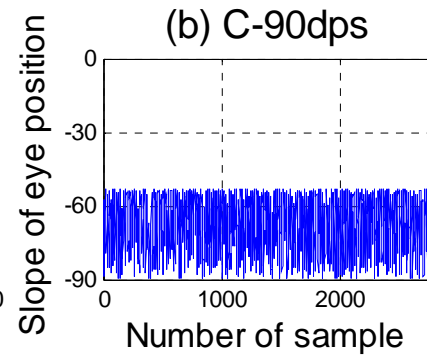
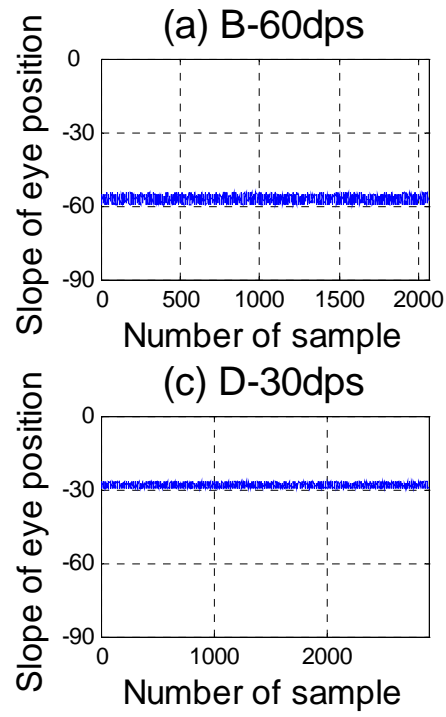
OKN eye position's
slope time series
of Subject WHL

Mean_30dps=-29.1dps \pm 0.6
Mean_60dps=-15.8dps \pm 10.2
Mean_90dps=-23.1dps \pm 15.6



OKN eye position's
slope time series
of Subject CN

Mean_30dps=-26.7dps \pm 1.9
Mean_60dps=-28.7dps \pm 8.6
Mean_90dps=-23.4dps \pm 12.0



OKN eye position's
slope time series
of Subject ZJ(4)

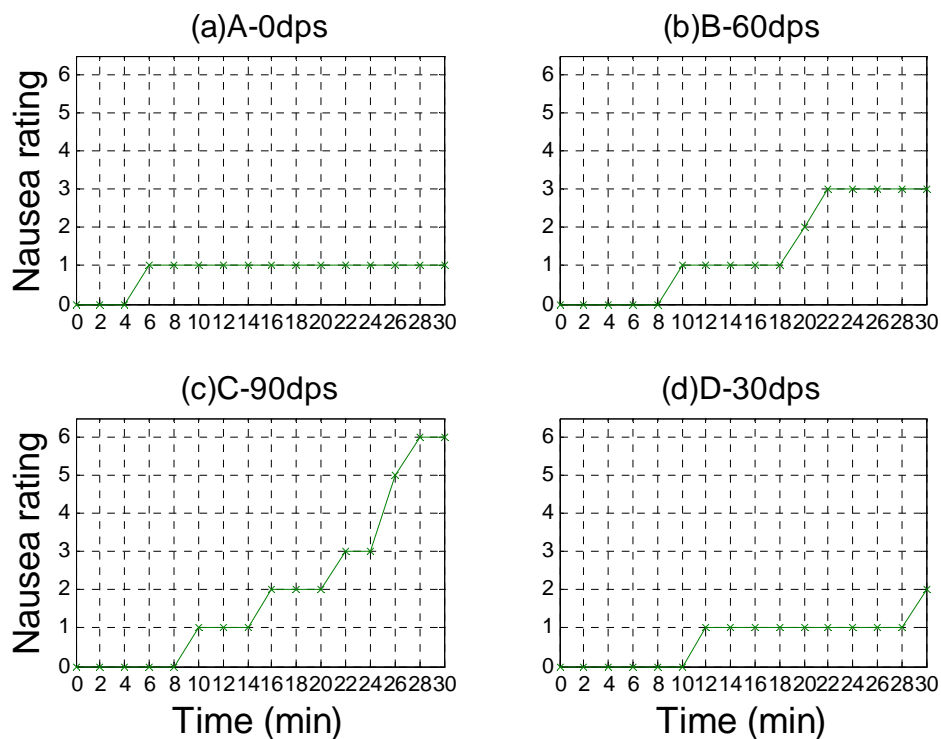
Mean_30dps=-28.4dps±0.9

Mean_60dps=-57.2dps±1.5

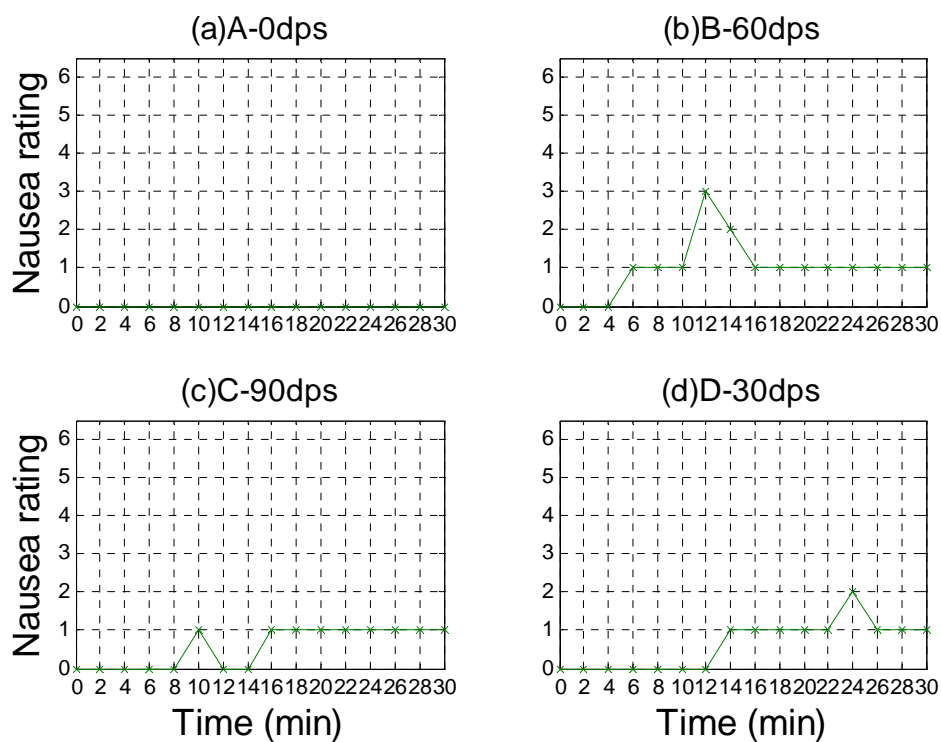
Mean_90dps=-66.6dps±10.0

Appendix 6-4 Individual plots of 7-point nausea rating time series

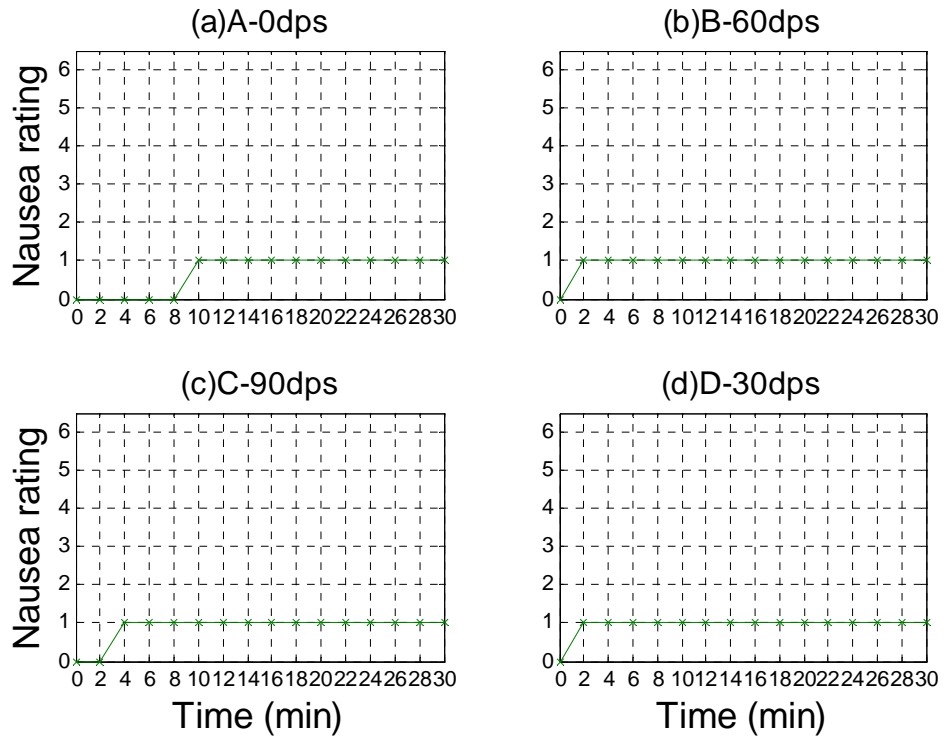
7-point nausea rating time series of Subject CLH



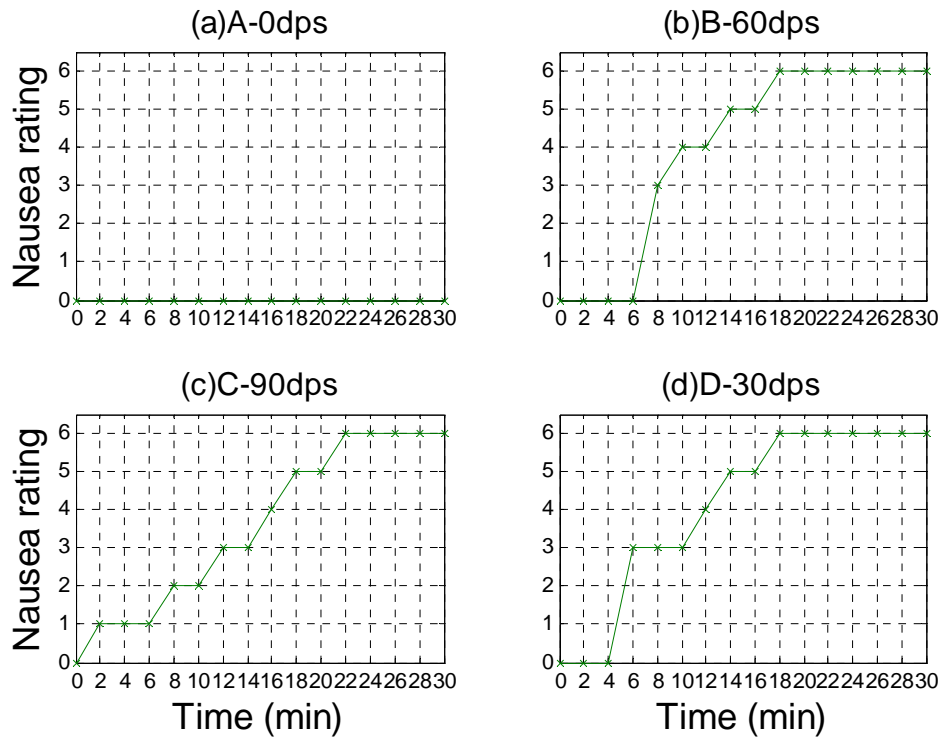
7-point nausea rating time series of Subject LZM



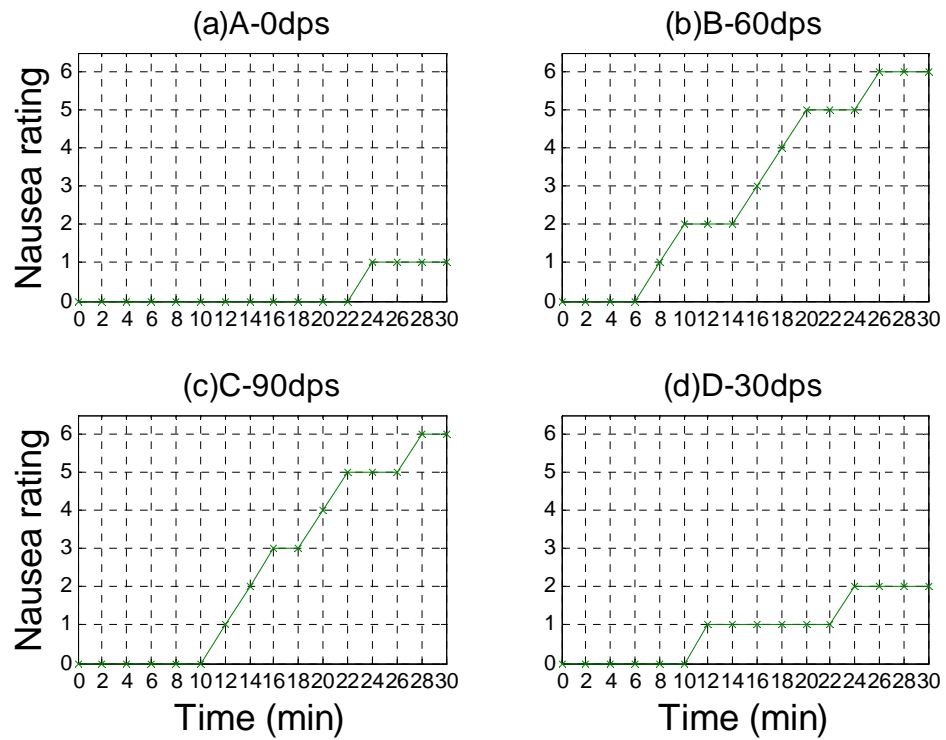
7-point nausea rating time series of Subject YTC



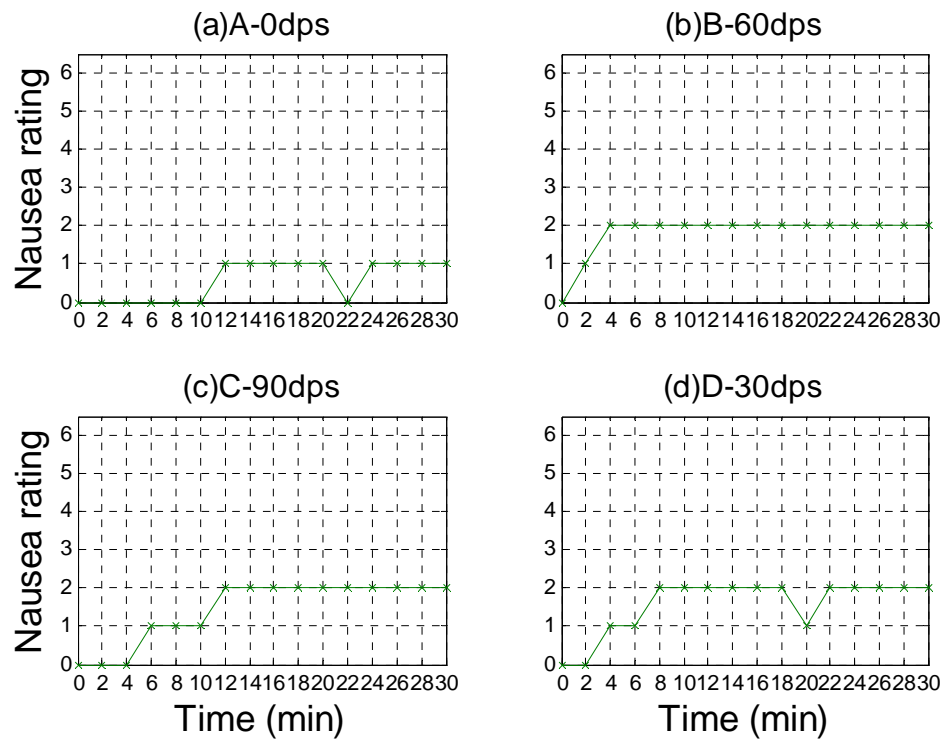
7-point nausea rating time series of Subject ZJ(1)



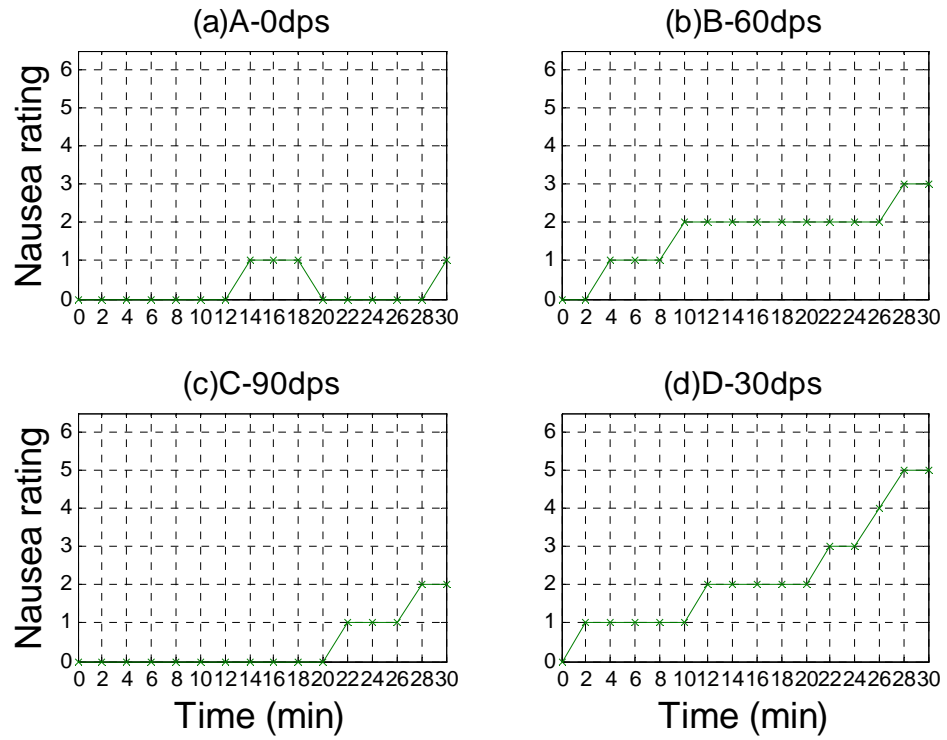
7-point nausea rating time series of Subject SYF



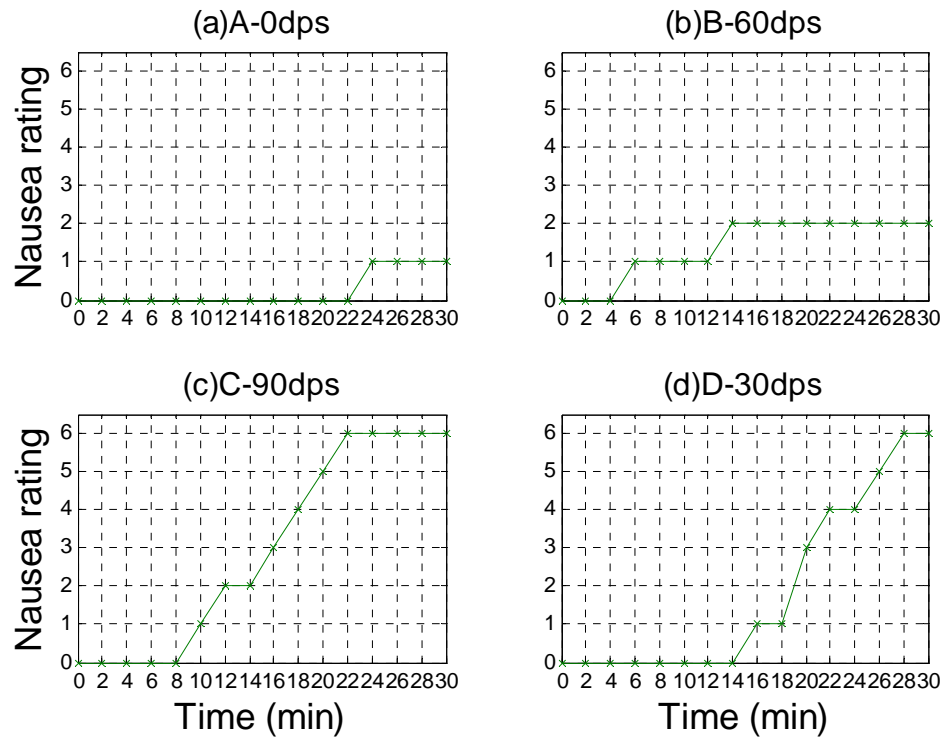
7-point nausea rating time series of Subject CP



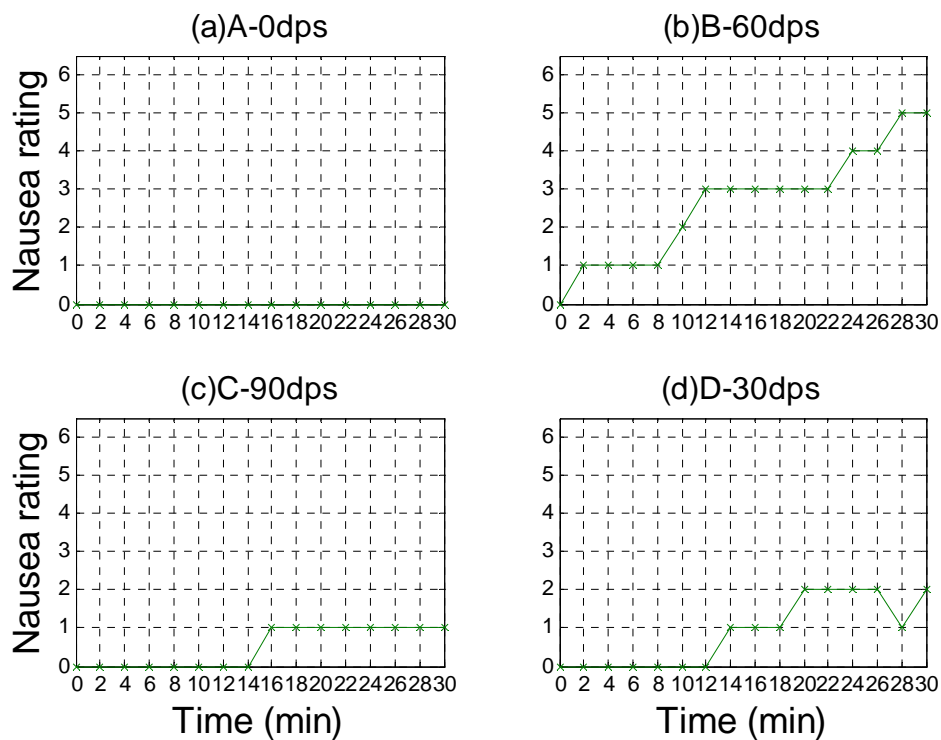
7-point nausea rating time series of Subject FQ



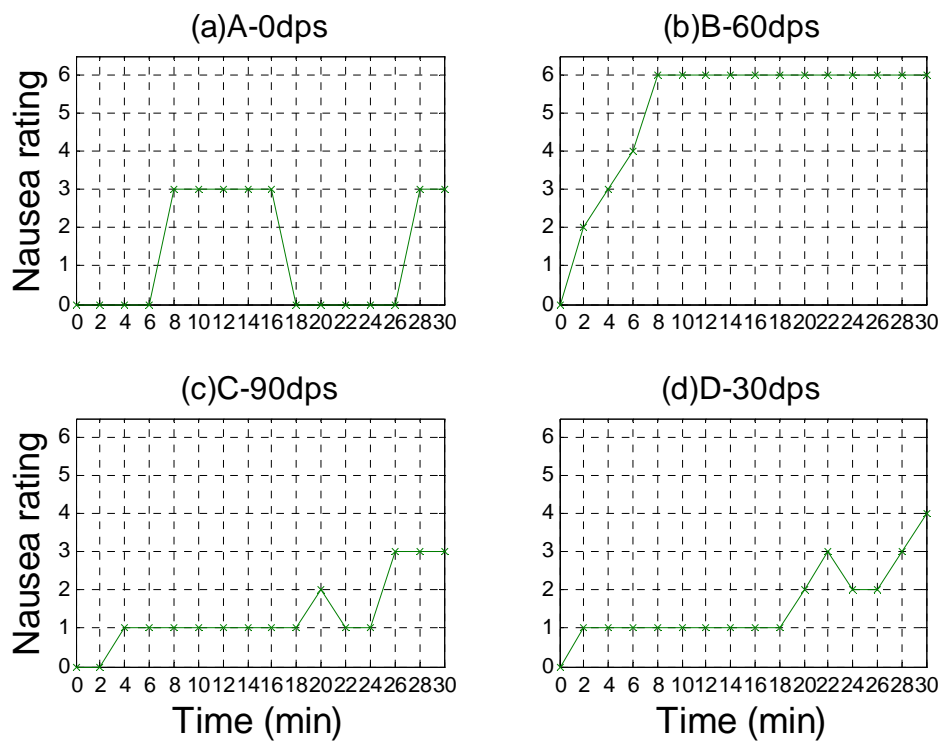
7-point nausea rating time series of Subject LZY



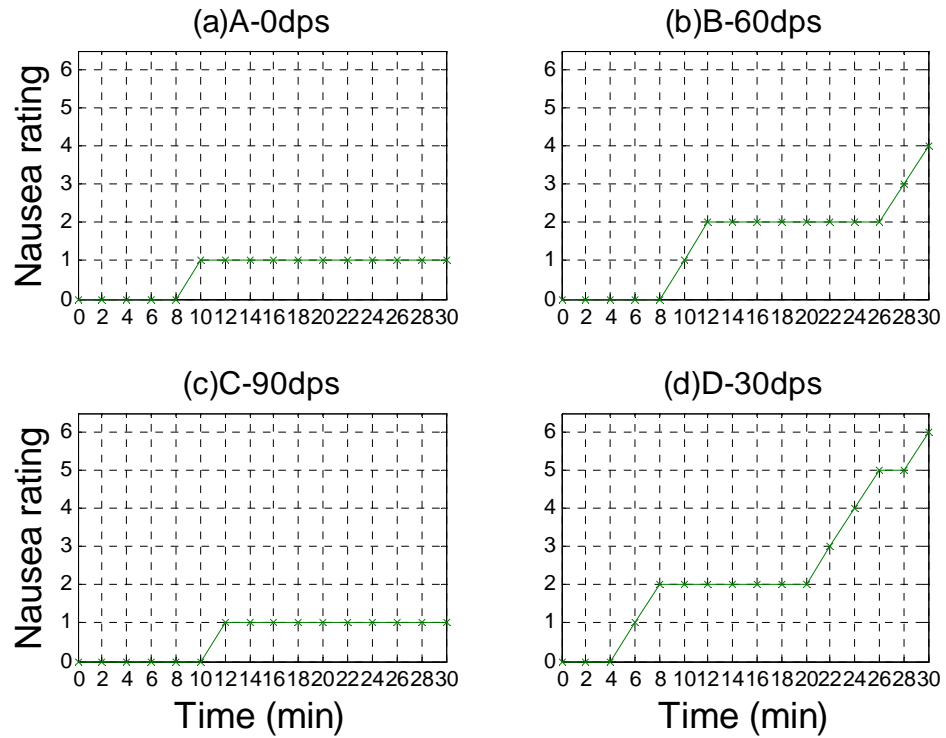
7-point nausea rating time series of Subject ZMZ



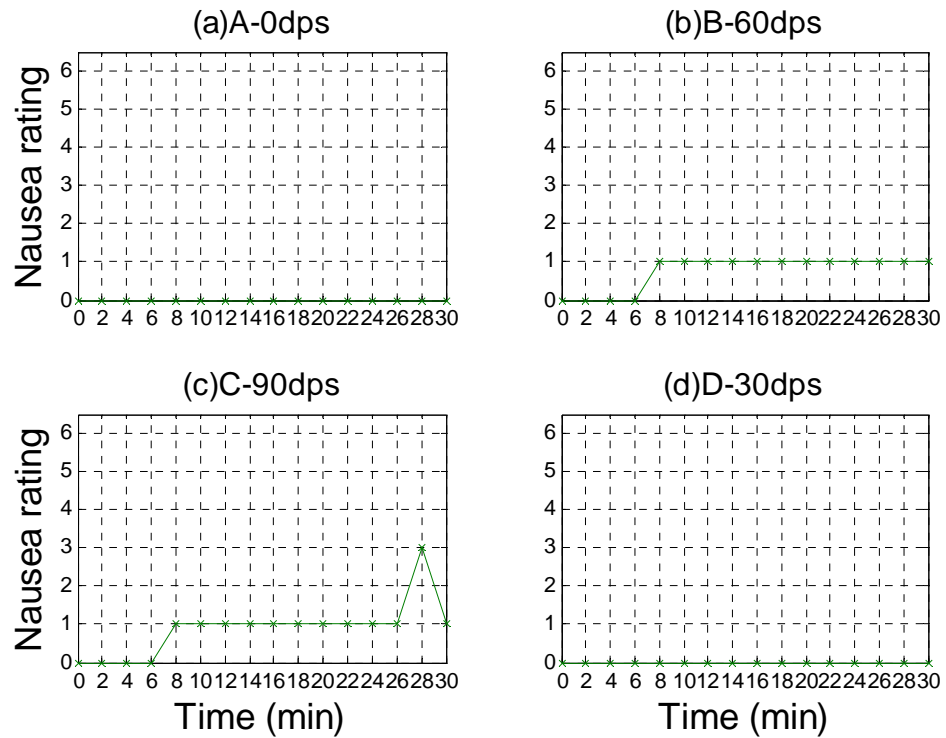
7-point nausea rating time series of Subject YYY



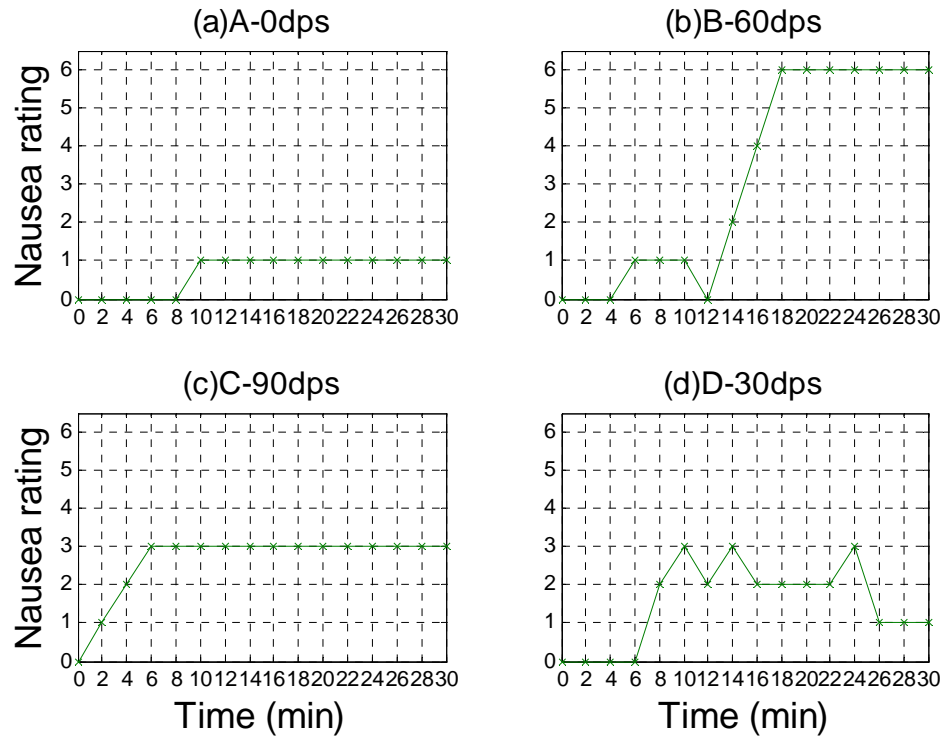
7-point nausea rating time series of Subject MHM



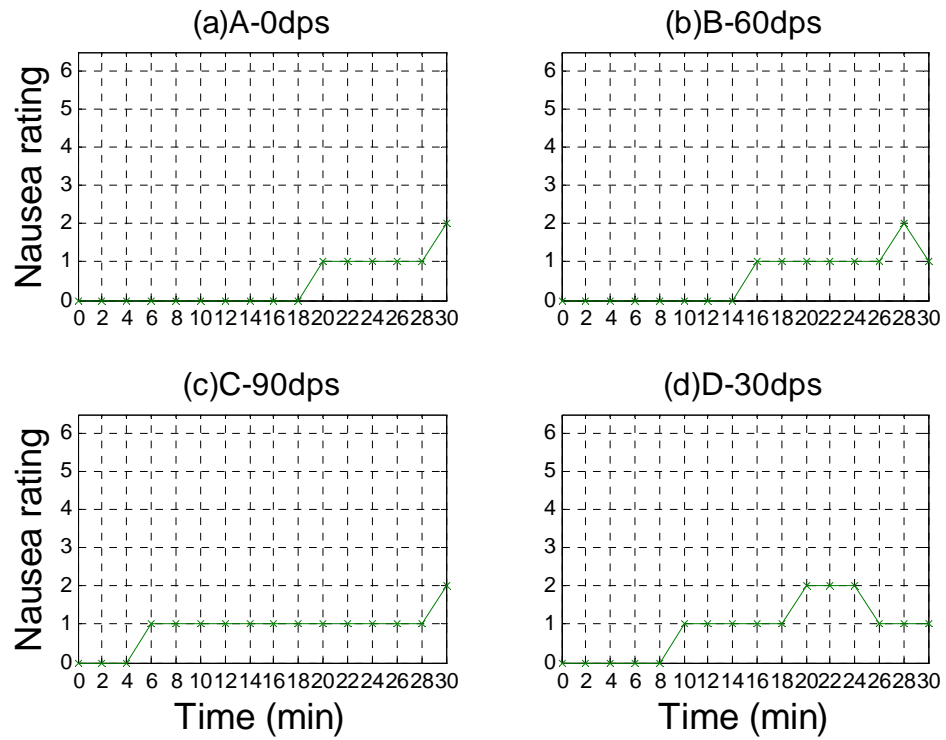
7-point nausea rating time series of Subject WHL



7-point nausea rating time series of Subject CN

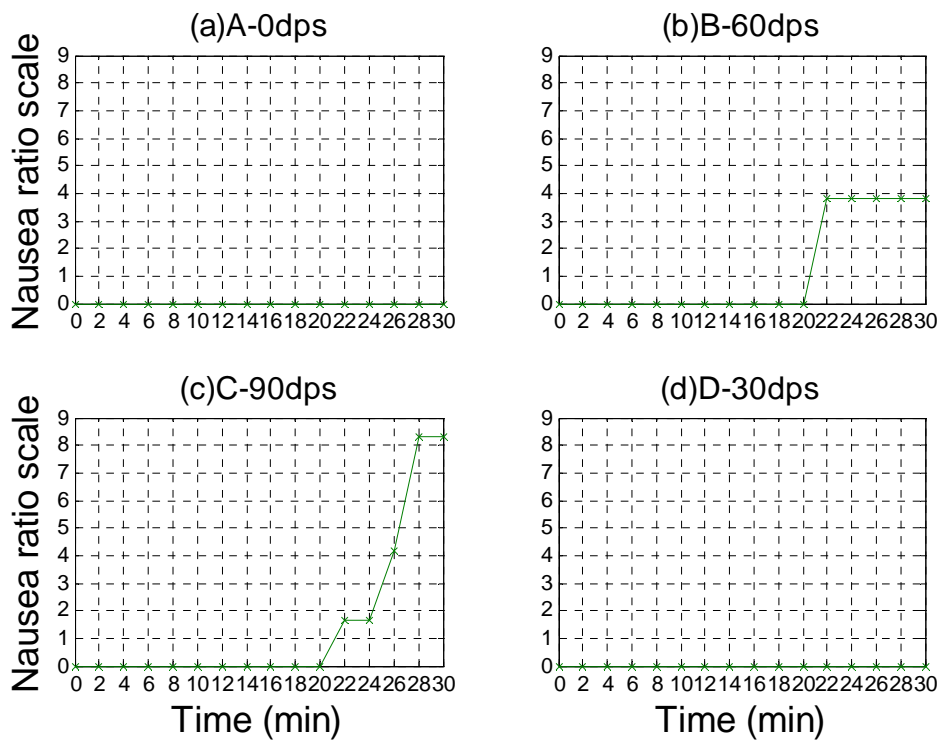


7-point nausea rating time series of Subject ZJ(4)

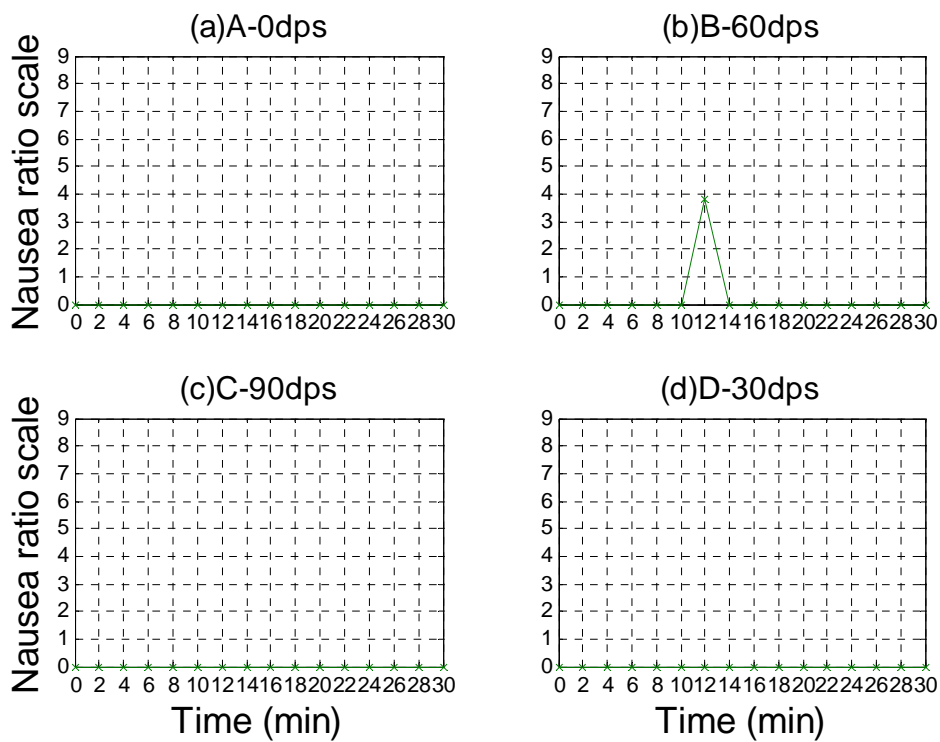


Appendix 6-5 Individual plots of modulus equalized nausea ratio scale data

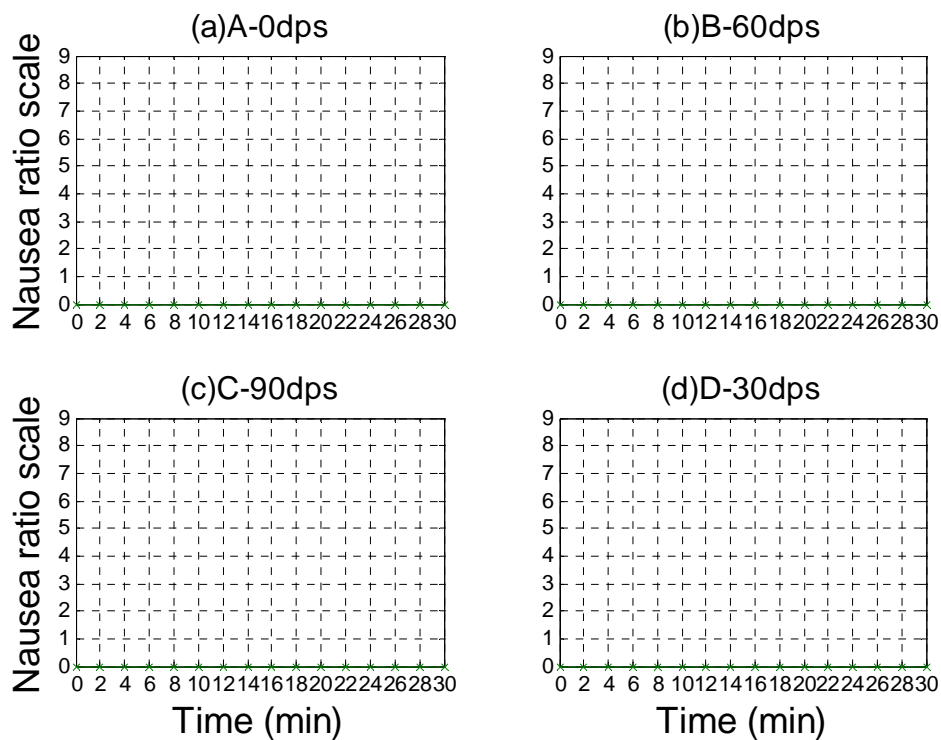
Nausea ratio scale data of Subject CLH



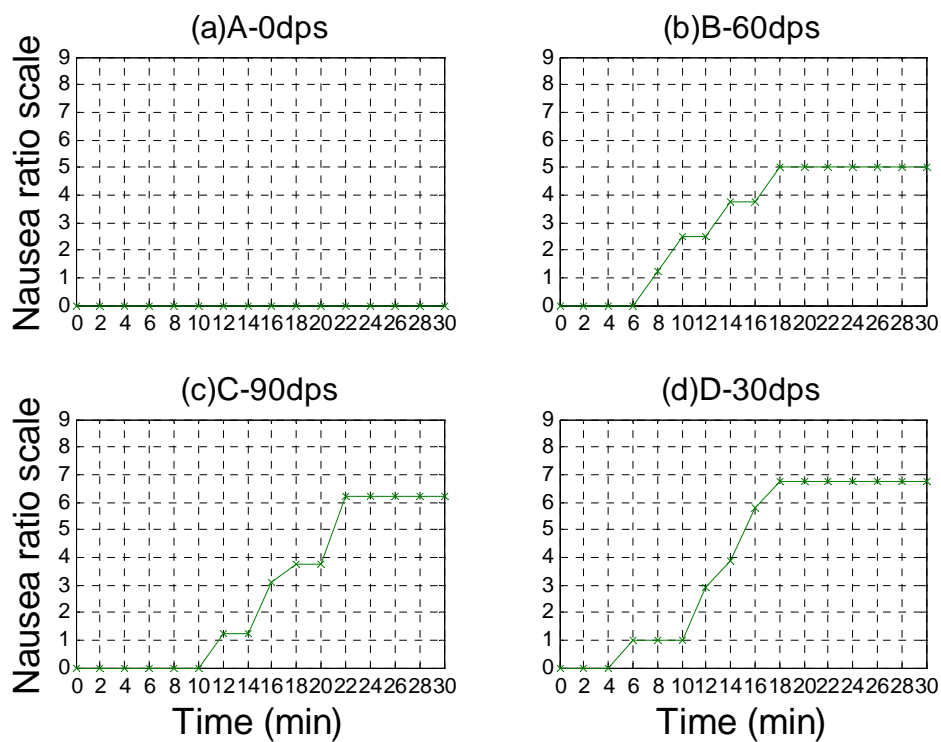
Nausea ratio scale data of Subject LZM



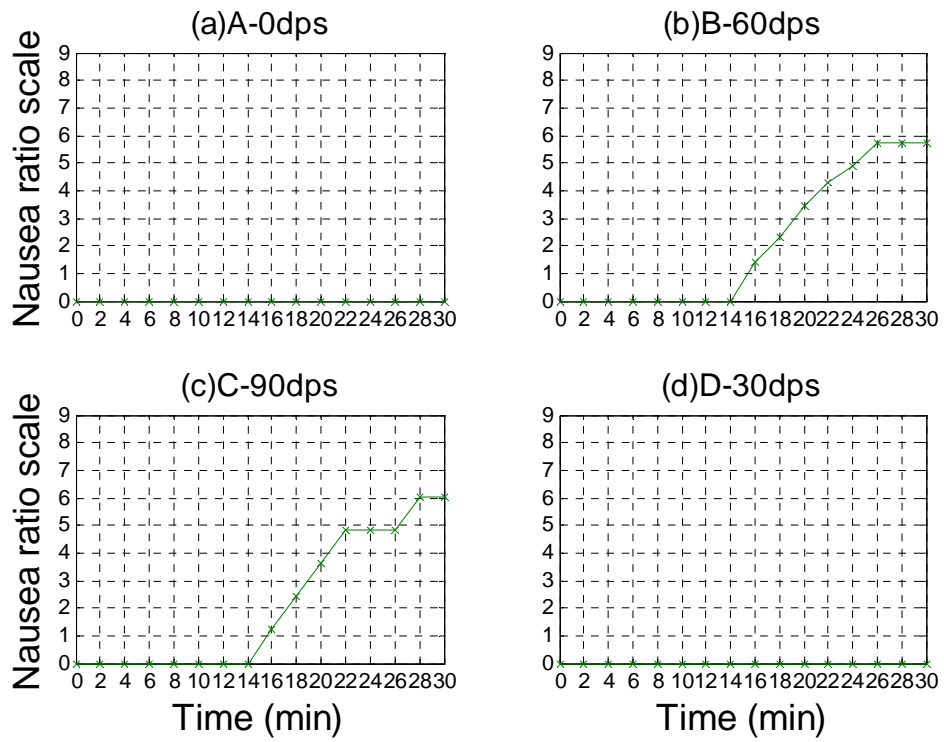
Nausea ratio scale data of Subject YTC



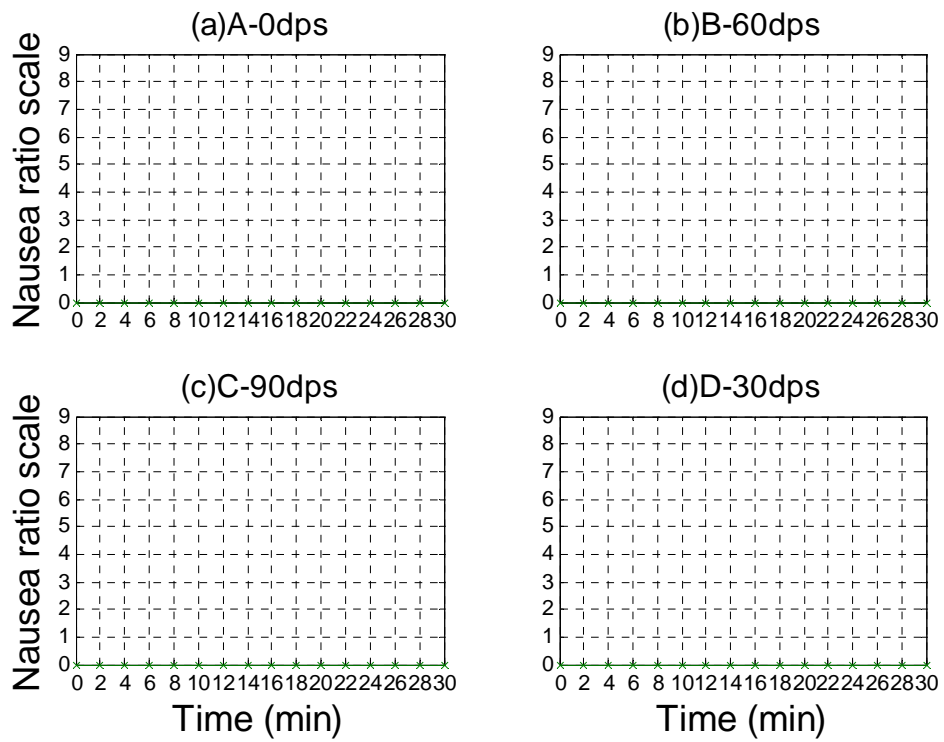
Nausea ratio scale data of Subject ZJ(1)



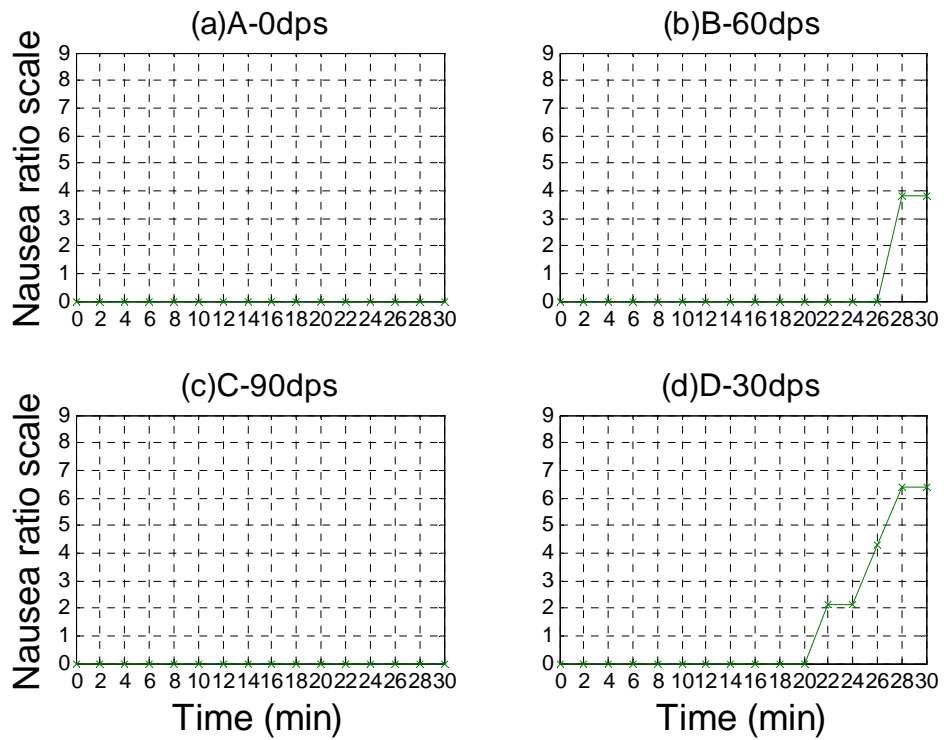
Nausea ratio scale data of Subject SYF



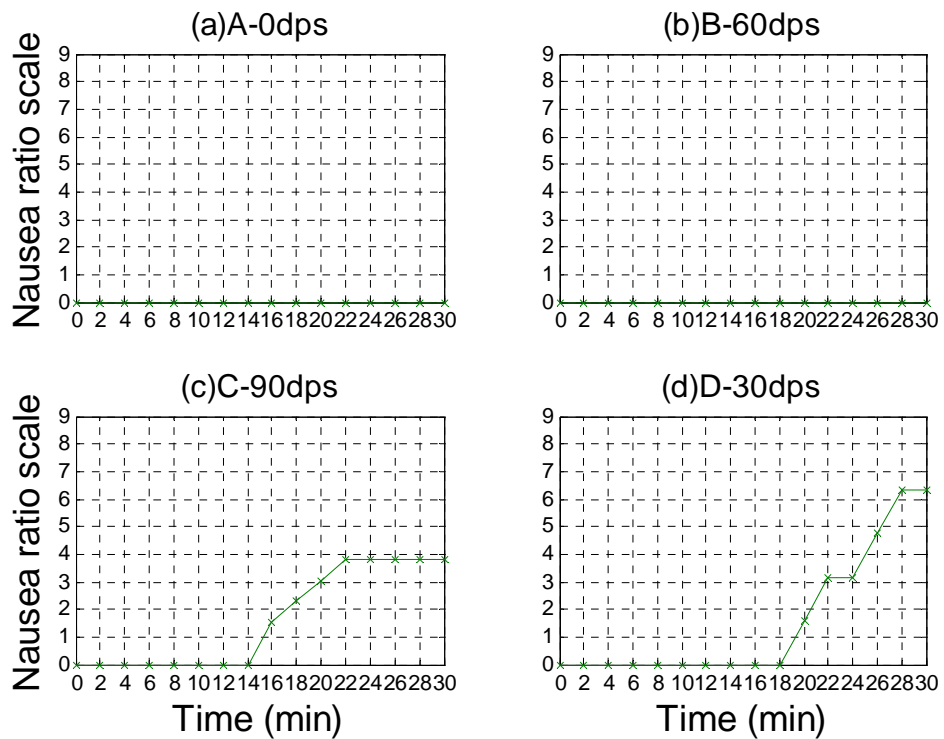
Nausea ratio scale data of Subject CP



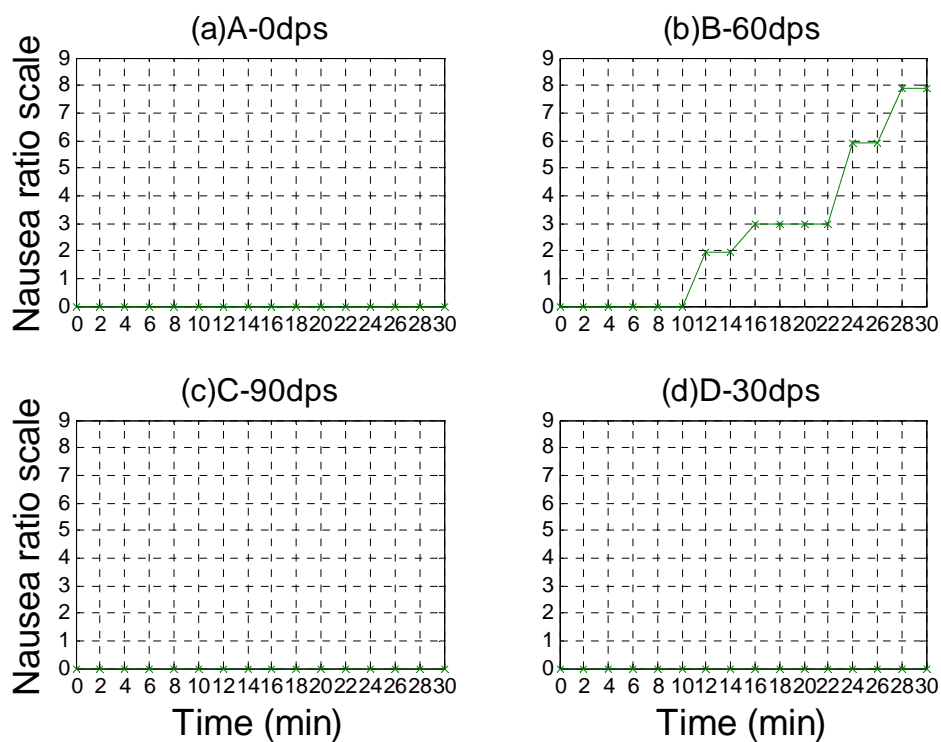
Nausea ratio scale data of Subject FQ



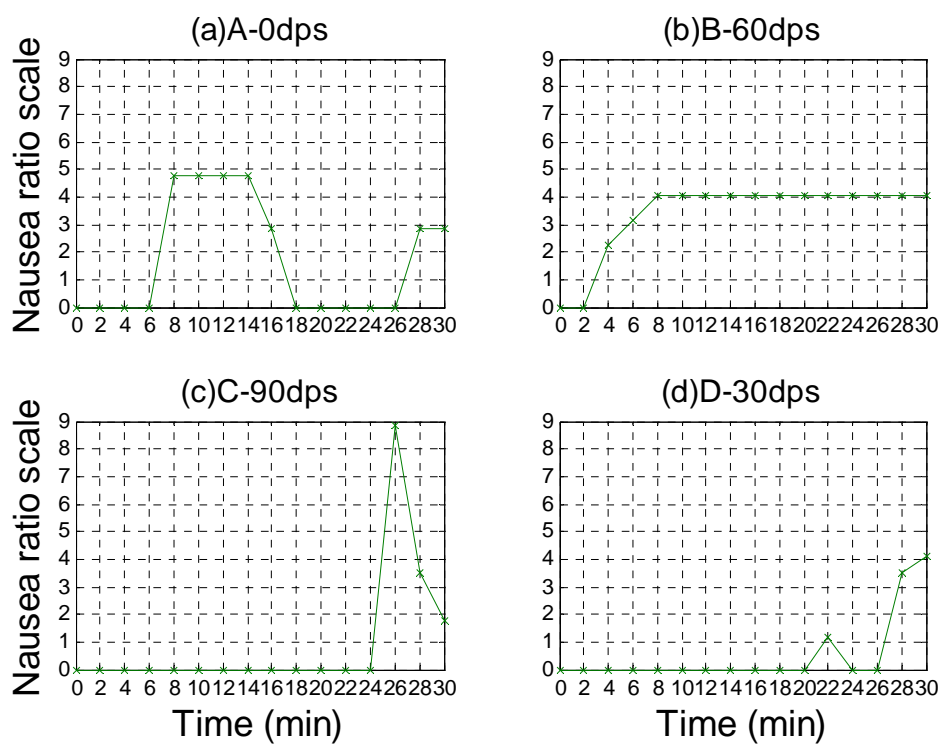
Nausea ratio scale data of Subject LZY



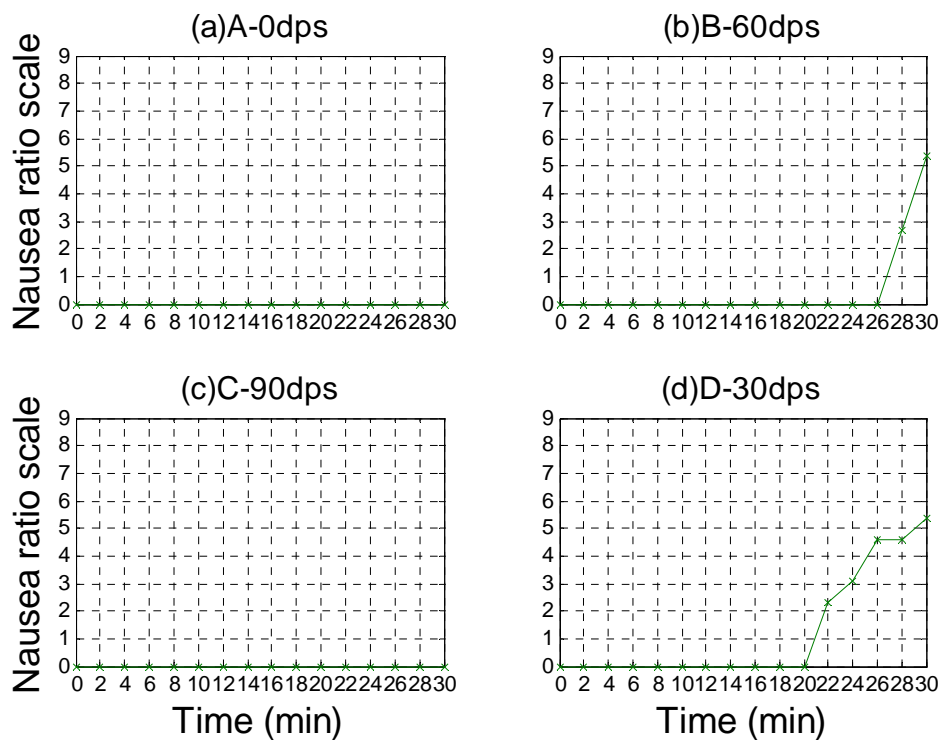
Nausea ratio scale data of Subject ZMZ



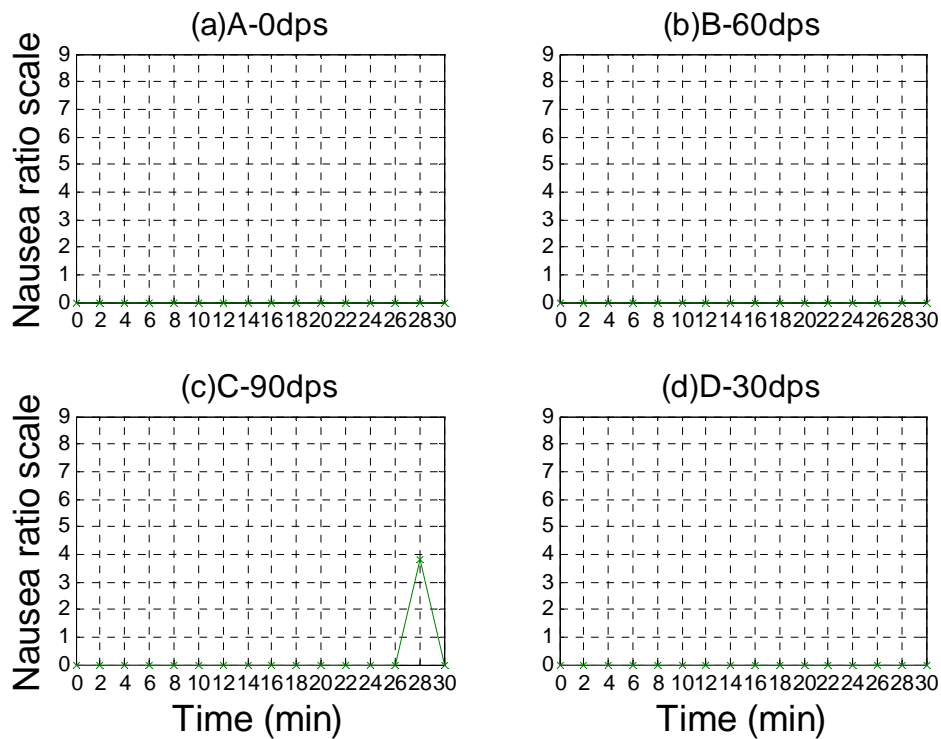
Nausea ratio scale data of Subject YYY



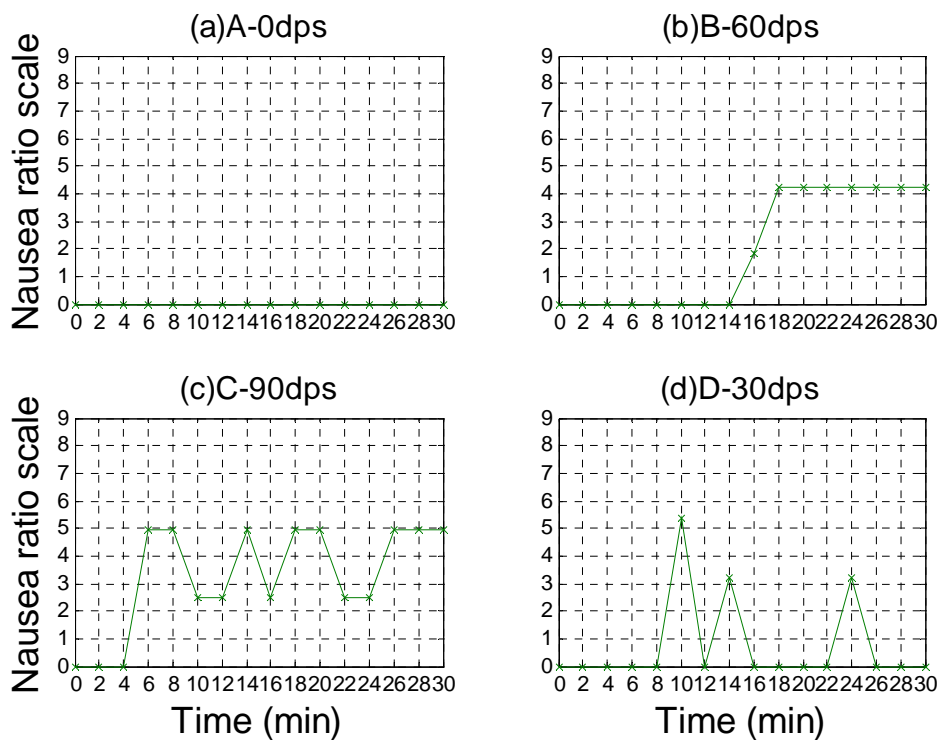
Nausea ratio scale data of Subject MHM



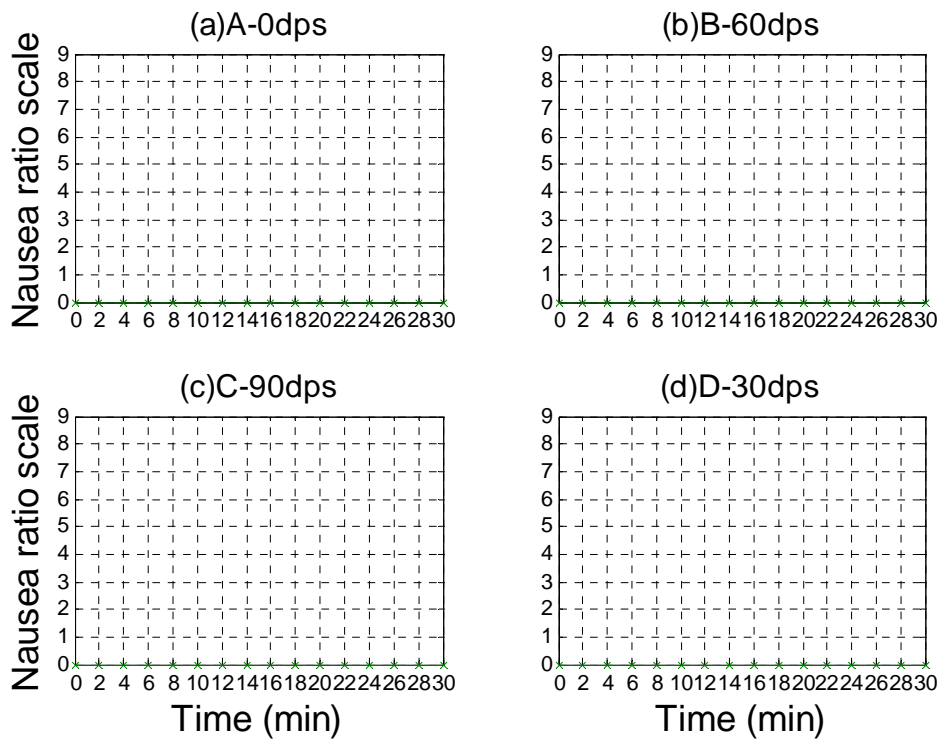
Nausea ratio scale data of Subject WHL



Nausea ratio scale data of Subject CN

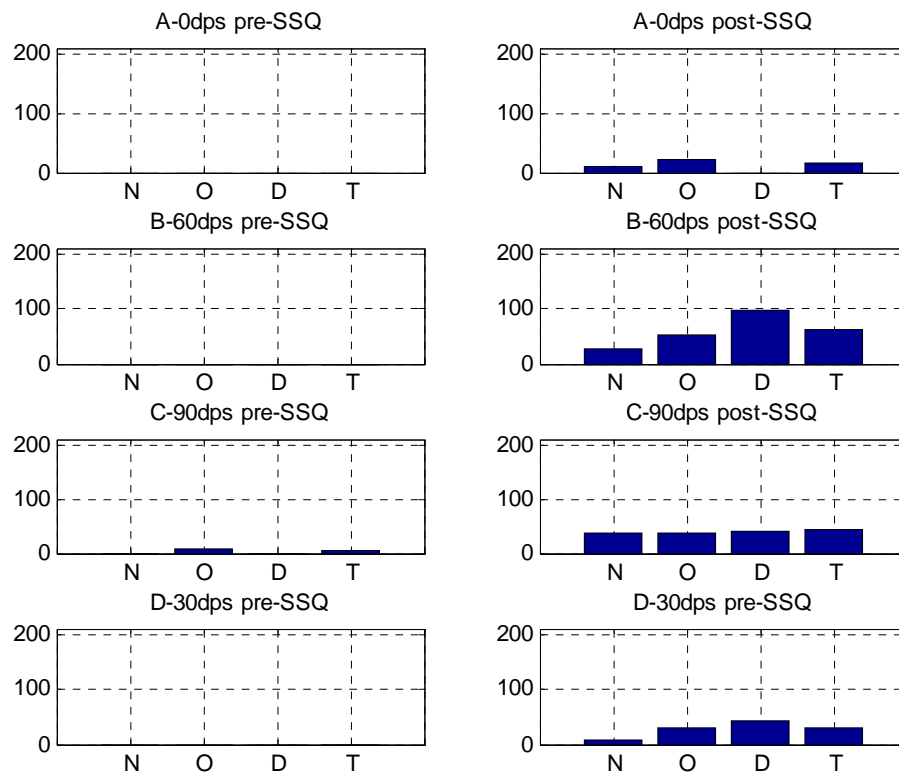


Nausea ratio scale data of Subject ZJ(4)

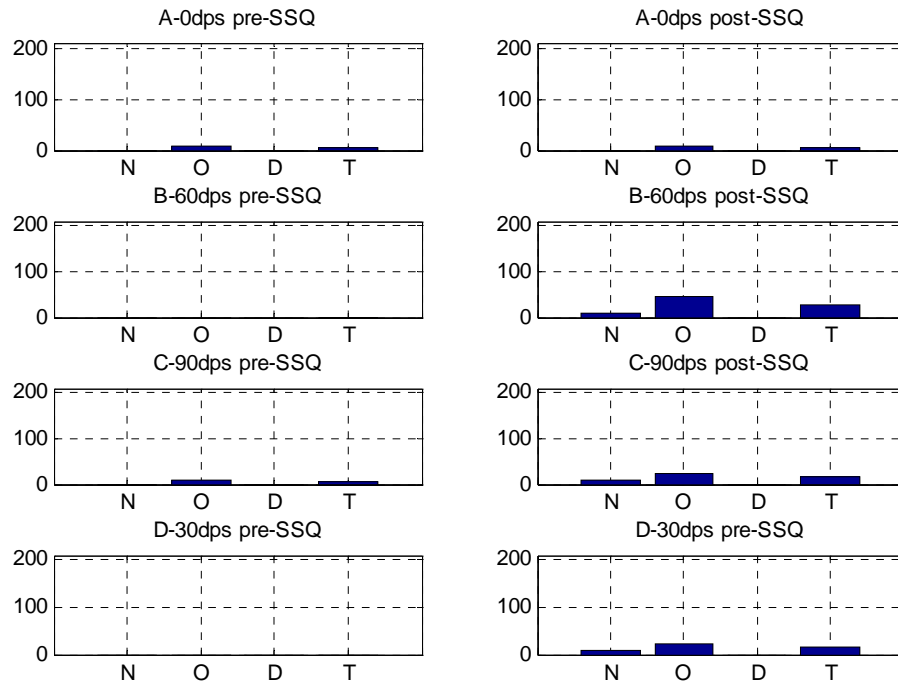


Appendix 6-6 individual plots of pre-& post-exposure SSQ scores

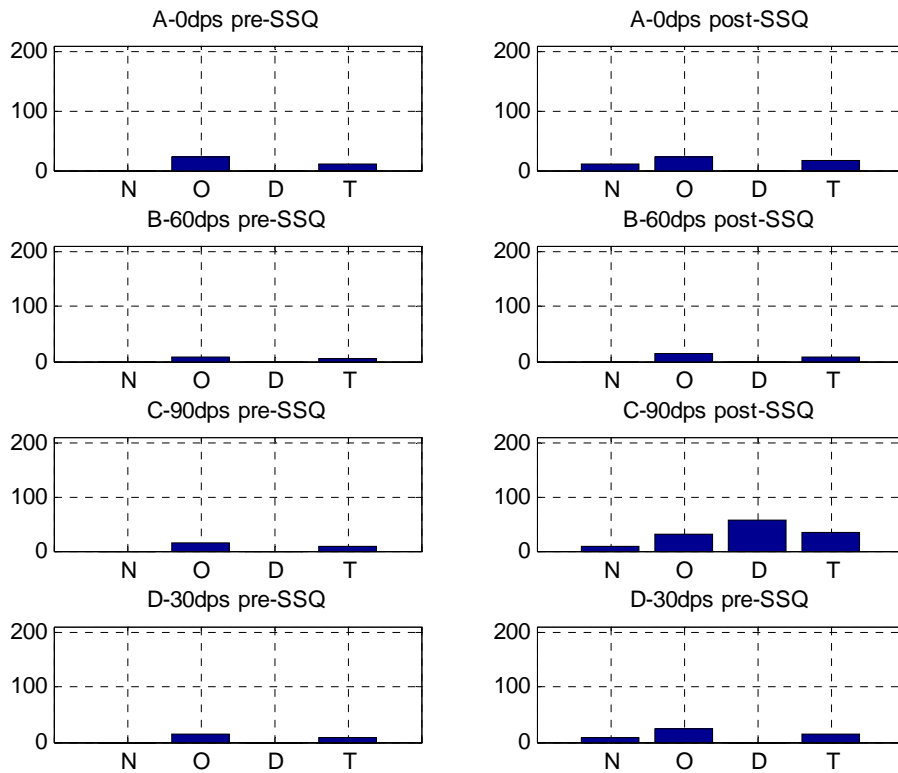
Pre- & Post- SSQ scores of subject CLH



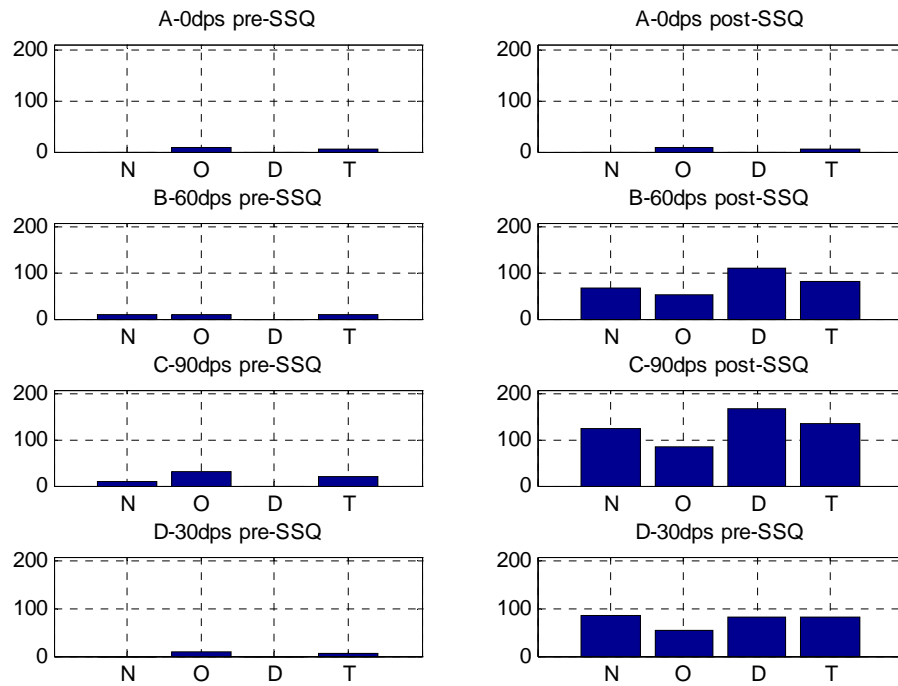
Pre- & Post- SSQ scores of subject LZM



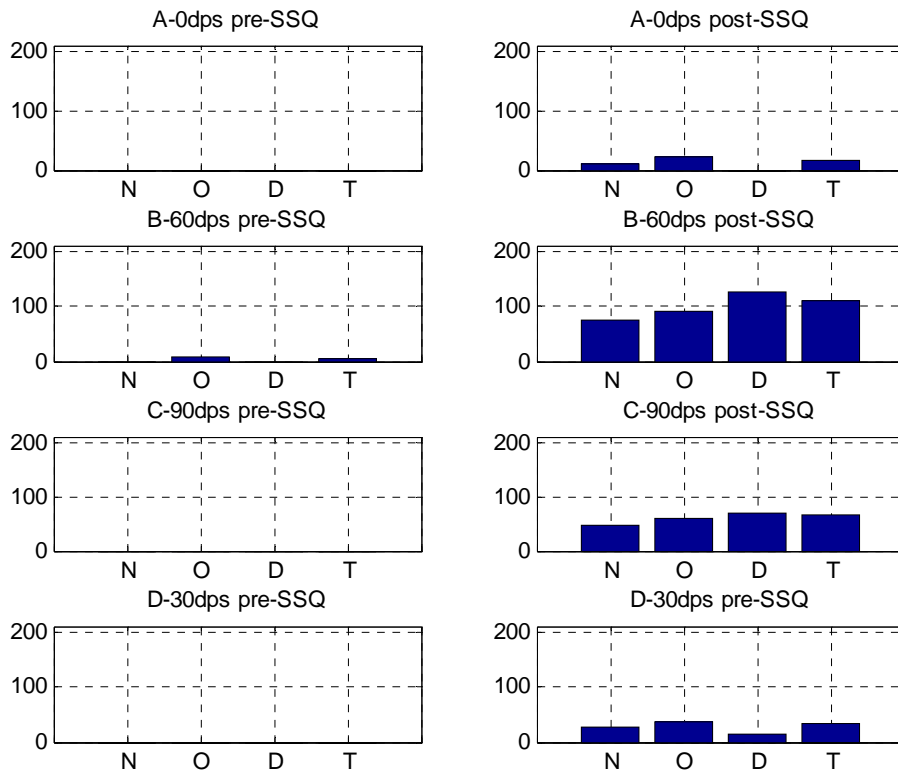
Pre- & Post- SSQ scores of subject YTC



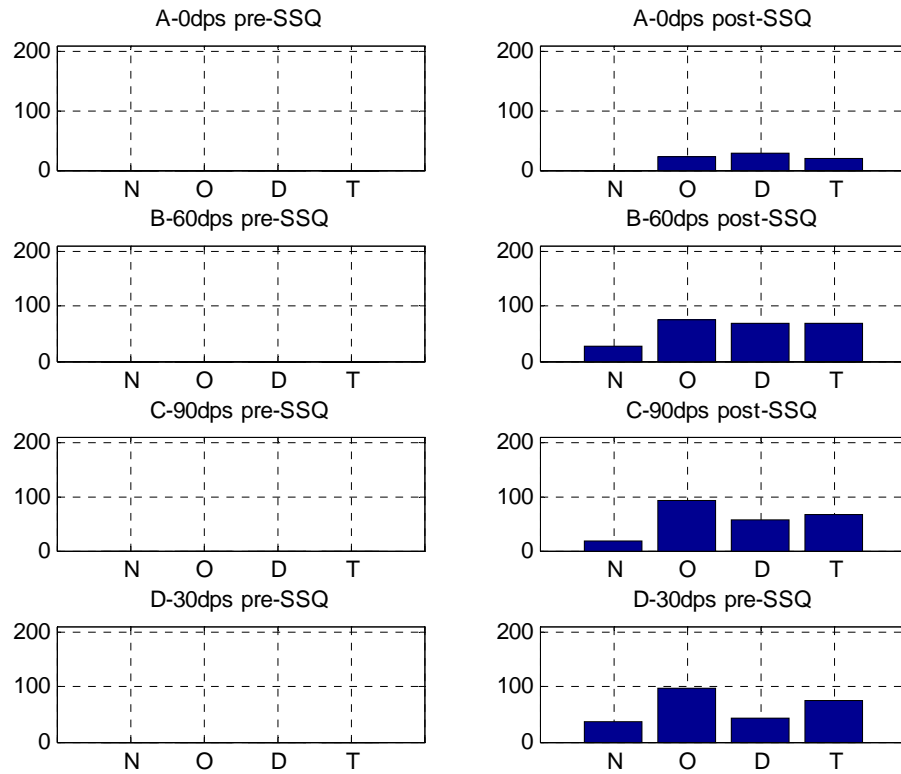
Pre- & Post- SSQ scores of subject ZJ(1)



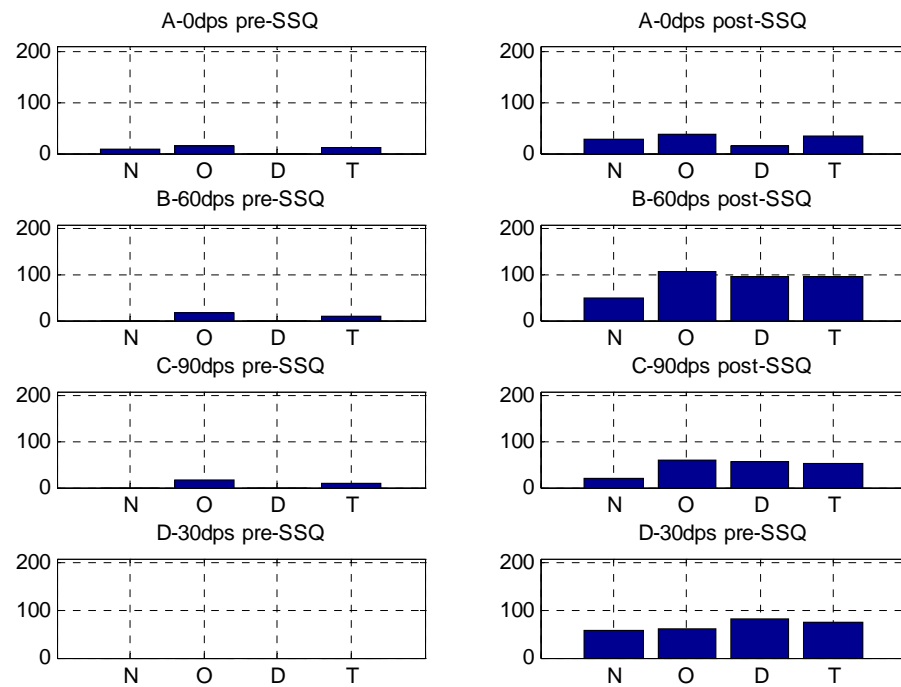
Pre- & Post- SSQ scores of subject SYF



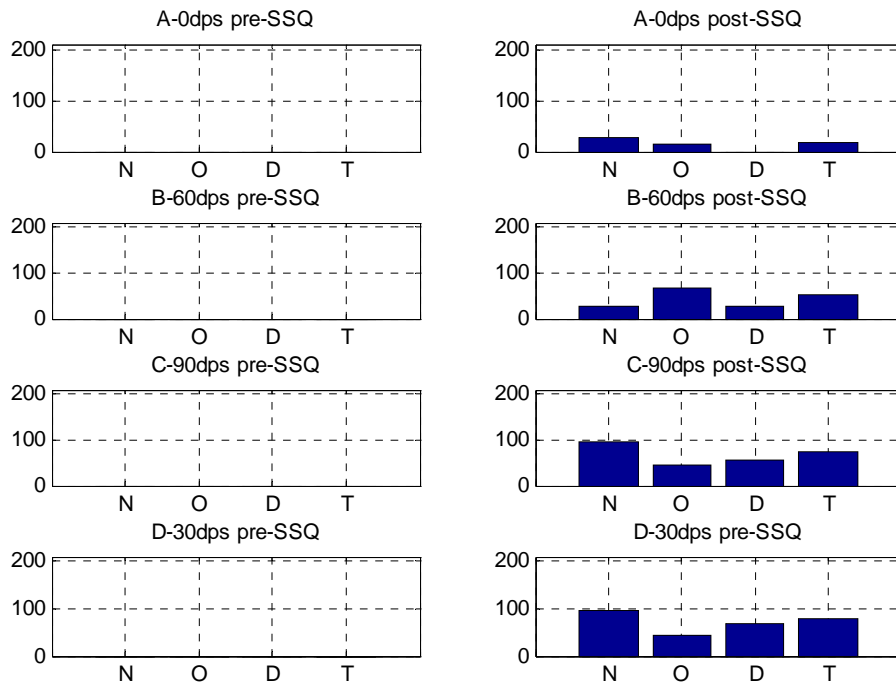
Pre- & Post- SSQ scores of subject CP



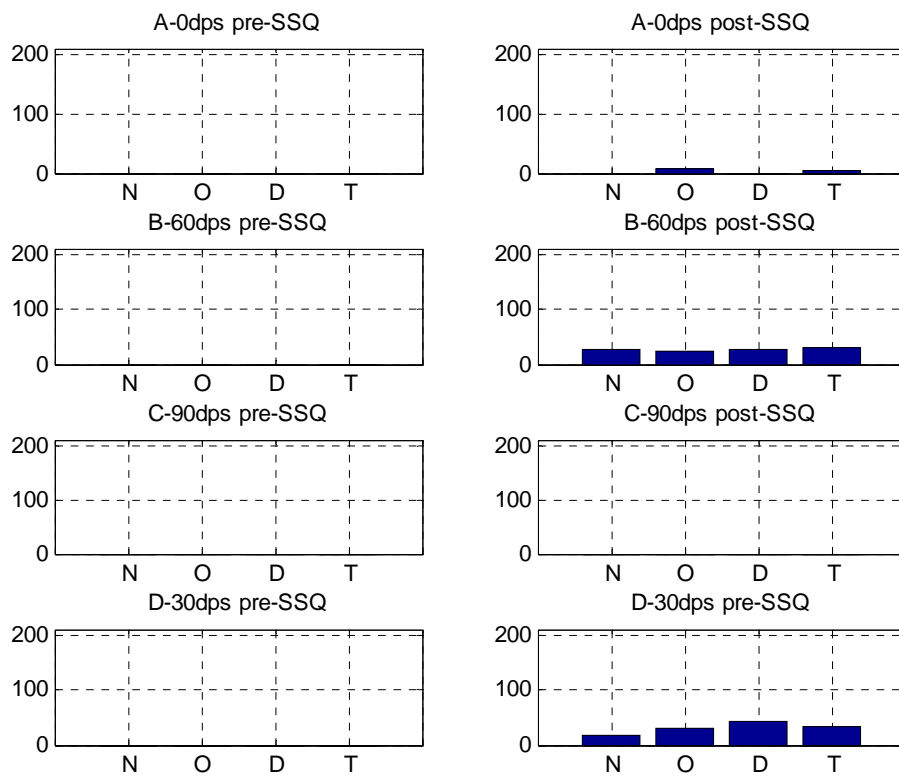
Pre- & Post- SSQ scores of subject FQ



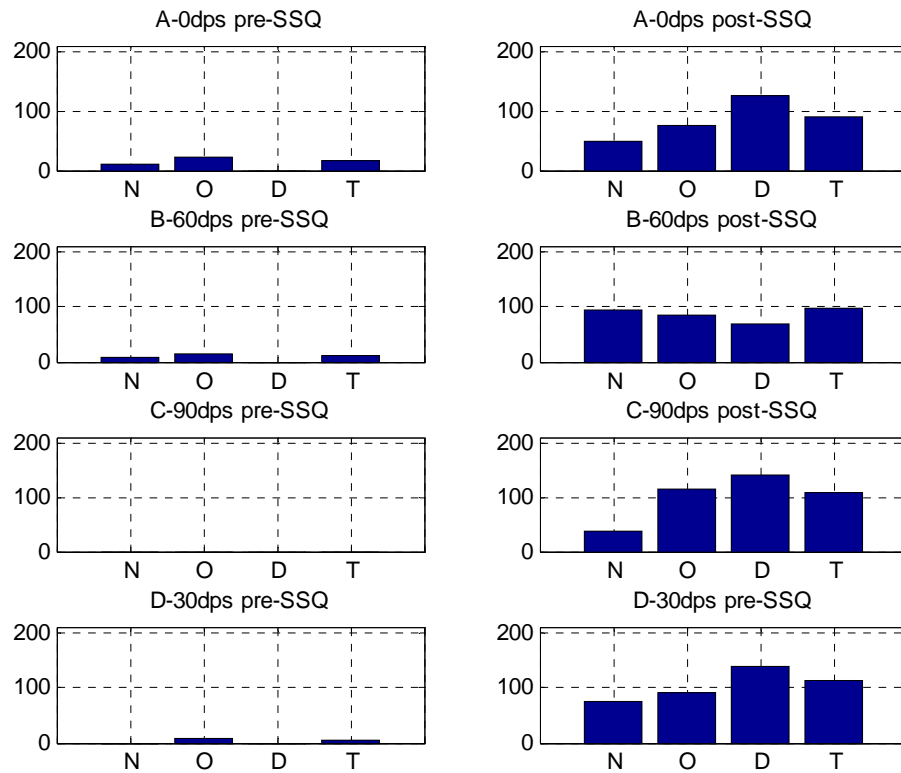
Pre- & Post- SSQ scores of subject LZY



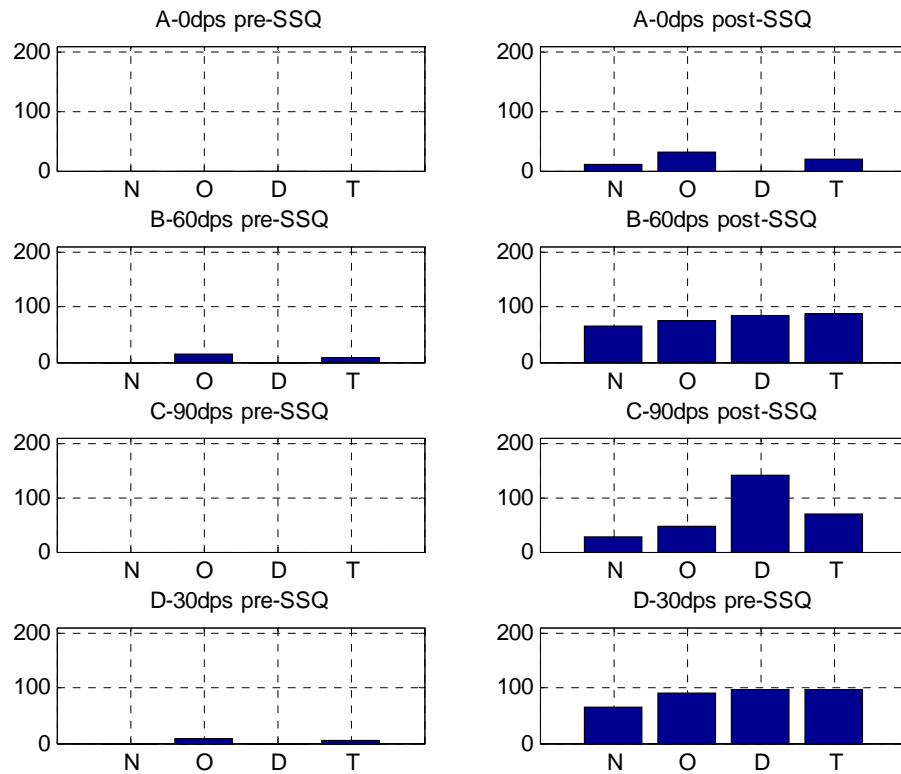
Pre- & Post- SSQ scores of subject ZMZ



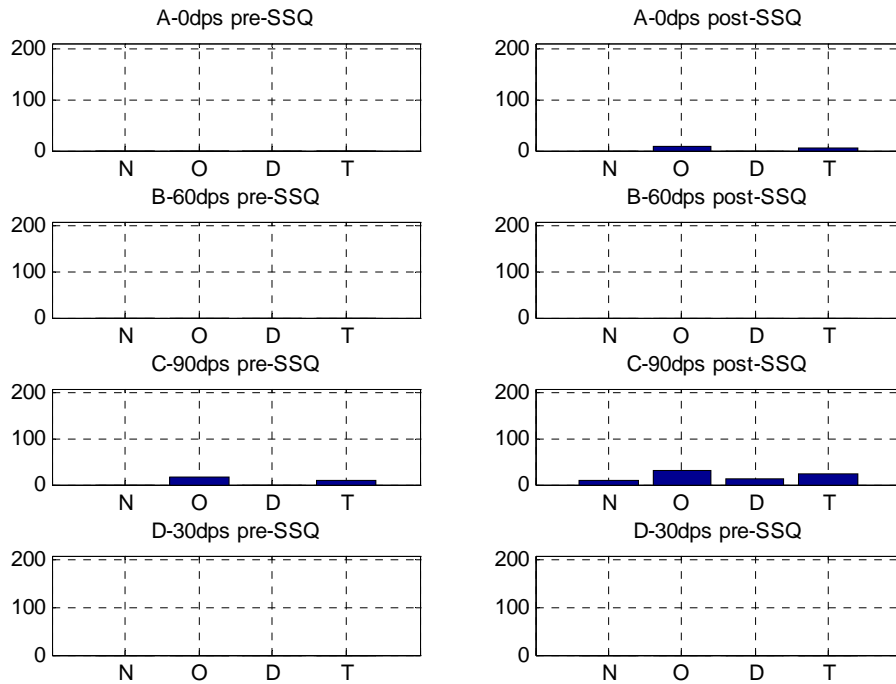
Pre- & Post- SSQ scores of subject YYY



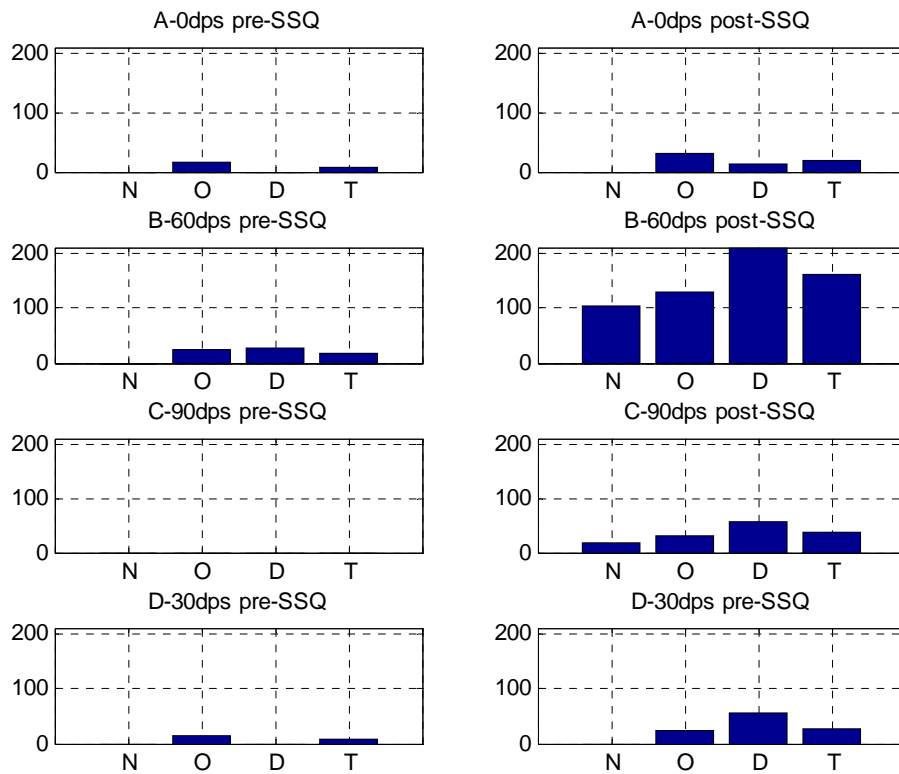
Pre- & Post- SSQ scores of subject MHM



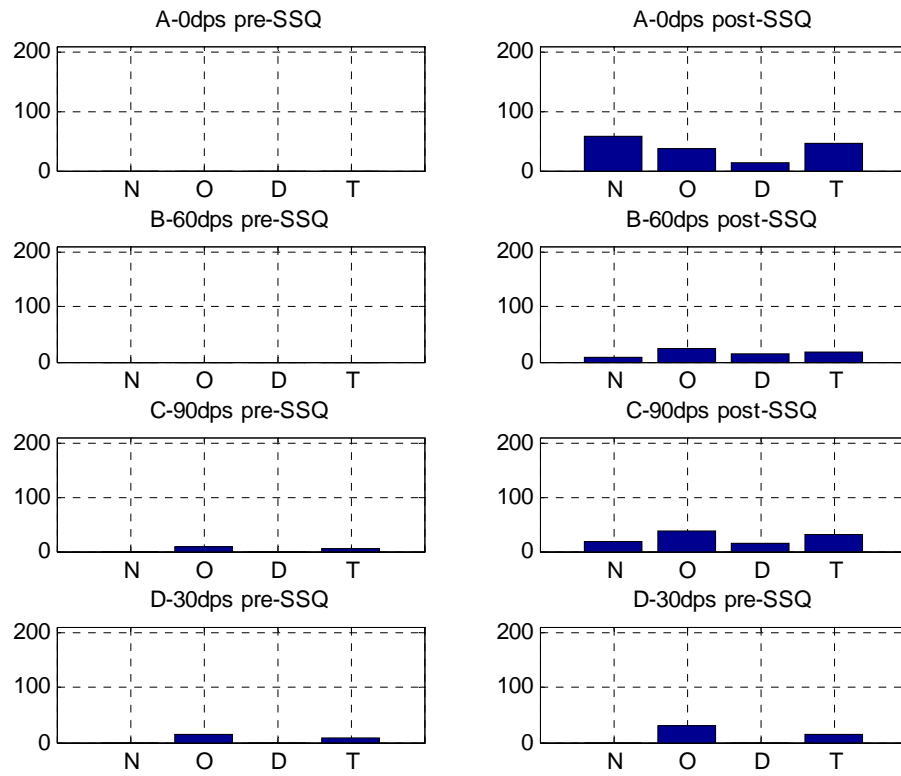
Pre- & Post- SSQ scores of subject WHL



Pre- & Post- SSQ scores of subject CN



Pre- & Post- SSQ scores of subject ZJ(4)



Appendix 7-1: grouping in experiment one

	2dps	14dps	34dps	Susceptibility	
Group I	1.4	9.8	12.1	moderately	24.3
	0.8	8.2	16.4	slightly	15.1
	1.5	8.9	18.2	slightly	18.0
	1.5	13.4	23.5	moderately	21.4
	1.9	4.6	24.1	very	15.4
	1.7	13.6	25.8	not at all	1.1
	0.8	1.4	28.6	very	37.1
Median	1.5	8.9	23.5	Median	18.0
	2dps	14dps	34dps	Susceptibility	
Group II	0.4	5.3	20.1	slightly	10.0
	1.3	4.3	12.6	very	36.0
	0.9	9.0	25.1	moderately	6.8
	2.0	12.4	22.7	not at all	1.0
	2.0	12.1	12.4	very	39.0
	1.9	7.7	33.8	moderately	18.0
	2.0	14.0	24.7	moderately	29.7
Median	1.9	9.0	22.7	Median	18.0

Appendix7-2: grouping in experiment two

Group I	30dps SPV	60dps SPV	90dps SPV	Susceptibility	
	26.7	54.0	81.8	moderately	19.3
	23.8	26.7	26.6	slightly	3.4
	27.6	49.4	47.9	moderately	28.1
	28.0	47.4	64.4	moderately	8.4
	28.0	19.3	26.9	slightly	17.0
	28.4	17.8	26.8	slightly	5.3
	29.1	15.8	23.1	slightly	22.0
Mean	27.4	32.9	42.5	Mean	14.8
Group II	30dps SPV	60dps SPV	90dps SPV	Susceptibility	
	24.8	22.6	15.5	very	15.4
	26.7	28.7	23.4	slightly	19.9
	27.7	51.9	24.0	slightly	15.4
	27.8	48.2	51.4	slightly	15.1
	28.0	58.1	44.1	slightly	18.0
	28.4	57.2	66.6	not at all	1.1
	29.2	52.4	57.8	moderately	16.5
Mean	27.5	45.6	40.4	Mean	14.5

Bibliography

Andre JT, Muth ER, Stern RM, Leibowitz HW.(1996) The effect of tilted stripes in an optokinetic drum on gastric myoelectric activity and subjective reports of motion sickness. *Aviat Space Environ Med.* Jan;67(1):30-3.

Balaban, C.D. and Parker, J.D. (1998). Neuroanatomic substrates for vestibulo-autonomic interactions. *Journal of Vestibular Research*, 8, 7-16.

Bense, S., Stephan, T., Bartenstein, P., Schwaiger, M., Brandt, T., and Dieterich, M. (2005) Fixation suppression of optokinetic nystagmus modulates cortical visual-vestibular interaction. *Neuroreport*, 16:887-890

Benson, A.J. (1984). Motion sickness. In: Dix,M.R.; Hood,J.D. (eds), *Vertigo* (pp. 391-426), John Wiley & Sons Ltd.

Benson, A.J., Hutt, E. C. B., and Brown, S. F. (1989).Thresholds for the Perception of Whole Body Angular Movement About a Vertical Axis. *Aviation, Space, and Environmental Medicine*, 60: p.205-213.

Binnie CD, Wilkins AJ (1998). Visually induced seizures not caused by flicker (intermittent light stimulation). In: Zifkin BG, Andermann F, Beaumanoir A, Rowan AJ, editors. *Reflex epilepsies and reflex seizures. Advances in neurology.* Vol. 75. Philadelphia: Lippincott-Raven Press, pp123-38.

Bles, W., Bos, JE., de Graaf, B., Grogen, E., and Wertheim, AH. (1998) Motion sickness: only one provocative conflict. *Brain research bulletin*, 47:481-487

Bock,OL and Oman, CM (1982). Dynamics of subjective discomfort in motion sickness as measured with a magnitude estimation method. *Aviat.Space Environ. Med.* 53:773-777.

Bonato F, Bubka A, Alfieri L. (2004) Display color affects motion sickness symptoms in an optokinetic drum. *Aviat Space Environ Med.* 2004 Apr; 75(4):306-11.

Bonato, F. Bubka, A. and Story, M. (2005) Rotation direction change hastens motion sickness onset in an optokinetic drum. *Aviation, space, and environmental medicine*, 76:823-827

Bos JE and Bles W. (1998). Modelling motion sickness and subjective vertical mismatch detailed for vertical motions. *Brain Res Bull.* 47(5):537-42.

Brandt, T. (1999) “Vestibular cortex: its locations, functions, and disorders” in *Vertigo*. In: Springer, pp.219-230.

Brandt, T., Dichgans, J., and Koenig, E. (1973) Differential effects of central versus peripheral vision on egocentric and exocentric motion perception. *Exp. Brain Res*, 16:476-491

Brandt, T., Paulus, W. & Straube, A. (1986). Vision and postural. In: Bles W, Brandt T. (Eds.) *Disorders of posture and gait* (pp.157-76), Amsterdam: Elsevier.

Brandt, T., Bartenstein, P., Janek, A., & Dieterich, M. (1998). Reciprocal inhibitory visual-vestibular interaction visual motion stimulation deactivates the parieto-insular vestibular cortex. *Brain*, 121, 1749-1758.

Buttner, U. & Buttner-Ennever, J.A. (1988). Present concepts of oculomotor organization. In: chapter 1 in *Neuroanatomy of the oculomotor system*, Elsevier, Amsterdam. New York: Oxford.

Byrne, M. D. & Gray, W. D. (2003). Returning Human Factors to an engineering discipline: Expanding the science base through a new generation of quantitative methods. Preface to the Special Section. *Human Factors*, 45(1), 1-4.

Chen, W. (2006). Effects of navigation velocities in fore-and-aft, lateral, yaw axes on cybersickness caused by exposure to a virtual environment. Thesis (M.Phil.)—Hong Kong University of Science and Technology.

Cheung BS, Howard IP, Money KE. (1991) Visually-induced sickness in normal and bilaterally labyrinthine-defective subjects. *Aviat Space Environ Med.* Jun;62(6):527-31.

Danieli B.; Lesma G.; Passarella D.; Silvani A.; Kennedy R.S.; Hettinger L.J.; Harm D.L.; Ordy J.M. and Dunlap W.P. (1996) Psychophysical scaling of circularvection (CV) produced by optokinetic (OKN) motion: individual differences and effects of practice. *Journal of Vestibular Research*, 6, pp.331-341.

Daunton, N. & Thomsen, D. (1979). Visual modulation of otolith-dependent units in cat vestibular nuclei. *Exp. Brain. Res.*, 37, 173-176

Dichgans, J. & Brandt, T. (1972). Visual-vestibular interaction and motion perception. In: Dichgans, J.; Bizzi, E. (eds), *Cerebral control of eye movements and motion perception* (pp.327-338), Basel-New York: S.Karger.

Dichgans, J. & Brandt, T. (1978). Visual-vestibular interaction: effects of self-motion perception and postural control. In: R.Held; H.W.Leibowitz; H.L.Teuber (eds), *Handbook of sensory physiology* Berlin (pp.755-804), Heidelberg: Springer-Verlag.

Diels, C. and Howarth, P.A. (2007) Visually induced motion sickness during single and dual axis motion, *Proceedings of The First International Symposium on Visually Induced Motion Sickness, Fatigue, and Photosensitive Epileptic Seizures (VIMS2007)*, Dec 10-11, 2007 - Hong Kong

Doya, K (1999). What are the computations of the cerebellum, the basal ganglia and the cerebral cortex? *Neural Networks* 12, 961–974.

Ebenholtz, S.M. (1992) Motion sickness and oculomotor systems in virtual environment. *Presence*, 1:302-305

Ebenholtz, S.M., Cohen, M.M. and Linder, B.J. (1994). The possible role of nystagmus in motion sickness: a hypothesis. *Aviat Space Environ Med*, 65, 1032-1035.

Flanagan, M.B., May, J.G. and Dobie, T.G. (2002). Optokinetic nystagmus, vection, and motion sickness. *Aviation, space and environmental medicine*, 73, 1067-73.

Flanagan MB, May JG, and Dobie TG. (2004). The role of vection, eye movements and postural instability in the etiology of motion sickness. *J Vestib Res*. 14(4):335-46.

Fletcher, W.A., Hain, T.C. and Zee, D.S. (1990). Optokinetic nystagmus and afternystagmus in human beings: relationship to nonlinear processing of information about retinal slip. *Exp Brain Res*, 81:41-52.

Fuchs, A.F. & Mustari, J. (1993). The optokinetic response in primates and its possible neuronal substrate. In *Visual Motion and its Role in the Stabilization of*

Gaze (pp343-369) Eds. F.A.Miles and J.Wallman Elsevier Science Publishers.

Golding, John F.; Kadzere, Priscilla; Gresty, Michael (2005) A Motion Sickness Susceptibility Fluctuates Through the Menstrual Cycle. *Aviation, Space, and Environmental Medicine*, Volume 76, pp. 970-973(4)

Golding (2006) Predicting individual differences in motion sickness susceptibility by questionnaire, *Personality and Individual Differences* 41 (2006) 237–248

Golding, J & Kerguelen, M (1992) A comparison of the nauseogenic potential of low-frequency vertical versus horizontal linear oscillation. *Aviation, Space, and Environmental Medicine*. Vol. 63, no. 6, pp. 491-497

Graybiel A, Wood CD, Miller EF, and Cramer DB. (1968) Diagnostic criteria for grading the severity of acute motion sickness. *Aerosp Med*. 39(5):453-5.

Guldin, W.O. & Grusser, O.J. (1998). Is there a vestibular cortex? *Trends in Neurosciences*, 21, 254-259.

Harding, G.F.A. and Harding, P.F. (2007) Photosensitive epilepsy and image safety. *Proceedings of The First International Symposium on Visually Induced Motion Sickness, Fatigue, and Photosensitive Epileptic Seizures (VIMS2007)*, Dec 10-11, 2007 - Hong Kong

Heeger (1987) A model for the extraction of image flow' in *J. Opt. Soc. Am.* Vol.4 No.8

Held, R. (1961). Exposure history as a factor in maintaining stability of perception and coordination. *J. Nerv. Ment. Dis*, 132, 26-32.

Henn, V.; Young, L.R. and Finley, C. (1974). Vestibular nucleus units in alert monkeys are also influenced by moving visual fields. *Brain Research*, 71, 144-149.

Hettinger, L.J., Berbaum, K.S., Kennedy, R.S., Dunlap, W.P., & Nolan, M.D. (1990). Vection and simulator sickness. *Military Psychology*, 2(3), 171-181.

Hettinger, L.J. & Ricco, G.E. (1992) Visually induced motion sickness in virtual environments. *Presence*, 1:306-310

Howard, I.P. (1986b). The perception of posture, self motion and the visual vertical. Chapter 18 in In: Handbook of Perception and Human Performance, New York, NY :John Wiley & Sons.

Howarth, PA. (2002) Virtual simulation sickness: is vection the only issue? In: Human Factors in the ages of virtual reality. Annual of the HFES Europe chapter, Dortmund, Oct 23-25, pp53-60

Hu and Hui (1997). Adaptation to optokinetic rotation-induced motion sickness without experiencing nausea. *Perceptual and Motor Skills*, June, 84(32), 1235

Hu, S., Davis, M.S., Klose, A.H., Zabinsky, E.M., Meux, S.P., Jacobsen, H.A., et al. (1997). Effects of spatial frequency of a vertically striped rotating drum on vection-induced motion sickness. *Aviat Space Environ Med*, 68, 306-311.

Hu, S., Stern R.M., Vasey, M.W., Koch, K.L. (1989) Motion sickness and gastric myoelectric activity as a function of speed of rotation of a circular vection drum. *Aerospace Medical Association*, 60:411-414.

Hu, S. & Stern, R.M. (1998). Optokinetic nystagmus correlates with severity of vection-induced motion sickness and gastric tachyarrhythmia. *Aviat Space Environ Med.*, 69, 1162-1165.

Hunter, M.C. and Hoffman, M.A. (2001). Postural control: visual and cognitive manipulations. *Gait Posture*, 13, 41-48.

Irwin, J.A. (1881). The pathology of sea sickness. *Lancet* ii, 907-909.

Jahn, K., Strupp, M., Krafczyk, S., Schuler, O., Glasauer, S. & Brandt, T. (2002). Suppression of eye movements improves balance. *Brain*, 125, 2005-2011.

Ji, J.T.T, Lor, F., and So, R.H.Y (2004) Integrating A Computational Model of Optical Flow into The Cybersickness Dose Value Prediction Model, Proceedings of the Human Factors and Ergonomics Society 48th Annual Meeting, 20-24 September, New Orleans, LA, USA, 2004

Katz, R.L. & Bigger, J.T. (1970). Cardiac arrhythmias during anesthesia and operation. *Anesthesiology*, 33, 193-213.

Kawakita T, Kuno S, Miyake Y, and Watanabe S. (2000). Body sway induced by depth linear vection in reference to central and peripheral visual field. *Jpn J Physiol.* 50(3):315-21.

Keller, EL. and Daniels, PD. (1975) Oculomotor related interaction of vestibular and visual stimulation in vestibular nucleus cells in alert monkey. *Experimental Neurology*, Volume 46, Pages 187-198

Kennedy, RS., Graybiel, A., McDonough, RC., and Beckwith, FD. (1968) Symptomatology under storm conditions in the north atlantic in control subjects and in persons with bilateral labyrinthine defects. *Acta oto-laryngologica*, 66:533-540.

Kennedy, R.S., Hettinger, L.J., & Lilienthal, M.G. (1990). Simulator sickness. In G.Crampton (Ed.), *Motion and space sickness* (pp.317-341). Boca Raton, FL: CRC Press.

Kennedy, R. S., Lane, N. E., Berbaum, K. S., and Lilienthal, M. J. (1993). Simulator sickness questionnaire: An enhanced method for quantifying simulator sickness. *The International Journal of Aviation Psychology*, 3(3), 203-220.

Kennedy, R.S. , Stanney, K.M. , Drexler, J.M. , Harm, D.L. (1999) Motion sickness and proprioceptive aftereffects following virtual environmental exposure. *Applied Ergonomics* Vol.30, 1999, P.27-38.

Koenig, E.J., Allum, J.H.K. and Dichgans, J. (1978) Visual-vestibular interaction upon nystagmus slow phase velocity in man, *Acta Otolaryngol* 85:397-410.

Krauzlis, R.J. (2005). The control of voluntary eye movements: new perspectives. *Neuroscientist*, 11:124-137

McGee, M.K. (1998) *Assessing Negative Side Effects in Virtual Environments*, Ph.D thesis, Industrial and Systems Engineering, Virginia Polytechnic Institute and State University, February 1998, Blacksburg, Virginia

Miles, FA.(1998). The neural processing of 3-D visual information: evidence from eye movements. *European Journal of Neuroscience*. Volume 10 Issue 3 Page 811 - March 1998.

Miyoshi, T. (1985) Role of the central and peripheral retina upon optokinetic nystagmus. *Acta Otolaryngol (Stockh) Suppl*, 419:53-61

Mustari & Fuchs, 1990, Discharge patterns of neurons in the pretectal nucleus of the optic tract in the behaving primate, *Neurophysiology*, Vol.64, pp77-89

Money, K.E. and Wood, J.D. (1968). neural mechanisms underlying the symptomatology of motion sickness. Fourth symposium on the role of the vestibular organs in space exploration, NASA SP-187.

Muratore, R. & Zee, D.S. (1979). Pursuit after-nystagmus. *Vision Res.* 19(9):1057-9.

Nawrot M, Rizzo M. (1995). Motion perception deficits from midline cerebellar lesions in human. *Vision Res*, 35(5):723-31.

Niemann, T., Lappe, M., Buscher, A., and Hoffmann, K-P. (1999) Ocular responses to radial optic flow and single accelerated targets in humans. *Vision research*, 39:1359-1371

Oman, C.M. (1982) A heuristic mathematical model for the dynamic of sensory conflict and motion sickness. *Acta Otolaryngol Supplementum*, 392:5-44

Oman, C.M. (1990). Motion sickness: a synthesis and evaluation of the sensory conflict theory. *Canadian Journal of Physiology and Pharmacology*, 68, 294-303.

Owen, N., Leadbetter, A.G. & Yarley, L. (1998). Relationship between postural control and motion sickness in healthy subjects – a reappraisal of the sensory conflict approach. *Brain Research Bulletin*, 47, 471-474.

Pereira, C.B., Strupp, M., Holzleitner, T. & Brandt, T. (2001). Smoking and balance: correlation of nicotine-induced nystagmus and postural body sway. *Neuroreport*, 12, 1223-6.

Reason, J.T. (1978). Motion sickness adaptation: a neural mismatch model. *J. R. Soc. Med*, 71, 819-829.

Riccio, G.E. & Stoffregen, T.A. (1991). An ecological theory of motion sickness and postural instability. *Ecological Psychology*, 3, 195-240.

Robinson, D.A., Gordon, J.L., and Gordon, S.E. (1986). A model of the smooth pursuit

eye movement model. *Biological cybernetics*, Vol.55, 43-57.

Schmid R, Zambbarbieri D, Sardi R.(1979). A mathematical model of the optokinetic reflex. *Biol Cybern.* 34(4):215-25.

Simpson, J.I., Giolli, R.A., Blanks, R.H.(1988) The pretectal nuclear complex and the accessory optic system, chapter 9 in *Neuroanatomy of the oculomotor system*, Elsevier, Amsterdam.New York.Oxford

So, R.H.Y., Lo, W.T. and Ho, A.T.K. (2002). Effects of navigation speed on the level of cybersickness caused by an immersive virtual environment. *Human Factors*, 43, 452-461.

So, R.H.Y. and Lor, F. (2004). *Computational Ergonomics: a possible extension of computational neuroscience? Definitions, possible benefits, and a case study on cybersickness.* Contemporary Ergonomics, Taylor & Francis.

So, R.H.Y., Finney, C.M. and Goonetilleke, R.S., "Motion sickness susceptibility and occurrence in Hong Kong Chinese." *Contemporary Ergonomics 1999*, Taylor & Francis.

Stanney, K.M., Salvendy,G., Desisinger, J., Dizio, P., Ellis, S., Ellison, J., Fogleman, G., Gallimore, J., Singer, M., Hettinger, L., Kennedy, R., Lackner, J., Lawson, B., Maida, J., Mead, A., Mon-Williams, M., Newman, D., Piantanida, T., Reeves, L., Riedel, O., Stoffregen, T., Wann, J., Welch, R., Wilson, J., Witmer, B, (1998). Aftereffects and sense of presence in virtual environments: Formulation of a research and development agenda. *International Journal of Human-Computer Interaction*, 10(2), 135-187.

Stanney, KM. & Kingdon, KS. (2002) Dropouts and aftereffects: examining general accessibility to virtual environment technology. *Proceedings of the Human Factors and Ergonomics Society 46th annual meeting.*

Stern,R.M., Hu,S., Anderson,R.B., Leibowitz,H.W. & Koch,K.L. (1990). The effects of fixation and restricted visual field on vection-induced motion sickness. *Aviat Space Environ Med*, 61, 712-715.

Stern, R.M., Hu, S., LeBlanc, R., and Koch, KL. (1993) Chinese hyper-susceptibility to vection-induced motion sickness, *Aviat Space Environ Med*, 64:827-830.

Stevens, S.S.(1957).On the psychophysical law. Psychol Rev. 1957 May; 64(3):153-81.

Stoffregen, T.A. and Smart, L.J. (1998). Postural instability precedes motion sickness. Brain research bulletin, 47, 437-448.

Stoffregen, T.A., Hettinger, L.J., Haas, M.W., Roe, M.M., Smart, L.J. (2000). Postural instability and motion sickness in a fixed-base flight simulator. Human Factors, 42, 458-469.

Telban, RJ and Cardullo,FM. (2001). An integrated model of human perception with visual-vestibular interaction. American institute of aeronautics and astronautics (AIAA) Modeling and Simulation Technologies Conference and Exhibit, Montreal, Canada, Aug. 6-9, 2001

Treisman, M. (1977) Motion sickness: an evolutionary hypothesis.Science, 197:493-495

E. K. C. Tsang and B. E. Shi, "Estimating disparity with confidence from energy neurons," Neural Information Processing Systems Conference, Vancouver, BC, Dec. 2007. (to appear)

Waespe, W. and Henn, V. (1977b). Vestibular nuclei activity during optokinetic after-nystagmus (OKAN) in the alert monkey. Exp. Brain Res/ 30, 323-330.

Warwick-Evans, L.A. & Beaumont, S. (1991). An experimental evaluation of sensory conflict versus postural control theories of motion sickness. Ecol. Psychol., 7, 163-179.

Warwick-Evans, L.A., Sympns, N., Fitch, T. & Burrows, L. (1998). Evaluating sensory conflict and postural instability theories of motion sickness. Brain Research Bulletin, 47, 465-469.

Webb, NA.(2000). Visual acuity, eye movements, the illusion of motion and motion sickness with optokinetic stimuli. Ph.D thesis. University of Southampton, faculty of engineering and applied science institute of sound and vibration research (isvr), southampton, united kingdom, so17 3tj.

Webb, NA & Griffin, MJ. (2002) Optokinetic stimuli: motion sickness, visual acuity,

and eye movements. *Aviat Space Environ Med*, 73:351-358

Webb, NA & Griffin, MJ. (2003) Eye movements, vection and motion sickness with foveal and peripheral vision. *Aviat Space Environ Med*, 74:622-625

Widrow, B. and Lehr, M.A. (1990) 30 years of adaptive neural networks: perceptron, Madaline, and backpropagation. *Proceedings of the IEEE* Volume: 78, Issue: 9: 1415-1442

Willson, V.J., and Jones, G.M. (1979). *Mammalian vestibular physiology*. New York: plenum press.

Wolpert, D.M., Miall, R.C., and Kawato, M. (1998) Internal models in the cerebellum, *Trends in Cognitive Sciences*, 2:338-347.

Yang, TD and Pei, JS (1991) Motion sickness severity under interaction of vection and head movements. *Aviat Space Environ Med*. 1991 Feb;62(2):141-4.

Yates, B.J., A.D. Miller and J.B. Lucot. (1998) Physiological basis and pharmacology of motion sickness: an update. *Brain Research Bulletin*. 47, 395-406.

Young, LR. (1977). Visual-vestibular interaction. In sixth international symposium on Biocybernetics. Leipzig, East Germany

Zupan L.H., Merfeld, D. M. and Darlot, C. (2002). Using sensory weighting to model the influence of canal, otolith and visual cues on spatial orientation and eye movements. *Biological Cybernetics*, Vol. 86, 209-230.